

DISCLAIMER

"This book was prepared as an account of work sponsored by an agency of the United States Government. Neither the United States Government nor any agency thereof, nor any of their employees, makes any warranty, express or implied, or assumes any legal liability or responsibility for the accuracy, completeness, or usefulness of any information, apparatus, product, or process disclosed, or represents that its use would not infringe privately owned rights. Reference herein to any specific commercial product, process, or service by trade name, trademark, manufacturer, or otherwise, does not necessarily constitute or imply its endorsement, recommendation, or favoring by the United States Government or any agency thereof. The views and opinions of authors expressed herein do not necessarily state or reflect those of the United States Government or any agency thereof."

Available from the National Technical Information Service, U.S. Department of Commerce, Springfield, Virginia 22161.

NTIS price codes

Paper copy: \$14.00

Microfiche copy: \$ 3.50

**ANALYSIS OF RESERVOIR PRETREATMENT IN
CHEMICAL FLOODING: A LITERATURE REVIEW**

By

Harry Surkalo and George Pouska
Exoil Services
1301 Arapahoe
Golden, Colorado 80401

Rex D. Thomas
Technical Project Officer
Bartlesville Energy Technology Center
P.O. Box 1398
Bartlesville, Oklahoma 74003

Date Published—July 1980

Work Performed for the U.S. Department of Energy
Under Contract No. DE-AC19-79BC10027

U.S. DEPARTMENT OF ENERGY

TABLE OF CONTENTS

ABSTRACT	
INTRODUCTION	
Problem Statement	1
Study Objective	2
Methodology	2
PROCESS FUNDAMENTALS	
Adsorption	3
Precipitation	5
Cation Exchange	5
Fluid Displacement/Dispersion	7
Mobility Control	8
Miscellaneous	9
LITERATURE REVIEW	
Laboratory Studies	10
Patents	22
Field Studies	26
Bell Creek Field	27
North Burbank Field	38
El Dorado Field	41
Ranger Zone - Wilmington Field	42
Salem Field	42
Mobil - Four Field Tests	44
Louden Field	47
Benton Field	48
Pembina Field	49
Lawry Farm, Bradford Field, Phase II	50
Loma Novia Field	50
Big Muddy Field	51
Higgs Unit	52
NOMENCLATURE	53
BIBLIOGRAPHY	56
APPENDIX	62

ABSTRACT

This paper is a state-of-the-art literature review of pertinent information on the topic of preflush for chemical flooding. Three areas of information were included in the search: laboratory studies, patents, and field application studies.

Preflush of a reservoir prior to chemical flooding can be beneficial in several ways. The ultimate economic benefit which is sought from a preflush can be the result of reduced surfactant consumption, improved slug performance, and/or increased reservoir contact.

There are numerous chemical and physical processes which may occur during a preflush injection. Those which have been cited most frequently in the literature include the following: reduction in surfactant adsorption on reservoir clays, reduction in surfactant precipitation due to multivalent cations, and added mobility control to improve reservoir sweep efficiency. Reduction of sulfonate losses has clearly been found to be the most frequently identified purpose of a preflush. This goal is accomplished by means of fluid displacement, cation exchange, or other sacrificial replacement process.

The literature review has shown the laboratory studies to be the most valuable source of current technology. Field studies completed to date provide less up-to-date information presumably because of the greater time lag associated with a field project. The patents proved to be the least important source of information. Typically, the descriptions of processes and/or exact chemical formulations are vague or omitted completely.

INTRODUCTION

The economics of micellar-polymer flooding are directly related to two factors: (1) the large investment in chemicals, which can run as high as 60 percent of total project costs; and (2) the amount of oil recovered. Preflush treatments can reduce the amount of expensive chemicals necessary for the same recovery; or alternatively, for the same chemical costs, increase the amount of oil recovered. With the large economic benefit potentially available from the use of preflush in chemical flooding programs, the chemical and physical processes which control preflush effectiveness must be thoroughly understood.

PROBLEM STATEMENT

Many experimental studies have been completed on processes critical to preflush performance. Among these are works on surfactant adsorption and cation exchange characteristics with reservoir clays. Although the published literature in this area is extensive, few of the studies were specifically directed toward preflush. Only in the past few years have several researchers designed experimental programs to help define the parameters which control preflush effectiveness. Because of the recency of this work, the information available has not yet been collected and summarized in a single source.

Although numerous patents describe specific preflush techniques or specific preflush chemicals, process details are generally presented in a vague or cursory manner. Thus, the value of this source of published information to promote understanding of preflush behavior is minimal.

STUDY OBJECTIVE

The objective of this state-of-the-art literature review is to gather all the available pertinent information and summarize it. In this report, the literature review is divided into three sections: (1) reports on laboratory studies, (2) patents, and (3) reports of field application studies.

With this information, an experimental core flooding program is being developed, and results of this study will be published soon. Six-inch radial Berea discs are being used for most of this study. The objective of this work is to apply the techniques and chemicals discussed in the literature to a single, integrated core flooding program. In addition to gathering tertiary oil recovery and oil cut data, chemical analyses are being performed on produced fluids to provide a history of chemical composition. These data should be useful in analyzing the specific process details provided from previous works and determining ultimate preflush effectiveness as measured by tertiary oil recovery.

METHODOLOGY

An extensive computer-assisted literature search was completed to gather all pertinent publications which might be germane to the preflush topic. After reviewing and categorizing this first collection of papers, the references from these works were investigated yielding a second generation of publications for the review.

All of the papers collected were critically analyzed, and the portions dealing with preflush were summarized. These summaries were compiled, and they are presented in this report at three levels of detail as follows:

1. A brief overview of preflush fundamentals as indicated by the literature survey is presented in the section entitled, "Process Fundamentals."
2. Slightly more detail is available in the section entitled, "Literature Review." Here the individual papers are summarized with their pertinent conclusions included.
3. The appendix provides extensive detail with excerpts from selected papers. Mathematical developments as well as experimental results are also included. Nomenclature was modified to be consistent among the several publications included in the appendix.

PROCESS FUNDAMENTALS

Preflush of a reservoir prior to chemical flooding can be beneficial in several ways. The ultimate measure of preflush effectiveness is the economic benefit it provides. Total chemical costs may be reduced due to reductions in surfactant consumption. Tertiary oil recovery may be increased due to improved slug performance and/or increased reservoir contact.

The chemical and physical processes which may occur during a preflush injection are numerous: adsorption, precipitation, cation exchange, fluid displacement, and mobility control. Some have been clearly demonstrated in laboratory and field experiments; others have been hypothesized but not proven.

ADSORPTION

It has been demonstrated repeatedly that petroleum sulfonates and other surfactants are subject to adsorption in reservoir

rock, especially clays. This loss of surfactant, mostly prevalent at the leading boundary of the slug can alter the slug composition sufficiently to impair micellar stability and decrease tertiary oil recovery. Thus, a primary focus of research has been on the determination of this adsorption and the effect of numerous process parameters.

Investigators have identified many factors which influence surfactant adsorption — at least under some circumstances. Among these are the following: ionic strength, type of ions, temperature, pH, and surfactant type.

Based on experimental studies⁶⁸ at the University of Florida, two mechanisms have been proposed for surfactant adsorption.

1. The first mechanism is believed to be due primarily to electrostatic attraction of surfactant anions to positively charged crystal sites. This leads to a well defined adsorption plateau with the "shoulder" at an equilibrium surfactant concentration near the critical micellar concentration (CMC). This produces a Langmuir-like adsorption isotherm modified by hemicelle formation.

2. The second mechanism is believed to be due to the attraction of surfactant anions to multivalent cations in the exchange sites. These cations are postulated as "bridges" between the adsorbent surface and the adsorbed surfactant. If calcium is present, this mechanism leads to an adsorption isotherm with a maximum because the insoluble calcium surfactants are resolubilized in the presence of excess surfactant.

Research on surfactant adsorption at the University of Texas⁶⁷ has produced a physical model which simulates experimen-

tal isotherms well. The mathematical model envisions lateral interactions between adjacent adsorbed surfactant molecules and the formation of a second layer. Complete coverage is represented by a bilayer.

Experiments at Columbia University⁷⁰ have identified the importance of many parameters on surfactant adsorption. Among the most significant was the effect of sulfonate purity and oil in the surfactant system. Adsorption was discovered to decrease as the chain length of the oil increased. These phenomena as well as many others will be the subject of continuing research by personnel at Columbia University.

PRECIPITATION

Closely related to surfactant adsorption is precipitation; in fact, sometimes the two effects may be inseparable. A mechanism has been proposed based on precipitation which involves either cation exchange with brine or extraction of multivalent cations from the clay adsorbent to result in surfactant precipitation and subsequent dissolution by excess surfactant. This mechanism leads to an apparent adsorption isotherm with a maximum.

Analysis of precipitates showed these materials to be of the form CaA_2 where "A" is the surfactant anion. No appreciable sodium was found in the precipitate although sodium concentrations in solution were reasonably high.

The kinetics of precipitation has been studied by Walker, Somasundaran, and others^{68,70} and found to be dependent on electrolyte type, concentration, and degree of mixing.

CATION EXCHANGE

Closely associated with surfactant losses due to adsorption/precipitation is the cation exchange potential of most

clays found in reservoir rock. These clays will exchange monovalent cations for divalent ones and vice versa. The direction of the exchange is a function of the respective ions involved as well as their relative concentrations in the fluid and on the clay. Cation exchange represents a potential threat to micellar slug performance because of two conditions:

1. Surfactant systems typically have extremely low divalent cation concentrations because monovalent cations are required to maintain sulfonate solubility.
2. Many connate brines have a high divalent cation concentration.

Because of these conditions, there is a tendency for cation-exchange with divalent cations from the clay replacing the monovalent cation in the chemical slug.

Preflush can provide a substantial benefit under these circumstances by reducing the divalent cation concentration on the clay before sulfonate injection. The cation exchange which would have occurred between the sulfonate and clay now is seen between the preflush and clay. Thus, the preflush is frequently designated as a sacrificial agent, because the monovalent cations in the preflush are sacrificed in favor of the monovalent cations in the slug.

Almost all studies dealing with preflush have investigated the effect of ion exchange because it is a cardinal factor in preflush performance. From these studies have come data specifying the cation exchange capacities of the commonly encountered clays and the equilibrium constants for the various exchange processes. Other conclusions of importance follow.

1. At relatively low frontal velocities (< 4 ft/day), the ion exchange processes are rapid enough to ensure local equilibrium throughout the system.
2. Several ion exchange waves are generally set off by preflush injection. These waves travel at a lower velocity than that of the salinity wave, which is composed of a concentration variation of nonsorbed anions. This means that the injected composition will generally traverse only a relatively small distance into the reservoir, whereas the new compositions resulting from the exchange process persist much longer.
3. Preflush may be designed to completely condition the reservoir clays. This is seldom practical, however, because of the large volumes of fluid required. If soluble minerals are present, conversion may be essentially impossible. Alternatively, the preflush may be designed to suppress cation exchange by ensuring that the ratios of divalent and monovalent species are matched for the connate and preflush brines.

FLUID DISPLACEMENT/DISPERSION

The most obvious function of a preflush is to displace the reservoir brine which presumably is incompatible with the surfactant slug. By replacing the connate brine with a more suitable brine, the preflush acts as a buffer. The amount of isolation provided by a given size of preflush is a complex determination, even in the absence of cation exchange considerations, because of the structure of fluid flow through a porous media. In addition to the diffusion that can be expected at any interface of miscible fluids of different composition, there is dispersion resulting from fluid flow. In a reservoir, the dispersion effects may be greater than diffusion effects.

At moderate flow rates, the porous medium will create a slightly asymmetrical mixed zone (trailing edge elongated) with the convective dispersion coefficient almost proportional to the mean fluid velocity. The dispersion coefficients for a reservoir can be predicted from the physical properties of the system.

The interaction of fluid dispersion with the ion exchange isotherms can produce a variety of concentration waves in a reservoir. These waves may be self-sharpening, indifferent, or non-sharpening in the absence of dispersion. With dispersion, the self-sharpening waves attain a constant pattern as the opposing forces balance. Indifferent waves would neither sharpen nor spread in the absence of dispersion. With dispersion these waves spread proportional to the square root of the distance traveled. With non-sharpening waves, the spreading caused by variation of the concentration velocities with composition is added to dispersion, and soon the wave becomes so diffuse that dispersion is no longer significant. In this case, the wave spread is proportional to the distance traversed.

MOBILITY CONTROL

A possible application of preflush to improve tertiary oil recovery involves the injection of a polymer solution or other chemical system which forms a gelatinous precipitate in-situ. The proposed benefit is a result of improved reservoir sweep efficiency. The injection of the low mobility fluid preferentially into the more permeable zone of the reservoir creates a more uniform reservoir environment when the chemical slug is injected. Although this technique is completely divorced from the other processes previously described, it may have merit in some applications. This concept has been described in at least four patents^{32,49,64,65} and one article¹⁵ but there are no known field applications of the process.

MISCELLANEOUS

Several other preflush techniques are briefly described in the literature. One patent claims to reduce surfactant losses by injecting a sacrificial chemical which coats the clay with a polymolecular layer or film⁵⁶. As described, the process is alleged to be distinct from adsorption control techniques, but details of the process are not given.

Another special preflush technique employs the use of wetting agents such as polyphosphates and borates to enhance the performance of other sacrificial agents⁷.

LITERATURE REVIEW

A comprehensive review of publications dealing specifically with pretreatment for chemical flooding processes uncovered a few articles and patents. In contrast, a review of publications dealing with the processes pertinent to preflush disclosed numerous sources of information. There are scores of references on the subject of surfactant adsorption on clays. Likewise, the topic of cation exchange has been well researched. Because of the overwhelming number of publications in these and other associated areas, no attempt was made to summarize or catalog all of these works as a part of this report. Instead, only those publications dealing directly with preflush and the current chemical flooding research which comes to bear on preflush are included in this literature review.

These works have been segregated into three groups: laboratory studies, patents, and field studies. Brief summaries are provided for each publication reviewed within the framework. The most pertinent work has been included in greater detail in the appendix. These excerpts include some of the theoretical developments as well as data and figures with a common nomenclature.

Laboratory Studies

This section provides a summary of ten laboratory-based studies dealing with preflush and the processes which control preflush. Included among the ten are the most recent findings of the Department of Energy-sponsored programs at the Oak Ridge National Laboratory, University of Texas, University of Florida, and Columbia University.

The most comprehensive report published to date devoted to cation exchange and its effect on preflush performance has been written by a group of researchers at the University of Texas and Shell Development Company. G.A. Pope, L.W. Lake, H.J. Hill, and F. Helfferich collaborated on a three-part presentation^{59,52,30}.

The theoretical development is presented in a two-part paper which indicates how chemical flood design is affected by multiple cation exchange, adsorption, and dispersion processes. The third part of the paper reviews the results of an experimental core-flooding program and compares them with the theoretical predictions.

This study is summarized below and the mathematical development and experimental results are given in detail in the appendix.

The performance of a chemical flood is affected by the concentrations of the ionic species in the vicinity of the surfactant and polymer.

The theoretical development reveals how changes in composition can result from cation exchange, adsorption, and dispersion processes. The theory is based on the concept of "coherence" and mass-action equilibrium. Experimental evidence suggests that a divalent cation-surfactant complex may form,

thereby complicating the interaction of the ion exchange species in proximity to the surfactant.

Surfactant adsorption in Berea cores was significantly reduced by lowering divalent cation concentration in the surfactant, dissolving carbonate minerals, and converting clays to the sodium form.

Numerous conclusions were made from results of this work. Among the most significant are the following:

1. Generally, one or more ion exchange waves are set off by preflush injection. These waves travel at a lower velocity than the salinity wave, which is composed of a concentration variation of nonsorbed anions. This means that the injected composition will generally traverse only a relatively small distance into the reservoir, whereas the new compositions resulting from the exchange process persist much longer.
2. Preflush size may be estimated based on the complete reconditioning of the reservoir clays. Such a preflush would seldom be practical. However, if the fastest ion exchange wave is slow, the composition generated by the new salinity and old clay composition will determine the environment of the chemical slug for most of its travel. Alternatively, the preflush can be designed to suppress cation exchange by ensuring that the ratios of divalent and monovalent species are matched for the connate and preflush brines.
3. When slug sizes are small and dispersion is relatively large, the effect of dispersion is significant on calculated conditions.

4. A fluid which is matched to the reservoir clays with respect to ratios of divalent and monovalent species (but different over-all composition) will, nevertheless, cause cation exchange to occur in the mixing zones between injected and in-situ fluids. This phenomenon is caused by fluid dynamic dispersion.
5. If a displacing fluid has an adsorption isotherm so that its front would be a self-sharpening wave in the absence of dispersion, the actual concentration profile tends to resemble an asymptotic profile that traverses the porous media without changing shape. Under typical conditions, this phenomenon is more important under field rather than laboratory applications.
6. For simple aqueous solutions of sodium, calcium, and magnesium chlorides, mass-action isotherms adequately represent the experimental data. With respect to cation exchange, the calcium and magnesium can be treated as a single specie. This does not imply that the two cations are equivalent in their effect on surfactant systems.
7. Preflushing to convert clays completely to the sodium form may be essentially impossible when soluble minerals are present. Even in the absence of soluble minerals, large volumes of preflush are needed for total conversion.
8. Surfactant adsorption in Berea is dominated by adsorption of a divalent cation/surfactant interaction specie and/or acid-soluble minerals.

F.W. Smith of Atlantic Richfield Company⁶⁹ has reported on a laboratory preflush study involving both Berea and reservoir

rock. This study was designed to determine the effects of ion exchange on preflush efficiency. The effect of precipitation and complex ion formation was not considered. Test results closely followed predicted behavior based on mathematical analysis.

A summary of the conclusions reached from this work follows. A more detailed account is included in the appendix.

1. The level of salinity of preflush brine is important to the efficiency of ion exchange conditioning--large volumes of low or moderate-salinity brine may be required for elution of divalent cations, but the elution rate can be much higher with more saline brines.
2. With regard to elution of divalent cations by a preflush brine, calcium and magnesium ions can be treated as a single ionic species.
3. At relatively low frontal-advance rates, of 2 to 4 ft/day, the ion-exchange processes are rapid enough so that local equilibrium exists throughout the system.
4. Studies of increasing and decreasing calcium concentrations in the Second Wall Creek core showed no evidence of calcium adsorption hysteresis.
5. The cation exchange capacities of the Second Wall Creek cores were considerably greater than the capacity of a Berea outcrop core.
6. The affinity of a Second Wall Creek core for calcium ions was observed to increase substantially with reduction of brine salinity.

7. Given experimental information on the cation exchange capacity, shape of exchange isotherm, and compositions of connate and preflush brines, idealized estimations of reservoir preflush efficiency can be made. Either the described one-dimensional model described in the paper or its analytical approximation may be used.

C.S. Chiou and H.L. Chang of Cities Service Company completed an important study¹² of preflush design. Although the experimental portion of the study was brief, the findings were significant regarding the importance of ion exchange between divalent and monovalent cations in the reservoir clays and connate water. The mathematical model which they developed incorporating ion exchange and dispersion matched experimental data closely.

The following conclusions are taken from the report of these studies. The work is described in greater detail in the appendix.

1. A mathematical model may be used to predict the ionic displacement in both laboratory experiments and field pilot tests.
2. Based on the assumed cation exchange capacity, ion exchange rate law and dispersion characteristics of the flooding system, the ionic composition in the effluent can be simulated for three different types of preflush; a dilute connate brine, a divalent/monovalent balanced dilute brine, and a brine without divalent ions.
3. Of all three types of preflush investigated, only the diluted connate brine will result in an increase in divalent ion concentration in the front of the chemical

slug. This design may impair the effectiveness of a chemical slug.

4. As far as the ion exchange reaction between the flooding and rock clay is concerned, the divalent ion variation is emphasized in the flooding process. The divalent ions have a greater percent change due to ion exchange than monovalent ions.
5. The preflush performance in a chemical waterflooding process should be determined by the following factors:
 - a. types of preflush design
 - b. size of preflush
 - c. cation exchange capacity of reservoir rocks
 - d. dispersion characteristics of porous media
 - e. ionic composition in the chemical slug

Thomas Campbell of P.Q. Corporation recently published the results of his brine-displacement studies using Berea cores¹⁰. Alkaline systems including sodium orthosilicate, sodium hydroxide, sodium silicate, and sodium carbonate were tested. These were compared to plain sodium chloride solutions. Results show that the alkaline systems were effective in removing the divalent cations from the connate brine. These observations are generally consistent with the findings of other investigators referenced in this report.

The specific conclusions drawn by Campbell are included here. A more detailed description of his work is included in the appendix.

1. Highly alkaline preflushes $\text{pH} > 11$ are very effective in reducing hardness ions to very low levels in reservoir brine prior to injection of surfactant solutions.

2. High salinity preflush solutions are less effective in reducing hardness ions to low levels due to continued ion-exchange from the clays in the Berea cores.
3. The less alkaline sodium silicates, such as 2.0 ratio sodium silicate, are not as effective as sodium orthosilicate, mainly due to the lower alkalinity of the solution.
4. The use of sodium carbonate as a preflush chemical is very inefficient due to the high ion exchange peak induced by some action of the carbonate anion.
5. Dilute surfactant solutions had minimal effects on the elution of hardness ions from Berea cores.

Several investigations⁴² pertinent to preflush are concurrently in progress at the Chemistry Division of the Oak Ridge National Laboratory. Among these are the following:

1. Bleach plant effluent from pulping of wood by the Kraft process is being evaluated as a competitive adsorbate for petroleum sulfonate surfactant on minerals. The solids studied were montmorillonite and crushed Berea sandstone. Surfactant loss from solution was substantially less if the solid was contacted with dilute bleach plant effluent prior to contact with surfactant-containing solutions. Somewhat less diminution of surfactant loss was observed when the effluent was contacted with the solid simultaneously with surfactant. Bleach plant effluent displaced surfactant from montmorillonite when contacted with the solid subsequent to contact with the surfactant solution.

2. The effect of multivalent cations, particularly calcium and magnesium, on the performance of surfactants is an important factor in the design of a micellar system. Montmorillonite has been the primary clay tested because of its high ion exchange capacity. The concentration quotient for the sodium/calcium sorption reaction has been found to remain relatively constant for solutions containing various ratios of sodium to calcium except at very low sodium concentrations. Concentration quotients of this type are needed for use in predicting the sodium/calcium ratios in brines in contact with reservoir clays.

3. A theoretical study has been made of adsorption on mixtures of ion exchangers. The effect of variables such as the concentration of the ion being adsorbed, the concentration of the supporting electrolyte, loading, the values of the capacities and equilibrium constants for the various exchange processes, and the fraction of each adsorber in the mixture on the observed distribution coefficient has been investigated. A computer program has been written to facilitate the calculation of distribution coefficients for the adsorption of an ion on a given mixture of ion exchangers under a specified set of conditions.

Research at the University of Texas⁶⁷ on tertiary oil recovery processes has been directed in several areas. The investigation of direct interest to preflush studies is concerned with surfactant adsorption.

Work in surfactant adsorption was focused on a model that can explain maxima and minima in adsorption curves. The physical assumptions are that adsorption is a function of the con-

centration and composition of monomers in solutions, but not of concentration and composition of micelles; and that in mixed surfactants the micelles first formed are rich in the more hydrophobic component. Above the CMC (critical micellar concentration) the total monomer concentration increases and it gets richer in the hydrophil. The first effect tends to increase adsorption while the second tends to decrease it. These two competing effects are believed to lead to an adsorption maximum. The quantitative model was based on ideal equilibrium for micellization and adsorption, and it mirrors the complex behavior of experimental adsorption curves. An analysis showed that this adsorption behavior has a major influence on surfactant transport in flow through porous media. Under certain circumstances, effluent could contain surfactant at higher concentration or higher molecular weight than that injected.

Monoisomeric surfactants had simple Langmuir-type adsorption curves, but the plateau started at the CMC. Because this is not directly related to adsorption constants, the isomer that was most strongly adsorbed at low concentration did not necessarily have the highest plateau adsorption values. In a new dynamic model, rate effects in adsorption are expected to depend on micelle formation, not surface coverage.

A new physical model for surfactant adsorption has been proposed, and the resulting mathematical simulations have been shown to represent experimentally determined adsorption isotherms extremely well. The physical model envisions lateral interactions between adjacent adsorbed surfactant molecules and the formation of a second layer. Complete coverage is represented by a bilayer.

The surfaces were assumed to be heterogeneous, and the surface energies were assumed to be distributed in accordance with a

Gaussian distribution. This model will be subjected to further testing to confirm its validity.

Dinesh Shah and Robert Walker, Jr.⁶⁸ at the University of Florida are the principal investigators for a series of research projects dealing with enhanced oil recovery. Extensive work has been completed in the past four years, some of which is concerned with the phenomena associated with preflush processes. The experimentation with rock/fluid interaction is of special interest and a summary of their findings in this area follows.

Elementary analysis of calcium salts of several anionic surfactants confirmed that these materials can be represented by the formula CaA_2 when "A" is the surfactant anion. No appreciable amount of sodium was found in the precipitate even though some of the precipitates were formed from micellar solutions. The precipitation behavior of calcium lauryl sulfate has been studied for four constant concentrations of calcium. Precipitation was first observed; this was followed by precipitate dissolution when excess surfactant was added. On the basis of estimates of the CMC of the surfactant at the electrolyte concentration noted, it appeared that precipitate dissolution began for each calcium concentration before the CMC was reached.

Mechanisms have been postulated for both surfactant precipitation and precipitate dissolution. These emphasize surfactant dimerization and complex ion formation.

Distilled water extracted no appreciable amount of calcium or magnesium from cation exchanged kaolin, but that 1 wt-pct NaCl did. Moreover, earlier work with other clays suggested that brine can continue to extract multivalent cations from apparently well cation exchanged materials. The amounts of multivalent cations extracted by 1 wt-pct NaCl are sufficient to cause significant

surfactant precipitation. This suggests that ordinary saline preflushes may not eliminate surfactant losses due to multivalent cation precipitation.

On the basis of these and related observations, three adsorption mechanisms have been proposed as follows:

The first adsorption mechanism results in a Langmuir-like adsorption isotherm modified by hemimicelle formation. It is believed to be due primarily to electrostatic attraction of surfactant anions to positively charged crystal sites. This mechanism leads to a well defined adsorption plateau with the "shoulder" at an equilibrium surfactant concentration near the CMC.

The second adsorption mechanism is based on the attraction of surfactant anions to multivalent cations in the exchange sites. Multivalent cations are postulated as "bridges" between the adsorbent surface and the adsorbed surfactant. Owing to the solubility of calcium surfactants in excess of surfactant, this mechanism results in an adsorption isotherm with a maximum.

A third mechanism for apparent adsorption but actually based on precipitation involves either cation exchange with brine or extraction of multivalent cations from the adsorbent to result in surfactant precipitation and subsequent precipitate dissolution by excess surfactant. This mechanism would lead to an apparent adsorption isotherm with a maximum.

A recent paper written by P. Somasundaran of Columbia University covers surfactant losses in porous media⁷¹. A summary of the findings from this paper which are pertinent to preflush are included below.

Experiments have shown that the extent of sulfonate adsorption on reservoir rock is dependent on pH, temperature, ionic strength, and type of ions. Adsorption isotherms exhibit a maximum near the CMC under certain conditions. In this work, adsorption is considered to include losses due to precipitation, entrapment, etc. The adsorption losses depend markedly on pretreatment to the rock and surfactant. Because the adsorption phenomena is so complex, it was decided to study well characterized systems, and simplify the analysis.

Adsorption experiments using purified and as-received sulfonates show purification to reduce the adsorption maximum. The surfactant loss due to precipitation also varies with degree of purification. The maximum loss due to precipitation correlates with the total loss maximum. The adsorption isotherm obtained by isolating precipitation from the total losses still exhibited a maximum although less sharp.

The effect of oil was investigated and found to decrease both the adsorption and precipitation of surfactant. The reduction was more pronounced as chain length of the hydrocarbon increased. Because this effect may be one of the most important in controlling surfactant losses in field applications, it will be studied in detail by the investigators at Columbia.

When surfactant was added to solutions of divalent inorganic electrolytes, the surfactant precipitated. Continued addition of surfactant caused redissolution. In contrast, the precipitate formed from monovalent electrolytes did not redissolve with continued surfactant addition.

The kinetics of precipitation was studied as a function of electrolyte concentration. The rate of formation is dependent on the type of ions and degree of mixing. Sodium and potassium have

a lesser tolerance than ammonium and lithium salts, indicating the effect of the size of the ion.

It is postulated that the redissolution is due to solubilization by the micelles. This is supported by surface-tension data with calcium chloride because precipitation occurs before micellization. On the other hand, with aluminum nitrate, surface-tension data exhibit an apparent micellization region before precipitation. More detailed studies are being completed to verify these observations. Other possible mechanisms suggested for redissolution include aggregation of charged micelles and their redispersion and redissolution by complexation.

PATENTS

A review of the U.S. patents covering preflush processes and sacrificial chemical agents has revealed some useful information for this study. The specification of numerous chemical agents to be used in preflushes clearly has been the most valuable of the knowledge learned from the patents.

Typically, the descriptions of processes and/or exact chemical formulations are vague or omitted completely. Thus, the usefulness of patents for this type of information is minimal.

A brief description of the pertinent patents follows.

Harold Hill, et al of Shell Oil Company have received a patent (No.4,074,755) to control the ion exchange between the reservoir clays and injected fluids in a chemical flood³². The ionic composition of each injected fluid is arranged to provide a constant ratio of monovalent cation concentration to the square root of the divalent cation concentration among the several

fluids to be injected (refer to equation 6, appendix). As an example, by adjusting the composition of a preflush to yield the same concentration ratio as is found in the slug, any ion exchange which may occur will be substantially completed between the reservoir and the preflush, minimizing the ion exchange between the reservoir and the slug which follows.

Several U.S. patents consider the effect of adsorption in chemical flooding processes. One of the earlier patents (No.3,384,171) was issued to Harry Parker of Phillips Petroleum in 1968⁵⁶. Although the description of this patent does not specify adsorption per se, it claims to effect a benefit by injecting a clay-coating material which forms a polymolecular layer or film on the surface of the clay particles. Such a film acts to minimize deposition of surfactants in the slug on the clay. They also render the clay inert to water swelling action.

Numerous metal lignosulfonates are provided as examples of effective additives, as well as several other compounds.

Another patent which was issued shortly thereafter in April, 1969, was developed by Carl Brandner, et al of Mobil Oil Corporation (No.3,437,141)⁷. This improved method of oil recovery employs an aqueous solution of sacrificial inorganic additive to cover the majority of the adsorption sites in the reservoir.

Among the chemical additives specified are sodium carbonate, sodium polyphosphates and sodium borate. The polyphosphates and borate are wetting agents which are beneficial in reservoirs containing larger amounts of clay. These wetting agents are used in conjunction with the carbonate, the actual sacrificial agent.

In September 1969, another patent was issued to Mobil Oil Corporation³⁸. This patent (No.3,469,630) which was an invention

of Billy Hurd, et al, is substantially identical to No.3,437,141 described above. The same chemical additives are referenced in this patent as well as the same purpose of reducing the number of available adsorption sites.

Still another patent concerned with adsorption was issued to Joseph Reisberg of Shell Oil Company in April 1970. This patent (No.3,508,612) explains the use of a synergistic mixture of an organic sulfonate and a sulfated oxyalkylated organic surfactant as preflush⁶². It is claimed that the use of this preflush substantially reduces the degree of surfactant adsorption in the slug as well as several other benefits.

The synergistic mixture contains dissimilar anionic surfactants, one of which is an alkali metal or ammonium or amine salt of an organic sulfonate and one of which is an alkali metal or ammonium or amine salt of a sulfated oxyalkylated organic material.

The most recent patents which utilize a preflush to reduce adsorption of sulfonate from the chemical slug were issued in 1977 and 1979. The inventor of a block of four patents is George Kalfoglou of Texaco. The first of these patents, No.4,006,779 illustrates the use of a lignosulfonate salt in a preflush solution as a sacrificial agent to inhibit the deposition of surfactant in the microemulsion portion of the chemical flood on the reservoir matrix⁴⁵.

The second patent, No.4,133,385 extended this technology to include the use of an oxidized lignosulfonate salt⁴⁶. The third patent, No.4,142,582 named a chrome lignosulfonate complex as the sacrificial agent⁴⁷ while the fourth patent, No.4,157,115 reverts to the original sacrificial agent, a lignosulfonate salt⁴⁸.

In December 1968, George Bernard of Union Oil Company of California earned a patent (No.3,414,054) which claimed to reduce surfactant adsorption by use of a pyridine solution preflush⁵.

Several patents describe beneficial results from preflushes due to complexing or precipitation of divalent ions in the reservoir. The earliest of these is a patent by Lawrence Treiber of Pan Canadian Petroleum Corporation, issued in December 1968. This patent (No.3,414,053) describes the use of water soluble carbonate, such as sodium carbonate and an alkali metal hydroxide, such as sodium hydroxide, to inactivate the multivalent ions by precipitation⁷⁶.

A portion of the carbonate solution is injected first to precipitate any calcium ions. The hydroxide which follows is useful in precipitating magnesium because magnesium hydroxide is less soluble than the carbonate.

The remaining two patents which make direct reference to the benefit accrued from precipitation have been issued to Amir Sarem of Union Oil Company of California. Patent No.3,805,893⁶⁴ was issued in April 1974 and No.3,871,452⁶⁵ followed in March 1975.

In the first patent, Sarem explains the use of a preflush consisting of alternating slugs of an aqueous alkaline metal silicate solution and an aqueous solution of a chemical which reacts with the metal silicate solution to form a gelatinous precipitate. A small quantity of water is used as a buffer between the alternating slugs to prevent precipitation reaction from occurring too close to the injection well where injectivity might be restricted. Sodium orthosilicate and calcium chloride are given as examples of the two chemical agents.

The theory suggests that the reactant solutions tend to move to the more permeable zones where the resultant precipitate

reduces the permeability of that zone. The improved tertiary performance is a result of improved conformance and areal sweep efficiency rather than the chemical benefit afforded by most preflushes.

The second patent by Sarem adds another step to the alternating slug injection by including an alkaline metal hydroxide solution such as sodium hydroxide to the injection cycle. The addition of the caustic solution is claimed to provide the added benefit of divalent ion precipitation to the previous theory.

L. W. Holm, also of Union Oil Company, was issued a patent in March 1977 which is similar to Sarem's first patent. Holm, in patent No.4,011,908, describes the use of an alkaline metal silicate solution as a preflush³⁶. Although Sarem's patent predates that of Holm, Sarem's explanation of preflush performance is the more comprehensive.

In October 1974 a patent was issued to Bruce Knight and J.S. Rhudy of Marathon Oil Company. The concept for this patent, No.3,844,350, is similar in effect to Sarem's first patent; that is to improve tertiary performance by isolating the divalent cations in the more permeable zones thereby minimizing their interaction with the chemical slug which follows⁴⁹.

FIELD STUDIES

Included in this section are the reports of preflush work completed or contemplated for the numerous field demonstration projects of the past few years. Sometimes, preflush was designed to do no more than displace connate water ahead of the micellar slug, and sometimes the preflush design was more complex, with consideration for cation exchange, adsorption, precipitation and other factors relevant to ultimate tertiary oil recovery. Note

that preflush considerations have been attracting much more attention in the chemical flooding program recently. Research has shown the potential importance of preflush, and as a result the more recent field studies display a much more sophisticated approach to reservoir conditioning than some of the earlier field studies employed.

Bell Creek Field

A patented preflush system is a part of the Uniflood^R process being used at Bell Creek Field^{25,27}. This high pH silicate preflush is designed to efficiently remove Ca⁺⁺, Mg⁺⁺, and Fe⁺⁺ from the portions of the reservoir to be contacted with slug. The preflush employs several mechanisms in displacing the multivalent cations: displacement of reservoir brine, ion exchange with reservoir rock, and inactivation of clays by removal of bound water.

In addition, the preflush provides other benefits. It tends to make the reservoir rock water wet and provides favorable salinity and pH for the micellar-polymer system which follows. Occasionally it increases the volume of the reservoir contacted by the surfactant and polymer slugs.

During the evaluation of water-external micellar systems, several preflush compositions were evaluated. However, none were found which provided the multivalent cation displacement mechanisms described above at a reasonable cost.

In addition to the laboratory studies involving preflush systems, a field test was conducted in the Bell Creek reservoir. The purpose of this test was to confirm the mechanisms which prevail in the reservoir and determine chemical requirements for the sacrificial agents. The test consisted of: injecting 1,000

barrels of the high pH silicate preflush containing a methanol tracer into a well immediately outside the pilot area, allowing the solution to react in the reservoir for 56 hours and back flowing to produce the preflush solution. Samples of this produced fluid were analyzed for total alkalinity, methanol, and silicon concentrations. From this test, these conclusions were drawn:

1. 7.5 barrels of preflush was consumed per 100 barrels of pore volume contacted.
2. Reservoir carbonate minerals did not convert any of the preflush silicate to carbonate in solution.
3. Total silicon in solution increased due to dissolution of clays and sand.
4. Dilution of the preflush solution with reservoir water containing bicarbonate did not result in precipitation of silica.

Union Oil and Gary Energy Corporation have provided the following detailed account of the field test²⁵.

A key part of the Uniflood^R process is the alkaline silicate preflush. This preflush reduces adsorption of surfactant on clay minerals by disabling the reservoir's divalent cations that attack surfactants and by creating a high pH environment hindering the surfactant adsorption reaction. The use of a preflush slug can increase the efficiency of the Uniflood^R process by as much as 60 percent when calcium is present and by as much as 40 percent in calcium free systems for reservoirs with rock and fluid properties similar to Bell Creek. Therefore, using enough preflush solution to condition the entire effected reservoir will increase the amount of oil recovered by the process.

For these reasons, it is necessary to know how much preflush will be consumed in the reservoir as it does its job as a sacrificial agent. Although preflush consumption tests have been conducted on Bell Creek core material in the laboratory, the variability of the rock in the reservoir and the time consuming nature of the core tests have made it desirable to measure preflush consumption in the field. The following gives the results of the test conducted at Bell Creek.

Alkaline silicate preflush solution was prepared for the preflush consumption test at the micellar-polymer project injection plant by Gary Energy Corporation personnel. The composition of the preflush is as follows:

	<u>volume percent</u>
Bell Creek Produced Water	98.6
Caustic Soda (50 wt-pct NaOH)	0.66
Sodium Silicate (37.5 wt-pct)	0.53
NTA 150 (40 wt-pct NTA*)	0.10
Methanol	0.10

* Trisodium salt of Nitrilotriacetic Acid

The tank used for mixing the preflush ingredients was made of carbon steel with no internal coating and had a capacity of 1,000 barrels. An electrically driven stirrer was used for rapid mixing of the preflush solution.

Total alkalinity loss was determined by comparing the total alkalinity predicted from the methanol tracer concentration to that measured in the produced preflush solution. These two quantities are plotted on Fig. I vs. the total barrels produced.

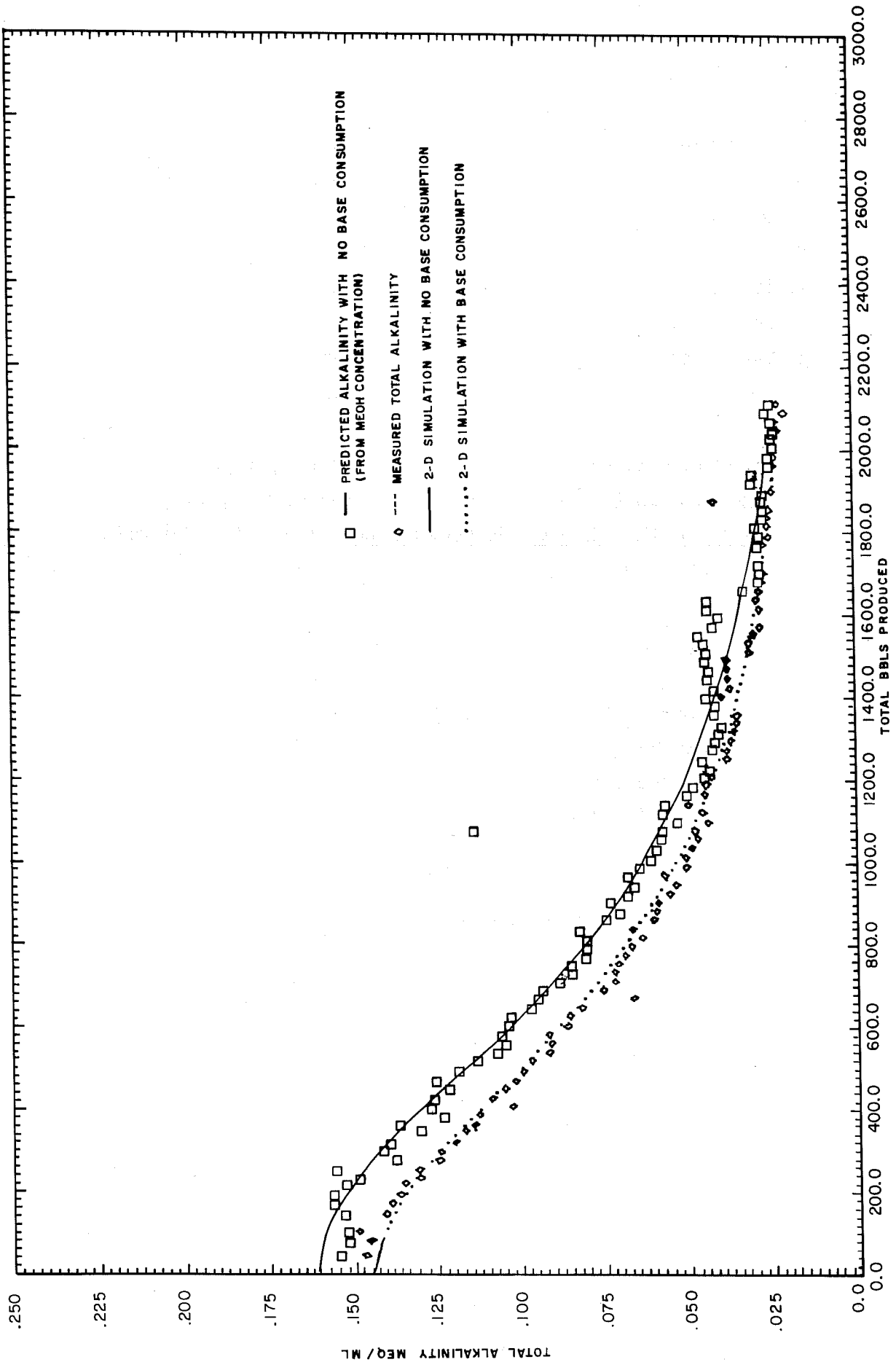


Figure I TOTAL ALKALINITY LOSS FROM PREFLUSH SOLUTION

The loss is determined by calculating the area between the total alkalinity curve derived from the methanol concentration (no base consumption) and the curve representing the measured total alkalinities. The area between the curves is equal to 3,217 gm-equivalents of base. To calculate the total alkalinity loss per unit of reservoir pore volume, it is necessary to know the volume of reservoir contacted by the preflush solution. This is determined by the volume of fluids injected, the dilution of the injected fluids by the water in place, and the drift rate of the reservoir fluids during the test. A computer simulation of the test was made to determine this contact volume.

The computer program uses finite difference methods to simulate a single well tracer test in two dimensions. The program was used to simulate the produced methanol concentration, which was then theoretically converted to total alkalinity. The base consumption reactions were represented in the program by a first order reaction occurring in the aqueous phase.

The best match of produced fluid concentration was obtained using the following input parameters to the program:

Porosity x Thickness = 3.0 ft.

Drift Rate = 2.5 ft./day

Radial Dispersion Coefficient Constant = 0.66 ft.

Angular Dispersion Coefficient Constant = 0.66 ft.

Reaction Rate Constant = 0.5 day⁻¹

Total Preflush Injected = 900 bbl.

The simulated produced fluid concentration curves are plotted in Fig. I, along with the measured values. The match is quite close, and the simulated curves are fairly sensitive to different input values of dispersion and drift rate. The input value of 900 bbl of total preflush injected gave a much better

match than 1,000 bbl, which is the amount of preflush intended for injection. This discrepancy could be due to an inaccurate measurement of the total amount of preflush in the mixing tank or to a production rate which was actually higher than the set value of 518 bbl/day.

The measured total alkalinity curve was modeled by assuming a constant reaction rate dependent only on the base concentration. This indicates that the reactions which occur are slow relative to injection rate. (If local equilibrium existed during the injection phase, most of the consumption would occur in the first fluids injected). Since the average flooding velocity during injection was 60 ft/day, the absence of local equilibrium during injection is reasonable. Also a contributing factor is the time it takes for the hydroxide and silicate ions to diffuse to the adsorption and cation exchange sites located in the less accessible pores.

It is unlikely, however, that the base consumption reaction is dependent only on the base concentration. After the adsorption sites are satisfied and the cation exchange sites are occupied by sodium, no further reaction should occur. The only possibility for a continued slow reaction would be if slightly soluble minerals such as gypsum or anhydrite were present in the formation. Since these minerals were not detected in any of the core samples which were analyzed and only low concentrations of sulfate were measured in the produced preflush solution, it is unlikely that they are present. Therefore, it will be assumed that after sitting in the formation for 56 hrs., the preflush and rock are in equilibrium and no further base consumption will occur.

In determining the volume of reservoir contacted by the preflush solution, we must know the following:

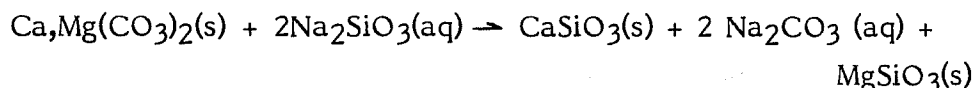
1. Minimum preflush concentration at which reaction still occurs.
2. Total volume which preflush solution contacts (with greater than the above minimum concentration).
3. Additional volume contacted due to drift.

The total alkalinity at which no further reaction occurs between preflush and reservoir rock is estimated to be 0.030 meq/ml. At this dilution of preflush with reservoir brine, all of the silicate and hydroxide will be converted to carbonate. This is supported by the produced preflush alkalinities plotted in Fig. I, which show little or no base consumption in produced fluids with total alkalinities less than 0.030 meq/ml.

The reservoir volume contacted by a solution with this concentration or greater was calculated to be 1,683 bbl by using the simulator with a zero drift rate and equal radial and angular dispersion coefficients of 0.66 ft. The additional reservoir contacted due to a drift velocity of 2.5 ft/per day was calculated to be 240 bbl. Therefore, the total reservoir pore volume contacted during the consumption test was 1,923 bbl.

The total alkalinity loss is therefore equal to 1.67 gm-equivalent of base per barrel of pore volume, which is the same as 7.5 percent of a pore volume of the design preflush solution.

Because silicate and hydroxide ions are more effective than carbonate in preventing sulfonate adsorption, reactions which convert silicate or hydroxide in solution are detrimental to the preflush. It has been shown in batch contacting tests that both siderite (FeCO_3) and dolomite $\text{Ca,Mg}(\text{CO}_3)_2$ react with high-pH silicate solution. The reactions which occur are as follows:



These reactions take place because the iron, calcium, and magnesium silicates are less soluble than their corresponding carbonates. Since the siderite and dolomite are slightly soluble, the divalent cations go into solution and immediately react with the silicate to form insoluble precipitates. This results in a conversion of the silicate ions in solution to carbonate ions.

The extent of reaction of preflush solution with carbonate minerals was determined by measuring the hydroxide, carbonate, and bicarbonate concentrations in the produced preflush solution. The amount of carbonate and bicarbonate expected with no conversion of carbonate minerals can be calculated from the methanol tracer concentration and the concentrations of carbonate and bicarbonate in the preflush and in the water in place. Fig. II shows the predicted carbonate plus bicarbonate concentrations along with the concentrations actually measured in the produced preflush solution. (Also see Fig. III).

As can be seen from Fig. II, the measured $\text{HCO}_3^- + \text{CO}_3^{=}$ concentration follows the predicted concentration very closely and is actually lower than the predicted concentration throughout most of the preflush production. This indicates that there is no significant reaction between the preflush solution and carbonate minerals in the formation around well 14-1.

Although no core samples from well 14-1 are available, examination of thin sections from nearby wells 14-2 and 14-3 indicated that siderite cement was present only in small amounts.

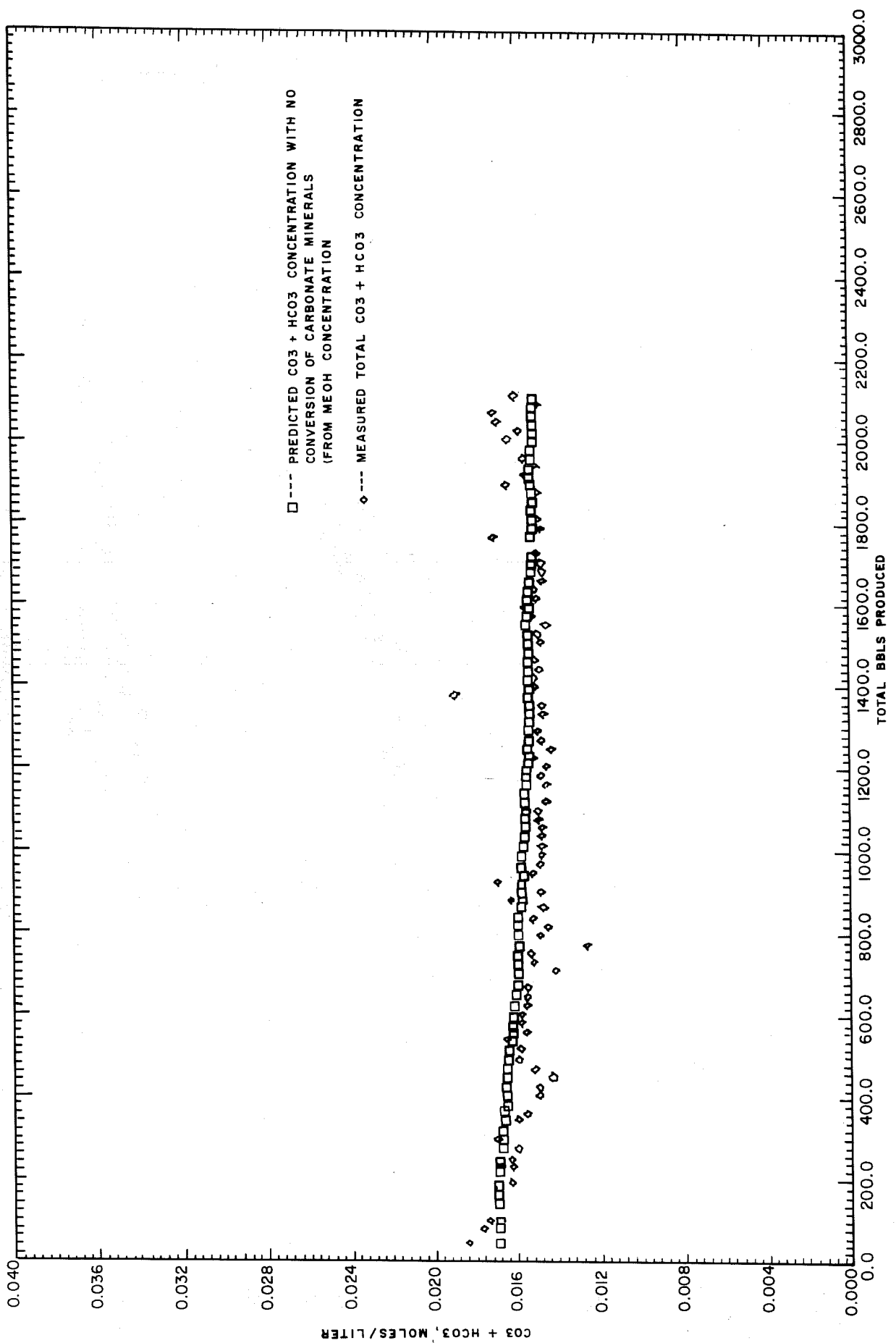


Figure II CONVERSION OF SILICATE TO CARBONATE BY RESERVOIR MINERALS

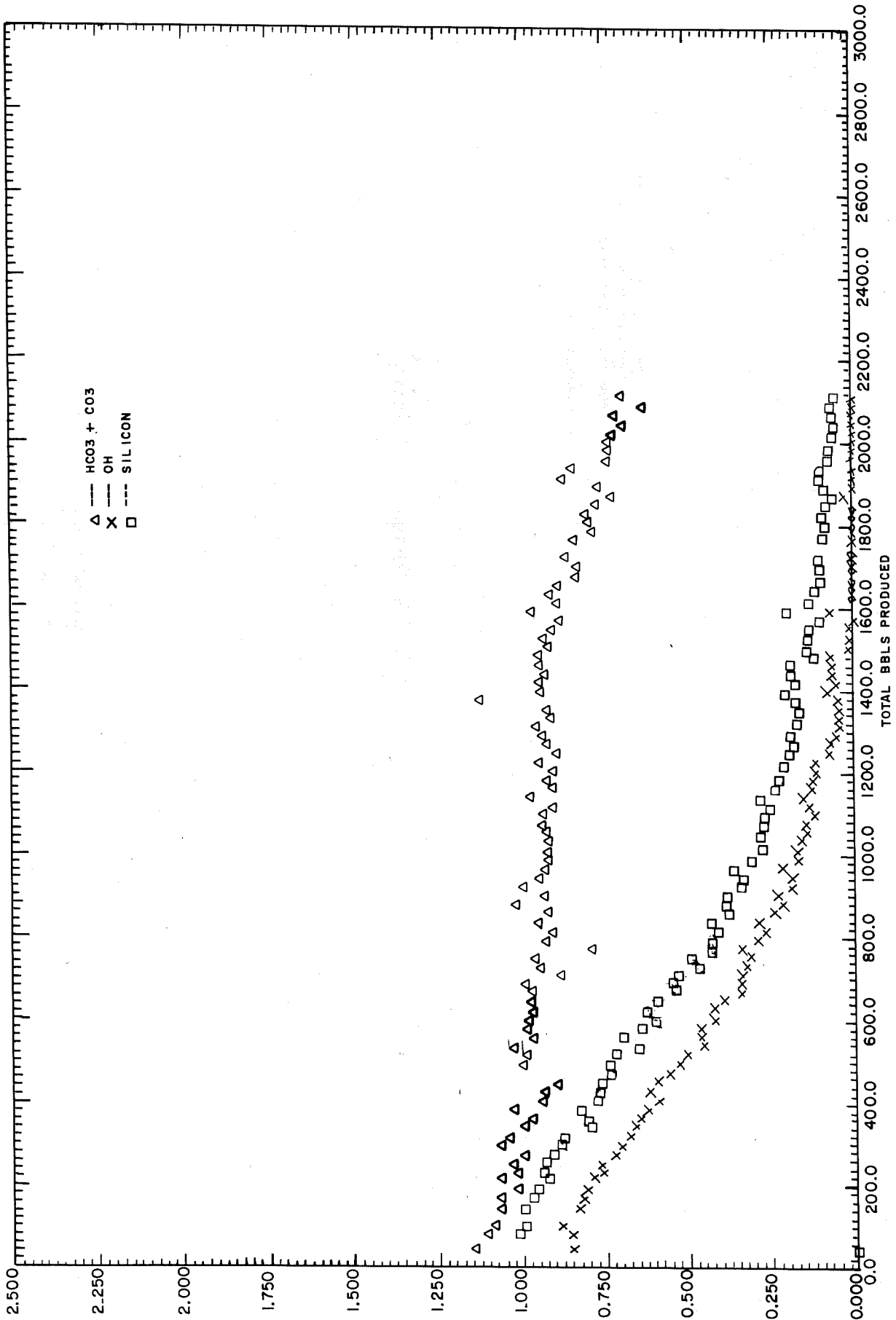


Figure III ACTUAL CONCENTRATIONS IN PRODUCED FLUIDS
(PRODUCED CONC/INJECTED CONC)

Therefore, there may be little or no siderite in well 14-1, but in the pilot area where larger amounts of siderite are known to be present, the reaction of silicate in solution with carbonate minerals may occur.

The apparent contradiction between the batch contacting tests and the core flow tests stem from rock compositional differences used in the test. The batch contacting test used a finely ground rock containing 50 percent siderite, whereas the core flow tests used Bell Creek core containing spotty distributions of very low siderite percentages. Additionally, the batch contacting tests had many orders of magnitude higher surface area per unit volume available for reaction than did the core flow tests resulting in the conclusion of a probable siderite reaction with high pH silicate solutions while the core flow tests, which more closely represent true reservoir conditions, reveal no probable silicate/siderite reaction.

In addition to the loss of silicate caused by reactions with carbonate minerals, it is possible that dilution with reservoir brine containing bicarbonate could cause a reduction in pH and precipitation of silica. The reaction which leads to the precipitation is:



The extent of this reaction depends on the concentrations of the various ionic species of silicate and carbonate which are in turn related to the pH of the solution. Calculations of the pH of this system were made based upon the literature values for dissociation constant of silicic acid and carbonic acid. In addition, the solubility of silica as a function of pH was obtained from the literature. To determine if precipitation of silica occurs when preflush is diluted with reservoir brine, the pH of the

system was calculated and measured in the laboratory for the full range of dilution ratios. The measured pH was then used to determine the solubility of silica at these dilutions. Fig. V shows the hydroxide concentration as a function of the volume fraction of preflush solution in the preflush-produced water mixture. Since the actual silicate concentration is always lower than the total solubility, we can say that no silica precipitation will occur due to dilution with reservoir brine.

Silicate loss was determined by measuring the silicon concentration and comparing it with the concentration which would be predicted from the methanol concentration. These two concentrations are plotted against the barrels produced in Fig. IV. As can be seen from the plot, the measured concentration of silicon is actually greater than that predicted with no loss. This means that sand and clay is being dissolved by the preflush solution in the reservoir, and there is a net gain of silicon in solution. This increase in silicon concentration is largest at the higher preflush concentrations as would be expected.

North Burbank Field

A fresh water preflush, followed by a saline preflush was used by Phillips Petroleum Company in the tertiary recovery pilot test at the North Burbank Unit⁷⁵. Based on laboratory design, a 0.4 PV of 15,000 ppm sodium chloride solution was scheduled for injection preceding the slug. The stated purpose of the preflush was to "condition the reservoir." However, no specific goals were designated in the field report, so the anticipated physical or chemical mechanisms can only be speculated.

Actual injection of the saline preflush in the North Burbank pilot unit was reduced from 0.4 to 0.2 PV. However, the preflush phase of the program was initiated about six months later than

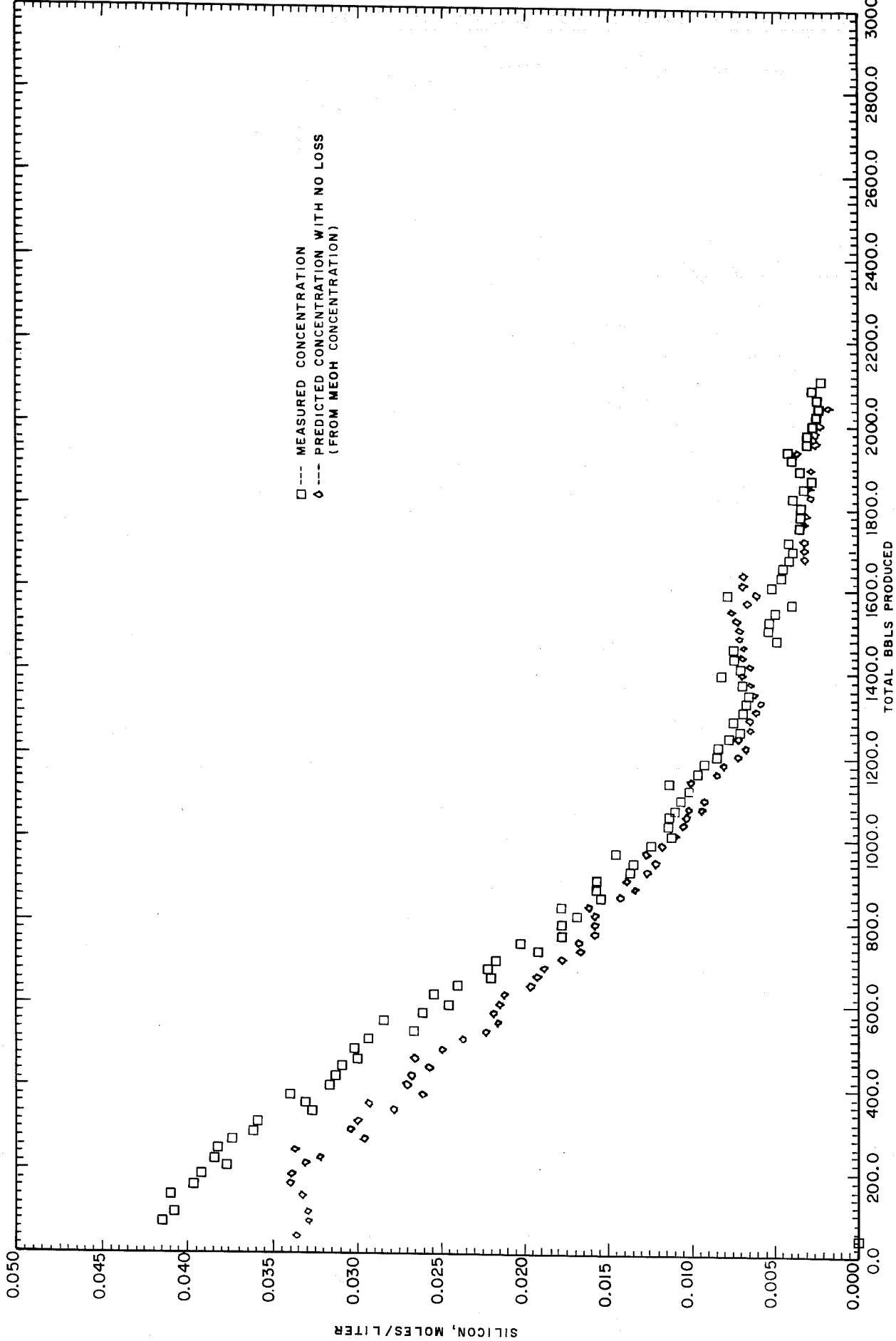
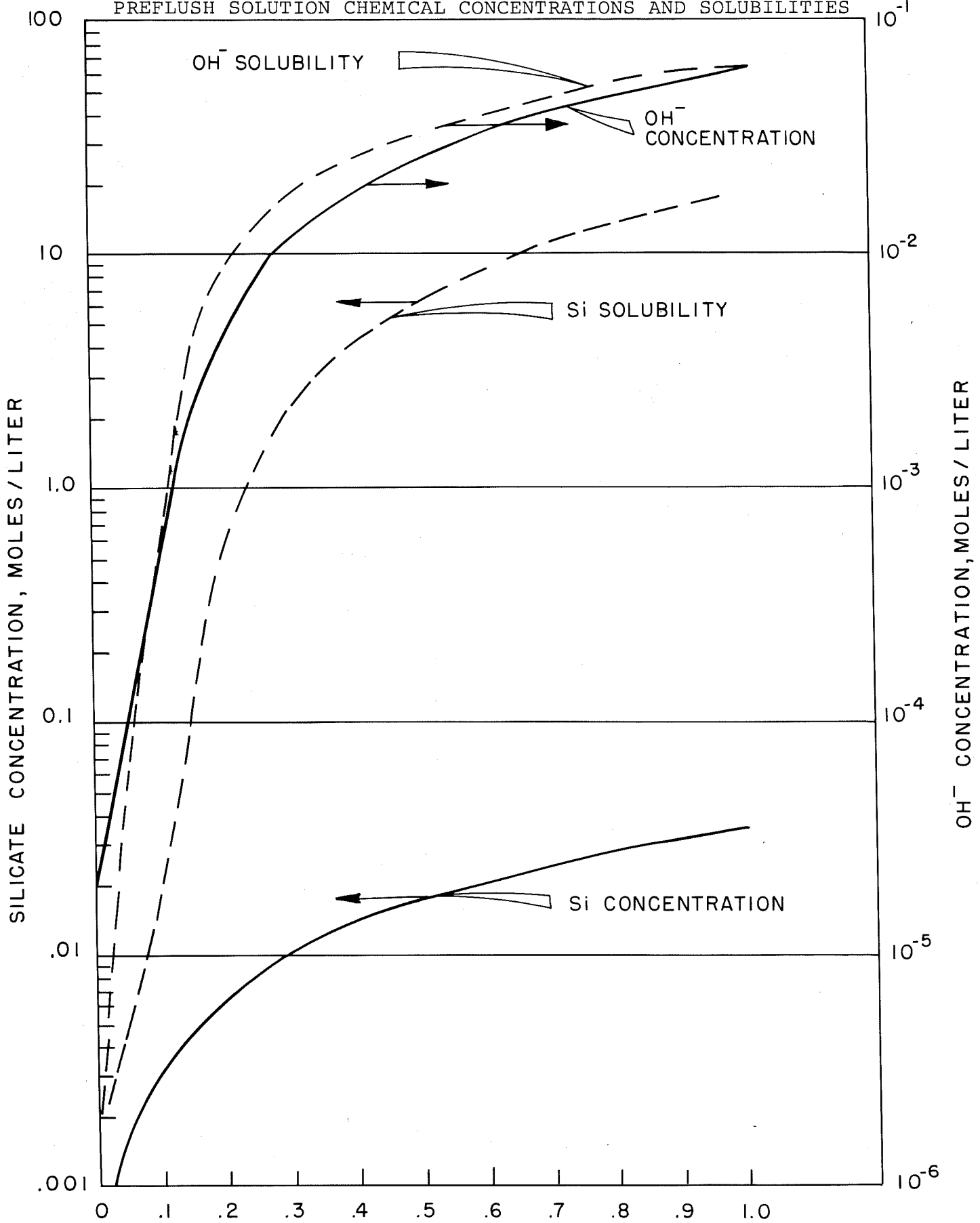


Figure IV TOTAL SILICON LOSS FROM PREFLUSH SOLUTION

Figure 1

PREFLUSH SOLUTION CHEMICAL CONCENTRATIONS AND SOLUBILITIES



$$x = \frac{\text{VOLUME PREFLUSH}}{\text{VOLUME PREFLUSH PROD. H}_2\text{O}}$$

planned at the time of the laboratory design. This delay in the injection schedule may have influenced the decision to reduce the size of the preflush.

El Dorado Field

Two distinct micellar-polymer floods were tested by Cities Service Company in their El Dorado field⁶³. The test in the Chesney lease consisted of an aqueous surfactant followed by a biopolymer. A small alkaline preflush was recommended from laboratory studies. Shell Development Company was the vendor for this portion of the test.

The test in the Hegberg lease was an oil-external surfactant slug followed by partially hydrolyzed polyacrylamide. A 0.76 PV saline preflush was used before slug injection. Phase I of the preflush contained 14,000 ppm sodium chloride in fresh water. Phase II increased the sodium chloride concentration to 29,000 ppm while adding more than 400 ppm of Ca^{++} and 250 ppm Mg^{++} . The ionic concentrations of Phase II were adjusted according to ion exchange theory to account for the effect of the Phase I injection where no divalent ions were added.

In both the Hegberg and the Chesney, the purpose of the preflush was to condition the reservoir water so that it could be better tolerated by the chemical slug. The efficiency of the chemical slug was realized to be dependent on the preflush.

Logging of several observation wells provided the necessary data to monitor the vertical and areal conformance of the preflush injection.

Ranger Zone--Wilmington Field

Based on laboratory core flood studies, a 1 wt-pct sodium chloride preflush was chosen by the City of Long Beach for use in the caustic flood in the Ranger Zone of Wilmington Field¹¹. This salt concentration matched the level found to be most effective in oil recovery with the caustic floods. The preflush water was softened Colorado River water. The total quantity of preflush was designed to be 0.20 PV.

A mini-injection test was completed in 1977 employing the same fluid systems chosen for the main project. Analysis of back flow samples was limited to alkalinity so evaluation of preflush performance was not possible.

Salem Field

A joint Texaco-Mobil test was completed in the Benoist reservoir in the Salem Field^{73,82,83}. The tertiary process used was the low-tension waterflood from Mobil. The first phase of the injection program was a three-part preflush. The first part was a softened fresh water injection equal to 0.22 PV. This water was injected to initiate displacement of the high salinity formation brine.

The second part of the pretreatment consisted of 0.103 PV of softened fresh water containing 6000 ppm sodium carbonate. The purpose of this slug was to facilitate removal of the remaining divalent ions by precipitation and to continue the displacement of formation brine.

The third part of the sequential preflush consisted of 0.196 PV of softened fresh water containing 6,000 ppm sodium carbonate, 6,000 ppm sodium chloride, and 1,000 ppm sodium tripolyphosphate.

This injection was designed to precondition the rock surfaces and to provide the saline environment to be used in the surfactant injection phase.

During this test periodic samples were drawn from producing wells for chemical analysis. Included in the analytical study were four different tracers used to monitor the flow patterns from each of the four injectors toward the center producer.

During the test, it was necessary to acidize the producer on several occasions to maintain adequate production rates. It was postulated that the mixing of various fluids near the well bore resulted in calcium carbonate precipitation. It was determined that calcium and magnesium levels were not lowered to near zero levels as expected.

Clearly, the preflush volume was insufficient. However, it has been recognized that the degree of insufficiency varied with permeability and length of flow path. Therefore, the subsequently injected surfactant was exposed to a variety of ionic concentrations, some of which were not optimum. This reduced the effectiveness and availability of the surfactant to mobilize oil and diminished the recovery of tertiary oil. The inadequacy of the oil mobilization was the result of one or a combination of the following:

1. Sacrificial chemicals used in the preflush did not satisfy formation adsorption requirements.
2. Adsorption requirements were greater than anticipated.
3. Conversion of the sodium sulfonate to a calcium or magnesium form, resulting in reduced surfactant performance.

Analytical studies clearly confirmed the conversion of water-soluble sodium sulfonate to oil-soluble calcium sulfonate. The mixing of streams with different compositions could have been responsible for the sulfonate conversion as it was theorized to have been responsible for the slugging of the producing well. On the other hand, the conversion could have occurred elsewhere in the formation. This theory is supported by the observation of calcium sulfonate at locations where the preflush had apparently adequately swept out the calcium ions. It is possible that some relatively inaccessible pores contained connate water and oil, neither of which was displaced during the preflush. Subsequent flooding with low-tension surfactant may have enabled some penetration and displacement, thereby providing the environment for the sulfonate conversion.

Mobil--Four Field Tests

The Mobil Research and Development Corporation completed four field tests involving displacement of reservoir brine by preflushes of various types⁷².

The first of the four tests was conducted in a mid-continent Pennsylvanian Age reservoir. The injection program was divided into two phases. The first phase involved displacement of reservoir brine with fresh water. Eight production wells were sampled, four each on opposite sides of a line of injection wells. The concentrations of calcium, magnesium, and salinity (as sodium chloride) were monitored. Initially, the reservoir brine contained 18 wt-pct sodium chloride, 12,000 ppm calcium, and 2,000 ppm magnesium. As the fresh water injection progressed, the ratio of calcium to salinity remained constant; likewise, the ratio of magnesium to salinity remained constant. These results indicate that with fresh water injection there was no source of divalent ions from the reservoir rock. Dilution resulted in proportional reduction of all ionic species.

The second phase of this program involved a single injection well and an observation well. Injection was as follows: 0.44 PV of softened fresh water, 1.93 PV of 5,400 ppm NaCl with bromide tracer spike, and 3.33 PV of unsoftened fresh water.

When the softened fresh water broke through at the observation well, the concentration of sodium, calcium, and magnesium dropped sharply as expected.

When the controlled salinity brine broke through, two significant observations were made. First, the bromide tracer was delayed by almost 20 percent, indicating significant adsorption of the sodium bromide at the leading edge. In addition, a large spike of calcium and magnesium was produced in spite of very low divalent ion concentration in the injected brine. The reservoir may have been functioning as a water softener in the regeneration cycle. The increased concentration of sodium with very low levels of calcium and magnesium in the injected fluid allowed a partial exchange with some of the divalent ions on the reservoir rock and clay. Another possible explanation of the high concentration of calcium and magnesium seen at the observation well at the time of brine breakthrough is a result of increased solubility of some calcium and magnesium salts as the sodium concentration increases.

After the production spike of divalent ions, the concentration slowly declined. A nearly constant concentration was reached by the time the softened fresh water broke through at the observation well.

The second of the four tests was completed in a Gulf Coast reservoir. A single injection well and a single observation well were used to determine the efficiency of reservoir brine displacement by a controlled salinity preflush. Reservoir brine

contained 6 percent sodium chloride, 1,000 ppm calcium and 200 ppm magnesium. The controlled salinity preflush contained 6,450 ppm sodium chloride. This fluid averaged approximately 20 ppm calcium and 4 ppm magnesium. Preflush injection amounted to 1.81 PV based on a radial flow pattern.

Chemical analysis of the produced fluids confirmed the efficient displacement of reservoir brine. Proportional reductions of sodium, calcium, and magnesium were realized. There was no evidence of any ion exchange phenomena or dissolution of divalent ions from the reservoir.

The third test was completed in another mid-continent reservoir of Pennsylvanian Age. In this case, the reservoir brine contained 16 percent sodium chloride, 9,000 ppm calcium, and 2,000 ppm magnesium. This brine was displaced by 8 PV of fresh water. The fresh water contained less than 600 ppm total dissolved solids, including less than 50 ppm each of calcium and magnesium.

As observed in the previous tests, the preflush provided a proportional reduction of all ionic species.

The last test was a near duplicate of the third. The preflush was conducted in a mid-continent reservoir. Connate water contained 7 percent sodium chloride, 3,000 ppm calcium and 1,000 ppm magnesium. This brine was displaced by 9.2 PV of softened fresh water.

Again, the chemical analyses of the samples from the observation wells indicated a proportional reduction of salinity and divalent cations.

Louden Field

A surfactant pilot test was conducted in Loudon Field, Illinois during the period 1969-71. Laboratory studies had revealed the need for a preflush ahead of the surfactant injection⁶⁰. The high-salinity reservoir water had to be isolated from the surfactant system because of the low-salinity tolerance of the sulfonate. Therefore, the use of fresh injection water in the surfactant and a low-salinity preflush was indicated.

High chemical costs precluded the use of complexing agents for the divalent ions in the reservoir. The only practical approach found was to precipitate the divalent ions using sodium carbonate. While the precipitation resulted in reduced permeabilities, the losses were not expected to be excessive. Ammonia was used with the sodium carbonate to help satisfy the base consumption of the reservoir.

The preflush was completed in two parts. Initially, 1.3 PV of a relatively fresh water (4,700 ppm sodium chloride, 5,000 ppm total dissolved solids) was injected to displace the highly saline reservoir water (64,000 ppm chlorides, 104,000 ppm total dissolved solids). The base preflush which followed was 0.098 PV of 8,100 ppm sodium carbonate and 4,300 ppm ammonia dissolved in softened fresh water. Sodium carbonate and ammonia were also added to the surfactant system, although at a reduced concentration.

Insoluble calcium carbonate gradually formed around the production well bore as a result of undisplaced high calcium brine mixing with injected sodium carbonate. This caused productivity losses that necessitated a minifrac stimulation and several subsequent acidizings. Permeability reductions elsewhere were not as severe.

The degree of divalent ion protection given the surfactant by the preflush was estimated from the calcium and magnesium concentrations found with the bases in the produced fluids. Surfactant samples taken from the production well contained less than 5 ppm calcium. At the leading edge of the surfactant, the magnesium concentration was as high as 150 ppm but quickly dropped to less than 40 ppm. These concentration levels were judged to be low enough for proper surfactant function.

Despite the effective protection of the surfactant from the resident divalent ions, tertiary oil recovery was less than anticipated. The probable cause for the disappointing performance of the surfactant was the high salinities found in the surfactant bank. Assuming a unit-mobility displacement, substantial reductions in salinity were expected with the preflush and again with the surfactant. Produced chlorides dropped from 64,000 ppm to 13,000 ppm with the preflush. However, instead of reducing further behind the leading edge of the surfactant, chlorides actually increased. It is theorized that because of the reduced mobility of the surfactant bank, the fluids invaded portions of the reservoir that were bypassed by the low salinity preflush. These pockets of high salinity connate water were mixed with the surfactant system.

Benton Field

Shell Development Company completed a series of tests in support of their pilot surfactant flood in the Benton Field, Illinois²². As a result of these tests, Shell recommended a small preflush with 9,000 ppm sodium chloride in fresh water followed by 5,000 ppm sodium tripolyphosphate in the sulfonate slug.

An experimental survey of several multivalent ion sequestering agents indicated that 0.5 wt-pct sodium tripolyphosphate

doubled the sulfonate system's tolerance for reservoir brine. With the sequestering agent the sulfonate slug remained effective with up to 25 percent reservoir brine. The ability of sodium tripolyphosphate to prevent the precipitation of multivalent cations was demonstrated by monitoring the pressure drop in core flood tests. The efficiency of the additive was clearly shown.

While the tolerance for brine was helpful, it was decided that further precautionary measures were necessary. Thus, a small preflush was injected to displace reservoir water from the surfactant. Sodium chloride concentration in the preflush matched the salinity of the surfactant slug.

Pembina Field

Mobil Oil Canada and Mobil Research and Development engineered a polyacrylamide polymer flood for use in Pembina Field, Alberta, Canada²⁸. Polymer injection was started in November 1971, and completed in September 1973.

Although no preflush was used, an extensive evaluation of the polymer-flood performance indicated the possible benefits of a preflush had it been used.

Several factors were identified as contributing to the limited and temporary production response. Water-rock interaction as well as formation water comingling reduced the polymer solution viscosity by 75 percent. Significant polymer adsorption was also realized. Tertiary process design should consider possible interactions between rock and injected fluid and take the necessary precautions to minimize the detrimental interactions. Preflush application is a logical candidate for this type of problem.

Lawry Farm, Bradford Field, Phase II

The Pennsylvanian Grade Crude Oil Association in conjunction with the Department of Energy has been conducting a micellar-polymer field test on the Lawry Farm in Bradford Field, Pennsylvania¹⁶.

In Phase I of the field test, only a fresh water preflush was used because the primary goal of this phase was to determine injectivity characteristics of the process fluids in the low-permeability sands.

During Phase II, which was a 24-hour field test, a 50,000 ppm sodium chloride preflush had been used. The effectiveness of the preflush brine to condition the reservoir fluids for slug injection was demonstrated in a series of core floods.

Tertiary oil recovery was compared for tests involving no preflush, 20,000 ppm sodium chloride, and 50,000 ppm sodium chloride. Oil recovery consistently improved with increasing salt concentration over the range studied.

The recommended volume of preflush was 0.10 PV. Actual fluid injection was 0.17 PV.

Loma Novia Field

Mobil Research and Development personnel designed a low-tension waterflood program for use in a watered-out section of Loma Novia Field, Texas²¹. The low-tension flood consisted of three injection phases. The first was the protective slug or preflush. Although specific chemical compositions were not listed for the field test, typical concentration was noted. For most applications, the sodium chloride concentration would be

between 1.0 and 2.0 wt-pct. This slug would normally be about 0.1 PV except with low salinity reservoir brines which are more compatible with the surfactant. In this case, the volume injected could be reduced. The primary purpose of this slug is to screen the low-tension surfactant from the reservoir brine and to base exchange the reservoir solids, replacing the magnesium and calcium with sodium ions. The rear portion of this slug will usually contain sodium tripolyphosphate and/or sodium carbonate to reduce surfactant adsorption and increase the water-wet condition of the reservoir.

Detailed analysis of the field test was not reported, and the effectiveness of the preflush can only be speculated.

Big Muddy Field

A saline preflush is anticipated by Conoco as one phase of the low-tension flood to be completed in the Big Muddy Field¹⁴. The stated purpose of this preflush is as follows:

"To establish the oil production base line and to achieve the desired pattern balance"

At this time, details regarding the preflush size and composition are not available.

No preflush fluids have been injected yet; however, the injection plant is being assembled. From flow sheets of this facility, it appears that the preflush will be simple saline solution rather than a more complex system employing sacrificial agents.

Higgs Unit

A field test of the Uniflood^R process was conducted⁵⁰ at the Higgs Unit, Texas, beginning in 1969. A very small (0.03 PV) preflush of polymer solution was designed to promote a more uniform sweep by the soluble oil.

No analytical study was conducted to determine the effectiveness of the preflush. With no additives to condition the reservoir, little benefit could be expected beyond displacement of reservoir water ahead of the soluble oil injection.

NOMENCLATURE

A	cross sectional area, L^2
A_i	function in Equation 45
a_i, b_i	parameters in Langmuir isotherm
B_{sp}	solubility product constant
C_i	fluid phase concentration of ith component, meq/ml V_p
\hat{C}_i	stationary phase concentration of ith component, meq/ml V_p
D_i	generalized chromatographic retardation term, <u>vol. aqueous phase</u>
D_s	surfactant retardation term V_p
f	fractional flow
F_i	rate of advance of concentration level "i" relative to overall fluid pore velocity
F_ξ	ratio of asymptotic mixing-zone length to maximum no-adsorption mixing-zone length
K_{ij}	ion-exchange equilibrium coefficient
K_l	longitudinal dispersion coefficient, L^2/t
L	total system length (linear)
l	characteristic dispersion length
m	number of nonionic species in the system
n	number of ionic species in the system
N_{Pe}^{-1}	inverse Peclet number (α/L)
q	volumetric flow rate, L^3/t
Q_v	cation exchange capacity, meq/ml V_p
r	Gapon ratio
S	phase saturation
t	time
v_{ci}	concentration velocity, dimensionless
$v_{\Delta ci}$	step velocity, dimensionless
$V_{A, B}$	slug size of fluid A, B, fraction V_p
V_p	pore volume
V_{pf}	preflood slug size, fraction V_p
V_{pd}	cumulative injection, fraction V_p
V_s	chemical slug size, fraction V_p

x fractional concentration of divalent cations in fluid phase,
meq/meq
 y fractional concentration of divalent cations in stationary
phase, meq/meq
 z linear position, L
 α dispersion parameter, L
 β separation factor; relative affinity for divalent cations
 ξ dimensionless position
 \emptyset porosity
 Δ difference
 γ, μ exponents in ion exchange equilibrium equations
 λ eigen value
 σ reciprocal characteristic velocity

SUBSCRIPTS

A, B, C	successive fluid injections
f	final concentrations
f _w	formation water
g	Gapon
max	maximum
m	mixing-zone or mass-action
n	nonsorbed ion
o	initial concentrations
or	residual oil saturation (after waterflood)
orc	residual oil saturation after chemical flood
pd	polymer drive
pf	preflood
s	surfactant
w	water
1	calcium ion
2	magnesium ion
3	sodium ion
4	total anion
5	complex
6	surfactant

SUPERSCRIPTS

^	stationary phase concentration
˘	moving spatial coordinate
*	excess calcium ion concentration
s	asymptotic quantity
o	a no-ion exchange or no-adsorption quantity

BIBLIOGRAPHY

1. Bae, J.H. & Petrick, C.B.: "Adsorption/Retention of Petroleum Sulfonates in Berea Cores, " SPE Journal, Oct. 1977, p. 353-357.
2. Bae, J.H., et al: "A Comparative Evaluation of Microemulsions and Aqueous Surfactant Systems," Improved Oil Recovery Symp. SPE-AIME, Tulsa, 1974.
3. Bernard, George G.: "Effects of Clays, Limestone and Gypsum on Soluble Oil Flooding," Improved Oil Recovery Symp. SPE-AIME, Tulsa, 1974.
4. Bernard, George G.: "Effect of Clays, Limestone and Gypsum on Soluble Oil Flooding," J. Pet. Tech., Feb. 1975, p. 179-180.
5. Bernard, George G.: "Secondary Recovery of Petroleum by Surfactant-Water Flooding," U.S. Patent No. 3,414,054, Dec. 3, 1968.
6. Boneau, D.F. & Clampitt, Richard L.: "A Surfactant System for the Oil-Wet Sandstone of the North Burbank Unit," Improved Oil Recovery Symp. SPE-AIME, Tulsa, 1976.
7. Brandner, Carl F., et al: "Multistep Method of Waterflooding," U.S. Patent No. 3,437,141, Apr. 8, 1969.
8. Bush, Darvell C. & Jenkins, Ralph E.: "CEC Determinations by Correlations With Adsorbed Water," SPWLA 18th Annual Logging Symp., 1977.
9. Campbell, Thomas C.: "A Comparison of Sodium Orthosilicate and Sodium Hydroxide for Alkaline Waterflooding," 47th Annual Calif. Regional Mtg. SPE-AIME, Bakersfield, CA, 1977.
10. Campbell, Thomas C.: "Chemical Flooding: A Comparison Between Alkaline and Soft Saline Preflush Systems for Removal of Hardness Ions From Reservoir Brines," Symp. on Oil Field and Geothermal Chemistry, Houston, 1979.
11. Carmichael, J.D.: "Caustic Waterflooding Demonstration project, Ranger Zone, Long Beach Unit, Wilmington Field, California," DOE Contract No. EF-77-C-03-1396.
12. Chiou, C.S. & Chang, H.L.: "Preflood Design for Chemical Flooding - A Study on Ion Exchange/Dispersion Process in Porous Media," Paper #376, AIChE, 84th National Mtg., Atlanta, 1978.
13. Cooke, C.E., Jr., et al: "Oil Recovery by Alkaline Waterflooding," Improved Oil Recovery Symp. SPE-AIME, Tulsa, 1974.
14. Conoco Oil Co.: "Big Muddy Field Low-Tension Flood Demonstration Project," Monthly and Annual Reports, Doe Contract No. DE-AC03-78SF01424.

15. Dabbous, Mahmoud K. & Elkins, Lloyd E.: "Preinjection of Polymers to Increase Reservoir Flooding Efficiency," Improved Oil Recovery Symp. SPE-AIME, Tulsa, 1976.
16. Danielson, H.H.: "Penn Grade Micellar Displacement Project," DOE Contract No. DE-AC21-76-MC-08002.
17. Danielson, H.H. & Paynter, W.: "Bradford Sand Micellar-Polymer Flood," Enhanced Oil Recovery and Improved Drilling Methods Symp. Proc., 1977.
18. Dreher, K.D. & Sydansk, R.D.: "Observation of Oil-Bank Formation During Micellar Flooding," Improved Oil Recovery Symp. SPE-AIME, Tulsa, 1976.
19. Ehrlich, R. & Wygal, R.J., Jr.: "Interrelation of Crude Oil and Rock Properties With the Recovery of Oil by Caustic Waterflooding," Improved Oil Recovery Symp. SPE-AIME, Tulsa, 1976.
20. Ely, Richard: "The Guerra Experiment - A Field Test of Tertiary Detergent Flooding," Improved Oil Recovery Symp. SPE-AIME, Tulsa, 1972.
21. Foster, W.R.: "A Low-Tension Waterflooding Process," J. Pet. Tech., Feb. 1973, p. 205-210.
22. French, M.S., et al: "Field Test of a Aqueous Surfactant System for Oil Recovery, Benton Field, Illinois," Improved Oil Recovery Symp. SPE-AIME, Tulsa, 1972.
23. Froning, H.R. & Treiber, L.E.: "Development and Selection of Chemical Systems for Miscible Waterflooding," Improved Oil Recovery Symp. SPE-AIME, Tulsa, 1976.
24. Gale, Walter & Sanvik, Erik I.: "Tertiary Surfactant Flooding: Petroleum Sulfonate Composition - Efficacy Studies," SPE Journal, Aug. 1973, p. 191-199.
25. Gary Energy Corp.: "Bell Creek Field, Micellar-Polymer Pilot Demonstration," Monthly and Annual Reports, DOE Contract No. EY-77-C-02-4207.
26. Glover, C.J., et al: "Surfactant Phase Behavior and Retention in Porous Media," SPE Journal, June, 1979, p. 183-193.
27. Goldberg, Arnold: "Bell Creek Field Micellar-Polymer Pilot Demonstration," DOE Contract No. ET-77-C-03-1802.
28. Groenveld, H., et al: "Pembina Polymer Pilot Flood," Improved Oil Recovery Symp., SPE-AIME, Tulsa, 1976.
29. Healy, Robert N., et al: "A Laboratory Study of Microemulsion Flooding," Improved Oil Recovery Symp., Tulsa, 1974.
30. Hill, H.J. & Lake, L.W.: "Cation Exchange in Chemical Flooding: Part 3 - Experimental," SPE Journal, Dec. 1978, p. 445-456.

31. Hill, H.J., et al: "Aqueous Surfactant Systems for Oil Recovery," Improved Oil Recovery Symp., SPE-AIME, Tulsa, 1972.
32. Hill, Harold J., et al: "Ion Exchange Controlled Chemically Aided Waterflood Process," U.S. Patent No. 4,074,755, Feb. 21, 1978.
33. Hirasaki, G.J. & Pope, G.A.: "Analysis of Factors Influencing Mobility and Adsorption in the Flow of Polymer Solution Through Porous Media," SPE Journal, Aug. 1974, p. 337-346.
34. Holm, Leroy W.: "Correlation of Oleic & Aqueous Micellar Processes for Tertiary Oil Recovery," Improved Oil Recovery Symp., SPE-AIME, Tulsa, 1978.
35. Holm, L.W. & Josendal, V.A.: "Reservoir Brines Influence Soluble-Oil Flooding Process," Oil & Gas J., Nov. 13, 1972, p. 158-168.
36. Holm, Leroy W.: "Micellar Flooding Process for Recovering Oil From Petroleum Reservoirs," U.S. Patent No. 4,011,908, March 15, 1977.
37. Hurd, B.G.: "Adsorption and Transport of Chemical Species in Laboratory Surfactant Waterflooding Experiments," Improved Oil Recovery Symposium, SPE-AIME, Tulsa, 1976.
38. Hurd, B.G., et al: "Method of Minimizing Adsorption of Surfactant From Flooding Water," U.S. Patent No. 3,469,630, Sept. 30, 1969.
39. Jennings, Harley Y.: "A Study of Caustic Solution-Crude Oil Interfacial Tensions," SPE Journal, June 1975, p. 197-202.
40. Jennings, H.Y., et al: "A Caustic Waterflooding Process for Heavy Oils," J. Pet. Tech., Dec. 1974, p. 1344-1352.
41. Jessen, F.W. & Johnson, C.A.: "The Mechanism of Adsorption of Lignosulfonates on Clay Suspensions," SPE Journal, September 1963, p. 267-273.
42. Johnson, James S., Jr.: "Chemicals for Enhanced Oil Recovery," Oak Ridge National Lab. Quarterly and Annual Tech. Progress Reports, DOE Contract No. W-7405-eng-26.
43. Johnson, J.S., Jr.: "Enhanced Oil Recovery by Micellar Floods: Chemicals From Wastes, Tracers, and Ion Exchange Aspects," Enhanced Oil & Gas Recovery & Improved Drilling Methods Symp. Proc., v. 1, p. B9/1 -B9/15.
45. Kalfoglou, George: "Lignosulfonates as Sacrificial Agents in Oil Recovery Processes," U.S. Patent No. 4,006,779, Feb. 8, 1977.
46. Kalfoglou, George: "Oxidized Lignosulfonates as Additives in Oil Recovery Processes Involving Chemical Agents," U.S. Patent No. 4,133,385, Jan. 9, 1979.

47. Kalfoglou, George: "Chrome Lignosulfonates as Additives in Oil Recovery Processes Involving Chemical Recovery Agents," U.S. Patent No. 4,142,582, March 6, 1979.
48. Kalfoglou, George: "Lignosulfonates as Additives in Recovery Processes Involving Chemical Recovery Processes," U.S. Patent No. 4,157,115, Jan. 5, 1979.
49. Knight, Bruce & Rhudy, John S.: "Oil Recovery Using Polymer Preslug," U.S. Patent No. 3,844,350, Oct. 29, 1974.
50. Knight, R.K. & Baer, P.J.: "A Field Test of Uniflooding at Higgs Unit," Improved Oil Recovery Symp. SPE-AIME, Tulsa, 1972.
51. Kossack, C.A. & Bilhartz, H.L., Jr.: "The Sensitivity of Micellar Flooding to Reservoir Heterogeneities," Improved Oil Recovery Symp. SPE-AIME, Tulsa, 1976.
52. Lake, L.W. & Helfferich, F.: "Cation Exchange in Chemical Flooding: Part 2 - The Effect of Dispersion, Cation Exchange and Polymer/Surfactant Adsorption on Chemical Flood Environment," SPE Journal, Dec. 1978, P. 435-444.
53. Lawson, J.B. & Dilgren, R.E.: "Adsorption of Sodium Alkyl Sulfonates on Sandstone," SPE Journal, Feb. 1978, P. 75-82.
54. Miller, R.J. & Richmond, C.N.: "El Dorado Micellar-Polymer Project Facility," J. Pet. Tech., Jan. 1978, p. 232.
55. Murphy, Charles L., et al: "A Successful Low-Tension Waterflood Two-Well Test," 51st Annual Tech. Conf. SPE-AIME, New Orleans, 1976.
56. Parker, Harry W.: "Aqueous Fluid Drive Oil Recovery Process," U.S. Patent No. 3,384,171, May 21, 1968.
57. Paul, G.W., & Froning, H.R.: "Salinity Effects of Micellar Flooding," J. Pet. Tech., Aug. 1973, p. 957-958.
58. Perkins, T.K. & Johnston, O.C.: "A Review of Diffusion and Dispersion in Porous Media, SPE Journal, Mar. 1963, P. 70-84.
59. Pope, G.A., et al: "Cation Exchange in Chemical Flooding, Part 1 - Basic Theory Without Dispersion," SPE Journal, Dec. 1978, p. 418-434.
60. Pursley, S.A., et al: "A Field Test of Surfactant Flooding, Loudon, Illinois," J. Pet. Tech., July, 1973, P. 793-802.
61. Reed, M.G.: "Formation Permeability Damage by Mica Alteration and Carbonate Dissolution," J. Pet. Tech., Sept. 1977, p. 1056-1060.
62. Reisburg, Joseph, et al: "Waterflood Oil Recovery Using Calcium-Compatible Mixture of Anionic Surfactants," U.S. Patent No. 3,508,612, Apr. 28, 1970.

63. Rosenwald, G.W.: "El Dorado Micellar-Polymer Demonstration Project," DOE Contract No. ET-78-C-03-1800.
64. Sarem, Amir M.: "Mobility-Controlled Caustic Flood," U.S. Patent No. 3,805,893, Apr. 23, 1974.
65. Sarem, Amir M.: "Mobility Controlled Caustic Flooding Process for Reservoir Containing Dissolved Metal Cations," U.S. Patent No. 3,871,452, Mar. 18, 1975.
66. Satter, A., et al: "Chemical Transport in Porous Media," 52nd Annual Fall Tech. Conf. SPE-AIME, Denver, 1977.
67. Schechter, R.S. & Wade, W.H.: "Tertiary Oil Recovery Processes Research at the University of Texas," Quarterly and Annual Tech. Progress Reports, DOE Contract Nos. EW78-5-19-0001, EY78-5-19-0001, DE-AAS19-78BC20001.
68. Shah, Dinech O. & Walker, R.D., Jr.: Research on Surfactant Polymer Oil Recovery Systems," University of Florida, Quarterly and Annual Tech. Progress Reports, DOE Contract No. FW-78-5-19-0008.
69. Smith, F.W.: "Ion Exchange Conditioning of Sandstone for Chemical Flooding," J. Pet. Tech., June, 1978, P. 959-968.
70. Somasundaran, P.: "Adsorption From Flooding Solution in Porous Media," Columbia University, July 1979, DOE Contract No. DE-AC19-79BC-10082.
71. Somasundaran, P. & Hanna, H.S.: "Adsorption of Sulfonates on Reservoir Rocks," 5th Symp. on Improved Methods for Oil Recovery, SPE-AIME, Tulsa, 1978.
72. Strange, L.K. & Cloud, W.B.: "Displacement of Reservoir Brine by Fresh Water - Four Field Case Histories," Improved Oil Recovery Symp. SPE-AIME, Tulsa, 1976.
73. Strange, L.K. & Tolash, A.W.: "Analysis of Salem Low-Tension Waterflood Test," Improved Oil Recovery Symp. SPE-AIME, Tulsa, 1976.
74. Taber, J.J.: "The Injection of Detergent Slugs in Water Floods," Petrol. Trans. AIME, v. 213, 1958, p. 186-192.
75. Trantham, J.C., Kleinschmidt, R.F.: "North Burbank Unit Tertiary Recovery Pilot Test," DOE Contract No. ET-76-C-03-1814.
76. Treiber, Lawrence E., et al: "Removal of Interfering Ions in Waterflood," U.S. Patent No. 3,414,053, Dec. 3, 1968.
77. Trogus, F.J., et al: "Static and Dynamic Adsorption of Anionic and Nonionic Surfactant," SPE Journal, Oct. 1977, p. 337-344.
78. Trogus, F.J., et al: "Adsorption of Mixed Surfactant Systems," 52nd Annual Fall Tech. Conf. SPE-AIME, Denver, 1977.

79. Trushenski, Scott P., et al: "Micellar Flooding - Fluid Propagation, Interaction, and Mobility," SPE Journal, Dec. 1974, P. 633-642.
80. Union Oil Co.: "Uniflood Soluble-Oil Flooding Process," Technology Sales Division.
81. Walker, Robert D., Jr., et al: "Cation Exchange, Surfactant Precipitation, and Adsorption in Micellar Flooding," Symp. on Chemistry of Oil Recovery, ACS, Anaheim, 1978.
82. Whitey, R.C. & Ware, J.W.: "Low-Tension Waterflood Pilot at the Salem Unit, Marion County, Illinois - Part 1 Field Implementation and Results," Improved Oil Recovery Symp. SPE-AIME, Tulsa, 1976.
83. Widmyer, Richard H., et al: "Low-Tension Waterflood Pilot at the Salem Unit, Marion County, Illinois - Part 2 Performance Evaluation," Improved Oil Recovery Symp. SPE-AIME, Tulsa, 1976.

A P P E N D I X

An extensive study of the phenomena controlling preflush performance was completed by G.A. Pope, L.W. Lake and F. Helfferich at the University of Texas and Shell Development Company^{52,59}. This theoretical development was presented in a two-part paper: "Cation Exchange in Chemical Flooding." Significant portions of the papers are included for reference.

INTRODUCTION

A key requirement for a successful chemical flood is to provide an adequate ionic environment for the surfactant to ensure that the desired interfacial activity, phase behavior, and mobility control are maintained. Aside from the in-place and injected ionic compositions and mixing through dispersion, crossflow, etc., this environment may be affected deeply by cation exchange with clays, solubility of minerals, and adsorption on rock.

The authors describe a fundamental theoretical analysis of cation exchange and adsorption phenomena in reservoir flooding. The treatment is applicable to multicomponent systems with any kind of equilibrium relations, specifically including interactions between components, but presumes idealized behavior with respect to fluid dynamics, absence of dispersion, immiscibility of aqueous and oleic phases, and conservation of local equilibrium. The treatment is an adaptation of multicomponent chromatographic theory to practical problems of chemical and related floods.

The basic problem is that the components involved in a chemical flood (water, cations, surfactant, polymer and oil) are coupled with respect to their transport properties, and only a theory of coupled, multicomponent systems can adequately describe their dynamic behavior. At first glance, one may be

inclined to assume that a mixture injected as a slug might transverse the reservoir as such, changing its composition a little by mixing with fluids ahead and behind or by loss to, or gain from, the rock over which it travels, but otherwise conserving its integrity. Multicomponent theory shows this idea is too naive. Rather, an injection sets off a set of "waves" (composition variations) that advance at different speeds and between which new compositions arise that bear little resemblance to the injected and previously present compositions, or any that could be formed from these by mixing. Moreover, the wave patterns generated by successive injections of different fluids may overlap and interfere and, thereby, modify injected compositions. Injected components thus generate their own environment through dynamic interactions. To be sure, it is not impossible, in principle, to operate under conditions ensuring that an injected active surfactant slug retains its favorable environment and thus its activity through most or all of the reservoir, but this often may prove impracticable. The task then is to design the flood so that a favorable environment is generated in situ.

THEORY

Definitions

The definitions, concepts, and theory presented in this section form the basis for the calculations and illustrations that follow. These ideas are abstracted from other works, which are the foundation for this application of multicomponent chromatographic theory to reservoir engineering.

Composition

If the fluid or stationary phase in a porous medium contains several components or species, then the complete set of

concentrations in the phase constitutes a composition. For n components, the composition is a n -dimensional vector, whose elements are the component concentrations.

Stationary Phase

The stationary phase in a porous medium constitutes the part of the rock matrix into which the dissolved species of the flowing phase may transfer. Therefore, a stationary-phase composition can be defined.

Profiles & Histories

A composition vector can describe the concentration of each species in the phase at every point in time and every location. When presenting the composition of the mobile or stationary phase, however, it frequently is more convenient to hold either the position or time variable constant, and vary the other. Composition (or concentration) plots that hold time constant are known as profiles. Similarly, composition (or concentration) plots holding the position constant are known as histories. A history with the constant position at the production well is a production or effluent history.

Waves and Their Sharpening Properties

A wave is a variation in composition advancing through the porous medium in the direction of fluid flow. Alternative terms used for wave are front, boundary, and transition.

Coherent chromatographic waves can be grouped into three classes that differ in their sharpening properties. In "nonsharpening waves," the concentration velocities are higher in the leading than in the trailing portions of the wave, and the

wave accordingly spreads in propagation. In "self-sharpening waves," the concentration velocities are lower in the leading than in the trailing portions, and the wave sharpens on propagation. Waves with uniform concentration velocities are "indifferent" with respect to sharpening behavior.

In nonsharpening waves, the spreading caused by the variation of the concentration velocities with composition is in addition to that caused by dispersion, and soon dominates. The wave eventually becomes so diffuse that dispersion is no longer significant, and the wave then spreads in proportion to the distance traveled ("proportionate" pattern).

Self-sharpening waves in the absence of any dispersion effects would become ideally sharp shock fronts. In reality, a steady-state width is attained in which the sharpening effect of the sorption isotherm and the spreading effect of dispersion balance one another ("constant" pattern).

Indifferent waves in the absence of dispersion would travel with constant width, that is, would neither sharpen nor spread. In reality, dispersion effects not combated by sharpening effects will cause spreading in proportion to the square root of traveled distance, according to linear dispersion theory.

Distance-Time Diagrams

A convenient representation of the propagation and interference of waves is the distance-time diagram. This diagram, with (normalized) distance and (normalized) time as coordinates, shows "trajectories" traced by given concentrations or compositions as they are propagated. A shock or step appears as a curve in the distance-time diagram, while a nonsharpening wave appears as a divergent trajectory bundle. Examples of distance-time diagrams can be found in Figs. 1 through 6.

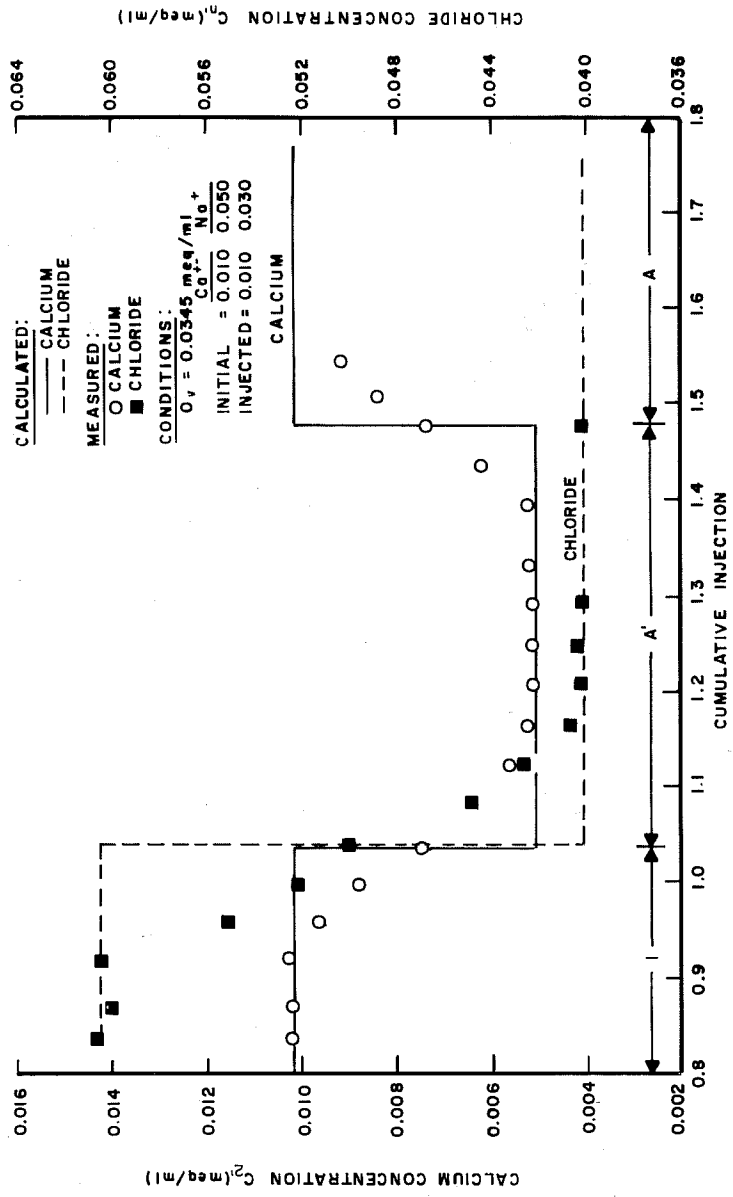
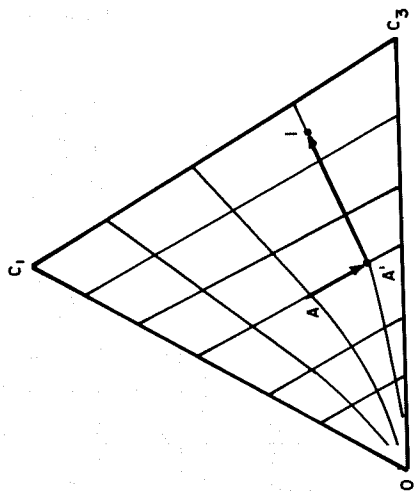
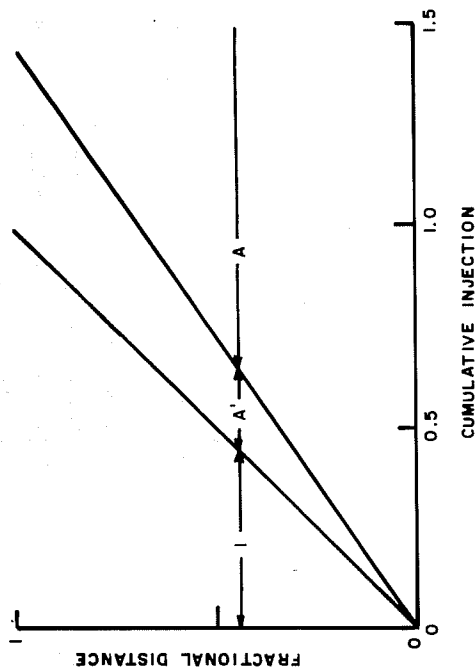


FIG. 1- Compositional route (schematic) distance-time diagram and production history calculated for the two-cation case and stated conditions. Experimental results from a 2-ft-long Berea core are shown for comparison

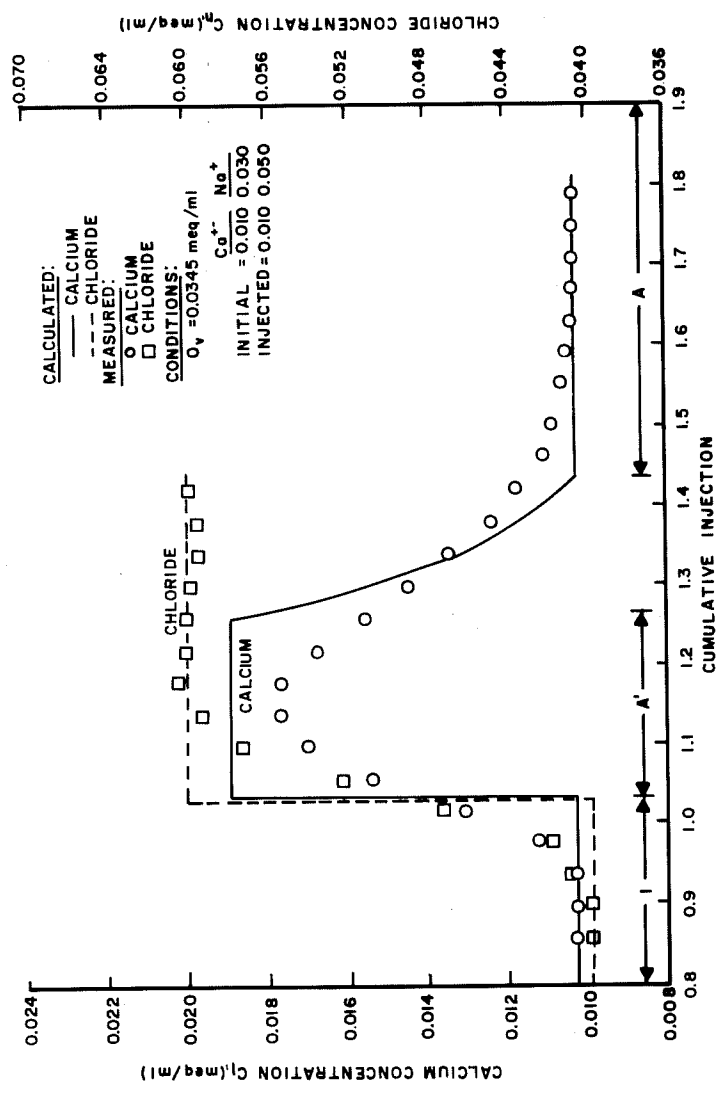
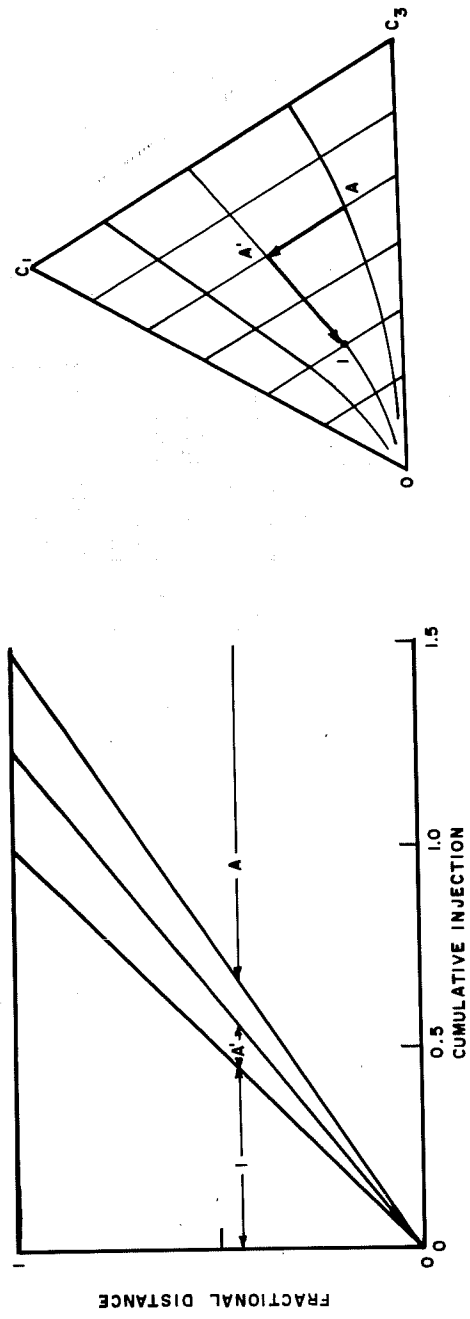


FIG. 2 — Composition route (schematic) distance-time diagram and production history calculated for the two-cation case and stated conditions. Experimental results from a 2-ft-long Berea core are shown for comparison.

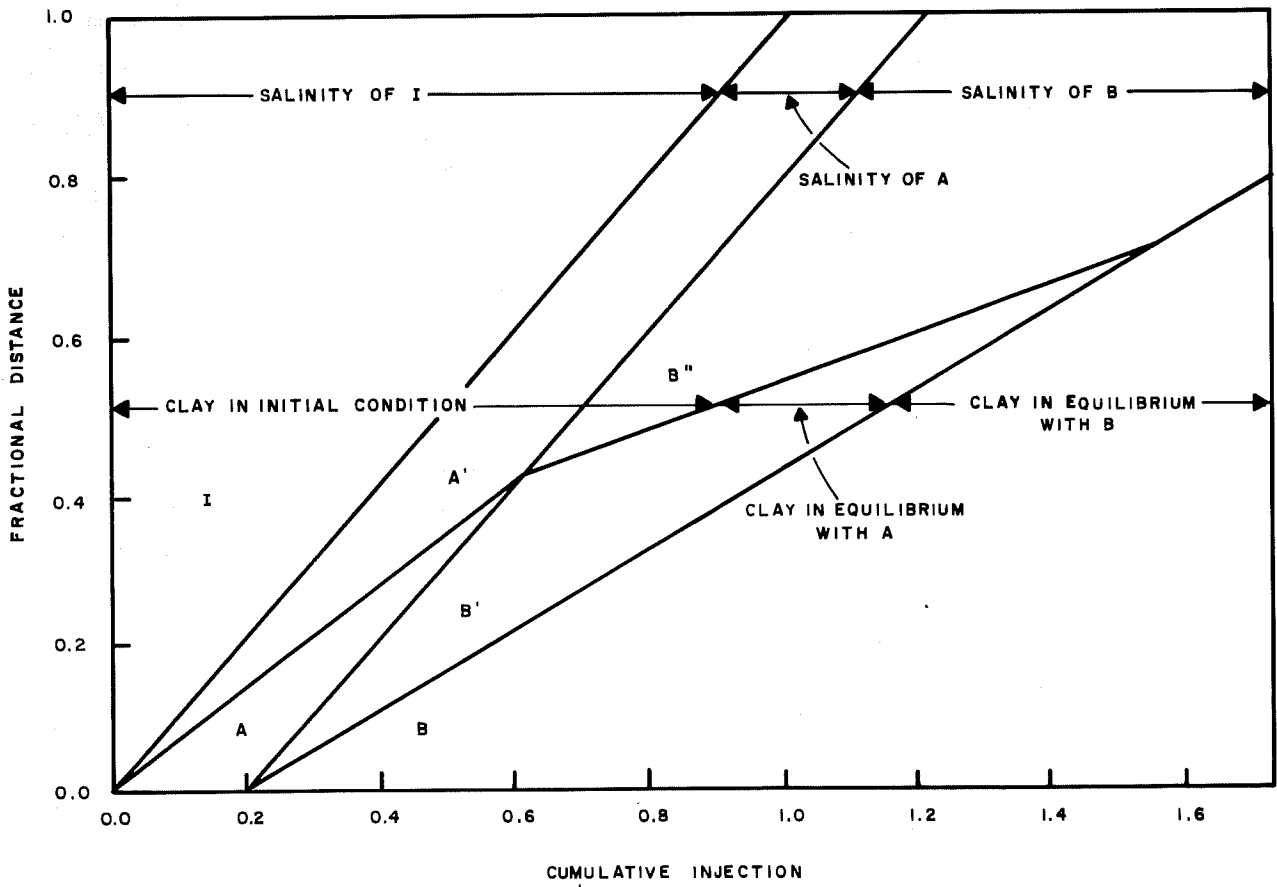
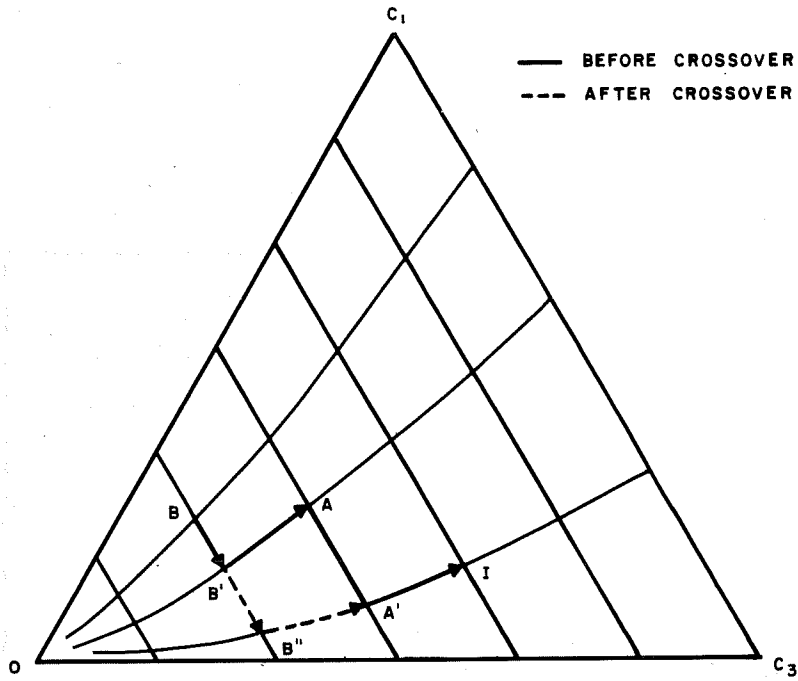


FIG. 3- Schematic composition-route and distance-time diagram for the two-cation, three-fluid case, calculated for the conditions in Table 1.

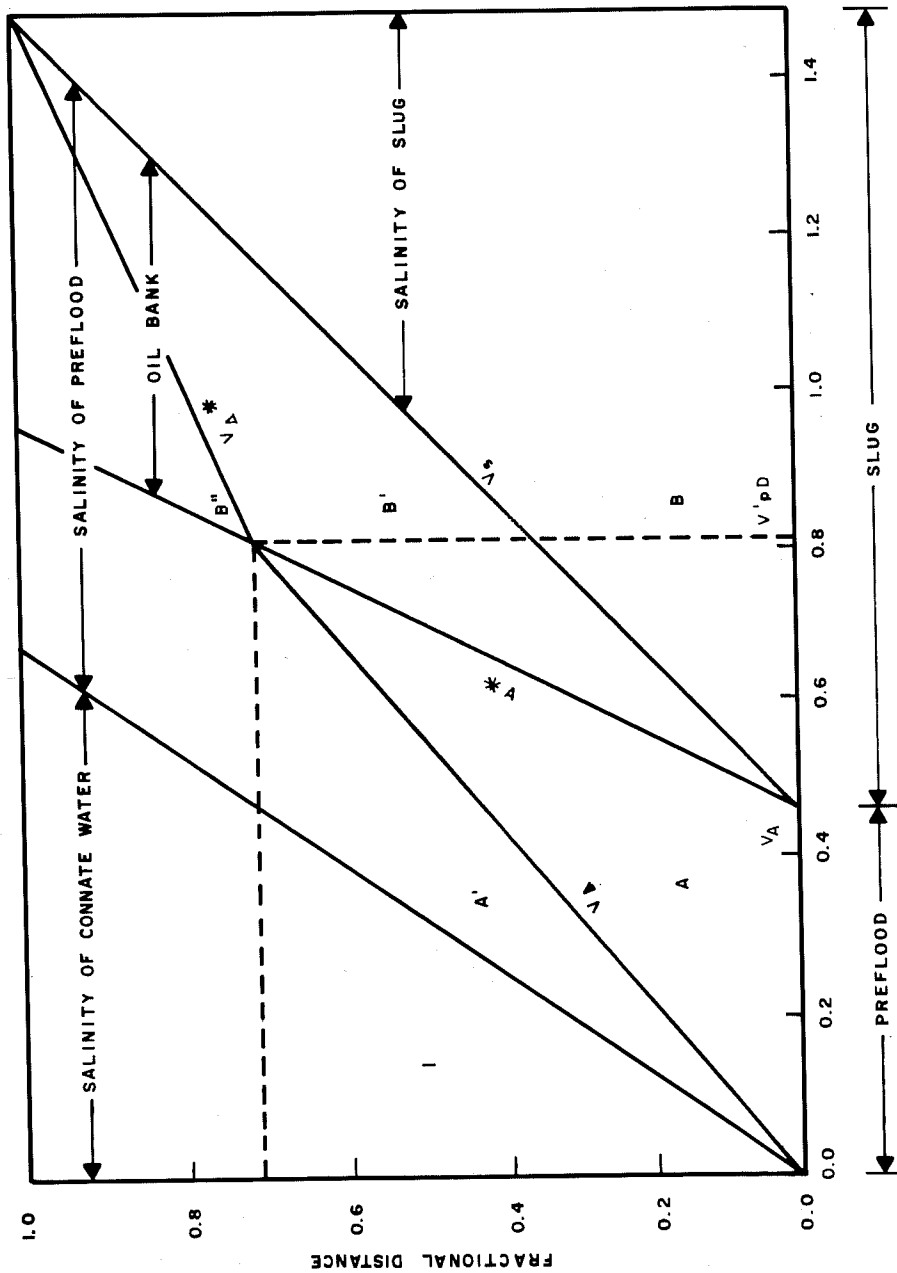


FIG. 4- Distance-time diagram for the two-cation case with surfactant and mobilized oil, calculated for conditions in Table 1, and with $S_{Or} = 0.3$, $S_{OrC} = 0$, $S_O^* = 0.6$, and $D_s = 0$.

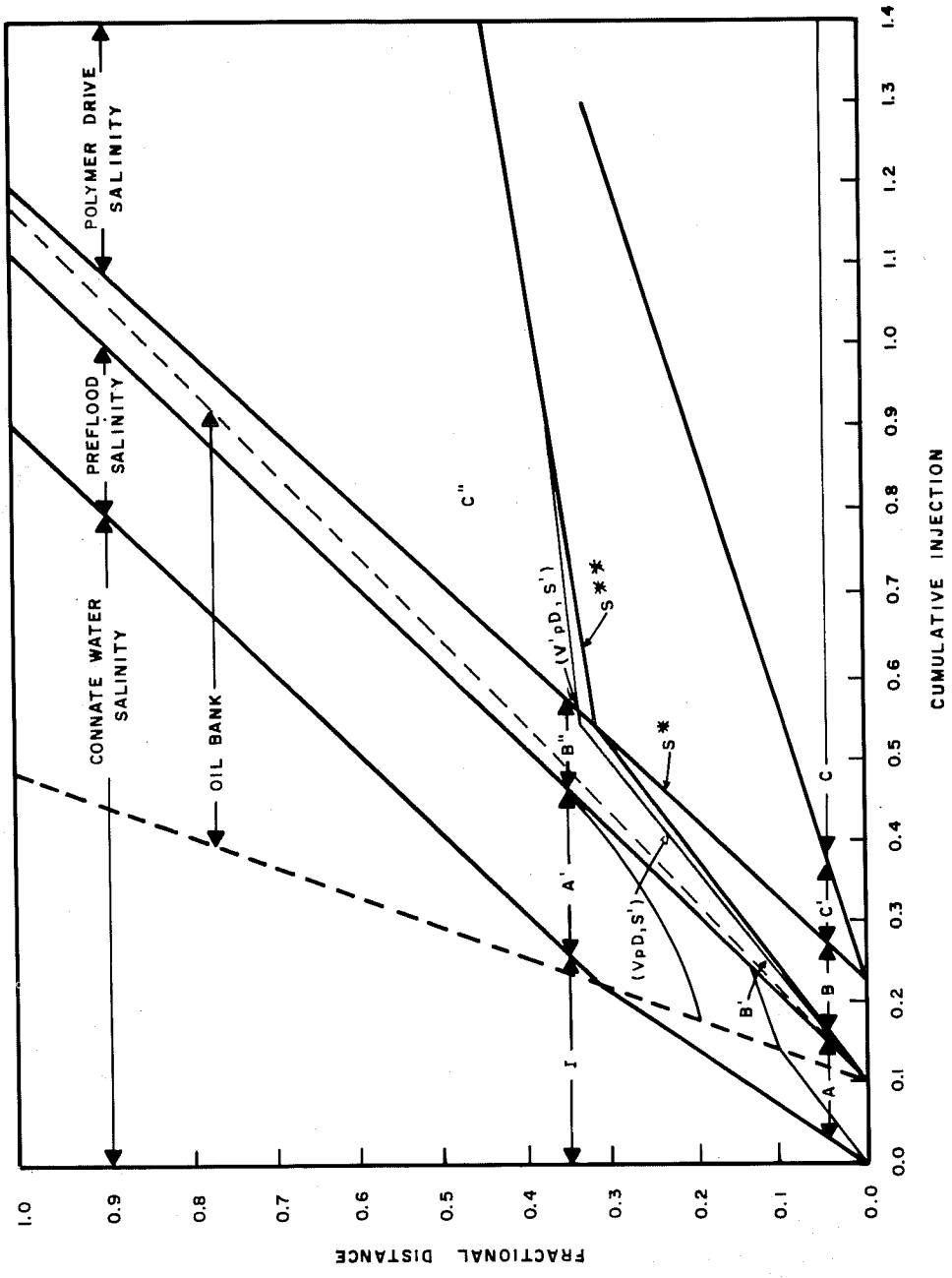


FIG. 5-- Distance-time diagram for chemical flooding sequence (preflood, chemical slug, and drive) with surfactant and mobilized oil, calculated for conditions in Table 2.

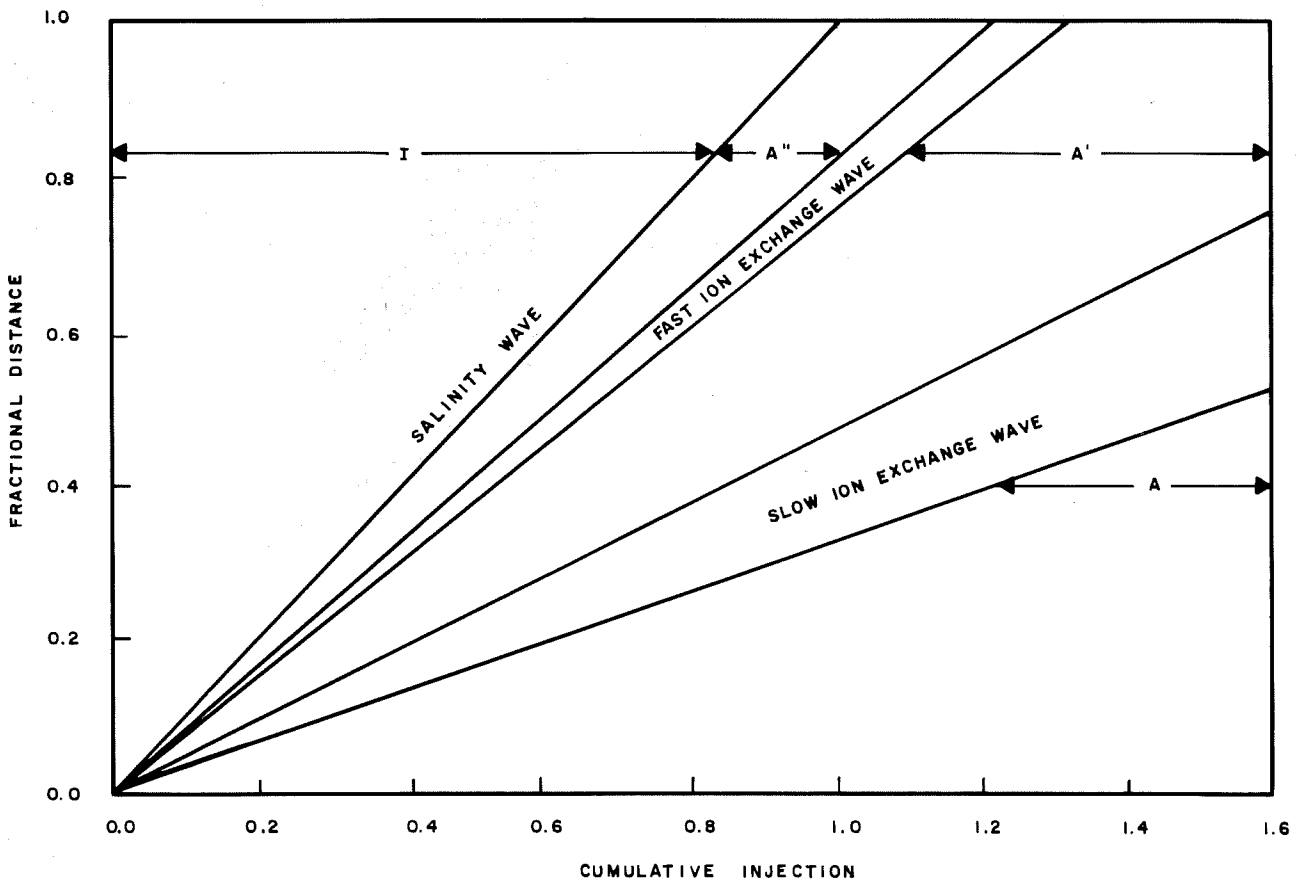
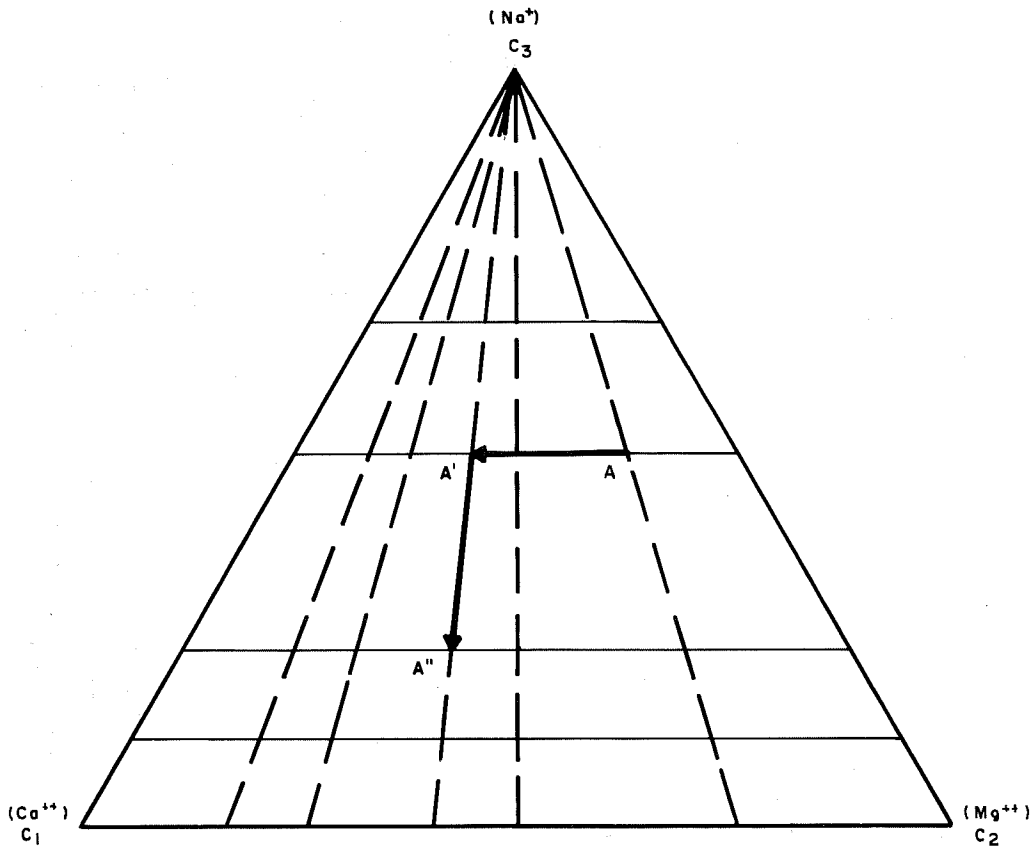


FIG. 6—Composition route and distance-time diagram for Ca^{++} Mg^{++} / Cl^- calculated for conditions in Table 3

Composition Space

A coordinate system whose axes are the concentration of all species is called composition space (also known as hodograph space). A composition is a point in such a space, and a wave is a curve connecting any two points.

If there are n components in a chromatographic system, the complete composition space has two n dimensions, one for each mobile-phase and stationary-phase concentration. However, if there is equilibrium between the mobile and stationary phases, the n dimensional, mobile-phase (or stationary phase) composition space suffices for a complete description. Moreover, conservation of electroneutrality requires the total concentrations of cations and anions (measured in equivalents) to be equal. This removes one degree of freedom and confines the physically possible compositions to an $(n - 1)$ -dimensional hyperplane, called a "simplex". This study uses mobile-phase composition simplexes for representation of composition-path grids and composition routes.

Composition Paths & Path Grids

We shall see that the concentration velocities of all species are equal along certain curves in composition space. This condition, known as coherence, will be discussed more fully later. For the present, it is sufficient to point out that coherence is a condition of stability that the system tends to attain, and that the requirement of coherence, along with the sorption equilibria, uniquely determine curves in composition space called composition paths. Moreover, the space is covered by families of such curves, so that each point in the composition space is at the intersection of two or more composition paths.

These families of curves, therefore, determine a grid (a "path grid") in composition space. Examples may be seen in Figs. 4 through 7.

Composition Rules

In contrast to a composition path, the composition route is the curve (in the composition space) representing the sequence of compositions in a particular system under given initial and injection conditions. We can distinguish between profile routes and history routes. Profile routes have sequences in space at given time, and history routes have sequences in space at given location. This study uses history routes, shown as arrows that, by convention, point in the direction of flow. Thus, the route is a sequence of arrows from the last injected composition to that present initially.

In a fully coherent system, the route will follow a sequence of paths, switching from one path to another at intersections. However, routes may contain noncoherent segments that do not follow any path, at least temporarily. In a sense, the path grid is a road map for the system, which by virtue of its tendency toward coherence, will seek to adapt its route to the paths.

Composition routes are useful adjuncts to distance-time diagrams because they show directly the concentrations of the species. The combination of a distance-time diagram, and a composition route diagram completely specifies all concentrations in a system at every position and time.

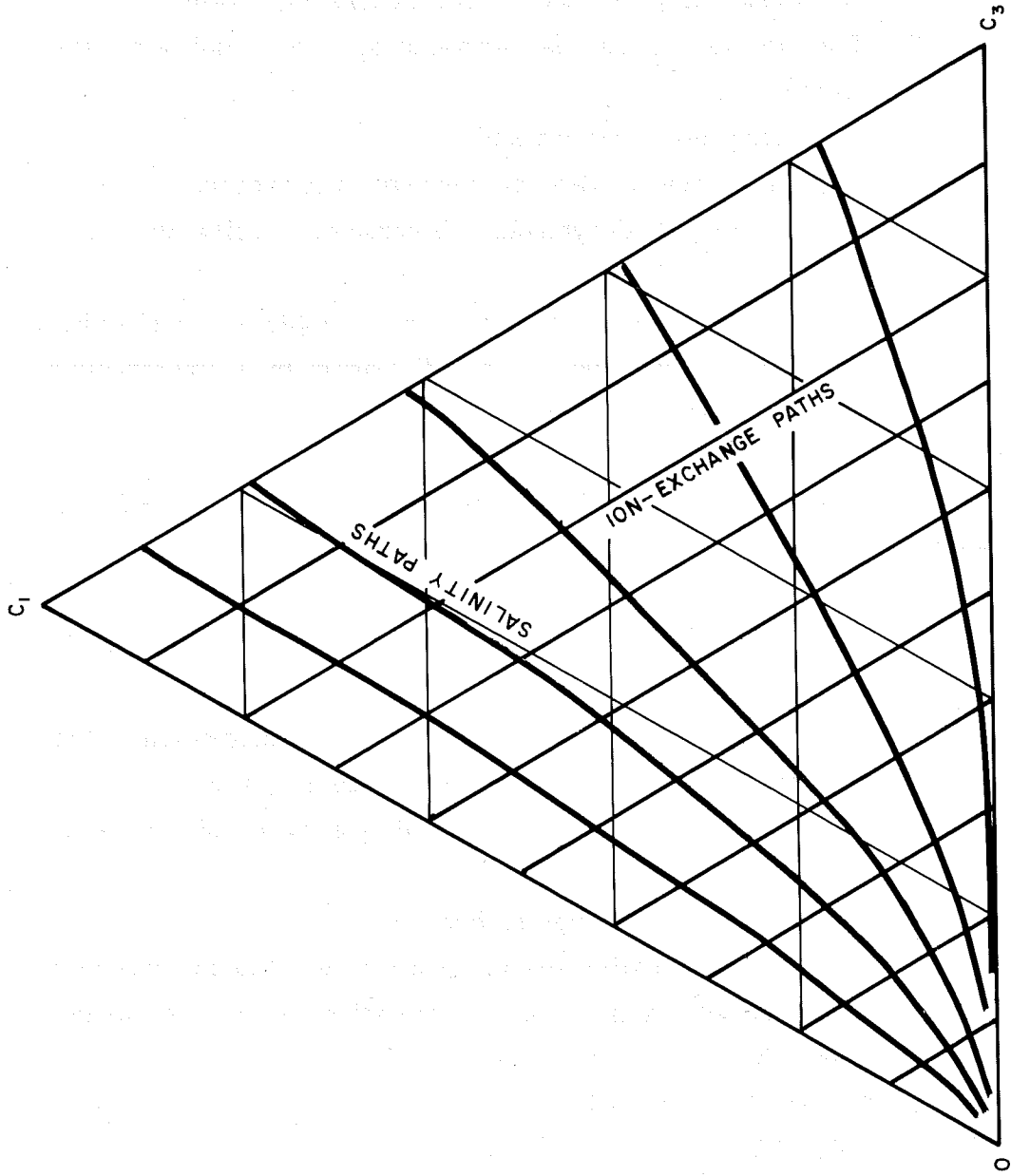


FIG. 7 - Composition-path diagram calculated for a two-cation system with Gapon or mass-action equilibrium.

ASSUMPTIONS

The theory is based on the following assumptions and idealizations.

1. The theory is presented in one-dimensional form.
2. The porous medium is quasi-homogeneous, uniform, and isothermal.
3. The fluids are incompressible.
4. The phases are in local equilibrium everywhere.
5. Effects of fluid-dynamic dispersion, capillarity, and gravity are neglected.
6. Oil is a separate, variant phase completely immiscible with the aqueous phase and displaced in a "piston-like" fashion by the surfactant.

In the calculated examples, the following additional conditions pertain.

7. Initial saturation and composition of the reservoir is uniform.
8. If several fluids are injected in succession, the injected composition of each is varied stepwise.
9. The cation exchange capacity of the reservoir clays is uniform and constant.
10. Inorganic anions are not sorbed.
11. Calcium-sodium cation exchange obeys the Gapon equation; (Eq. no. 5) calcium-magnesium-sodium cation exchange obeys the mass-action law.
12. The ionic contributions of surfactant and polymer are negligible.
13. If surfactant is sorbed, its isotherm is linear or has negative curvature (Langmuir type).

SUBSCRIPT CONVENTION

The system can have up to $n + m$ aqueous phase components, where $n - 1$ is the number of cationic species present. The n th species comprises all nonsorbing anions. Species $n + 1$, $n + 2$, etc., are surfactant (designated by a subscript s), polymer, etc., and may be sorbable. For specific examples, the subscripts 1 through 3 will refer to calcium, magnesium, and sodium, respectively.

GENERAL EQUATIONS

Electroneutrality

The requirement of solution electroneutrality is

$$\sum_{i=1}^{n-1} C_i = C_n \quad (1)$$

and for the stationary phase

$$\sum_{i=1}^{n-1} \hat{C}_i = Q_v \quad (2)$$

where Q_v is the cation-exchange capacity.

Equilibrium Relations

The general equilibrium relationship applicable to interfering species is

$$\hat{C}_i = F_i (C_1, \dots, C_n) \quad (3)$$

The theory is generally applicable to such equilibria. For noninterfering species, F_i is a function of C_i only.

For ion exchange, a broadly applicable formulation for binary exchange equilibria of cations i and j in multicomponent systems is

$$\frac{\hat{C}_i^{\mu_i}}{\hat{C}_j^{\mu_j}} = K_{ij} \frac{C_i^{v_i}}{C_j^{v_j}} \quad (4)$$

where K, v, and μ are empirical constants.

For the two-cation (calcium/sodium) examples, we specialize Equation 4 to

$$\frac{\hat{C}_3}{\hat{C}_1} = K_{31} \frac{C_3}{C_1^{0.5}} = K_{31}^r \quad (5)$$

an equation originally proposed by Gapon (r is termed the "Gapon ratio"). Based on Bolt's data, we take $K_{31} = 0.88$ (ml aqueous phase/meq)^{1/2}.

For the three-cation (calcium/magnesium/sodium) examples, we specialize Equation 4 to the mass-action equilibria with v and μ being reciprocal valences.

$$\frac{\hat{C}_3}{\hat{C}_1^{0.5}} = K_{31} \frac{C_3}{C_1^{0.5}} = K_{31}^r \quad (6)$$

$$\frac{\hat{C}_2}{\hat{C}_1} = K_{21} \frac{C_2}{C_1} \quad (7)$$

with $K_{31} = 0.15$ and $K_{21} = 0.5$ from van der Molen.

The electroneutrality conditions used to eliminate C_3 and \hat{C}_3 from Equation 5 enable \hat{C}_1 to be written explicitly as a function of C_1 and C_n for the two-cation cases.

$$\hat{C}_1 = Q_v / (1 + K_{31}r) \quad (8)$$

Material Balance

Under the listed assumptions, the differential material balance for species i is

$$\left[\frac{\partial}{\partial t} (S_w C_i + \hat{C}_i) \right]_z + \frac{q}{A\phi} \left[\frac{\partial (f_w C_i)}{\partial z} \right]_t = 0 \quad (9)$$

In terms of dimensionless distance and time variables ξ and V_{pd} , defined as

$$\xi \equiv \frac{z}{L} = \text{fractional length}$$

and

$$V_{pd} \equiv \frac{\int_0^t q dt}{A L \phi} = \text{cumulative injection in pore volumes}$$

Equation 9 reduces to

$$\left[\frac{\partial (S_w C_i + \hat{C}_i)}{\partial V_{pd}} \right]_{\xi} + \left[\frac{\partial (f_w C_i)}{\partial \xi} \right]_{V_{pd}} = 0 \quad (10)$$

Assumption 6 implies that S_w and F_w will be constant between step changes that are given by fractional flow calculations.

Concentration & Step Velocities

A useful concept is that of the "concentration velocity", defined as the speed with which a given concentration value is propagated in the direction of flow. Mathematically, the normalized concentration velocity, v_{ci} , of a given aqueous-phase concentration C_i of an arbitrary species is defined as

$$v_{ci} = (\partial \xi / \partial V_{pd}) C_i \quad (11)$$

Note that Equation 11 gives the change in fractional length per change in pore volume injected.

As expression for the concentration velocity is obtained from Equation 10 the differential material balance,

$$v_{C_i} = f_w / (S_w + D_i), \quad (12)$$

where the "retardation term," D_i is given by

$$D_i = (\partial \hat{C}_i / \partial V_{pd}) \xi / (\partial C_i / \partial V_{pd}) \xi = \left. \frac{d\hat{C}_i}{dC_i} \right|_{d\xi = 0} \quad (13)$$

The concept of concentration velocity is not applicable to propagation of a sharp step, in which concentrations are discontinuous. The step velocity can be obtained from an integral instead of differential balance, and obeys Equation 12 with a retardation term

$$D_i = \Delta \hat{C}_i / \Delta C_i \quad (14)$$

where the operator Δ indicates the difference in the values of the respective variable across the step.

The term D_i embodies the chromatographic retardation of the concentration or step velocity relative to the flow of the aqueous phase. For nonsorbed species (such as the anions), the stationary-phase concentration is and remains zero, so that $D_n=0$ and

$$v_{C_n} = f_w / S_w \quad (15)$$

a velocity equal to that of aqueous phase flow. In contrast, waves of any species whose variations in mobile-phase concentrations are accompanied by variations in stationary-phase concentration incur retardation because $D_i > 0$.

Equation 12 also provides a distinction among the three types of waves mentioned above. In an indifferent wave, v_{C_i} is

not a function of C_i . In a self-sharpening wave, v_{ci} decreases in the direction of flow (ξ increasing), while the opposite applies to a nonsharpening wave.

Salinity Waves and Ion Exchange Waves

The preceding analysis has shown that concentration variations of the nonsorbed anions are propagated at a different velocity than concentration variations entailing re-equilibrium of the stationary phase. We may, therefore, distinguish between "salinity waves", involving variations in anion concentration (salinity), but not in composition of the stationary phase while traveling at the velocity of aqueous phase flow, and "ion exchange waves" (or "sorption waves"), involving composition variations of the stationary phase, but not of the anions while traveling at lesser velocities.

Coherence

The solution to sets of first-order hyperbolic differential equations (such as Equation 10) may be obtained by any of several solution techniques, such as the method of characteristics. Here, however, we take advantage of the property that the bulk of chromatographic phenomena fall into what is referred to elsewhere as "coherent" waves. As is shown below, this property simplifies the calculation of composition profiles and histories.

The state of coherence exists much like the state of thermodynamic equilibrium for closed systems in that it is the state toward which all perturbations tend. As will be discussed below, the advantage of this is that composition paths may be calculated for any equilibrium relationship independent of the particular initial and boundary conditions. After the composition paths are calculated, it may be shown further that any variation in com-

position space, other than along a composition path, is non-coherent and reverts to the composition path.

Restricting the mathematical treatment exclusively to coherent waves is not possible in all cases because there may be regions of noncoherent waves in the time-distance space. The location of regions, however, may be inferred from the intersection of coherent waves. In each noncoherent region, the method of characteristics or a more involved application of the theory of coherence must be used to determine the composition. For the specific cases in this paper, we show that, granted assumptions 7 and 8, coherent waves will be attained immediately on the initiation of injection of any new composition into the system.

Coherence is a condition when the concentration velocities of all species at any given point in space or time are equal. This statement does not exclude the existence of several waves in a system, but does state that, if the waves are coherent, the concentration changes of all species must advance "in phase" in any single wave. Accordingly, the condition for coherence is for a nonsharpening wave,

$$v_{C_i} = v \quad \text{for } i = 1 \dots n + m \quad (16)$$

where v is the composition velocity common to all concentrations at the respective point in space and time. An analogous condition pertains for a coherent composition step. Coherence thus requires all retardation terms, D_i , to be equal in a particular wave,

$$D_1 = D_2 = D_{n+m} = D \quad (17)$$

Calculation of Composition and Coherent Step Velocities

The retardation term, D , of a composition in a coherent, diffuse wave can be obtained by solving an eigenvalue problem. The velocity of any given composition in such a wave is

$$V = f_w / (S_w + \lambda) \quad (18)$$

where λ is the eigenvalue associated with that composition. Comparison with Equations 12, 17, and 18 shows that $\lambda = D$. In an $n + m$ component system with one constraint (electroneutrality), any composition has $n + m - 1$ eigenvalues and thus can be propagated with $n + m - 1$ different eigenvelocities in coherent waves. If one species is not sorbed (anions), one eigenvalue is zero and corresponds to the salinity wave, with velocity given by Equation 15.

For cases with only two exchanging cations and nonsorbed anion ($n = 3, m = 0$), there is a salinity wave and only one ion exchange wave. Since this last wave travels at constant salinity C_n , its retardation term can be obtained directly by differentiation of the respective equilibrium equation. For the Gapon equilibrium Equation 5, one finds

$$D = \left. \frac{d\hat{C}_1}{dC_1} \right|_{dC_n=0} = \frac{Q_v K_{31} (C_n + C_1)}{2C_1^{3/2} (1 + K_{31}r)^2} \quad (19)$$

The velocity of a coherent step is obtained directly from Equation 12 with D_i given by Equation 14. Coherence requires all D_i for the step to be equal. For evaluation of the step velocity, the compositions on both sides of the step must be known. This usually requires prior construction of the composition route, described next.

Construction of Composition Path Grids

Composition paths are defined as curves (in the composition space), representing composition variations compatible with the coherence condition (Equation 16). Generally, their directions in the composition space are given by eigenvectors. In an $n + m$ component system with one constraint, there are $n + m - 1$ eigenvectors (number of components less number of constraints) for any composition, so that any point in the composition space is at an intersection of $n + m - 1$ paths.

In a system with $n + m - 1$ exchanging cations and nonsorbing anions, one eigenvalue corresponds to a salinity wave with variation of the anion concentration, but not of the stationary-phase composition. The other eigenvalues correspond to ion-exchange waves with variations of the stationary-phase composition, but not of the anion concentration.

In systems with only two exchanging cations, the composition paths are lines of constant salinity (ion-exchange paths) and curves of mobile-phase composition in equilibrium with constant stationary-phase composition (salinity paths).

In the general multi-cation case, the grid of the ion-exchange paths must be constructed by numerical integration in the eigenvector directions. For ion exchange equilibria obeying Equation 4, this procedure can be abbreviated using the relations,

$$\frac{dC_j}{dC_i} = \frac{\mu_i \lambda / \hat{C}_i - v_i / C_i}{\mu_j \lambda / \hat{C}_j - v_j / C_j} \quad (20)$$

valid for any pair of cations i and j . After elimination of the stationary-phase concentrations with Equations 2 and 4 and substitution of the respective nonzero eigenvalue for λ , the

exchange path corresponding to that eigenvalue can be calculated by integration of Equation 20.

Construction of Composition Routes

In general, a noncoherent composition variation acts as the source of a set of coherent waves. Such noncoherence may be induced by injection at the injection well or arise from interference of waves in the reservoir, as applications of the theory will show later.

The coherent waves originating from a common distance-time point of noncoherence are necessarily in the sequence of increasing velocities (counted in the direction of flow), for the fastest waves will have traveled farthest from the origin in any given time interval.

The construction of a composition route in a given path grid is illustrated schematically in Fig. 8. For simplicity, a two-dimensional grid of two sets of paths has been chosen. The "slow" and "fast" paths correspond to composition variations with low and high-composition velocities, respectively, and therefore, to slow and fast waves. The initial noncoherent wave is a composition variation from Points A (upstream side) to I (downstream side). The evolving route, representing the two coherent waves into which the initial wave is resolved, is points A to A' to I. This is the only route entirely along composition paths that meets the requirement that composition variations with high velocities (fast paths) are entirely downstream of those with low velocities (slow paths).

To be exact, the composition-path grid is calculated with the "differential" coherence condition that the derivatives $d\hat{C}/dC_i$ be equal and is strictly applicable to diffuse coherent

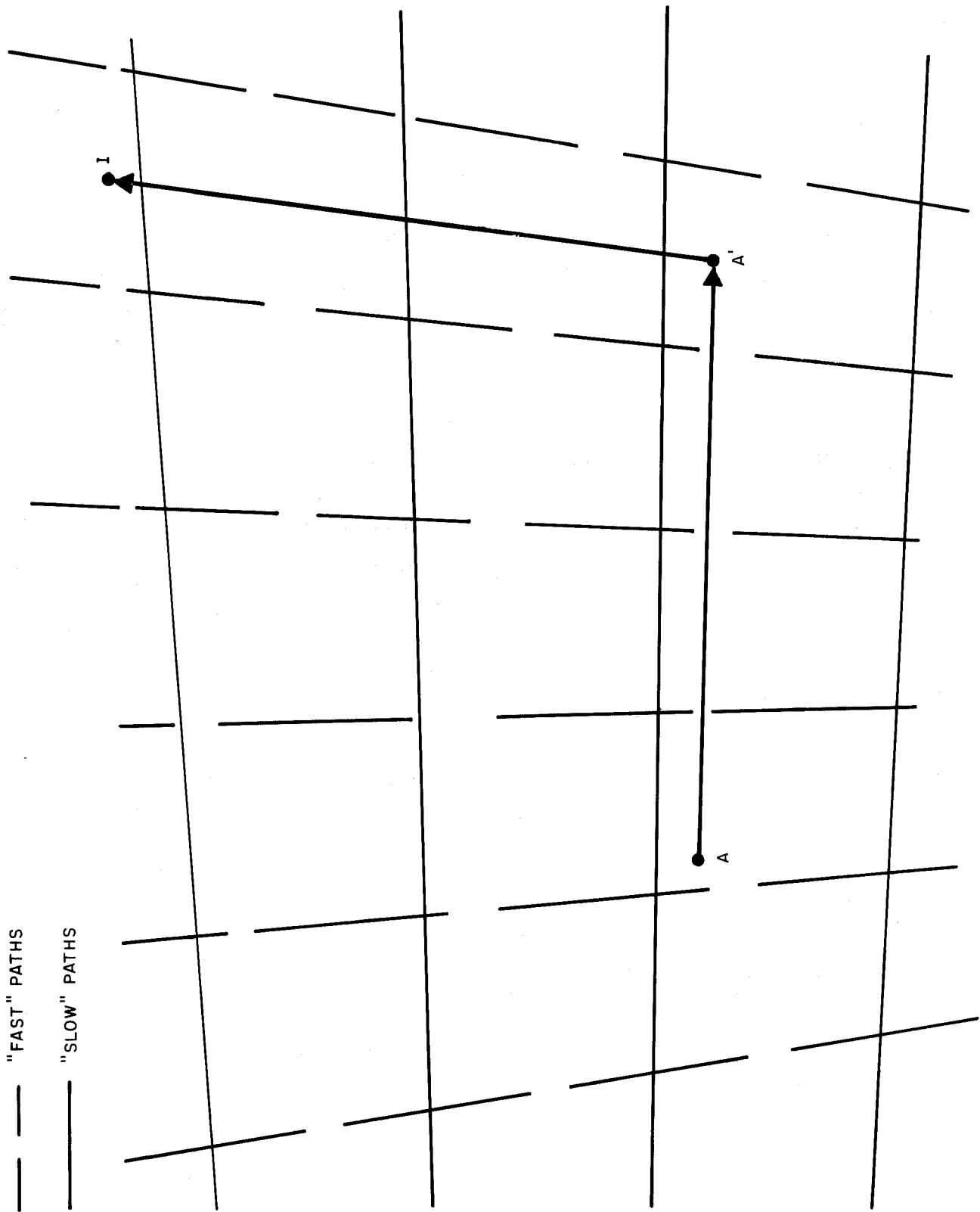


FIG. 8- Schematic composition route in two-dimensional path grid.

waves, but not to coherent steps. The last steps obey the "integral" coherence condition that the finite-difference ratios $\Delta\hat{C}_i/\Delta C_i$ be equal; pairs of points meeting this condition may not fall exactly on the same path if that path is curved. The sequence of waves is unaffected by this complication, but an exact route construction requires a correction so that the integral instead of differential coherence condition is met for those waves that are steps.

For complex initial or injection conditions, the composition route may change during the operation as faster waves interfere with slower waves of different origin from those preceding them. Examples of such behavior will be found below when applying the theory to cases with three or more fluids.

Construction of Distance-Time Diagrams, Composition Profiles and Composition Histories

Quantitative constructions of distance-time diagrams, profiles, and histories are based on the fundamental relation $v = d\xi/dV_{pd}$ for the normalized velocity. For any composition in a diffuse coherent step between constant compositions, the velocity is constant and the trajectory in the distance-time diagram (ξ, V_{pd} plane) is linear. Along such a trajectory, distance and time are related to one another by

$$\xi - \xi' = v(V_{pd} - V'_{pd}) \quad (21)$$

where v is the velocity of the respective composition (or step) and ξ' and V'_{pd} are the coordinates of the point of origin of the trajectory. This origin may be at the injection well ($\xi' = 0$) and onset of injection of a particular field, or at a point of wave intersection in the reservoir. For construction of a

profile at a given time V_{pd}^* , the location ξ^* of a concentration, composition, or step with velocity v and origin (ξ', V'_{pd}) is, from Equation 21,

$$\xi^* = \xi' + v (V_{pd}^* - V'_{pd}) \quad (22)$$

Similarly, for a history at a given distance ξ^* ,

$$V_{pd}^* = V'_{pd} + (\xi^* - \xi')/v \quad (23).$$

Construction starts from the initial and injection conditions which specify all points of origin of trajectories on the axes $\xi=0$ and $V_{pd}=0$. Coordinates of points of wave interference through crossover, etc., acting as origins of new trajectories, are found by either graphical construction in the distance-time plane or as solutions to Equation 21 for multiple injections.

In interference of a step with a diffuse wave, the step remains coherent, but the composition on either or both sides vary, thus, its trajectory is curved where it traverses the diffuse wave (unless the step is a salinity wave). The slope of the step trajectory at any point in terms of the compositions on its two sides is given by Equations 12 and 14. Of these two compositions, the one before intersection obeys its trajectory Equation 21, and the other can be obtained from it with the coherence conditions for step and diffuse wave. Substitution of these compositions in the step-velocity equation yields that velocity as a function of distance and time. The step trajectory then can be obtained by numerical integration of that equation, starting from the distance-time point of the first intersection with a composition trajectory of the diffuse wave. At the same time, this calculation defines the points of origin of the composition trajectories of the diffuse wave after intersection, so that these trajectories can be calculated with Equation 21.

If the routes of the interfering sharp and diffuse waves are on the same composition path (they are then necessarily in opposite directions), the step trajectory terminates the composition trajectories when intersecting them, and the composition on the other side of the step remains constant. Otherwise, the calculation of the curve-step trajectory remains the same.

If the step is a salinity wave, its slope remains unchanged. Points of origin of the new trajectories of the diffuse wave after intersection then are obtained, without integration, by simultaneously solving the trajectory equations for the step and the respective compositions before intersection.

Fig. 5 shows examples of such interferences. The ion-exchange waves of preflow and chemical slug, both on the same composition path, merge into a coherent pulse with a sharp front and diffuse rear and eventually degenerate into a single coherent step. While still interfering with one another, the waves are intersected by the salinity wave of the drive and change their trajectory slopes accordingly.

Interference of two diffuse waves generates a finite area of noncoherence in a distance-time plane. While such noncoherence eventually is resolved into coherent waves in the same way as a noncoherent step, its quantitative calculation requires numerical integration. The method of characteristics appears particularly suitable for this purpose. The same is true for gradual, noncoherent composition variations of the injected or connate fluid. This topic will be taken up later.

Two-Phase Flow

Two examples here involve formation of and two-phase flow in an oil bank. The relevant basic equations, adapted from a previous work, are summarized here for ease of reference.

By assumption, the surfactant advances with a sharp front, reduces residual oil saturation at that front from S_{or} to S_{orc} , and thereby accumulates an oil bank with oil saturation, S_o^* (Fig. 9).

The velocity, v_s , of the surfactant front (and oil bank rear) is given by Equation 12 with the appropriate substitutions,

$$v_s = 1/(1 - S_{orc} + D_s \text{ with } D_s) = \hat{C}/C_s \quad (24).$$

Material balances for the oil give velocities at the front and rear of the oil bank,

$$v = f_o^* / (S_o^* - S_{or}) \quad (25)$$

$$v_s = f_o^* / (S_o^* - S_{orc}) \quad (26).$$

Moreover, from Equations 24 and 26,

$$\frac{S_o^* - S_{orc}}{1 - S_{orc} + D_s} = f_o^* \quad (27).$$

The fractional flow of oil in the oil bank, f_o^* , is a function of the oil bank saturation, S_o^* . For given values of S_{orc} , D_s , and given the fractional flow dependence on saturation, S_o^* thus can be found as the value satisfying Equation 27.

RESULTS

The theory outlined in the preceding section is applied to several sample cases with increasing complexity.

FLOW →

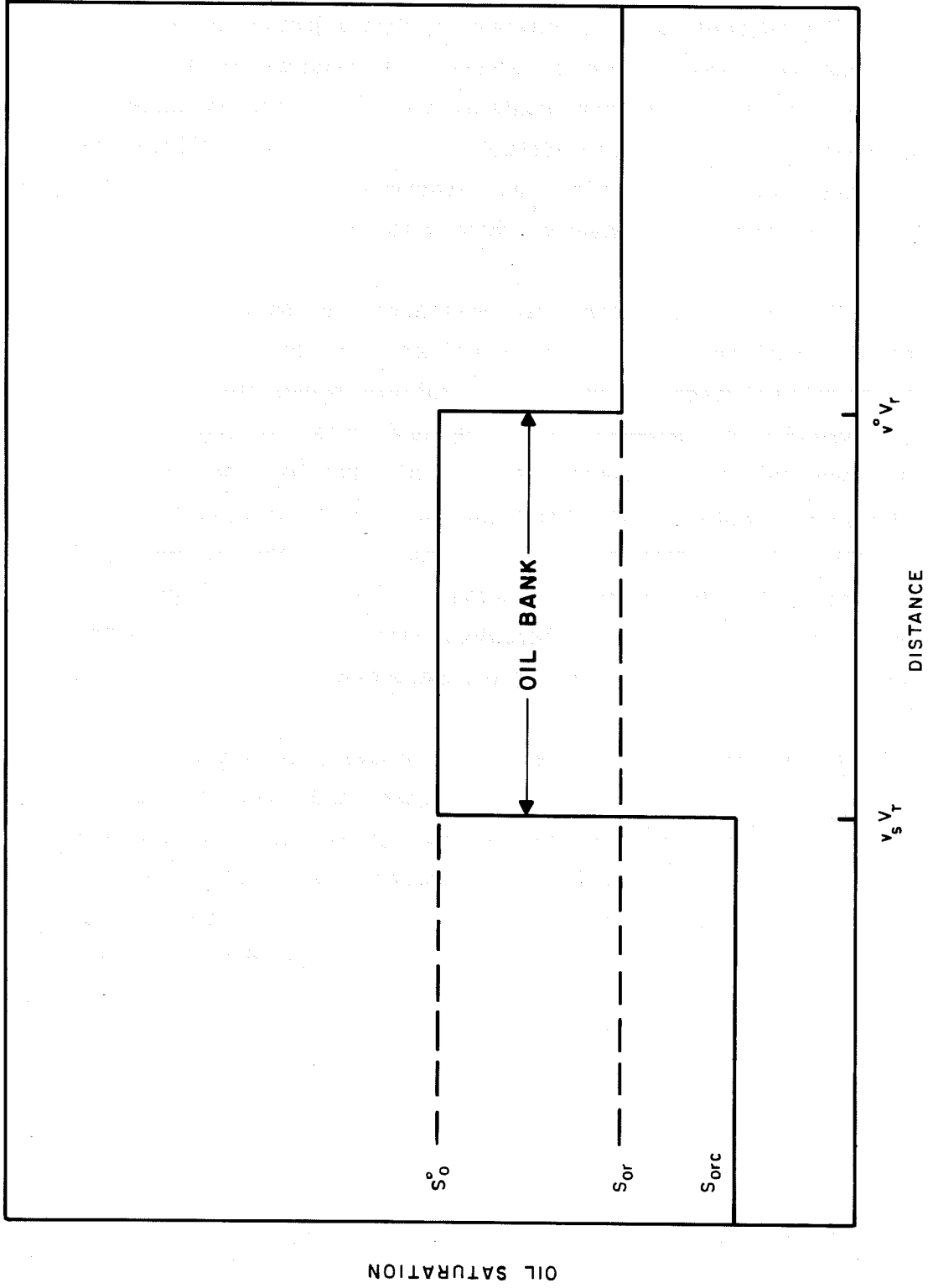


FIG. 9- Oil bank generated by surfactant that reduces residual oil saturation from S_{or} to S_{orc} .

Two Exchanging Cations, No Mobile Oil
And Two Fluids

The simplest case of interest is that injection of a binary aqueous salt mixture into a reservoir at residual oil saturation having connate water that contains the same salts at different concentrations. Since no surfactant is present to mobilize the oil, the aqueous saturation and fractional flow, S_w and f_w , remain uniform and constant at their initial values.

The preceding theoretical treatment has shown that composition variations under such conditions are propagated in the form of two types of waves: (1) salinity waves that travel at the velocity of aqueous-phase flow and entail a concentration variation of the nonsorbed anions, but not of the reservoir clays, and (2) slower ion exchange waves that entail a variation of the cation composition of the clays, but not of the concentration of the nonsorbed anions. The salinity waves are indifferent for sharpening behavior, whereas the ion exchange waves may be self-sharpening or nonsharpening.

In general, the injected fluid differs in salinity (anion concentration) from the connate water and will not be in equilibrium with the reservoir clays. Injection then produces two waves, a new composition is generated with salinity at the injected level, but within which the clays remain in their original state. The mobile-phase concentrations of the exchanging cations in that zone can be calculated from the equilibrium equations, given the injected salinity and the initial cation concentrations. Specifically, for calcium and sodium with Gapon or mass-action type equilibria, one finds for the calcium concentration in the zone between the salinity and ion exchange waves that

$$C_{1A'} = C_{nA} - \frac{C_{21}}{2C_{11}} \left[(C_{31}^2 + 4C_{nA} C_{11})^{1/2} - C_{31} \right] \quad (28).$$

A composition-path grid for the system (Fig. 7) has two sets of paths, one each for the salinity waves (constants \hat{C}_1 and \hat{C}_3) and the ion exchange waves (constant C_n). The paths in the figure have been calculated for Gapon or mass-action type equilibria, for which constancy of \hat{C}_1 and \hat{C}_3 demands $C_3/C_1^{1/2}$ to be constant, so that the salinity paths are given by

$$C_1 = \left(\frac{K_{31} \hat{C}_1}{\hat{C}_3} \right) C_3^2 = a C_3^2 \quad (29)$$

where "a" is a constant with different value for every path. The general behavior of the paths, however, is independent of the specific form of the equilibrium relations; the ion exchange paths are always lines of constant salinity. All salinity paths originate from the zero apex of the diagram and will show positive curvature if the preference of clays for the ion of higher valence (Species 1) increases with dilution, as is normally the case.

As noted earlier, the salinity waves are indifferent for sharpening behavior. The front of the injected salinity therefore is propagated as a set (fluid-dynamic dispersion being assumed negligible), regardless of its level. The ion exchange waves are usually self-sharpening (if the concentration of the cation preferred by the clays decreases across the wave in the direction of flow) and are nonsharpening for the opposite case.

The distance-time diagrams, composition routes, and production histories of two cases with NaCl, CaCl₂, and no oil are shown in Figs. 1 and 2. In the first example (Fig. 1), the injected salinity is lower than that of the connate water. Theory predicts the formation of an indifferent salinity wave and a self-sharpening ion exchange wave in between which exists a new zone where the calcium concentration is lower than in both the connate and injected fluids. In the second example (Fig. 2), the

TABLE 1

COMPOSITIONS OF TWO EXCHANGING CATIONS
(THREE FLUIDS) EXAMPLE

<u>Zone</u>	<u>Description of Composition</u>	<u>Concentrations (meq/ml)</u>			
		<u>C₁</u>	<u>C₃</u>	<u>C_n</u>	<u>C₁</u>
I	Initial connate water	0.010	0.050	0.060	0.0185
A'	Salinity A with clays in equilibrium with initial clay	0.005	0.035	0.040	0.0185
B''	Salinity B with clays in equilibrium with initial clay	0.001	0.014	0.015	0.0185
A	Injected Solution A	0.01	0.030	0.040	0.011
B'	Salinity B with clays in	0.002	0.013	0.015	0.011
B	Injected Solution B	0.004	0.011	0.015	0.031
Q _v =	0.0262 meq/ml				

injected salinity is higher than that of the connate water. Theory predicts the formation of an indifferent salinity wave and a non-sharpening ion exchange wave with an intervening zone in which the calcium concentration is higher than in both the connate and injected fluids.

Regarding quantitative detail, agreement is excellent for intermediate calcium levels and mean wave velocities, but not for sharpness of waves. A calculation neglecting fluid-dynamic dispersion, an important effect (especially in short-core laboratory experiments) cannot be expected to give a good match. Dispersion can produce diffuseness of self-sharpening and indifferent waves and can add to the diffuseness of nonsharpening waves, as indicated in the experimental production histories in Figs. 1 and 2. The effect of dispersion removes the last discrepancy between theory and experiment in the two examples above. This is discussed later.

Two Exchanging Cations, No Mobile Oil And Three Fluids

This example illustrates the type of response that arises from two successive injections of fluids of different compositions. For ease of comparison, the conditions are identical with those in Fig. 1 except that injection of the first fluid, instead of being continued indefinitely, is followed by injection of a second.

The composition route and distance-time diagram of this case are shown in Fig. 3, and Table 1 lists all occurring compositions. As with the start of injection of Fluid A, the change-over to injection of Fluid B produces two waves; a faster salinity wave and a slower ion exchange wave. The salinity wave from the second injection overtakes the ion exchange wave from the first

injection, as is apparent from the distance-time diagram. (Of course, if injection of the first fluid continues for long enough time, this will not occur before the production well is reached). Where these two waves meet, a simultaneous noncoherent variation of salinity and clay composition momentarily exists. Like non-coherence at the injection point, this noncoherence in the reservoir acts as the source of two noncoherent waves, of which the faster salinity wave now is downstream of the ion exchange wave. One might say the two waves have "crossed-over."

The composition variations generated by such a crossover of coherent waves can be recognized in both the distance-time and composition-paths diagrams. The distance-time diagram reflects the superposition of the patterns of injected salinities (propagated at the velocity of aqueous-phase flow) and of clay compositions in equilibrium with the injected fluids (propagated at the lesser velocities of the ion exchange waves). The new composition B'' that occurs when the waves cross has the salinity of injected Fluid B, but is in equilibrium with clays in their original state.

The schematic composition-route diagram in Fig. 3 traces the evolution of the response. Before crossover, the routes are produced by the two injections and are constructed as in previous examples. The composite route B-B'-A-A'-I, reflecting the compositions before crossover, cannot persist because it contains a faster wave (B'-A) upstream of a slower wave (A-A'). As these two waves cross, they eliminate the intermediate zone of composition A, and the composition variation from B' to A' momentarily becomes a single, noncoherent step. This noncoherence is resolved into two new coherent waves, of which the slower ion exchange wave is now upstream of the salinity wave. Accordingly, the new route from B'' to A' is through B'', and B'' corresponds to the composition of the new zone between the waves.

In the example in Fig. 3, both ion exchange B-B' and A-A' are self-sharpening. In such a case, the ion exchange waves B-B' and B'-B'' will eventually merge into a single, coherent, self-sharpening wave, B-B''.

Fig. 3 also shows that the ion-exchange wave of the first injection changes its velocity (trajectory slope) as it crosses the salinity wave of the second injection. Such a velocity change is the rule because the wave occurring after crossover is between different compositions than it was before.

Two Exchanging Cations, Surfactant And Mobilized Oil And Three Fluids

For the next complication, the authors introduce a surfactant contained in the second injected fluid that reduces oil saturation, thereby producing an oil bank. As stated in the initial assumptions, oil is considered to be a completely immiscible separate phase. Under Assumption 13, the surfactant front is self-sharpening and propagates as a step when the waves cross. Only two new effects then have to be accounted for: (1) the variation in pore space available for the aqueous phase, caused by displacement of oil and formation of oil bank, and (2) two-phase flow within the oil bank.

The first two examples including mobilized oil will show how a preflood can be sized so that it will just suffice to precondition the reservoir ahead of the surfactant front all the way to the production well. For this purpose, only the response behavior ahead of the surfactant front need be considered. A distance-time diagram for such a case is shown in Fig. 4. The ionic compositions of the preflood and surfactant slug have been taken to be the same as in Table 1. The following additional conditions were selected: (1) residual oil saturation at the

start of the flood ($S_{or} = 0.3$); (2) complete oil displacement by surfactant ($S_{orc} = 0$); (3) Equation 27 satisfied at an oil bank saturation ($S_o^* = 0.6$); and (4) no surfactant is sorbed ($D_s = 0$).

The distance-time diagram shows the following three waves to be of concern: (1) the surfactant front (also rear of oil bank) with velocity v_s , (2) the oil bank front with velocity v^* , and (3) the ion-exchange wave with velocity v_Δ while ahead of the front bank and v_Δ^* while within the oil bank. With reference to Fig. 4 and with the general Equations 12 and 24 through 27,

$$v_s = \frac{1}{1 - S_{orc} + D_s} \quad (30)$$

$$v^* = \frac{S_o^* - S_{orc}}{(S_o^* - S_{or})(1 - S_{orc} + D_s)} \quad (31)$$

$$v_\Delta = \frac{1}{1 - S_{or} + D_1} \quad (32)$$

$$v_\Delta^* = \frac{1 - S_o^* + D_s}{(1 - S_{orc} + D_s)(1 - S_o^* + D_1)} \quad (33)$$

Fig. 4 has been constructed with these equations and the respective data for saturations and retardation terms, D_i . The size of the preflood, V_A , has been so adjusted that the ion-exchange wave, which preconditions the reservoir clays, is not overtaken by the surfactant front until it arrives at the production well ($\xi = 1$).

The minimum size of preflood required for such complete preconditioning is

$$(V_A)_{\min} = D_i - D_s \quad (34)$$

Should the ion-exchange wave be nonsharpening instead of self-sharpening, the calculation would be exactly the same,

except that the retardation term, D_1 , now is evaluated for the rear of that wave,

$$D_1 = d\hat{C}_1/dC_1 \Big|_{C_1 = C_{1B}} \quad (35).$$

In the presence of any number of additional exchanging cations, the calculation would be the same, with D_1 now referring to the slowest ion-exchange wave or, if that wave is nonsharpening to its rear.

Complete reconditioning of the reservoir clays in accordance with Equation 34 may be impractical. Alternatives that then may be considered are as follows.

1. Suppress the ion-exchange wave or waves by choosing a preflood that is in equilibrium with the clays in their original state (e.g., matched Gapon ratios of connate water and preflood).
2. Adjust conditions so that the surfactant quickly overtakes the ion-exchange wave or waves of the preflood and then travels in a favorable ionic environment.

In both instances, the surfactant would travel during most or all of its traverse in an ionic environment with salinity of the injected chemical slug and in equilibrium with the clays in the original state. The salinity of the slug therefore would have to be chosen so as to produce an active environment under these conditions.

Two Exchanging Cations, Surfactant And Mobilized Oil
And Four Fluids

An actual chemical flooding sequence usually contains at least four fluids: preflood, chemical slug, and polymer drive, in addition to the connate water. A distance-time diagram for such a case with four fluids is shown in Fig. 5. The diagram has been calculated for the conditions listed in Table 2 and with the same methods as in previous examples. Table 2 also provides the compositions of the various zones that appear in the diagram. The following new features are apparent from Fig. 5.

1. The salinity wave of the preflood is overtaken by the front of the oil bank and changes its velocity because of altered fractional flows and saturation in the oil bank.
2. Surfactant sorption retards the surfactant front (and oil bank rear) relative to the salinity wave of the chemical slug.
3. Because oil is not completely displaced ($S_{orC} > 0$), the salinity waves in and behind the oil bank travel at greater-than-unit velocity.
4. Injection of the chemical slug produces a nonsharpening ion exchange wave, whose merger with the slower ion exchange wave of the preflood creates a curved boundary in the distance-time diagram.

In the example shown, the preflood was not large enough for complete reconditioning of the reservoir. The surfactant travels most of the time in an ionic environment dictated by the salinity of the injected chemical slug and by the reservoir clays in the

TABLE 2

COMPOSITION FOR TWO EXCHANGING CATIONS
WITH OIL (FOUR FLUIDS) EXAMPLE

<u>Zone</u>	<u>Concentrations (meq/ml)</u>		
	<u>C₁</u>	<u>C₃</u>	<u>C_n</u>
I	0.244	0.904	1.148
A	0.0204	0.0738	0.0942
A'	0.0025	0.0917	0.0942
B	0.0268	0.01368	0.1536
B'	0.0445	0.1091	0.1536
B''	0.0065	0.1471	0.1536
C	0.0065	0.0184	0.0249
C'	0.0005	0.0244	0.0249
C''	0.0002	0.0247	0.0249

$$Q_v = 0.042 \text{ meq/ml}, S_{orc} = 0.05, D_s = 0.015, S_{or} = 0.32, S^* = 0.485.$$

original cationic compositions (Zone B''). Under the conditions selected for the calculation, this environment contains much less calcium than the injected slug, the initial connate water, and the environment early in the flood when the surfactant travels over preconditioned clays (Zone B').

The only additional major complexity involved in Fig. 5 is the curved boundary of the surfactant slug's ion exchange wave after this wave intersects the preflood ion exchange wave. We therefore describe only how this curved boundary is calculated, leaving the calculation of other waves to other methods. If the preflood ion exchange wave intersects the leading edge of the slug's ion exchange wave at (V'_{pd}, ξ') , after this point a shock front will continue across which the calcium concentration changes from B'' concentration to a concentration given by

$$\frac{\xi}{V_{pd} - V_A} = \left(1 - S_{orc} + \frac{d\hat{C}_1}{dC_1} \right)^{-1} \quad (36)$$

from Equation 22. From Equation 19, this defines C_1 as a function of ξ and V_{pd} in the shaded region S^* . The velocity of the shock for $\xi' < \xi < \xi''$ and $V'_{pd} < V_{pd} < V''_{pd}$ is, from Equation 14,

$$\frac{d\xi}{dV_{pd}} = \left[1 - S_{orc} + \left(\frac{\hat{C}_{1B''} - \hat{C}_1}{C_{1B''} - C_1} \right) \right]^{-1} \quad (37)$$

where the subscript B'' refers to \hat{C}_1 and C_1 evaluated at composition B'' (Table 2). Integration of Equation 37 subject to the boundary condition $\xi(V''_{pd}) = \xi'$ will yield the curved boundary of region S^* . This must be done numerically as \hat{C}_1 and C_1 are functions of ξ and V_{pd} from Equation 36.

A similar calculation will yield the curved boundary of the slug's ion exchange wave after it crosses the polymer-drive salinity wave.

While Fig. 5 gives a good general idea of the type of response generated by a chemical flooding sequence of this kind, its quantitative detail will be only as good as the reservoir satisfies the original assumptions. The highly complex media of real reservoirs have not been considered, and even in an idealized medium, the following additional effects must be considered.

1. In the presence of more than two exchanging cations, each injection sets off more than one ion-exchange wave.
2. Surfactant adsorption and cation exchange are usually interdependent and therefore produce coupling of the respective waves.
3. Fluid-dynamic dispersion makes all waves more diffuse and may generate additional perturbations.
4. A surfactant may produce complete solubilization partition between water and oil or form more than two fluid phases.

The first two effects can be accounted for in the general theory presented here. The third, dispersion, is discussed later. The fourth, partitioning between fluid phases and more complex phase behavior, requires an extension of multi-component chromatographic theory used here to multiphase flow and is not considered here.

Three Exchanging Cations, No Mobile Oil And Two Fluids

We consider only a case with three cations (calcium, sodium, and magnesium) and two fluids. More complex cases, however, are

handled readily with a combination of the general methods applied here and in the preceding examples.

As theoretical treatment has shown, injection of a fluid different from connate water in such a three-cation system generally produces three waves; one salinity wave and two ion exchange waves. As in simpler cases, the salinity wave travels at the velocity of aqueous phase flow and is indifferent to sharpening behavior, whereas the ion exchange waves are slower and may be self-sharpening or nonsharpening.

Fig. 6 shows the composition route and distance-time diagram of a sample case. The compositions of the connate and injected fluids and of the various newly generated zones are listed in Table 3. The composition route is drawn in a path grid for constant, injected salinity and thus represents only the two ion exchange waves. In the reservoir, these waves are upstream of a salinity wave across which the salinity changes from the injected value to the connate value, while the clay composition remains unaltered. The end point "A" of the route in the diagram thus is the composition having injected salinity and being in equilibrium with clays in their original state. Once A" has been calculated and plotted in the composition-path grid, the construction of the composition route from A (injected composition) to A" with the principle outlined previously is straightforward: the route takes a slow then a fast path and therefore goes through A". The respective wave velocities are obtained with Equation 12 and the appropriate substitution for the retardation term D_1 . In the sample case shown, both ion exchange waves are nonsharpening.

In response to more complex injection conditions, the crossovers of ion exchange waves from different injections occur in essentially the same manner as the crossover between an ion exchange and a salinity wave, discussed previously.

TABLE 3

COMPOSITIONS OF THREE EXCHANGING CATIONS EXAMPLE

<u>Zone</u>	<u>Concentrations (meq/ml)</u>			
	<u>C₁</u>	<u>C₂</u>	<u>C₃</u>	<u>C_n</u>
I (initial)	0.120	0.132	1.304	1.556
A''	0.467	0.335	0.198	1.000
A'	0.300	0.200	0.500	1.000
A (injected)	0.134	0.360	0.506	1.000

The general formulation of the eigenvalue problem makes the approach outlined here applicable to systems with any number of exchanging cations, as well as systems which also contain other species (such as surfactant and polymer) whose sorption interacts with cation exchange. With a greater number of interfering species, one loses the convenience of working with simple, two-dimensional composition diagrams. Also, care now must be taken with the definition of salinity waves, as the only waves uncoupled from others and advancing at the velocity of aqueous-phase flow are those of species neither sorbed nor partitioning into oil. If the surfactant is ionic, sorbable, and interacting with cation exchange, the ion exchange waves will have variations of total anion concentration (but not of concentrations of non-sorbed, inorganic anions).

CONCLUSIONS

1. A method has been presented for calculating several first-order effects of multicomponent cation exchange and sorption in a chemical flood using the concepts of chromatography with interference. Specific examples of the coherent resolution are illustrated for the cases of two and three exchanging cations.
2. In general, one or more ion exchange waves are set off that travel at lower velocity than the salinity wave, which is composed of a concentration variation of non-sorbed anions. This means that the injected composition will generally traverse only a relatively small distance into the reservoir, whereas the new compositions resulting from the exchange process persist much longer.
3. A method is presented for estimating the size of a preflood required for completely reconditioning the

reservoir clays. Such a preflood probably seldom will be practical. However, if the fastest ion exchange wave is slow, the composition generated by the new salinity and old clay composition will determine the environment of the chemical slug for most of its traverse. This composition then would indicate an active chemical slug. In many cases, this composition can be designed given the assumptions of this study.

Alternatively, it may be possible or desirable to adjust the injected compositions so that cation exchange is suppressed, or at least minimized. All that is required for a typical brine preflood is that the ratio, $C_i^{V_i}/C_j^{V_j}$, be matched for the connate and preflood brines. Second-order effects not considered here may cause some exchange to occur even in this case. For the surfactant and polymer solutions, additional interactions must be taken into account.

Lake and Helfferich followed with a paper which included the effects of dispersion on the theoretical model described above. Thus, the interaction of cation exchange, polymer/surfactant adsorption and fluid-dynamic dispersion in a porous media was studied. Again, substantial portions of the report are reproduced for reference ⁵².

INTRODUCTION

Assumptions

The assumptions used here are similar to those used earlier, except that (1) fluid-dynamic dispersion is not neglected, (2) all material-balance relations are restricted to single-phase flow (there is no oil in the system), and (3) the system can have no more than five components; calcium, (C_1 - meq/ml) - a divalent cationic component; sodium (C_2 - meq/ml) - a monovalent cationic component; chloride or total salinity (C_3 - meq/ml) - nonadsorbing anionic component; surfactant (C_4 - meq/ml) - an adsorbing component; and polymer (C_5 - ppm) - a nonionic adsorbing component. Note that all concentrations for C_1 through C_4 (including the stationary phase concentrations) are in milliequivalents per milliliters of pore volume.

The foregoing assumptions restrict somewhat the usefulness of the following results when predicting the behavior of real systems. Nevertheless, these results effectively illustrate the combined influence of dispersion, cation exchange, and polymer/surfactant adsorption on a chemical flood's environment.

STATIONARY PHASE, PROFILES, AND HISTORIES

The stationary phase may be the clay (cation exchange) or rock (polymer/surfactant adsorption). We designate stationary phase concentrations with a superscript $\hat{}$.

GENERAL EQUATIONS

Material Balance

Subject to these assumptions, the one-dimensional convective-diffusion equation describing transport of species "i" in a porous medium is

$$0 = \frac{\partial (C_i + \hat{C}_i)}{\partial t} + \frac{q}{A\phi} \left(\frac{\partial C_i}{\partial z} \right) - \frac{\partial}{\partial z} \left(K_\ell \frac{\partial C_i}{\partial z} \right) \quad (38)$$

$i = 1, \dots, 5$

where K_ℓ is the longitudinal dispersion coefficient.

$$\text{The inverse Peclet number} = N_{Pe}^{-1} = \frac{K_\ell A\phi}{qL} \cong \frac{\alpha}{L}$$

With this, Equation 38 reduces to

$$\frac{\partial (C_i + \hat{C}_i)}{\partial V_{pd}} + \left(\frac{\partial C_i}{\partial \xi} \right) - \frac{\partial}{\partial \xi} \left(N_{Pe}^{-1} \frac{\partial C_i}{\partial \xi} \right) = 0 \quad (39).$$

Note that this definition of the Peclet number is not the same as that defined earlier. The definition used in Equation 39, however, is the more convenient in scaling dispersion to systems of different lengths. This Peclet number may be converted to the earlier one by multiplying N_{Pe}^{-1} with the ratio system length to characteristic particle diameter.

Equilibria Relations

Here, the equilibrium isotherm between sodium and calcium on the clays and in the flowing phase is assumed to follow a relation first proposed by Gapon and later investigated by Bolt,

$$\frac{\hat{C}_2}{\hat{C}_1} = K_{21} \frac{C_2}{\sqrt{C_1}} = K_{21}^r \quad (40)$$

where r is the Gapon ratio.

Equation 40 is only one of several relationships proposed in the literature to represent sodium-calcium exchange on formation clays. Its use here presumes no superiority of this equation over other isotherms. Subsequent work and the work of others elsewhere has shown isotherms of the "mass-action" or "Kerr" type to be slightly more accurate when representing sodium-calcium exchange. Equation 40 is, nevertheless, entirely adequate for most purposes and considerably simpler to implement in the mathematical development.

For adsorption of surfactant and polymer species, we assume that a Langmuir isotherm applies,

$$\hat{C}_i = \frac{a_i c_i}{1 + b_i c_i} \quad i = 4 \text{ or } 5 \quad (41)$$

There is some question about whether the surfactant-polymer adsorption is completely reversible. For the illustrations in this report, we use Equation 41 only for single-step changes (concentration increasing) in the polymer or surfactant influent concentration, so there is no need to include an irreversible adsorption term in Equation 41. Since we use this equation for both surfactant and polymer adsorption, many of the conclusions deduced below will be applicable to either.

If C_{fi} is the concentration of surfactant or polymer in the injected fluid (the final concentration) Equation 41 may be written as

$$\hat{C}_i = \frac{C_{fi} (1 + C_{fi} b_i) C_i}{C_{fi} (1 + b_i C_i)} \quad (42).$$

$$i = 4 \text{ or } 5$$

Electroneutrality

Following Assumption 3, solution electroneutrality is

$$C_3 = C_1 + C_2 \quad (43)$$

and stationary phase electroneutrality is

$$Q_v = \hat{C}_1 + \hat{C}_2 \quad (44)$$

where Q is the cation exchange capacity.

In view of Equations 43 and 44, C_1 , C_2 , and C_3 are no longer independent species. We arbitrarily choose to solve for calcium and chloride concentration so that Equation 39 now may be written generally as

$$\frac{\partial A_i}{\partial V_{pd}} + \left(\frac{\partial C_i}{\partial \xi} \right) - \frac{\partial}{\partial \xi} \left(N_{Pe}^{-1} \frac{\partial C_i}{\partial \xi} \right) = 0 \quad (45)$$

$$A_1 = C_1 + \frac{Q_v}{1 + K_{21} \left(\frac{C_3 - C_1}{\sqrt{C_1}} \right)} = C_1 + \frac{Q_v}{1 + K_{21} r} \quad i = 1, 3, 4, 5 \quad (46)$$

$$A_3 = C_3$$

$$A_i = C_i + \frac{a_i C_i}{1 + b_i C_i} \quad i = 4 \text{ or } 5$$

where the first of these equations follows from eliminating C_2 and \hat{C}_2 between Equations 40, 43, and 44, and the second follows from the chloride anion being nonadsorbing.

To solve for C_1 , we integrate Equations 45 and 46 numerically using finite elements (Galerkin's method) Equation 45 for

C_1 is coupled to C_3 making it necessary to solve for C_1 and C_3 simultaneously. Here, we use an analytic solution for C_3 , since chloride is nonadsorbing, to couple the chloride and calcium equations.

Analytic Solution For Chloride Concentration

The approximate solution for Equations 45 and 46 with $i = 3$ and the following boundary and initial conditions $C_3(0, V_{pd}) = C_{3f}$ is $C_3(\xi,) = C_{30}$

$$\frac{C_3 - C_{30}}{C_{3f} - C_{30}} = \frac{1}{2} \left[1 - \operatorname{erf} \left(\frac{\xi - V_{pd}}{2\sqrt{N_{Pe}^{-1}} V_{pd}} \right) \right] \quad (47)$$

The solution for the complete sequence of formation water, preflow, slug, and polymer drive can be found by superposition.

$$\begin{aligned} C_3(\xi, V_{pd}) = & C_{3fw} + \left(\frac{C_{3pf} - C_{3fw}}{2} \right) \cdot \left[1 - \operatorname{erf} \left(\frac{\xi - V_{pd}}{2\sqrt{N_{Pe}^{-1}} V_{pd}} \right) \right] \\ & + \left(\frac{C_{3s} - C_{3pf}}{2} \right) \cdot \left\{ 1 - \operatorname{erf} \left[\frac{\xi - (V_{pd} - V_{pf})}{2\sqrt{N_{Pe}^{-1}} (V_{pd} - V_{pf})} \right] \right\} + \left(\frac{C_{3pd} - C_{3s}}{2} \right) \\ & \cdot \left\{ 1 - \operatorname{erf} \left[\frac{\xi - (V_{pd} - V_{pf} - V_s)}{2\sqrt{N_{Pe}^{-1}} (V_{pd} - V_{pf} - V_s)} \right] \right\} \end{aligned} \quad (48)$$

for a linear system. Equation 48 applies only for $V_{pd} > V_{pf} + V_s$. For $V_{pf} < V_{pd} < (V_{pf} + V_s)$, the last term should be omitted; for $0 < V_{pd} < V_{pf}$, the last two terms should be omitted, making Equation 48 the same as Equation 47.

The boundary conditions selected for the numerical solution are the total fluxes specified at the inflow and outflow end of this system.

$$\left(C_i - N_{Pe}^{-1} \frac{\partial C_i}{\partial \xi} \right)_{\xi=0} = C_{if} \quad i \neq 3 \quad (49)$$

$$\left(\frac{\partial C_i}{\partial \xi} \right)_{\xi=1} = 0 \quad i \neq 3 \quad (50)$$

Accuracy of Solutions

These are three sources of error in the above procedure.

1. Errors in the analytic solution, Equation 47, resulting from the disagreement between the boundary conditions for the analytic solution and those used by the numerical solution, Equations 49 and 50. These errors should be greatest at small V_{pd} and large N_{pe}^{-1} . For $V_{pd} > 0.1$ $N_{pe}^{-1} < 0.5$, the average error caused by using Equation 47, instead of the more complicated exact solution, is usually less than the error in the numerical solution of Equation 46. This level of accuracy is acceptable in the current application.
2. Time truncation errors that arise because of the finite differencing of the time variable. There are, in addition to time truncation errors, errors originating from the spatial truncation. These errors are much smaller than time truncation errors in the finite-element methods we are using (nonsmooth cubics as basic functions). In general, time-step sizes were chosen to keep the total average numerical error below 3%.
3. Errors caused by oscillations result from the inability of the finite-element program to solve Equation 45 if the various waves or fronts become too sharp. For single-phase problems, this occurs when the second-order term becomes much less than the other terms (the equation loses its parabolic character). This problem, in principle, can be surmounted by choosing more node

points. In practice, computing time and core storage requirements limit the maximum number of node points. As before, however, we are able to use enough node points for $N_{pe}^{-1} > 0.0005$ to reduce the average error to less than 3%.

These precautions keep the accuracy to the analytical and numerical solutions at an acceptable level. The current analytical-numerical approach, therefore, will yield results similar to those reported earlier using a completely numerical solution scheme to solve the material-balance equations.

RESULTS

Throughout this section we will refer to inverse Peclet numbers of 10^{-2} and above as "laboratory" scale dispersion. Inverse Peclet numbers of 10^{-3} and below are termed "field" scale dispersion. The laboratory scale N_{pe}^{-1} is that which we have found exhibited by surfactant slugs in 0.5 to 2-foot long laboratory cores. The 10^{-2} value is somewhat larger than that, but still in approximate agreement with, values quoted in the literature for inert tracers in outcrop sandstone cores. The field scale value, on the other hand, is somewhat arbitrary, being based on values obtained from the Esso Tracer test method.

History Match on Ion-Exchange Experiments

Figs. 10 and 11 show data from experiments in a 2-foot long Berea core with no oil present that are suited ideally to the assumptions. In Fig. 10, the concentration of chloride in the brine initially present in the core was 0.04 meq/ml; the chloride concentration in the injected fluid was 0.06 meq/ml. Fig. 11 represents the reverse experiment of Fig. 10, with initial and injected chloride being 0.06 and 0.04 meq/ml, respectively. In

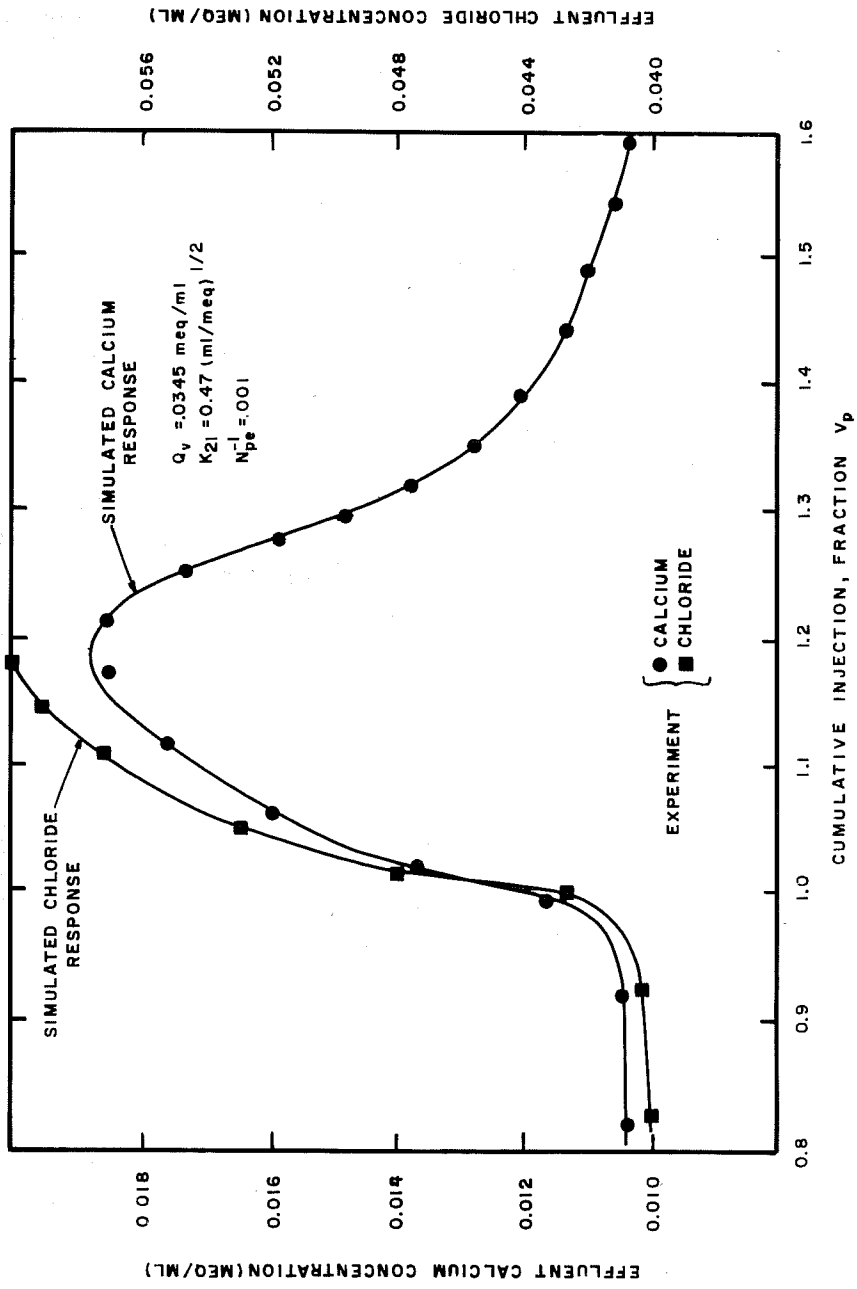


FIG. 10- Effluent history match of ion-exchange experiment in a 2-ft Berea core.

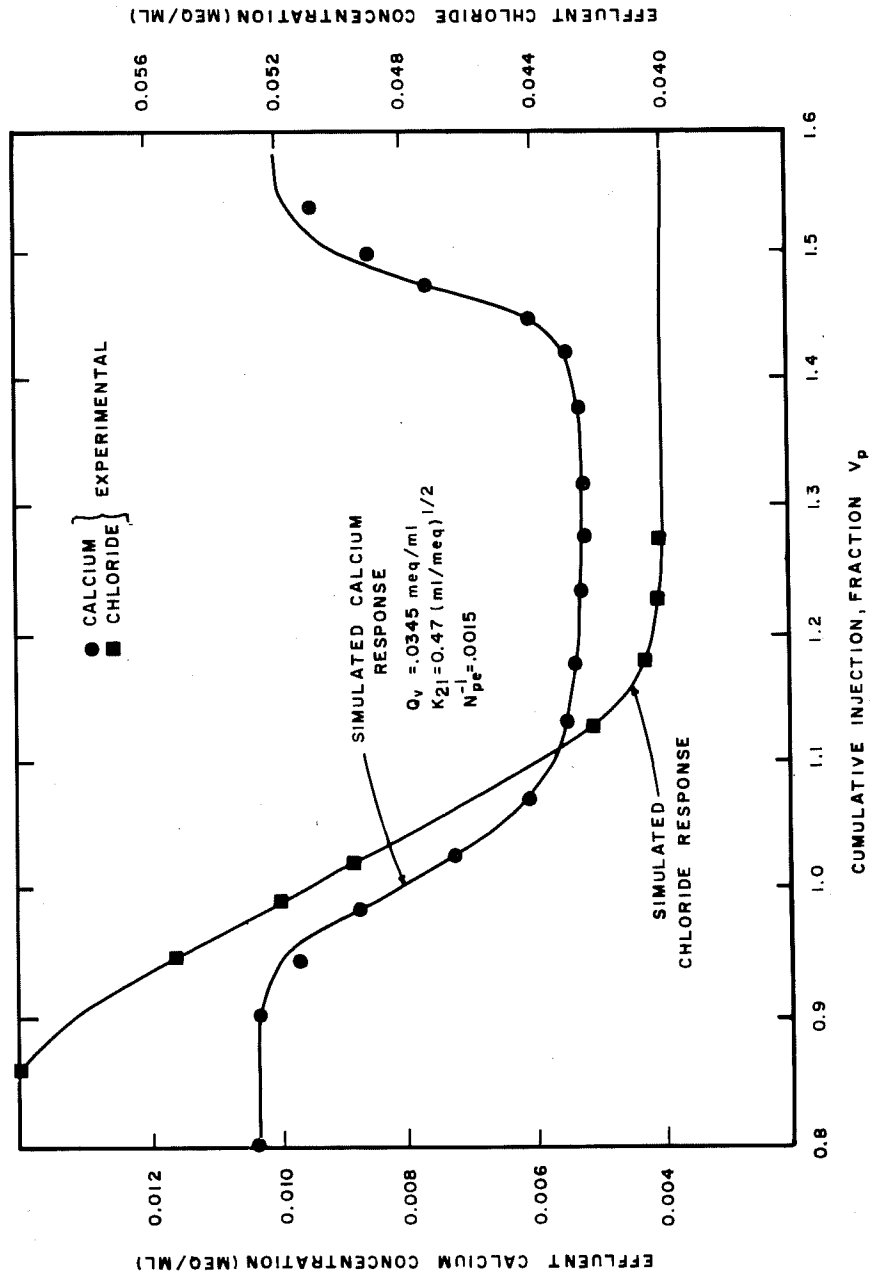


FIG. 11— Effluent history match of ion-exchange experiment in a 2-ft Berea core.

both experiments, the calcium concentration in the initial and injected fluids was 0.0103 meq/ml.

Figs. 10 and 11 also show the effluent history match of the solutions to Equations 45 and 48 ($V_{pf} = V_s = 0$), with the experimental results. Both figures show good agreement between theory and experiment, even though they required slightly different inverse Peclet numbers. This is somewhat surprising since these two figures represent sequential experiments run on the same core with the same fluids. Both N_{pe}^{-1} and K_{21} are best fit numbers, however, and this difference probably is within experimental uncertainty.

The effluent history matches Figs. 10 and 11 provide a useful comparison between the results of the no-dispersion theory, and the dispersion theory described here. The no-dispersion theory gives correct mean-wave velocities and intermediate zone compositions, but gives waves that are too sharp. The dispersion theory, on the other hand, predicts correct intermediate compositions, but also accurately reproduces the relative spread of the waves. The implication is that dispersion theory is needed if the extent of spread is important.

Entire Chemical Flooding Sequence

Fig. 12 shows the calculated calcium concentration profile at $V_{pd} = 0.7$ cumulative injection for an entire chemical flooding sequence. The slug sizes and injected concentrations are given in Table 4. Fig. 12 shows the profiles calculated at laboratory and field-scale dispersion levels and also shows the no-dispersion limit.

The main concern in Fig. 12, regarding the effectiveness of the chemical slug, is the loss of calcium cations to the reser-

TABLE 4

INJECTED AND INITIAL CONCENTRATIONS AND SLUG SIZES FOR
FIGURE 12

	<u>Formation Water</u>	<u>Preflood</u>	<u>Chemical Slug</u>	<u>Polymer Drive</u>
Total salinity, meq/ml	1.153	0.0942	0.153	0.0249
Calcium, meq/ml	0.244	0.0204	0.017	0.0065
Sodium, meq/ml	0.909	0.0738	0.136	0.0184
Slug size, fraction V_p	Initial	0.10	0.12	---

TABLE 5

INJECTED AND INITIAL CONCENTRATION AND SLUG SIZES FOR
FIGURE 15

	<u>Chloride (meq/ml)</u>	<u>Slug Size (fraction V_p)</u>	<u>Polymer (ppm)</u>
Formation water	1.6	Initial	---
Preflood	0.3	0.5	---
Chemical slug	0.2	0.1	800
Polymer drive	0.5	---	1000

Polymer adsorption: $\hat{C}_5 = (0.05 + C_3^2) C_5$

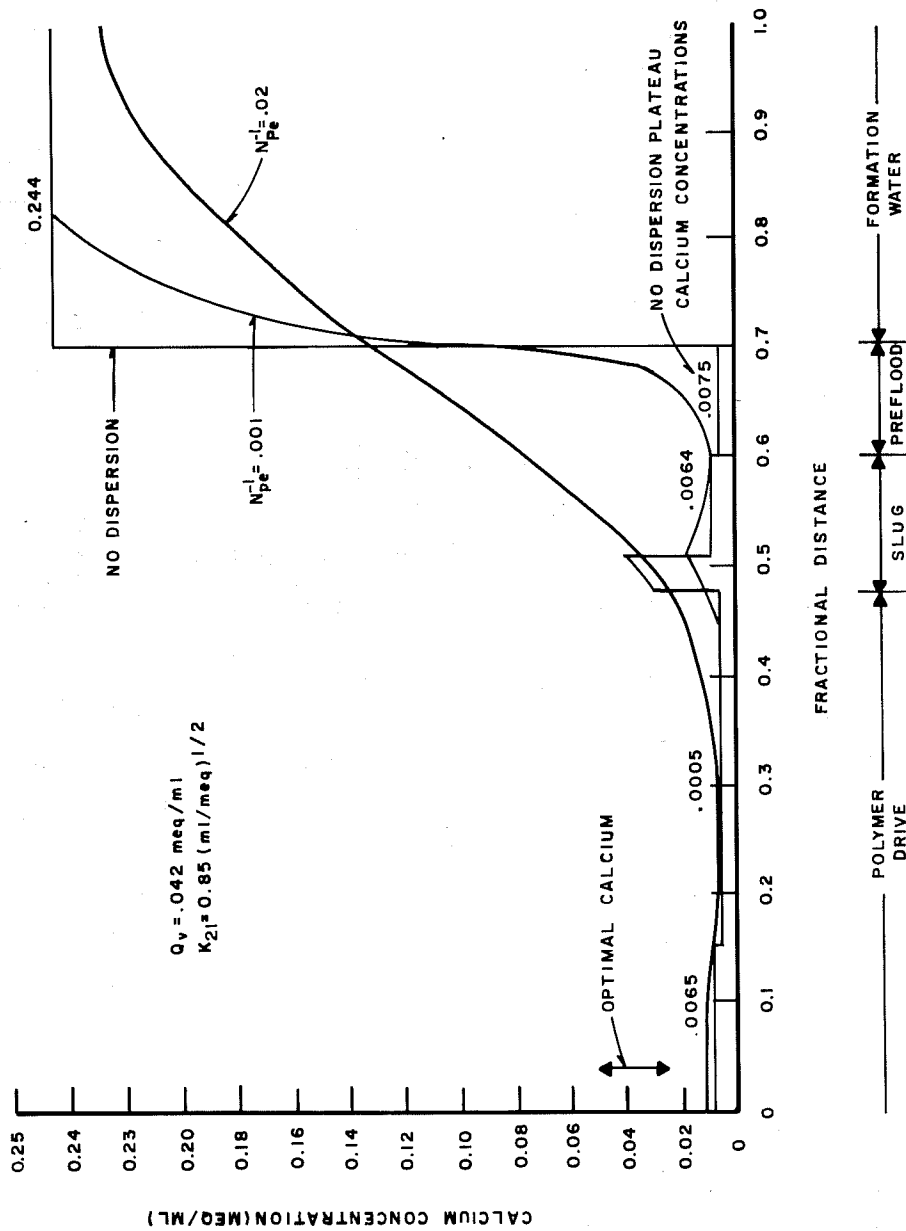


FIG. 12- Calcium profile at $0.7 V_p$ cumulative injection for typical chemical flood sequence.

voir clays. Based on the no-dispersion curve, this can result in a calcium concentration of 0.0064 meq/ml, which is lower than what was injected (0.017 meq/ml) and lower than that required for an "optimal" calcium concentration in the slug's presence. With field-scale dispersion, the situation is even worse, as the dispersion erodes the locally high calcium concentration at $\xi = 0.51$. With laboratory scale dispersion, the mixing is so large as to completely obliterate this local maximum, but mixing with formation water ahead of the preflood will restore the slug's calcium concentration to the optimal region. Thus, it appears that under some circumstances, dispersion can compensate for the detrimental effects of cation exchange. It is not possible to make a general statement in this regard, but clearly the inclusion of dispersion in the calculation can modify results calculated from methods that assume no dispersion, particularly when dispersion is large and/or slug sizes are small.

Dispersion Induced Ion Exchange

When a fluid is displaced by another fluid with different total salinity and calcium concentrations, but with the same Gapon ratio, the no-dispersion methods predict no change in the concentration of component i on the clay ($\hat{C}_{10} = \hat{C}_{1f}$). Dispersive mixing between the two fluids, however, causes the fluids to mix and to alter r . The result of this mixing is a change in the concentration of component i on the clay in the mixing zone between the two fluids, even though the clays have equal compositions ahead and behind the mixing zone. Such a phenomenon has been observed in laboratory experiments, and is the result of a linear mixing phenomenon, dispersive mixing, occurring simultaneously with nonlinear adsorption, as evidenced by the term r in Equation 40.

The basis for this section is an experiment where $C_3 = 1.66$ meq/ml, $C_1 = 0.28$ meq/ml solution was displaced by $C_3 = 0.166$

meq/ml, $C_1 = 0.0039$ meq/ml solution in a Berea core. For both solutions, r was about 2.6. The calcium concentration effluent history of this experiment is given in Fig. 13 along with the simulation at two dispersion levels. $N_{pe}^{-1} = 0.0041$ was the experimentally observed dispersion. Fig. 13 shows the simulation result was only a quantitatively good fit. Adjusting Q_v and K_{21} would probably improve the fit, but experimental uncertainties in this particular experiment would render parameters thus obtained of questionable value.

Shown also in Fig. 13 is the dispersive effluent history with no ion exchange. The calculated solution less the no-ion exchange solution is a measure of the importance of the dispersion-induced ion exchange.

$$C_1(\xi, V_{pd}) - C_1^0(\xi, V_{pd}) = C_1^*(\xi, V_{pd}) \quad (51)$$

This difference, termed the excess calcium concentration, is shown in Fig. 14, for one of the cases in Fig. 13, as a function of position and cumulative injection. The most important question addressed by Fig. 14 is whether deviations caused by the dispersion-induced cation exchange grow or decay with time. The largest effects apparently occur ahead of the point $\xi = V_{pd}$ and are calcium deficiencies (C_1^* negative). These differences evidently grow with time. Of more importance in chemical flooding, since the slug usually would be adsorbing, are the effects behind the point $\xi = V_{pd}$. These differences are actual calcium excesses (C_1^* positive). The maximum excesses in the $\xi < V_{pd}$ region evidently also grow fairly fast at first and then grow much slower later on. Moreover, the region over which the non-zero excess extends also grows with time. Differences such as these occur over a region that easily could contain a typically small chemical slug, but the maximum excess calcium concentration is only about 0.006 meq/ml, which is within the tolerance of many surfac-

tant formulations. Because this mixing-zone effect is dispersion induced, the effect is less predominant at small N_{pe}^{-1} (actually) vanishing in the limit of $N_{pe}^{-1} \rightarrow 0$). The converse of this is that the dispersion-induced, cation exchange effect should decrease with increasing N_{pe}^{-1} . This is true until dispersion becomes so large as to completely override all other effects. The denominator of the error function argument in Equation 47 is a measure of the dispersion of a front. Because this quantity contains V_{pd} , in addition to N_{pe}^{-1} , it follows that the effect should grow with time. Moreover, since it also follows from Equation 47 that the mixing-zone length grows as the square root of V_{pd} , it is consistent that the region over which the effect is important also should grow. The excess concentrations become negative again in the region $V_{pd} > \xi$ (Fig. 14). This is the result of small oscillations in the numerical solution that do not alter the basic conclusions in Fig. 14.

Simulation of Polymer Behavior With a Chloride-Dependent Isotherm

One of the first uses envisioned for a low-salinity preflood was to lower the surfactant and polymer adsorption on the rock. Another study has shown that the adsorption of these large molecules increases with the total salinity of the fluid. This section demonstrates the effect of this dependency on the effluent history of the polymer concentration.

Table 5 shows the injected concentrations and slug sizes used in this set of simulations. The adsorption isotherm for this case is linear in polymer concentration and quadratic in chloride concentration and quadratic in chloride concentration (Table 5). Fig. 15 shows the results of the two simulation runs and one purely dispersive (no adsorption) analytic solution for polymer effluent history. With the preflood, the effluent

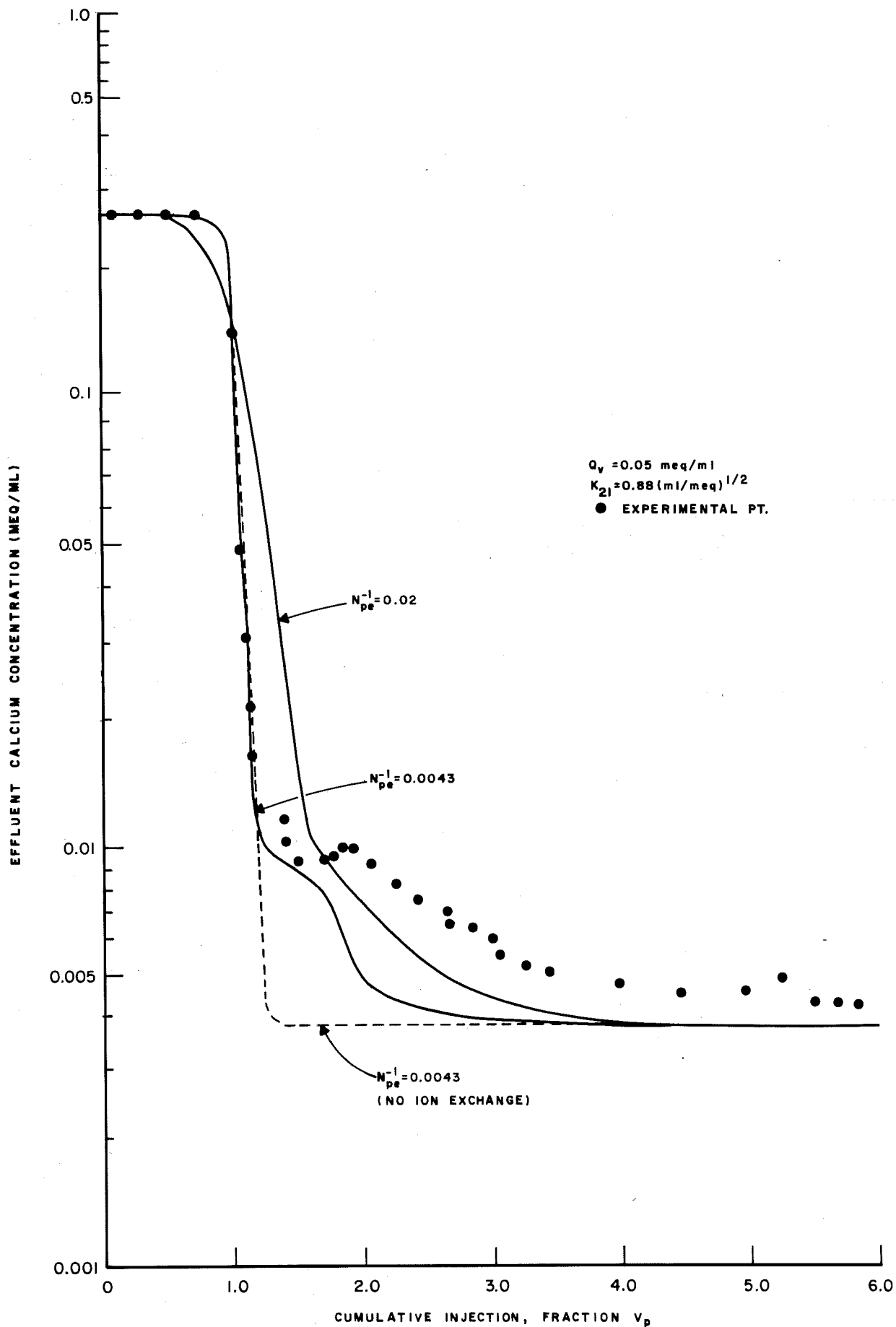


FIG.13—Effluent calcium concentration and sensitivity to Peclet number for demonstration of dispersion-induced ion exchange.

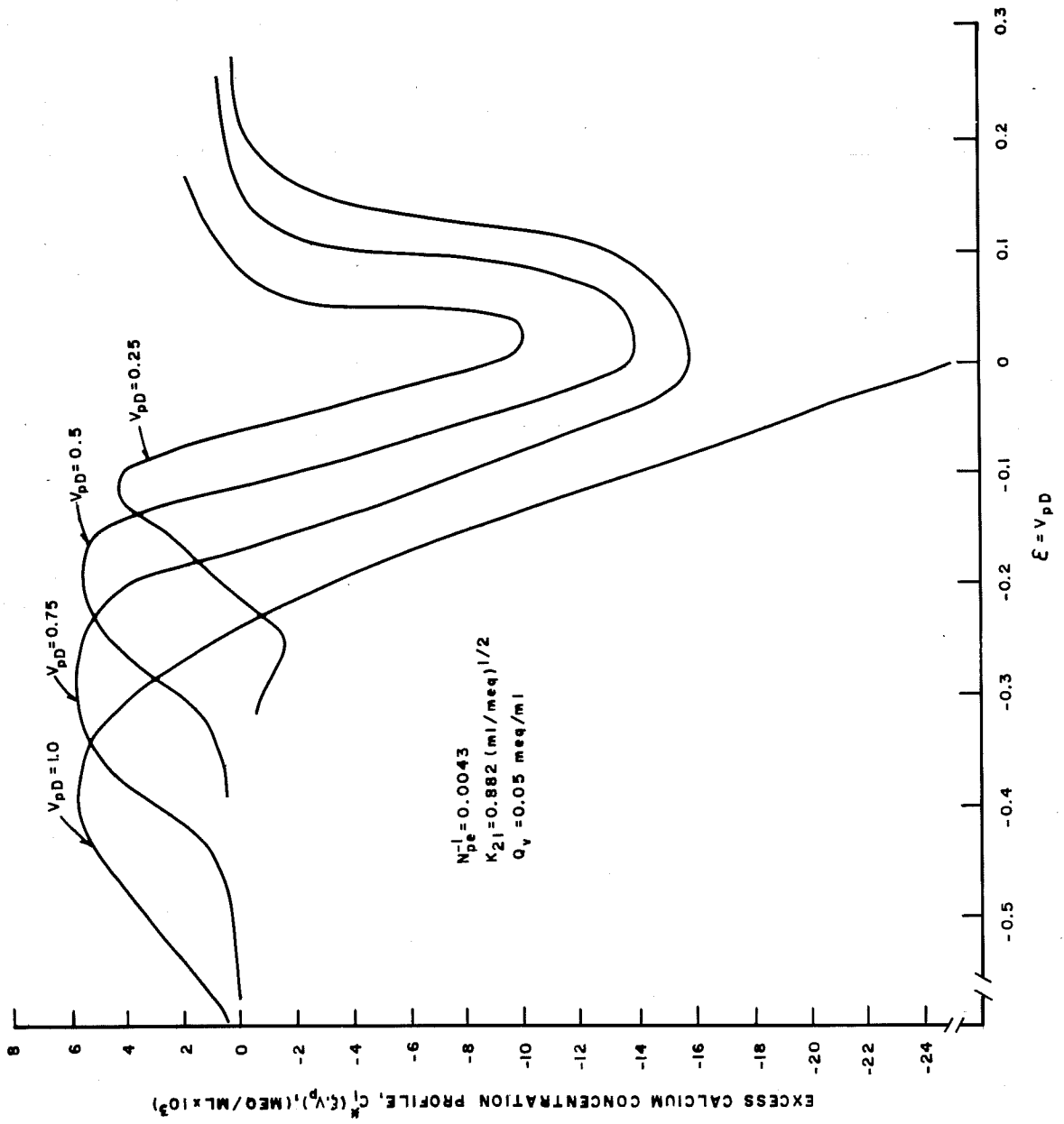


FIG. 14- Excess calcium concentration profile for various cumulative injections.

history is only slightly different from the analytic solution effluent history. This is because the preflood keeps the polymer front's total salinity environment low enough so that the adsorption is small. For the no-preflood case, the situation changes considerably. Now the front is sharper than before because the mixing with the more-saline formation water causes the lower polymer concentrations to adsorb much more than when the slug was preceded by a preflood. Because the slug and polymer drive themselves have low chloride concentrations, a substantial portion of this adsorbed polymer desorbs back into the solution. This causes the effluent polymer concentration to be actually greater than the injected polymer concentration, a phenomenon occasionally observed with both the chemical and the polymer in actual practice. Usually some material remains on the rock, even at low-fluid polymer concentration and total salinity. If this effect is pronounced, the effluent polymer concentration may not necessarily exceed the injected polymer concentration, but the total polymer lost would almost certainly be much larger with no preflood.

Asymptotic Mixing Zones

Self-sharpening waves in homogeneous porous media experience two competing physical phenomena. Dispersion tends to spread out the wave in proportion to the square root of time, and the effect of the adsorption isotherm, on the other hand, tends to sharpen the wave, causing a discontinuous shock in the absence of dispersion. These phenomena tend to balance each other producing, in an asymptotic sense, a wave that does not change shape with time and one that is independent of the system's initial conditions. That is, an initially sharpened wave will spread to this limit while an initially dispersed wave will sharpen to this limit. This section explores this asymptotic wave through the extended example of a Langmuir isotherm and the numerical scheme described

above. Although for simplicity we restrict ourselves to a Langmuir isotherm, the technique and results apply equally to any chromatographic process with a self-sharpening wave.

This study follows earlier work on general self-sharpening waves caused by adsorption isotherms.

If the simplest type of displacement occurs, that of one miscible fluid of unit concentration displacing another in a one-dimensional, linear, homogeneous porous medium, solutions to Equations 45 and 46 would give the concentration of the displacing fluid at all positions and times. If, however, the balance between dispersion and adsorption is attained, and the isotherm is one that would produce a shock in the absence of dispersion, the shape of the wave will become constant, and the wave itself will progress through the porous medium in simple translation. When this happens, the wave (viewed in a coordinate system that moves with the average position of the displacing front) will be independent of time. Transforming Equations 45 and 46 into the spatial coordinate $\xi' = \xi - v_{\Delta C} V_{pd}$, where $v_{\Delta C}$ is the dimensionless step velocity, yields,

$$\left(1 + \frac{d\hat{C}}{dC}\right) \left(\frac{\partial C}{\partial V_{pd}}\right)_{\xi'} - \left[\left(1 + \frac{d\hat{C}}{dC}\right) v_{\Delta C} - 1\right] \left(\frac{\partial C}{\partial \xi'}\right)_{V_{pd}} - N_{Pe}^{-1} \left[\frac{\partial^2 C}{\partial (\xi')^2}\right]_{V_{pd}} = 0 \quad (52)$$

The step velocity is the velocity the shock would have in the absence of dispersion. Note that $v_{\Delta C}$ has meaning only if the wave is self-sharpening. The subscript for C (4 or 5) will be omitted because this section deals with one-component systems only. The quantity $v_{\Delta C} V_{pd}$, termed the adjusted cumulative injection, is the position the fluid front would have if there were no dispersion and no displacing fluid initially in the system. From these remarks, we assume that the wave is moving

by simple translation and, therefore, that the first term of Equation 52 will be zero. This results in the following differential equation for the asymptotic concentration profile.

$$\left[(v_{\Delta C} - 1) + v_{\Delta C} \frac{d\hat{C}}{dC} \right] \frac{dC}{d\xi'} + N_{Pe}^{-1} \left(\frac{d^2 C}{d\xi'^2} \right) = 0 \quad (53)$$

Integrating once with the boundary conditions that $(dC/d\xi')_{\xi \rightarrow +\infty} = 0$ and $C(+\infty) = 0$ yields

$$v_{\Delta C} \hat{C} + (v_{\Delta C} - 1) C + N_{Pe}^{-1} \left(\frac{dC}{d\xi'} \right) = 0 \quad (54)$$

Since the displacing fluid's injected concentration is unity, a second integration of Equation 54 will occur between the limits of $C = 0.9$ and $C = 0.1$.

$$\Delta \xi_m^S = \xi_{C=0.1} - \xi_{C=0.9} = - N_{Pe}^{-1} \int_{C=0.1}^{C=0.9} \frac{dC}{v_{\Delta C} \hat{C} + (v_{\Delta C} - 1)C} \quad (55)$$

The quantity $\Delta \xi_m^S$, defined as the asymptotic mixing-zone length, is a measure of a front's length. This is the limit that self-sharpening dispersive waves approach with time.

Further use of Equation 55 must involve the specific isotherm, Equation 42 with $C_f = 1.0$. Substituting Equation 42 into Equation 55 and integrating yields

$$\Delta \xi_m^S = N_{Pe}^{-1} \left(\frac{1 + \hat{C}_f}{\hat{C}_f} \right) [\ln(9)] \left(1 + \frac{2}{b} \right) \quad (56)$$

Equation 56 has used the definition of $v_{\Delta C} = 1/(1 + \hat{C}_f)$.

The mixing-zone length for a nonadsorbing dispersive wave is from Equation 47

$$\Delta\xi_m^0 = \xi_C = 0.1 - \xi_{C=0.9} = 3.625 \sqrt{N_{Pe}^{-1} V_{pd}} \quad (57)$$

Note that $\Delta\xi_m^S$ is time-independent, while $\Delta\xi_m^0$ is proportional to the square root of time.

Fig. 16 shows the behavior of the transient mixing zone, $\Delta\xi_m$, as a function of the adjusted cumulative injection calculated by the numerical technique described above. The middle curve is that of a nonadsorbing mixing zone that obeys Equation 57. The lower curve is that of a self-sharpening front that is initially sharp and becomes more dispersed with time. The upper curve is that of an initially dispersed front that sharpens with time. Both of the latter cases tend to (but do not attain within the finite system) the limit described by Equation 56. The adsorption isotherm, nevertheless, causes the mixing-zone length to be smaller at the end ($v_{\Delta} C V_{pd} = 1$) of the displacement than would be anticipated from pure dispersion.

From Equation 57, the maximum value that the nonadsorbing mixing-zone length can attain is a $V_{pd} = 1.0$.

$$(\Delta\xi_m^0)_{\max} = 3.625 \sqrt{N_{Pe}^{-1}} \quad (58)$$

We shall use Equation 58 as a reference quantity for Equation 56. The ratio of asymptotic mixing-zone length to maximum nonadsorbing length is

$$F\xi \equiv \frac{\Delta\xi_m^S}{(\Delta\xi_m^0)_{\max}} = \frac{\sqrt{N_{Pe}^{-1}}}{3.625} \left(\frac{1 + \hat{C}_f}{\hat{C}_f} \right) \ln(9) \left(1 + \frac{2}{b} \right) \quad (59)$$

This quantity is a function of the three parameters N_{Pe}^{-1} , \hat{C}_f , and b . Fig. 17 presents Equation 59 graphically. Over much of the range of parameters, particularly low \hat{C}_f or high N_{Pe}^{-1} ,

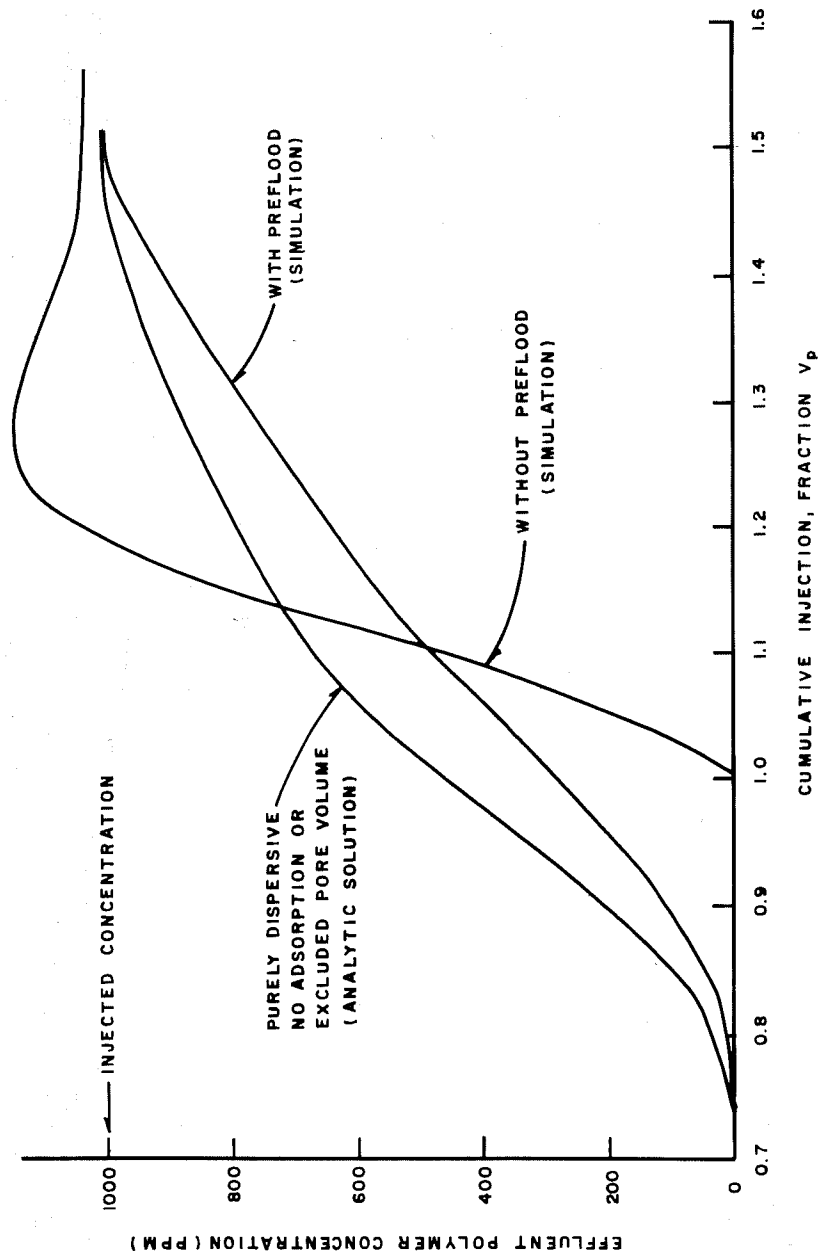


FIG. 15- Effluent polymer concentration for a chloride-dependent isotherm.

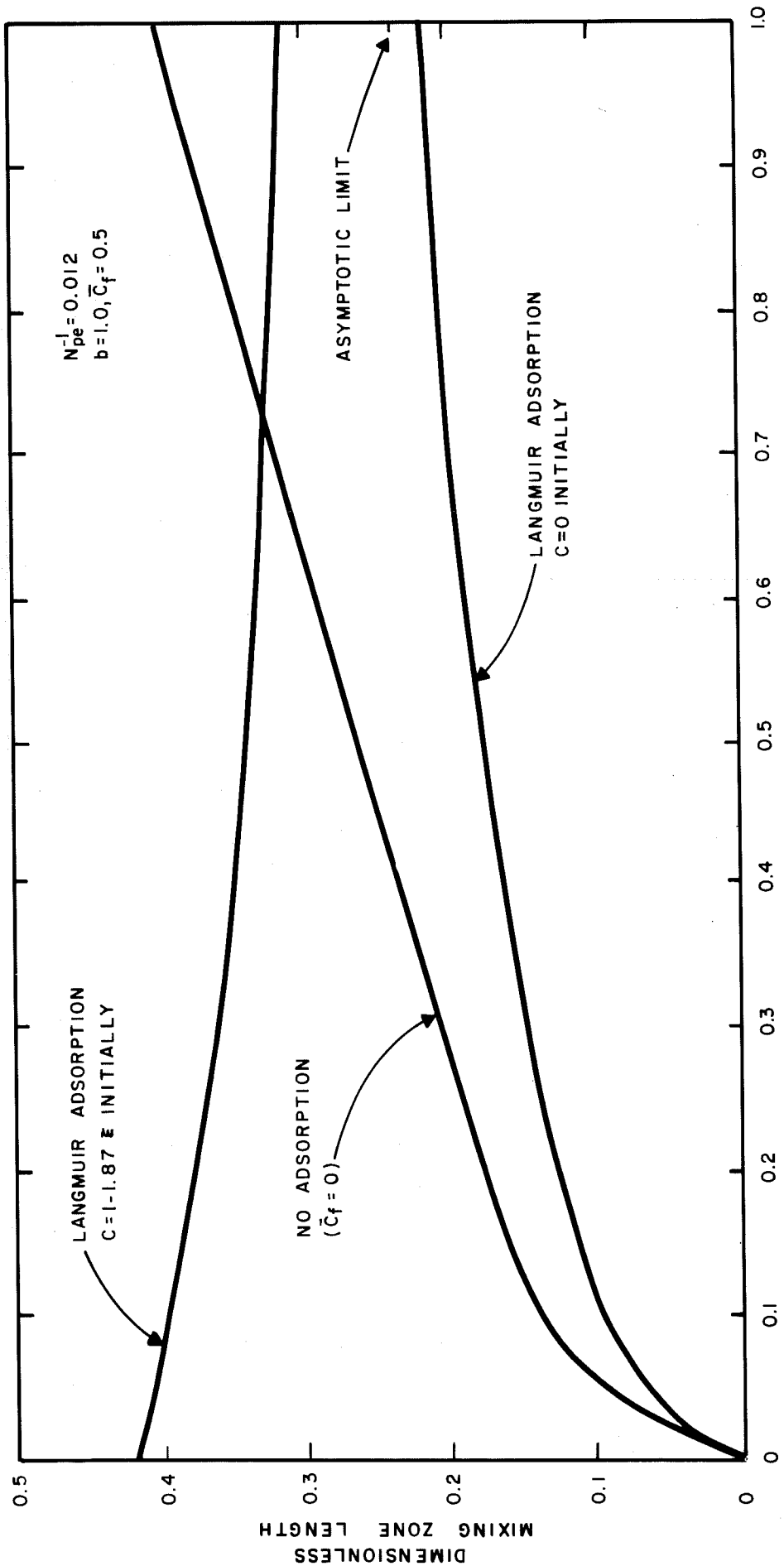


FIG. 16 — Comparative behavior of adsorbing and nonadsorbing mixing zone lengths.

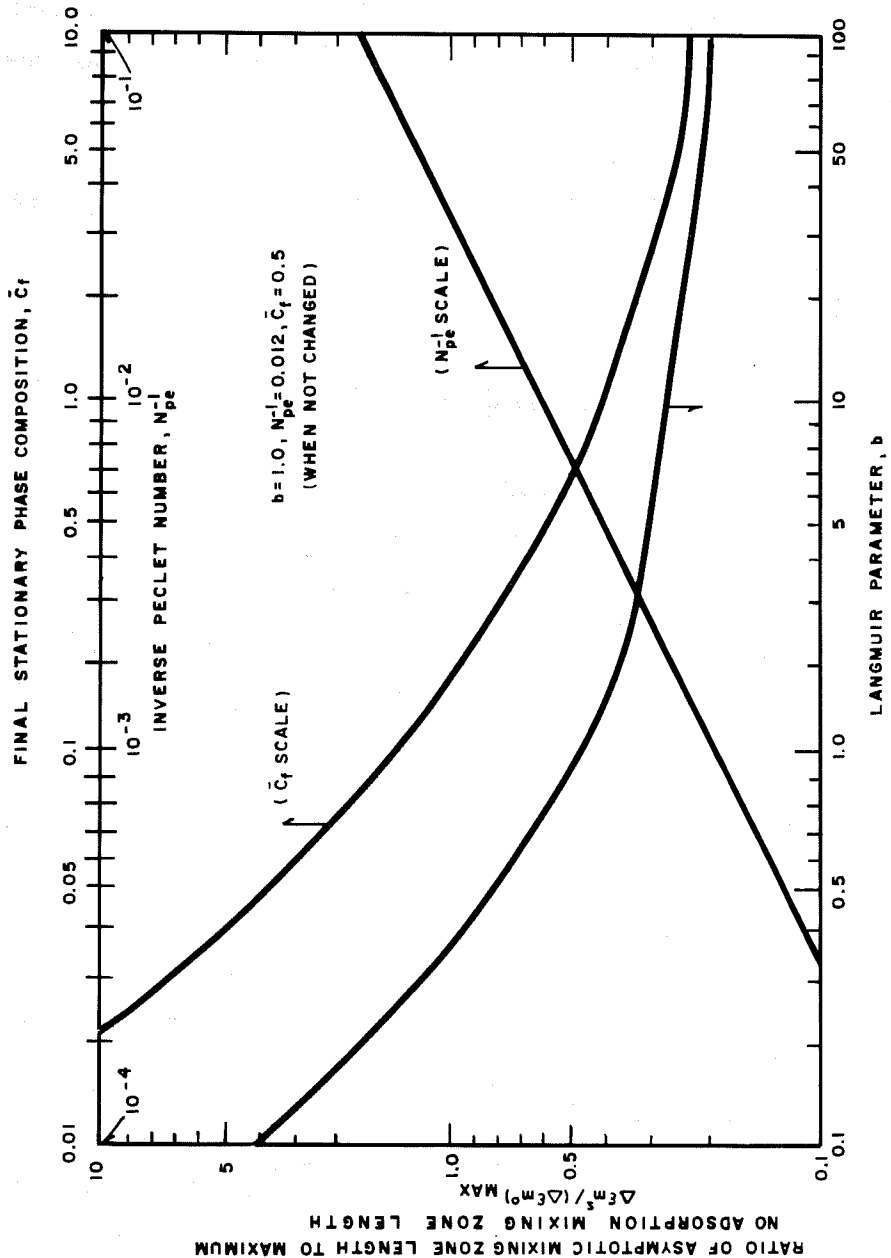


FIG. 17- Ratio of stabilized mixing zone length to maximum no adsorption mixing zone length

the asymptotic mixing-zone length is greater than the maximum purely dispersive mixing-zone length ($(\Delta\xi_m^S/\Delta\xi_m^O)_{\max} > 1.0$). On the other hand, for low N_{Pe}^{-1} , high C_f , or high b , the asymptotic mixing-zone length is less than the maximum purely dispersive mixing-zone length. The implications of this are difficult to see from Equation 59 because it is a comparison of a mixing-zone length $(\Delta\xi_m^S)$ evaluated at $V_{pd} \rightarrow \infty$ with a mixing-zone length $\{(\Delta\xi_m^O)_{\max}\}$ evaluated at $V_{pd} = 1$.

If we let $(\Delta\xi_m)_{\xi=1}$ be the mixing-zone length of an initially sharpened adsorbing front when it reaches the effluent end, then for $F_\xi > 1$,

$$(\Delta\xi_m)_{\xi=1} \ll (\Delta\xi_m^O)_{\max} \ll F_\xi (\Delta\xi_m^O)_{\max} \quad (60)$$

and for $F_\xi \ll 1$,

$$(\Delta\xi_m)_{\xi=1} \ll F_\xi (\Delta\xi_m^O)_{\max} \ll (\Delta\xi_m^O)_{\max} \quad (61)$$

Dividing inequalities in Equations 60 and 61 by the maximum nonadsorbing mixing-zone length (which is always positive) and keeping only the first (the strongest) inequalities yields

$$\frac{(\Delta\xi_m)_{\xi=1}}{(\Delta\xi_m^O)_{\max}} < 1 \quad \text{for } F_\xi > 1 \quad (62)$$

and

$$\frac{(\Delta\xi_m)_{\xi=1}}{(\Delta\xi_m^O)_{\max}} < F_\xi \quad \text{for } F_\xi < 1 \quad (63)$$

The inequality in Equation 62 yields no new information since the maximum adsorbing zone length is always less than the maximum nonadsorbing mixing-zone length. The inequality in Equation 63 along with Equation 59, on the other hand, provides insight into

how much the adsorption of the mobile-phase component will decrease the mixing-zone length over that expected from nonadsorbing dispersion theory.

Fig. 18 schematically illustrates the situations described by the inequalities in Equations 62 and 63. In the upper plot, the asymptotic mixing-zone length is greater than the maximum nonadsorbing mixing-zone length ($F_\xi > 1$). In the lower plot, the converse is true ($F_\xi < 1$). The difference between the actual mixing zone length ($\Delta\xi_m$) of an adsorbing front and the mixing-zone length of a nonadsorbing front ($\Delta\xi_m^0$) will be greater when $F_\xi < 1$ (Fig. 16). We now attempt to deduce which situation described in Fig. 16 applies to laboratory and field-scale displacements.

Typical values of the three parameters in Equation 59 are $\hat{C}_f \approx 0.05$ for surfactant or polymer adsorption 0.001 (field scale) $N_{Pe}^{-1} < 0.01$ (lab scale) $90 < b < 200^{13}$. The limit of Equation 59 for large b is

$$\frac{\Delta\xi_m^S}{(\Delta\xi_m^0)_{\max}} = \frac{\sqrt{N_{Pe}^{-1}}}{3.625} \left(\frac{1 + C_f}{C_f} \right) \ln(9) \quad (64)$$

Equation 64 is a useful result since b usually is poorly known and large enough to justify the approximation. Physically, what Equation 64 implies is that as the isotherm becomes more nonlinear ($b \rightarrow \infty$), there is a point beyond which the wave will not sharpen further. These numbers yield

$$\begin{aligned} F_\xi \text{ (lab scale)} &= 1.27 \\ F_\xi \text{ (field scale)} &= 0.4 \end{aligned} \quad (65)$$

or for the inequalities in Equations 62 and 63,

$$\text{(laboratory scale)} \quad \frac{(\Delta\xi_m)_{\xi=1}}{(\Delta\xi_m^0)_{\max}} < 1 \quad (66)$$

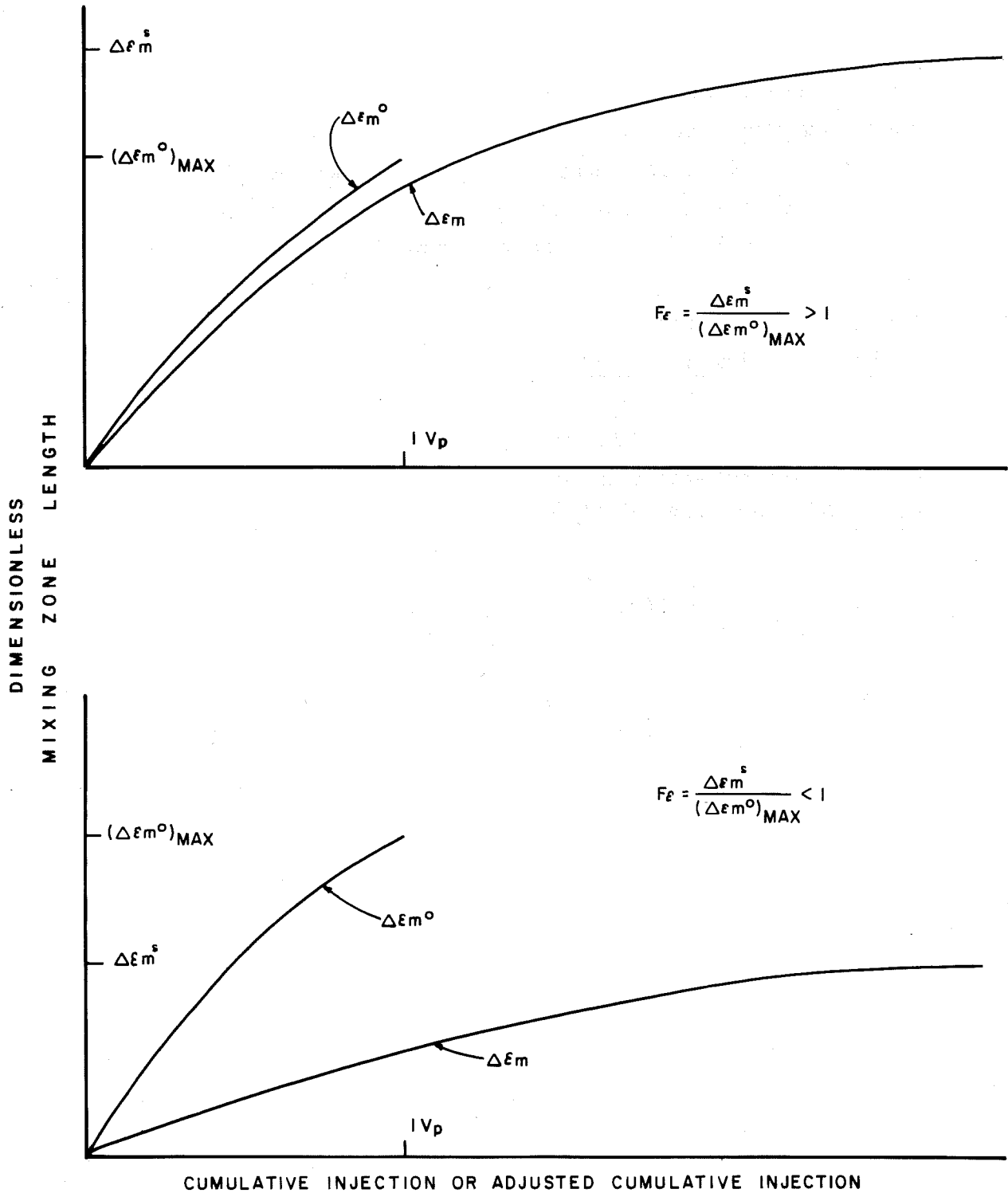


FIG. 18— Schematic illustration of the behavior of mixing zone lengths in finite systems.

$$\text{(field scale)} \quad \frac{(\Delta\xi_m)_{\xi=1}}{(\Delta\xi_m^0)_{\max}} < 0.4 \quad (67).$$

Hence, on the field scale the Langmuir isotherm will sharpen the dimensionless mixing-zone length $(\Delta\xi_m)$ more than it will on the laboratory scale, relative to the respective no-adsorption, mixing-zone lengths $(\Delta\xi_m^0)$. Conversely, laboratory measurements of dispersion of surfactant solutions are not likely to be affected greatly by adsorption effects, provided the \hat{C}_f value is not much greater than 0.05. This conclusion is true for one-sided (or continuous) chemical fronts. For finite slugs, the adsorption remains the important, regardless of N_{pe}^{-1} value, because of the depletion and possible chromatographic separation of the surfactant and polymer.

We have found that the actual mixing-zone length approaches the asymptotic limit exponentially. This is another departure from nonadsorbing dispersion theory with a mixing-zone that grows proportionally to the square root of time. It appears, moreover, that the time constant of this growth rate increases as the asymptotic mixing-zone length decreases. This implies that a small $\Delta\xi_m^0$ will be attained at a smaller V_{pd} than a larger asymptotic mixing-zone length.

CONCLUSIONS

1. The scheme of coupling a finite-element numerical simulation for calcium concentration to the analytic solution for chloride concentration is satisfactory for modeling the effects of dispersion and two-cation exchange reactions in chemical flooding.
2. When slug sizes are small and dispersion is fairly large, the inclusion of dispersion can modify results calculated by methods that assume no dispersion.

3. A fluid with a Gapon ratio that is in equilibrium with the reservoir clays (but with a different over-all composition), nevertheless, will cause cation exchange to occur in the mixing-zone between the injected and in-situ fluids. This phenomenon is caused by fluid dynamic dispersion and can be an important effect in systems with moderately large dispersion where a highly calcium sensitive slug is used.

4. If a displacing fluid has an adsorption isotherm so that its front would be a shock in the absence of dispersion, the actual concentration profile (including dispersion) tends to resemble an asymptotic profile that traverses the porous medium without changing shape. This phenomenon is new to the petroleum literature in that it predicts asymptotic mixing-zone lengths that are independent of time and inversely proportional to the Peclet number. Moreover, it appears that, given reasonable values of the parameters involved, this phenomenon is more important under field than under laboratory conditions.

In continuation of the theoretical study described above, H.J. Hill and L.W. Lake of Shell Development Company completed an experimental study in cores³⁰. The results of their efforts are reported below.

DISCUSSION OF EXPERIMENTAL DATA

Most flow experiments were conducted in Berea cores, except for one experiment that was conducted in a sand pack prepared from disaggregated Berea sand. X-ray diffraction analysis of these two disaggregated sands showed that both contained quartz, feldspar, dolomite, and clay. The Berea sand also contained siderite (FeCO_3). Clay fractions contained illite, kaolinite, and chlorite. About 50% of the Tar Springs clay fraction was chlorite and 70% of the Berea clay fraction was kaolinite.

Cation-exchange capacity, Q_v , certain other core data, and experimental conditions are summarized in Table 6-B, where experiments are identified with a letter or number code. Table 7-B gives analytical data for solutions used in the floods. In Table 7, the primary identification code marks the solution with which the rock was equilibrated before the first displacement. Solutions used in successive floods are identified by successive letters of the alphabet.

Experimental results are illustrated in the figures and summarized in Tables 8 and 9. For each solution pair used in a displacement experiment, the net gain or loss of calcium and magnesium from the solutions was determined by material balance. Since gain by the solutions represented loss by the core and vice versa, the solution material balances measured $\Delta\hat{C}_1$ and $\Delta\hat{C}_2$. These values of $\Delta\hat{C}$ were used with the independently determined value of cation-exchange capacity, Q_v , and the known values of the appropriate solution concentration ratios to obtain values

TABLE 6

CORE DATA AND EXPERIMENTAL CONDITIONS

	EXPERIMENT				
	<u>R</u>	<u>1230</u>	<u>1094</u>	<u>1095</u>	<u>E-1</u>
Core Data					
Identity	Berea	Berea	Tar Springs	Berea	Berea
Dimensions, in.	2 x 24	2 x 2 x 24	1 x 24	1 x 24	2 x 2 x 22
Orientation	Vertical	Vertical	Vertical	Vertical	Horizontal
Porosity		0.22	0.38	0.38	0.23
Permeability, md		180			1,020
Q_v , meq/ml	0.034	0.039	0.019	0.017	0.039
Temperature, °F	77	85	85	85	168
Frontal rate, **ft/day	2.0	2.0	1.0	1.0	2.0
Comments		Acidized	Sand Pack	Sand Pack	

* Cylindrical

** Frontal rate = qL/V_p .

TABLE 7

SOLUTION DATA FOR FLOW EXPERIMENTS
(Concentrations in meq/ml at Temperature of Experiment)

<u>Experiment</u>	<u>Ca⁺⁺</u> <u>(C₁)</u>	<u>Mg⁺⁺</u> <u>(C₂)</u>	<u>M⁺⁺</u> <u>(C₁₂)</u>	<u>Cl⁻</u>	<u>Surfactant⁻</u>	<u>SO₄⁼</u>	<u>Volume</u> <u>Injected</u> <u>($\frac{v}{p}$)</u>
R	0.0103			0.040			3.00+
RA	0.0103			0.060			1.8
RB	0.0103			0.040			1.58
1230	0.1147	0.0000		0.1147			3.00+
1230A	0.0625	0.0000		0.5563			3.32
1230B	0.1003	0.0000		1.655			3.86
1230C	0.0000	0.0000		0.2497			4.33
1230D	0.0000	0.0000		0.0796	0.0118	0.0000	2.94
1230E	0.0000	0.0000		0.300			3.95
1094	0.1720	0.0953		1.257			4.85
1094A	0.0127	0.0074		0.0932			4.43
1094B**			0.0153	0.0730	0.0569	0.0256	3.78
1094C**			0.0055	0.0220			2.60
1094D			0.0000	0.1310			21.25
1094E**			0.0000	0.073	0.0592	0.0265	1.20
1094F**			0.0000	0.040			2.93
1095	0.0172	0.0953		1.257			4.70
1095A	0.0127	0.0074		0.0932			7.96
E-1	0.142	0.159		0.576			2.07
E-1A	0.0051	0.0056		1.576			1.98
E-1B	0.0117	0.0115		0.2537			2.14
E-1C	0.0278	0.0241		0.0976			2.09

*Solution RA displacing Solution R constitutes Experiment RA. Similar convention for all experiments.

**Solutions contained 600 ppm Dow Pusher 700 (TM). No other solutions contained polymer.

TABLE 8

ISOTHERM CONSTANTS - EXPERIMENTS WITHOUT SURFACTANTS
(Calculated for Concentrations Expressed in meq/ml at Temperature of Experiment)

Experiment	K_{m31}	K_{g31} (ml/meq) $^{1/2}$	K_{m21}	K_{g21} (ml/meq) $^{1/2}$	K_{m321}	K_{g321} (meq/ml) $^{1/2}$	N_{Pe}^{-1}	Root	Best Fit
RA	0.0053	0.470					0.0015	Small	Either
RB	0.0053	0.470					0.0015	Small	Either
1230A	0.0102	0.832					0.0025	One	K_m
1230B	0.0155	No Root					0.0020	Large	K_m
1230C	0.0072	1.078					0.0030	One	Either
1230	0.0110	0.955					0.0025		K_m
average									
1094A	0.0143	No Root	0.900	No Root	0.011	No Root	0.0013	One	K_m
1095A	0.0540	1.094	0.58	0.44	0.064	1.01	0.0030	Large	K_m
E-1C	0.0037	0.530	0.95	0.77	0.0037	2.4	0.0050	Small	K_m

TABLE 9

ISOTHERM CONSTANTS - SURFACTANT EXPERIMENT (1094 B-C)
(Calculated for Concentration in meq/ml @ 85°F)

	Figure		Source
	15	16	
Mass action, K_{m321}	0.011	0.011	From 1094A
Inverse Peclet, N_{Pe}^{-1}	0.0013	0.0013	From 1094A
Langmuir, a	0.293	3.5	History match
Langmuir b, ml/meq	30	800	History match
Mass action, K_{m51}		0.048	History match
Mass action, K_C , ml/meq		120	History match
Mass action, K_{321}			
Curve 2	10,000		Assumed
Curve 3	0.011		Assumed
Curve 4	0.0010		Assumed

for the constants in the isotherm Equations 4 through 7. There are generally two K values for each applicable isotherm equation and each set of data. Where this was the case, Table 8 indicates which of the two roots (K values) gives the best fit of the experimental data. It is this value that is tabulated.

Table 8 also gives values of the inverse Peclet number N_{Pe}^{-1} , which best describe dispersion observed in experiments. These values were obtained by history matching the experimental chloride-ion waves. In some displacements there was evidence of viscous instability, gravity instability, or heterogeneity effects. We chose to represent these effects in the model as dispersion, i.e., with higher inverse Peclet numbers.

Two-Cation Displacements, no Surfactant

For Experiment R, the Berea was saturated and equilibrated with a solution containing 0.04 meq/ml NaCl and 0.1 meq/ml CaCl₂. After the effluent concentrations became constant, the core was flooded with the original solution. This last displacement is designated Experiment RB in the tables. Experimental data (Fig. 19) show that cation exchange occurred and was reversible without obvious hysteresis effects. Model curves shown in Fig. 19 were calculated from the mass-action equation, but Gapon's equation describes the data equally well (Table 8). Lake and Helfferich used these same data and Gapon equilibria in the preceding sections.

In preceding and other flow experiments at low temperatures (60 to 95°F), it has been observed that steady-state concentrations of calcium and magnesium in effluent samples are usually slightly above the injected level. As shown later, experiments at higher temperatures yield much larger excesses that are associated with mineral dissolution. To eliminate, or at least minimize, interference from soluble minerals, Experiment

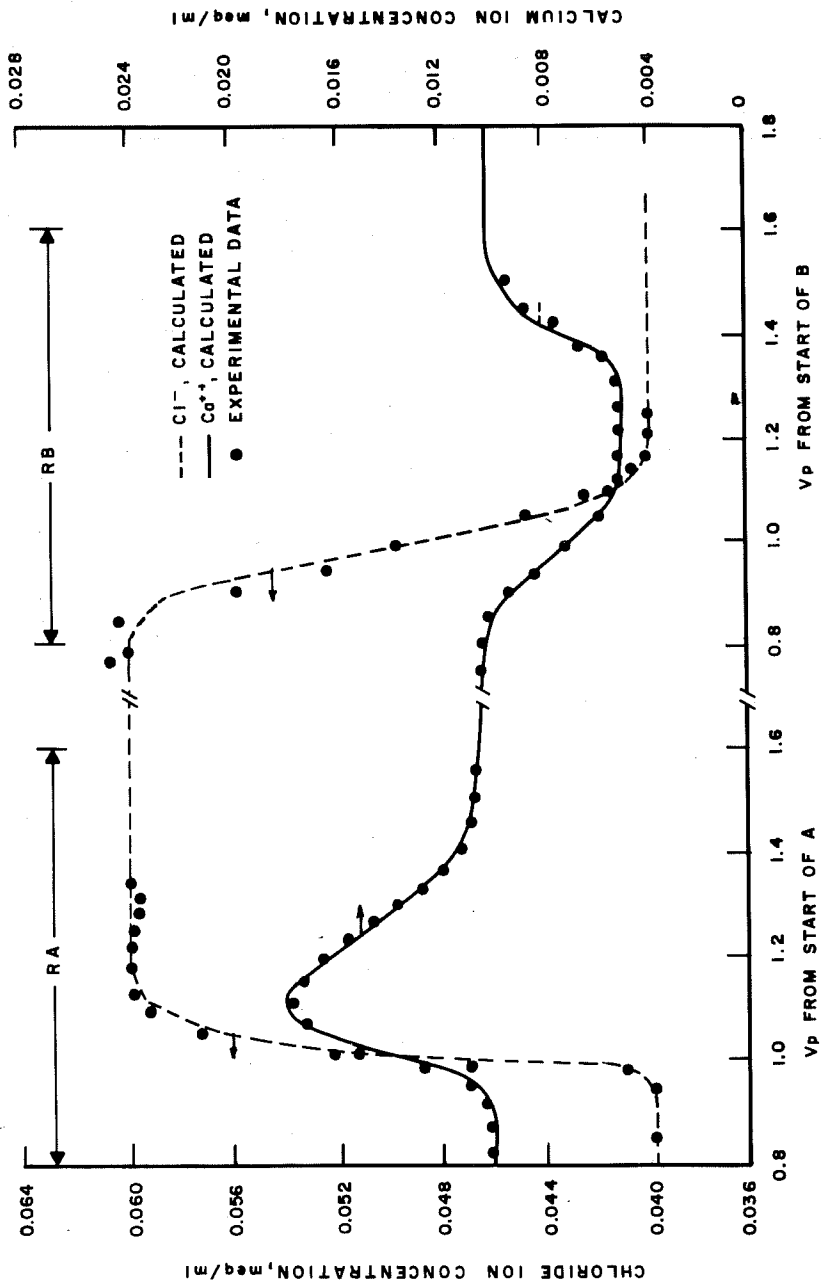


FIG. 19— Cation exchange; constant calcium concentration.

1230 was conducted in a Berea core after preconditioning floods designed to dissolve all minerals soluble in 0.1 N HCl and finally to restore core surfaces to a condition of equilibrium with near neutral pH (6.5 to 7.5) solutions. All preconditioning floods contained CaCl_2 , but no sodium or magnesium salts. The final equilibrating solution was 0.115 meq/ml CaCl_2 and C_1 should have been equal to Q_V . From this totally Ca^{++} form of clays, the core was displaced incrementally (1230A, B, and C) to the totally Na^+ form. Sodium-calcium mass-action solution ratios, C_3^2/C_1 , varied from zero to ∞ and total salinity as chloride-ion concentration varied from 0.115 to 1.665 meq/ml. Total excess calcium produced during the three displacements equaled 0.038 meq/ml of pore volume. This compares favorably with the value of 0.039 meq/ml obtained when the core in the sodium form later was subjected to a single displacement with CaCl_2 solution. On completion of the flow experiments, Q_V values were obtained for four small samples taken from the core. Values varied from 0.034 to 0.038 and averaged 0.036 meq/ml.

Material balance determinations of the excess calcium produced in each incremental displacement were used to determine the best fit value of the particular isotherm constants as given in Table 8. Since $C_3 = 0$ for displacements 1230A, and $C_1 = 0$ for displacement 1230C, only one value of K is obtained for each displacement. This eliminates choosing between two values by history matching procedures. Individual displacement values for isotherm constants were averaged and used to calculate the model results given in Fig. 20. As indicated in Table 8, the Gapon isotherm would not yield a solution for displacement 1230B and the known value of Q_V . For this case, K_{g31} values obtained from 1230A and 1230C were averaged, and this average K_{g31} was used to calculate all three displacements. Considering all three displacements, the mass-action isotherm describes the experimental data somewhat better than the Gapon isotherm. However, the results are essentially identical for Displacement 1230C.

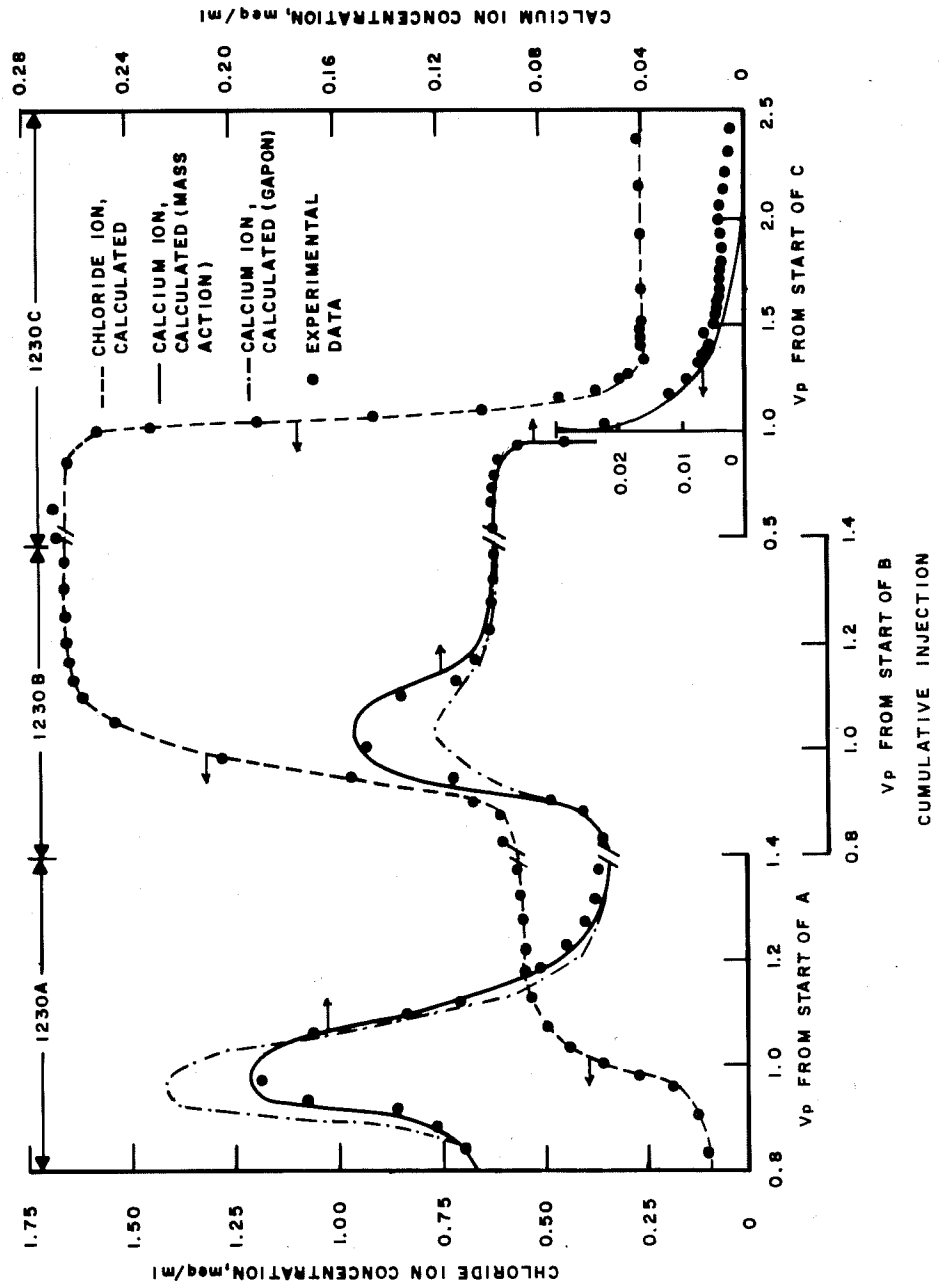


FIG. 20- Mass action vs Gapon equations.

This last displacement can be viewed as a preflood undertaken to reduce Ca^{++} concentration and total salinity before injecting a chemical slug. Displacement of total salinity was efficient, but Ca^{++} ion concentration in effluent after 2 PV injection was still 0.0004 meq/ml (80 ppm). Model results are lower, but model history shows that the long tailing of Ca^{++} is the result of the "mixing-zone" effect described by Lake and Helfferich.

Three-Cation Displacements, No Surfactants

Solutions containing both Ca^{++} and Mg^{++} were used in experiments in sand packs prepared from disaggregated Tar Springs (1094) and Berea sand (1095). Isotherm constants for the three-cation system (Table 8) could not be calculated for Gapon equilibria in the Tar Springs sand pack. Mass-action constants could be calculated for both packs and gave a slightly better fit of experimental data for the experiment yielding a Gapon solution (1095A). Model calculations for this last experiment (using the mass-action isotherm) are compared with experimental data in Fig. 21.

The isotherm constant, K_{m21} , for the Tar Springs sand pack was 0.95, indicating within experimental error that the clays in this pack exhibited zero selectivity between calcium and magnesium. Accordingly, the displacement was calculated as a two-cation displacement using the sum of Ca^{++} and Mg^{++} concentrations as one divalent cation, C_{21} . The resulting K_{m321} value is given in Table 8. Although the Berea sand pack gave both Gapon and mass-action constants, indicating the clays had about a two-fold preference for Ca^{++} over Mg^{++} , calculation as a two-cation displacement gives a good representation of the experimental data (Fig. 22). Experiment E-1C in a Berea core at 168°F gave a K_{m21} value of 0.95 and a K_{g21} value of 0.77, both indicating that

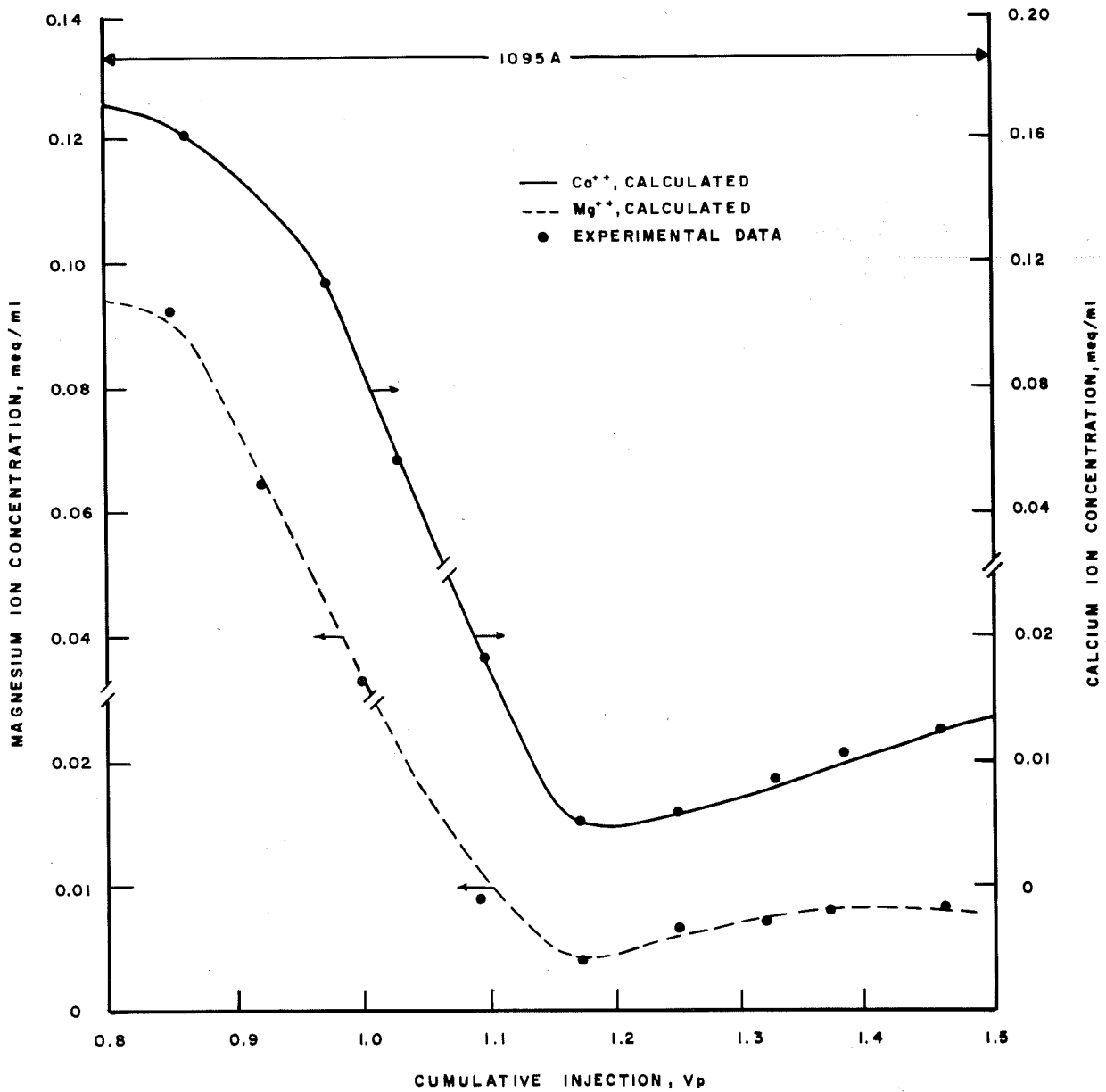


FIG. 21- Experiment 1095A as three-cation exchange

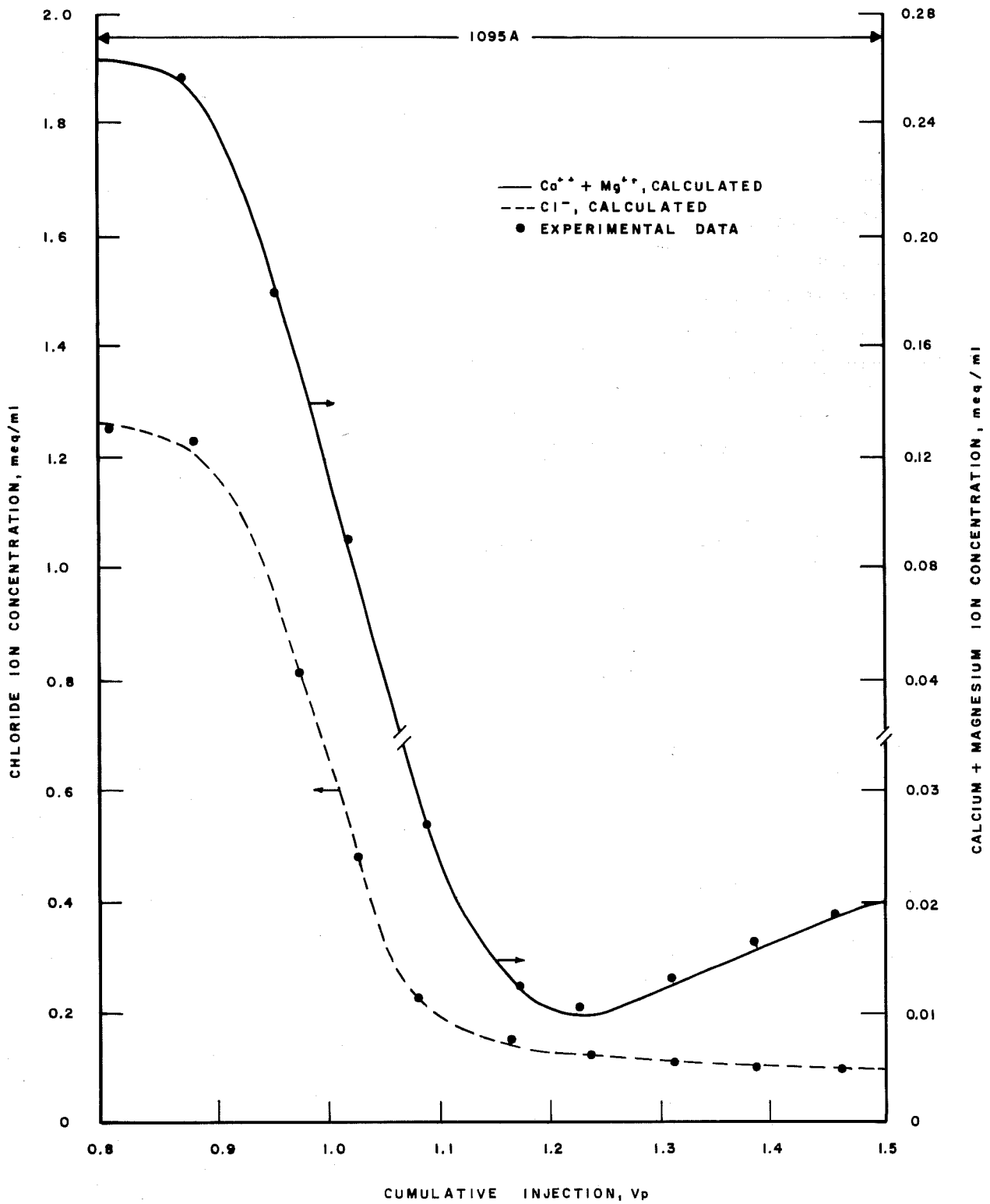


FIG. 22— Experiment 1095A as two-cation exchange.

this experiment also can be treated as a two-cation displacement. These results thus support Smith's conclusion that calcium and magnesium can be treated as a single divalent cation.

Smith's data were for Second Wall Creek and Berea sandstones. Considering these results, three different sandstones are shown to contain clays that do not exhibit enough selectivity between calcium and magnesium to be of practical significance in pre-flood considerations. Clay types are predominantly chlorite and kaolinite, but illite and small amounts of montmorillonite are present in at least one sand. These results essentially agree with those reported by others for natural soils and montmorillonite clay.

Cation Exchange at Elevated Temperature;
Mineral Dissolution

In low temperature experiments, effluent solutions usually reach a constant divalent-ion concentration of 0 to 20 ppm above the injected level. We have (as did Smith) attributed this to mineral dissolution. For these increased concentrations, we found that the model does not require addition of a solubility equilibrium expression if the steady-state concentrations for both the initial and final solutions are used in the exchange-isotherm calculations.

At elevated temperature (168°F), the discrepancy for Berea cores can be much higher, particularly when the solution salinity is high. In Experiment E-1, we observed produced divalent-cation concentrations that were as much as 0.035 meq/ml (700 ppm) higher than we were injecting. Total chloride-ion concentration of this solution was 1.58 meq/ml (56,000 ppm Cl⁻). Average divalent-ion effluent concentration after more than 2 PV was only 0.003 meq/ml (60 ppm) higher than injected, but during the first part of

Experiment E-1A (Fig. 23) individual samples varied widely from the average. Later displacements (E-1B and E-1C) at lower salinity showed decreasing average discrepancy and less variation between samples. After more than 8 PV, near the end of E-1C, average effluent, C_{12} , was 0.0015 meq/ml (30 ppm) higher than injected solutions, C_{12} . Concentrations in Table 7 for E-1 and E-1A are actual injection solution data. Calcium and magnesium concentrations for E-1B and E-1C are steady-state effluent averages that were used to calculate the K values given for this experiment in Table 8. Model results shown in Fig. 23 were calculated from the mass-action, two-cation isotherm using the tabulated values of solution concentration and K_{m321} . Simulation for the last displacement (E-1C) was good considering that chloride data showed that heterogeneity or instability effects were rather pronounced.

We believe these results indicate mineral dissolution. Adequate prediction of ionic concentrations in actual reservoirs will require knowledge about minerals present, their solubility as a function of temperature and total solution composition, and their abundance. Given this information, appropriate solubility functions can be incorporated into the model.

Displacements With Surfactants

Fig. 24 gives experimental data for a surfactant displacement in the Tar Springs sand pack. The displacing solution contained a mixture of two petroleum sulfonates. Nominal average equivalent weight of the two was 460 and 330, and these were used in proportions to provide an over-all average equivalent weight of 410. The displacing solution contained 0.047 meq/ml of this sulfonate mixture, 0.011 meq/ml NEODOL 25-3S, and 0.6% isobutyl alcohol, in addition to the other components listed in Table 7. Surfactant was delayed about 0.1 PV, peaked at about 1.1 times

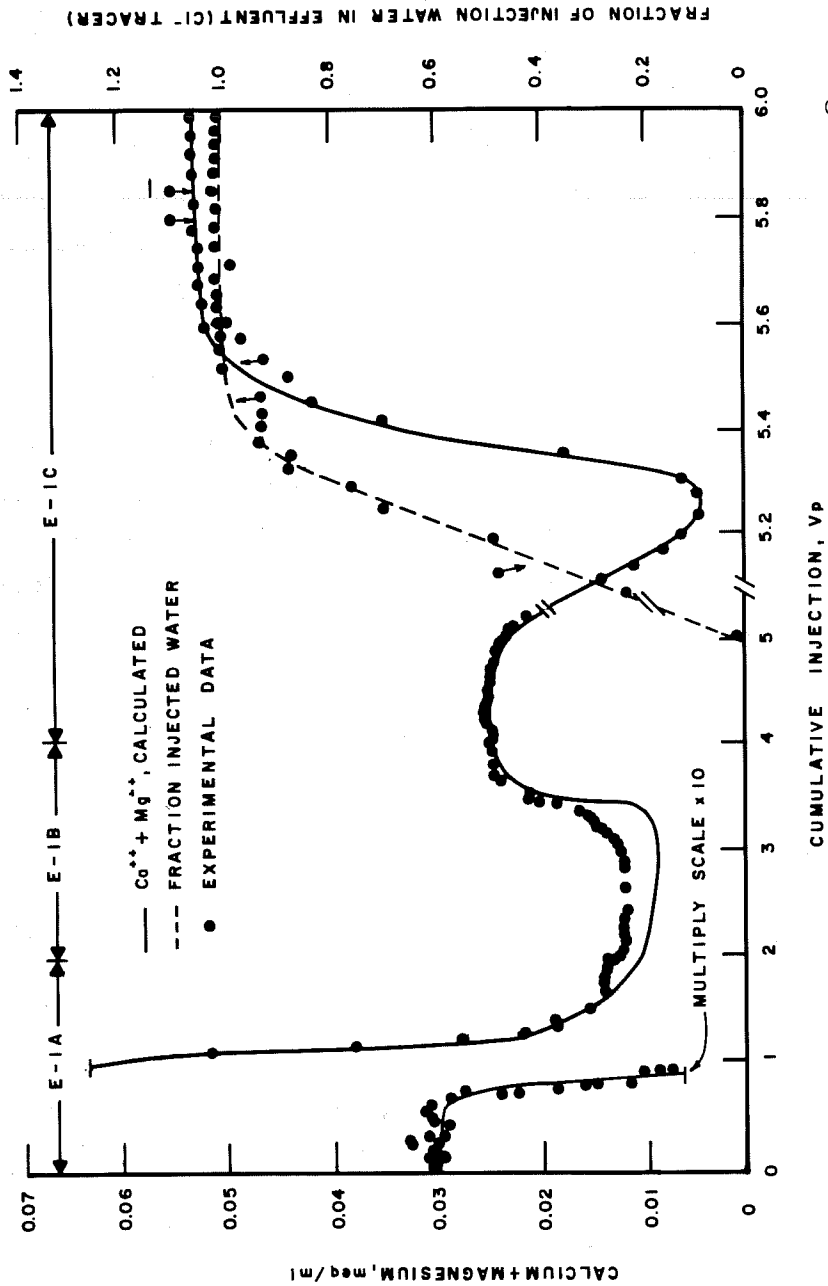


FIG. 23— Mineral solubility and cation exchange at 168°F.

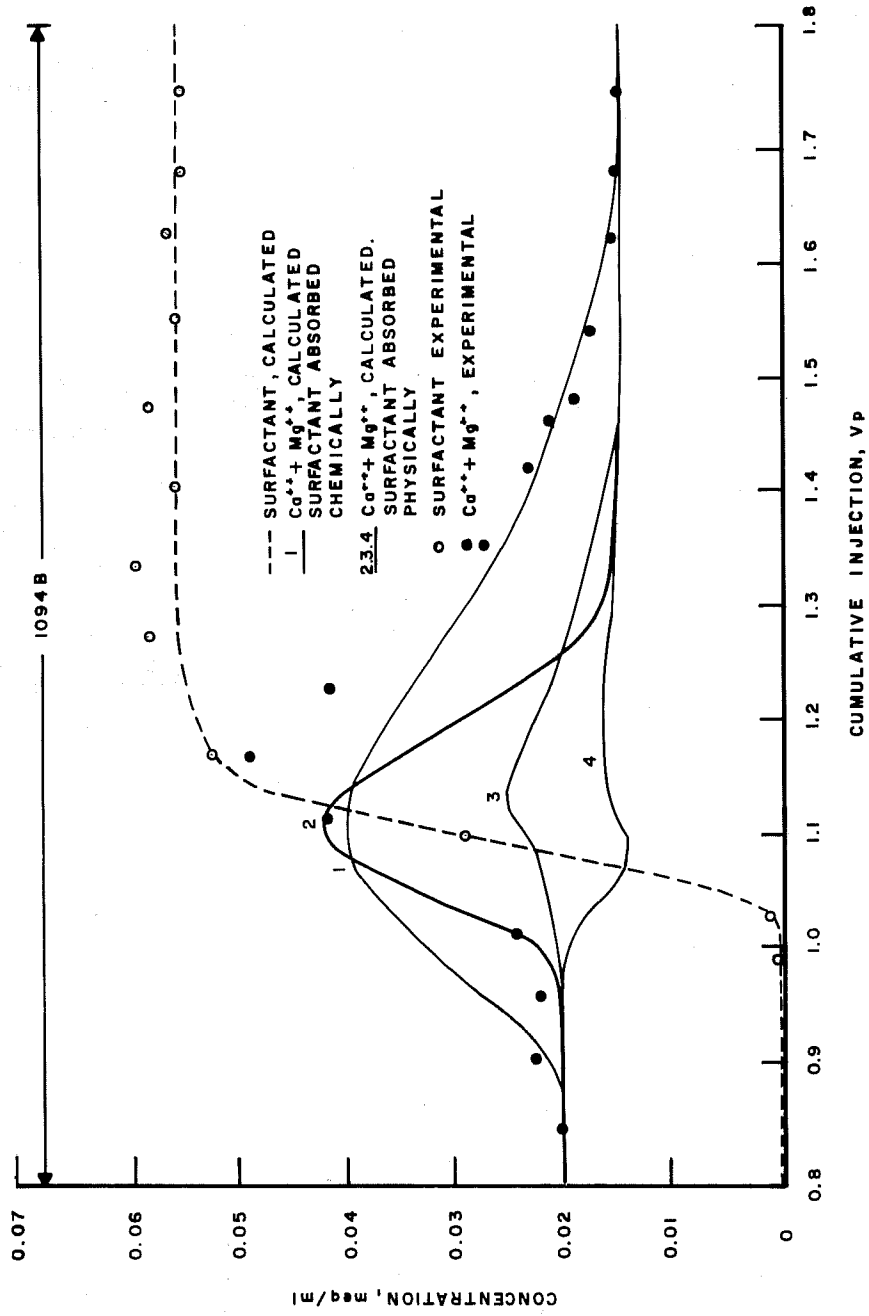


FIG. 24— Cation exchange; chemical vs. physical surfactant adsorption.

injected level, then returned to injection level. Divalent-cation concentration peaked slightly ahead of the surfactant peak and at a value about 3-4 times the injected level, then slowly declined to the injected level at 1.6 PV.

Our first efforts to simulate production history for this experiment also are shown in Fig. 24. We assumed that the cation exchange isotherm constant and inverse Peclet number determined for the previous displacement in this pack applied to the present displacement. We further assumed that adsorption of surfactant followed the Langmuir-type isotherm,

$$\hat{C}_6 = \frac{a C_6}{1 + b C_6} \quad (68)$$

where C_6 is surfactant concentration and \hat{C}_6 is adsorbed surfactant concentration in meq/ml of pore volume. This relation, with the values of a and b given in Table 9, yields the calculated surfactant curve in Fig. 24. The history match is good, except for the "overshoot" in experimental surfactant concentration.

To calculate divalent-ion concentration, additional knowledge is required regarding distribution of cations between adsorbed surfactant and the equilibrium solution. Curves 1 through 4 were obtained from various assumptions as follows:

Curve 1

Adsorption is chemical. The surfactant anion exchanges for an anion at the adsorbent surface and anion concentration in the flowing solution remains constant.

Curves 2 through 4

Adsorption is physical, anion is lost from the flowing solution. Electroneutrality then requires an equivalent loss of cations. We assumed that the cation associated with

adsorbed surfactant then could undergo exchange reaction as follows:



and, that mass-action isotherm applies. Thus,

$$\frac{\bar{C}_3^2}{\bar{C}_{21}} = \bar{K}_{321} \frac{C_3^2}{C_{21}} \quad (69)$$

where M^{++} represents $\text{Ca}^{++} + \text{Mg}^{++}$, and $^-$ indicates counter ions of the adsorbed surfactant.

Curves 2 through 4 are calculated for the values of K_{321} given in Table 9. Curve 2 is for the case of essentially all adsorbed surfactant in the sodium form. For Curve 4, about 65% of the adsorbed surfactant is in the calcium form. Actual divalent-cation effluent concentration reached a peak level later than calculated and about 20% higher than the maximum concentration predicted from any of the four assumptions.

Results of these simulations show that a different set of mechanisms leading to delayed but increase divalent-cation concentration is required to describe the experimental data. For the simulation given in Fig. 25, the following assumptions were used.

1. Langmuir chemical adsorption was assumed; a and b (given in Table 9) were selected to give adsorption about equal to experimental material-balance loss of surfactant for Displacements 1094B and 1094C (polymer drive following surfactant).
2. "Complex" formation was assumed, $M^{++} + \text{surfactant}^- \rightleftharpoons M \text{ surfactant}^+$ described by mass-action equilibria,

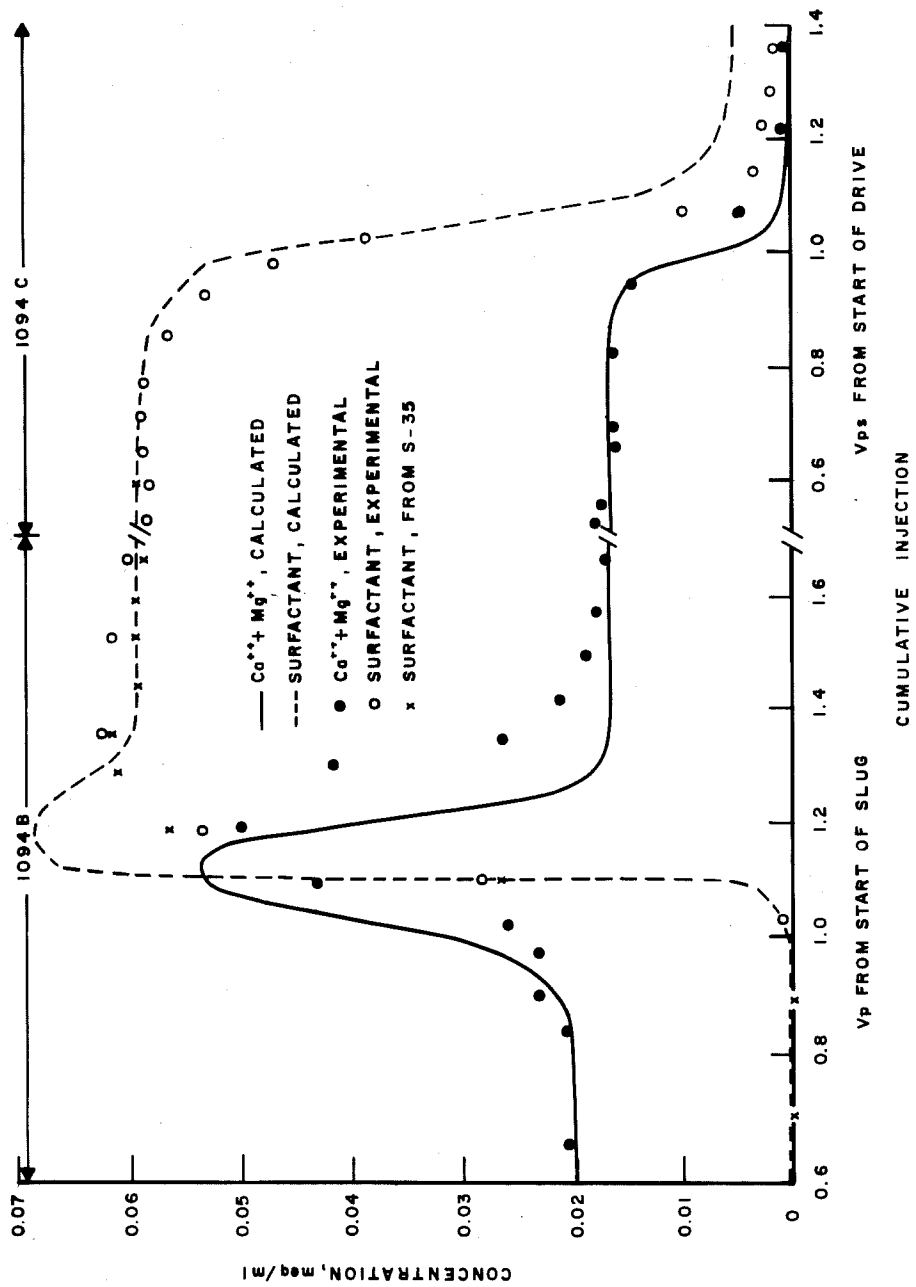
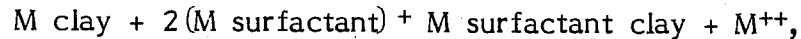


FIG. 25- "Surfactant complex" exchange and chemical adsorption.

$$K_C = \frac{C_5}{C_{21}C_6} \quad (70)$$

where C_5 is the concentration of the "complex".

3. Another assumption was cation exchange of the new specie.



described by

$$\frac{\bar{C}_3^2}{\bar{C}_{21}} = K_{m521} \frac{C_3^2}{C_{21}} \quad (71)$$

Constants, K_C and K_{m521} , used to calculate the history match simulation in Fig. 23 are given in Table 9.

We do not consider the match entirely adequate and recognize the speculative nature of the assumptions with their inherent difficulties, such as our failure to include micelle equilibria. Nevertheless, the simulation is appreciably better than those given by other assumptions. Surfactant left in the sand pack at the end of the simulation is, however, about 25% less than the 0.0037 meq/ml PV derived from the experimental data.

Chromatographic separation of the surfactant components has been reported by some investigators. Others have found no separation in their systems. To indicate whether separation of components was important in Experiment 1094B, we include tracer amounts of a linear alkyl benzene sulfonate (equivalent weight = 340) radioactively tagged with Sulfur-35. Fig. 25 shows that this tracer arrived coincidentally with the other surfactants.

Following the displacement shown by Fig. 25, we flooded the Tar Springs sand pack with 22 PV of pure sodium chloride solution

(1094D). We found (Fig. 26) that the cation exchange pulse of divalent ions was completely out of the pack after about 5 PV. Residual levels (~ 8 ppm) of divalent cations persisted after 20 PV. At this point, we flooded the pack with crude oil and waterflooded with the pure sodium chloride solution. Divalent-ion concentration in produced aqueous phase did not change. Displacement 1094E consisted of injecting the previously described surfactant system dispersed in pure sodium chloride solution. This was followed by Polymer Drive 1094F, also in pure sodium chloride solution. We observed a sharp increase in divalent-cation concentration as surfactant appeared in the effluent (Fig. 26). We have not attempted to simulate the data shown in Fig. 26.

The Berea sand pack (Displacement 1095) was subjected to displacements identical with Displacements 1094 A, B, C, D, E, and F. Each displacement gave results similar to those presented in 1094. In the displacement with surfactant and polymer drive in pure sodium chloride, the divalent-ion pulse arriving with surfactant was slightly larger than that shown for Displacement 1094E and F in the Tar Springs sand. This behavior contrasts sharply with Displacements (1230D and E) conducted in the acid-washed consolidated Berea core (Fig. 27). In the absence of carbonate minerals, we obtained no increase in divalent ion as sodium surfactant flowed through the core. These comparisons show that acid-soluble minerals are the dominant source of the divalent-cation pulses observed when surfactant flowed through the unacidized rock in the two sand packs.

The data in Fig. 27 also show that the surfactant front arrived at the outflow end of the core almost simultaneously with the nonadsorbing chloride-ion front. Since the surfactant solution contained only about $\frac{1}{2}\%$ total surfactant, this is an extremely small apparent frontal loss of surfactant. However,

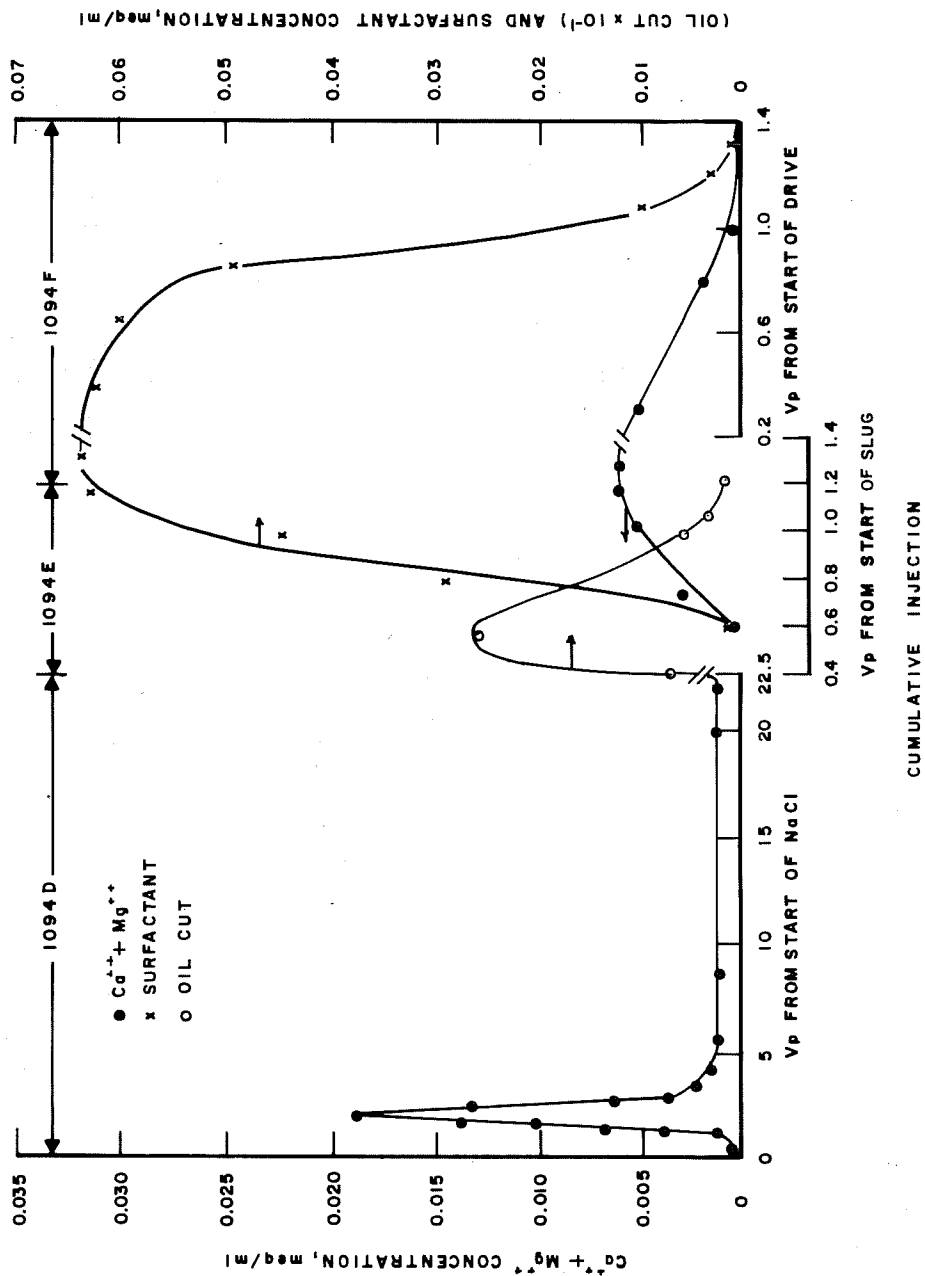


FIG. 26— Divalent cation produced by surfactant after NaCl
 preflood.

determining surfactant loss for this system by frontal lag is complicated because the system is subject to excluded pore volume in consolidated rock (Displacement 1230E). The excluded pore volume effect is not related to polymer, since neither surfactant flood nor its displacing solution contained polymer. When the observed $0.105 V_p$ excluded pore volume is added to the $0.02 V_p$ frontal lag, a total surfactant loss of $154 \mu\text{eq/gm}$ rock is obtained. This compares with the value of $158 \mu\text{eq/ml}$ from material-balance calculations, but contrasts rather sharply with the value of $830 \mu\text{eq/ml/gm}$ obtained for the Berea sand pack displacements with divalent-cation present (comparable to Experiments 1094B and 1094C). Thus, divalent cations and/or carbonate minerals play a dominate role in the adsorption of surfactant from this formulation.

To obtain some independent information about surfactant/divalent cation interactions, we measured apparent calcium ion activity as a 0.003 meq/ml solution of CaCl_2 was diluted with an 0.0565 meq/ml solution of the sodium surfactant system. To indicate the effects of dilution and changes in ionic strength, we first diluted a sample of the CaCl_2 solution with a solution equivalent to replacing the surfactant in the surfactant solution with NaCl . A comparison of the two sets of data (Fig. 28) shows clearly that either surfactant and calcium do interact or that the electrode response is altered severely by the presence of surfactant. Two observations argue for interaction; electrode response during the last five incremental additions a slope about equal to the slope of the line for dilution with salt water and electrode response to nonsurfactant systems was normal after the experiment was completed.

Careful observation during the dilution experiment revealed no evidence of surfactant precipitation. We believe, therefore, that divalent cation/surfactant interaction is indicated. If the

simple complex described by Equation 70 is assumed the only interaction, values of K_C can be calculated for each experimental point. These values vary from 23 to 66, averaging 43. We used a value of 120 to obtain the history match in Fig. 25. Our experience with the divalent cation electrode system indicated that exposure to the subject surfactant at concentrations of 0.05 meq/ml can significantly alter electrode response. We believe, therefore, that the data in Fig. 28 have only qualitative significance.

Froning and Treiber suggested that certain clay minerals may have normally unexposed exchange sites that are exposed by the surfactant²³. If the counter-ions for these newly exposed sites are divalent cations, a new source of these ions is available. Such a mechanism might explain the observed divalent ion pulses in Experiments 1094 and 1095. Unless, however, the acid pretreatment in Experiment 1230 exposed these sites, our results argue that such sites do not exist in Berea sand.

There are undoubtedly alternative mechanisms that can explain our observations. Those we have used are sketchy and will be revised significantly as research continues. The essential point is that new knowledge about interactions between components of the reservoir and the solutions we inject into the reservoir is essential if we are to improve oil-recovery processes and simulation of these processes. We have discussed some aspects of cation exchange, adsorption, divalent cation/surfactant interaction, and mineral dissolution. We have not considered interactions with the oil phase in the reservoir, and we are confident these interactions can be significant and ultimately will have to be included in any reasonably complete model.

CONCLUSIONS

1. Cation exchange equilibria exert an important influence on the ionic composition of aqueous fluids flowing through reservoirs containing clay minerals.
2. For simple aqueous solutions comprised predominantly of sodium, calcium, and magnesium chlorides, mass-action isotherms adequately represented all of our experimental data. The Gapon isotherm describes significant amounts, but not all data satisfactorily.
3. For the specific cases we studied, solution concentrations adequately represented the data; activities were not tested.
4. As previously reported by Smith, calcium and magnesium can be treated as a single divalent specie for purposes of cation exchange calculations. This in no way implies that Ca^{++} and Mg^{++} have the same effect on surfactant systems.
5. Preflooding to convert clays totally to the sodium form may be essentially impossible when soluble minerals are present. Even though soluble minerals are absent, large volumes of preflow may be required.
6. Given the cation exchange capacity, experimental data for the mass-cation constant, and analytical data for the in-situ waters, the mass-action isotherm can be used to optimize design of preflows.
7. Limited evidence suggests that divalent cation/surfactant interaction exhibits characteristics of complex-ion formation.

8. Surfactant adsorption in Berea rock is dominated by adsorption (exchange) of a divalent-cation/surfactant interaction specie and/or acid-soluble minerals.

9. Further knowledge regarding interactions between the surfactant system and reservoir components, such as rock minerals, crude oil, and divalent cations, is required before calculation of the changes in the ionic environment of a surfactant flowing through the reservoir can be accomplished satisfactorily.

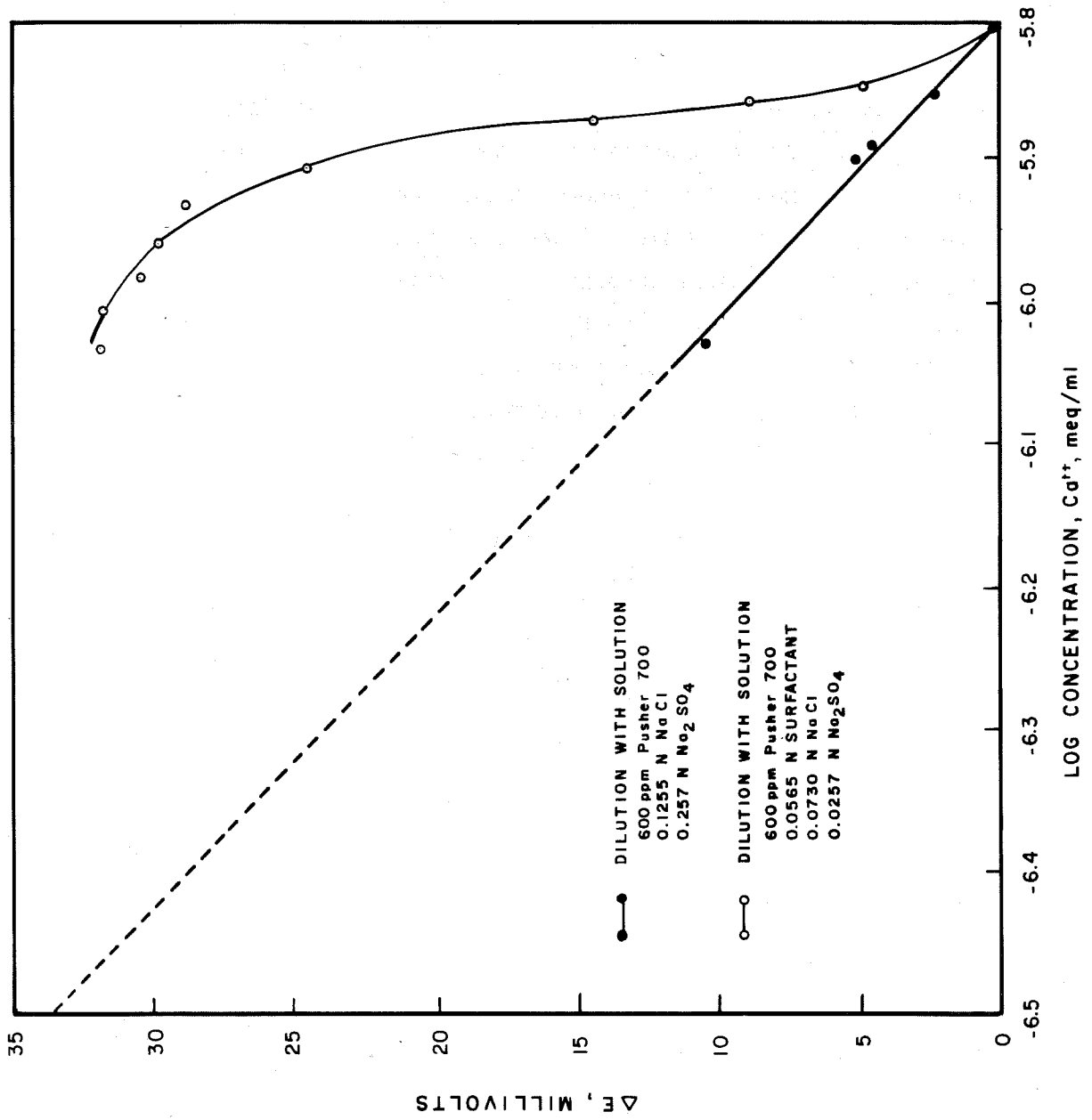


FIG. 28- Surfactant-calcium ion interaction; Orion divalent cation electrode.

The following account is taken from the report of F. W. Smith entitled "Ion-Exchange Conditioning of Sandstones for Chemical Flooding"⁶⁹.

INTRODUCTION

One current obstacle to the widespread use of certain tertiary oil recovery processes is the reservoir ionic environment that injected fluids must withstand. Those processes based on micellar fluids containing substantial quantities of anionic surfactants (such as petroleum sulfonates) may be particularly vulnerable to the effects of high salinity or moderately high multivalent-cation concentration. Even when acceptable chemical formulations exist for specific ionic conditions, oil displacement efficiency may suffer if the reservoir brine composition is not reasonably constant throughout the reservoir. Reservoir conditioning is attempted primarily for these reasons. By injecting a brine of the desired composition ahead of a slug of micellar solution, the most favorable circumstances for effective performance of the chemicals may be established.

This study examines the efficiency of preflushing in situations where ion exchange phenomena are important. In particular, the replacement of divalent cations (such as calcium and magnesium) by less offensive monovalent cations (such as sodium) was studied. The effects of soluble minerals like gypsum or anhydrite were not considered; their behavior can be described adequately by relatively straightforward solubility relationships. Also, the use of chemicals in the preflush brine to react with divalent cations by precipitation or complex ion formation was not determined. It is hoped that this study can be used to determine whether such chemical treatments are needed.

Basic Considerations

Ion exchange is a process in which an ion bound to a surface is replaced by another ion of like electrical charge from a surrounding solution. In the simplest exchange cases, the total ionic charge on the surface does not change, nor does the bulk concentration of ionic charge in the solution. Thus, even though the solution chemical composition may change, salinity will not change when defined as total equivalents of cations per unit volume.

Among the usual components of sandstone petroleum reservoirs, clay minerals are well known for their ion exchange properties. The cation exchange capacities vary from about 10 meq (milliequivalents)/100 gm of kaolinite to about 100 meq/100 gm of montmorillonite.

Other sandstone materials reported to possess ion-exchange properties are quartz, feldspars, and organic matter. The exchange capacities of quartz and feldspars are usually quite low, but the capacity of solid organic matter may be as high as 150 to 500 meq/100 gm.

The major factors that appear to influence cation exchange and, thus, preflush efficiency are cation exchange capacity, brine composition, shape of exchange isotherms and brine salinity.

Fig. 29 shows two hypothetical exchange isotherms of an ion exchanging substance in contact with a solution containing two cationic species. These curves represent the quantity of one species adsorbed on the ion exchanger as a function of its relative concentration in solution. The variable x describes the fractional concentration of the species of interest when concentrations are expressed in equivalents per unit volume. Thus,

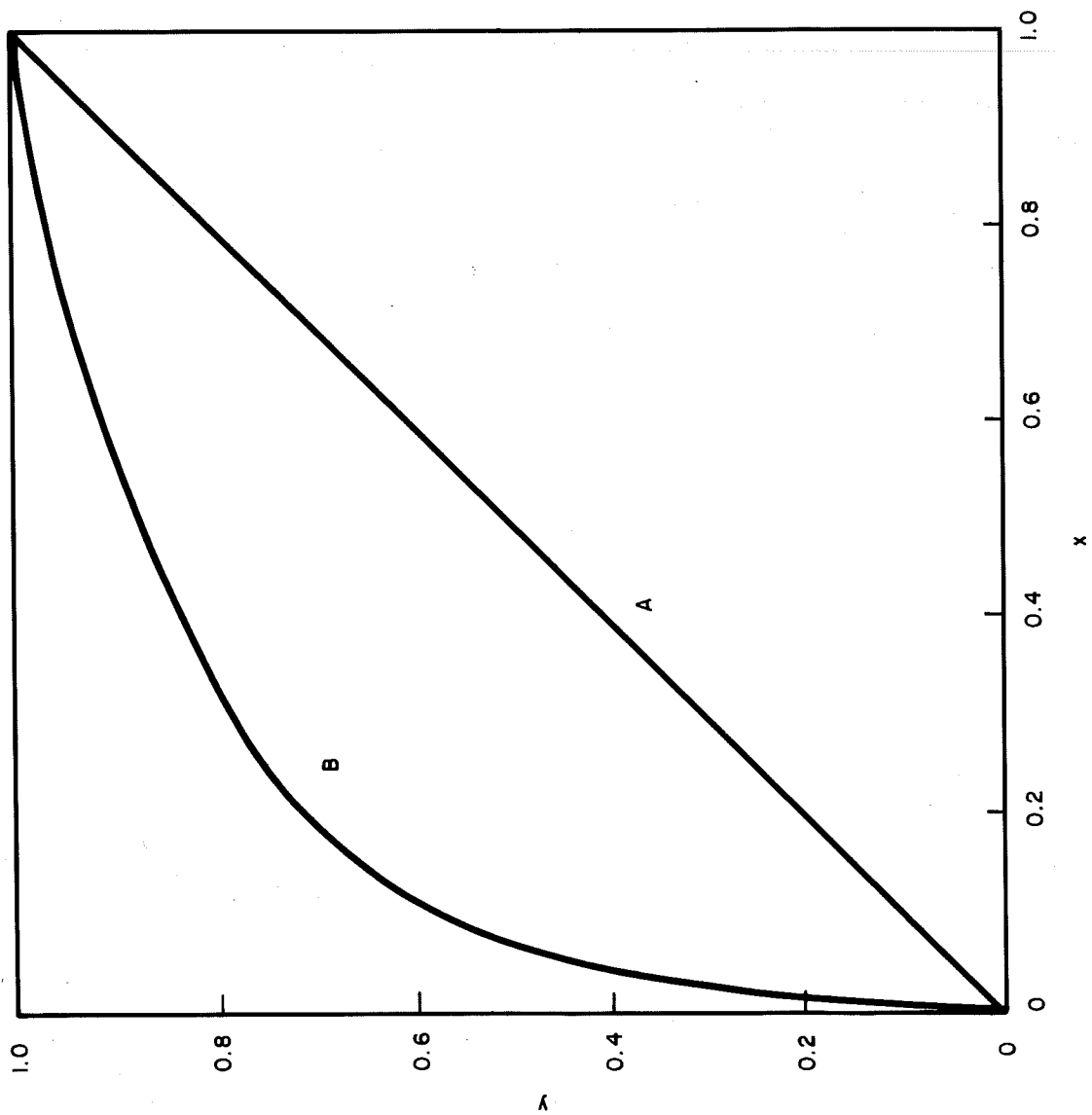


FIG. 29— Hypothetical ion-exchange isotherms.

$$X = C/C_t \quad (72)$$

where C is the concentration of cations in solution. The variable y gives the adsorbed quantity of the species of interest as a fraction of the Q_v , " y " and " x " describe the adsorbed and dissolved concentrations of divalent cations, respectively, in a system also containing a species of monovalent cations. Because of the electrical charge, 1 mol of divalent ions is equivalent to 2 mol of monovalent ions.

Curve A in Fig. 29 represents an exchange isotherm where the exchanger has no greater affinity for divalent ions than for monovalent ions. The dimensionless, adsorbed concentration y is always equal to the bulk solution concentration x . However, Curve B is more typical of real ion exchange systems. Divalent ions are attracted more strongly to the exchanger than monovalent ions, and the fraction of exchange sites occupied by divalent ions is greater than the fraction in solution. At low divalent ion concentrations, relatively small changes in equilibrium solution concentration cause large changes in divalent-ion adsorption levels. At high divalent-ion concentrations, the adsorption level is high and not very sensitive to changes in solution composition.

The curves of Fig. 29 can be approximated by an equation of the form

$$y = x / \left[x + (1 - \lambda) / \beta \right] \quad (73)$$

where β , the "separation factor," reflects the affinity of the ion exchanger for divalent ions. As used here, β is the ratio of relative adsorption levels of the two ionic species:

$$\beta = \frac{y/x}{(1-y)/(1-x)} \quad (74).$$

A value of $\beta = 1$ gives Curve A of Fig. 29, and increasing values of β produce the typical convex exchange isotherms corresponding to greater attraction for divalent ions. A selectivity coefficient (which implies validity of the mass-action law by incorporating the valences of the two ionic species) also may be used to describe ion exchange equilibria, regardless of their theoretical bases. Modifications of Equation 73 were found to be satisfactory, but this does not imply that other expressions would not be suitable.

EXPERIMENTAL CHARACTERIZATION OF CORES

All procedures were performed at an ambient temperature of $74 \pm 2^\circ\text{F}$. Table 10 describes the properties of the cores used. Berea cores were studied because of their widespread use in laboratory experiments and Second Wall Creek cores from the Salt Creek field, Natrona County, Wyoming, were studied because the reservoir is a candidate for micellar flooding. Table 10 gives values for the dimensionless dispersion coefficient, $K_1/(v_f l)$, for three cores. These values were determined by displacing a brine from the cores with a brine of the same chemical composition at a different concentration level. The effluent concentration data were used in the standard manner to evaluate the dispersion coefficient. The data suggested a small amount of dead-end pore volume in the cores, but this was ignored.

Table 10 also gives Q_v values for three cores determined for sodium-calcium exchange. Because of the nearly identical experimental behavior of Berea Cores MS3 and MS4; the Q_v and dispersion coefficient were obtained only for Core MS4. The ion exchange capacity for Second Wall Creek cores is three to

TABLE 10

PHYSICAL PROPERTIES OF CORES

	<u>Berea Cores</u>		<u>Second Wall Creek Cores</u>	
	<u>MS3</u>	<u>MS4</u>	<u>SC3</u>	<u>SC4</u>
Permeability, md	Not determined	195	98	32
Porosity, %	22.3	22.4	22.7	21.5
Length, cm	30.1	30.1	27.0	29.7
Pore volume, ml	134.9	135.3	32.4	32.4
Dimensionless dispersion, $K/(v_F L)$	Not determined	0.0051	0.0068	0.036
Q_v , meq/ml of PV	Not determined	.047	.175	.147

TABLE 11

X-RAY DIFFRACTION ANALYSIS OF CORES

<u>Sample</u>	<u>Quartz</u> (percent)	<u>Feldspar</u> (percent)	<u>Kaolinite</u> (percent)	<u>Kaolinite +</u>		<u>Montmorillonite</u>
				<u>Chlorite</u>	<u>Illite</u>	
Core SC3 (whole rock)	87	7	5			
Core SC3 (<0.5)	Low			High		Intermediate
Core SC4 (whole rock)	92	5	2			
Core SC4 (<0.5)	Low			Intermediate		High
Berea (whole rock)	94	1	5		Trace	
Berea (<0.5)		Low	Intermediate		High	

TABLE 12

BRINE COMPOSITIONS

	Ion Concentration (meq/liter)		
	<u>Second Wall Creek</u>	<u>Madison</u>	<u>Preflush*</u>
Na ⁺	194.0	31.0	250.0
Ca ⁺⁺	1.2	15.2	---
Mg ⁺⁺	6.8	3.8	---
Cl ⁻	130.0	19.3	219.3
HCO ₃ ⁻	70.4	1.9	1.9
SO ₄ ⁼	1.6	28.8	28.8
Total Salinity	202.0	50.0	250.0

*Preflush brine prepared from soft Madison brine with addition of 200 meq/liter of NaCl.

four times that of Berea cores. X-ray diffraction analyses of disaggregated whole rock (Table 11) indicate that the most abundant material of substantial ion exchange capacity in both rocks is kaolinite. However, the amount of kaolinite present is not consistent with the relative exchange capacities. Table 11 shows that by separating the samples into small particle-size fractions, montmorillonite becomes evident in the Second Wall Creek material but not in Berea material. Recently, Froning and Treiber also reported the presence of montmorillonite in Second Wall Creek sandstone. Because of its high Q_v value, montmorillonite could be responsible for the differences in exchange capacities between the two types of rock. There was no X-ray evidence of appreciably soluble minerals, such as gypsum or anhydrite, in either sandstone.

Fig. 30 illustrates sodium-calcium exchange isotherms for Second Wall Creek Core SC3. The four sets of data shown represent results of individual experiments. Three experiments were conducted at a salinity of 0.250 meq/ml., the strength of the preflush brine proposed for the Second Wall Creek reservoir. Two experiments were performed with calcium concentration increasing and one with calcium concentration decreasing. The three groups form a relatively smooth curve with no evidence of hysteresis. The fourth set of data was obtained at a total salinity of 0.050 meq/ml., the strength of the Madison brine with which the reservoir was waterflooded. The shape of this isotherm shows a considerably greater affinity of the core for the calcium than at the high salinity, which can affect the concentration profile of divalent ions when Madison brine is displaced from the core by preflush brine.

Fig. 31 shows the exchange isotherm for Core SC4 with calcium concentration decreasing at 0.25 meq/ml. The shape of the curve is qualitatively similar to that of Core SC3, but it suggests a somewhat greater affinity for calcium ions.

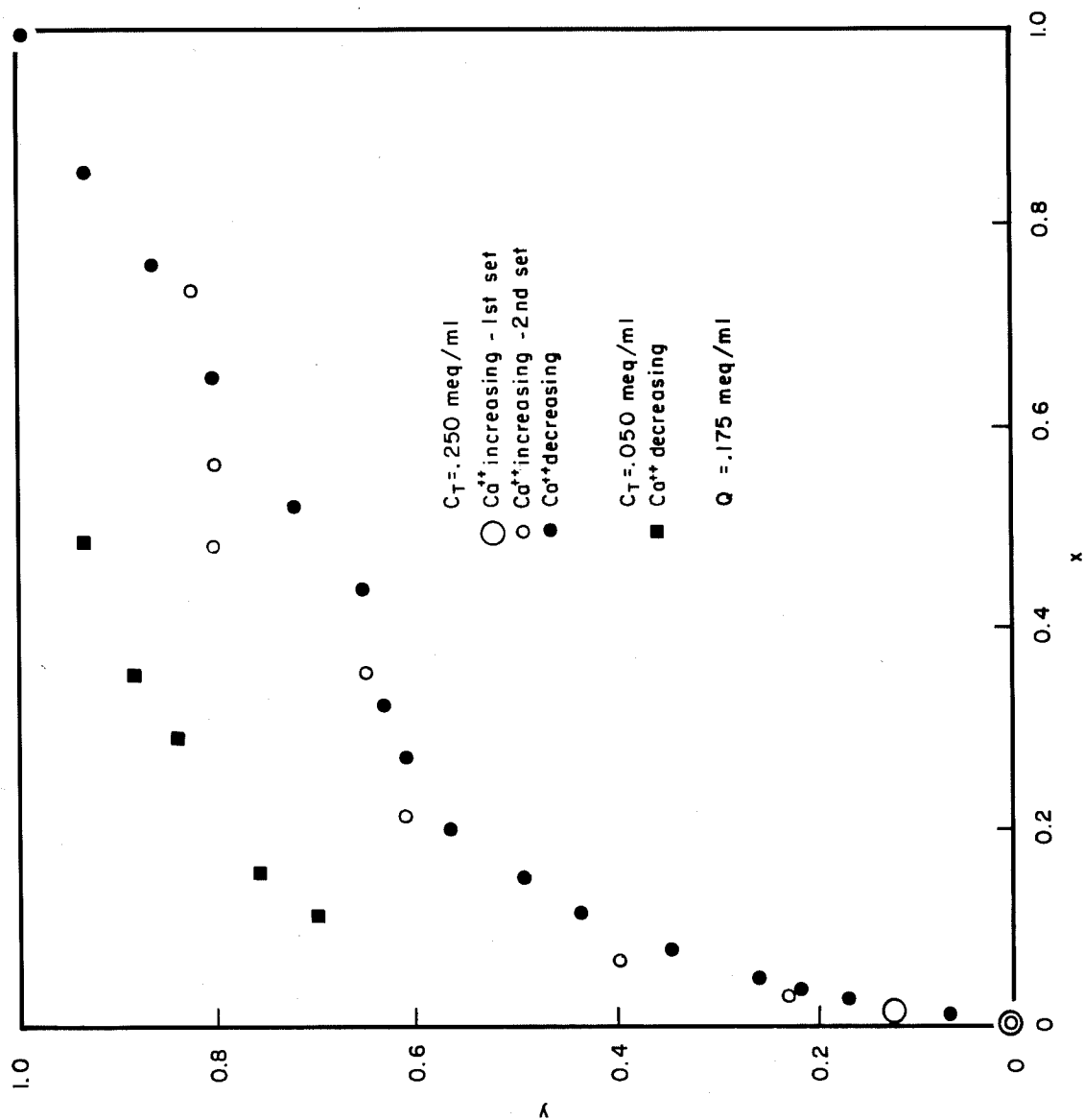


FIG. 30 - Calcium-sodium ion exchange in Second Wall Creek Core SC3.

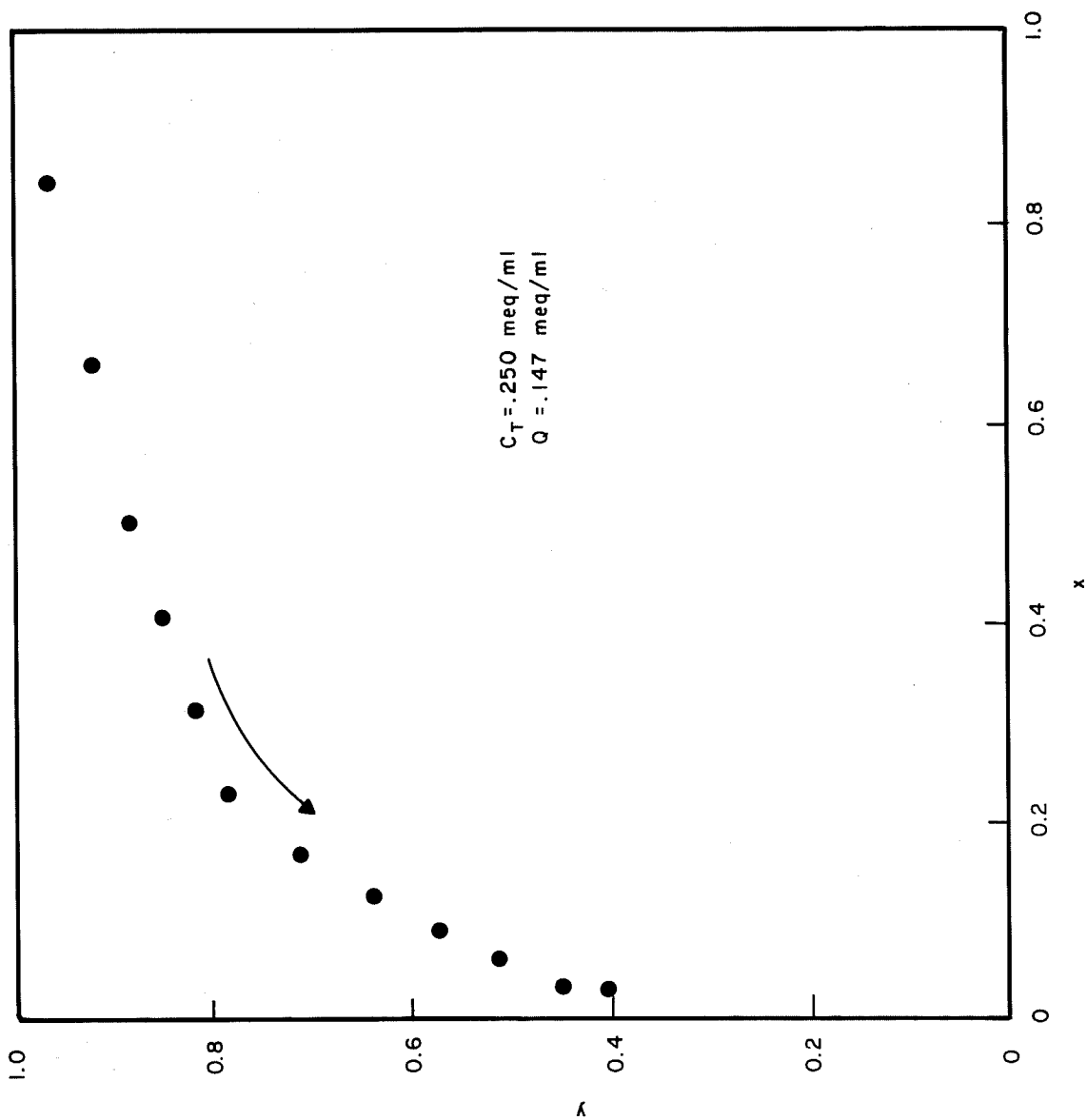


FIG. 31— Calcium-sodium ion exchange in Second Wall Creek Core SC4.

Core SC4 exhibited a preference for calcium ions as did the Second Wall Creek cores. However, the calcium increasing exchange curve did not coincide with the calcium decreasing curve. It was not clear whether the apparent hysteresis was real or was an experimental artifact.

COMPARISON OF EXPERIMENTAL WITH CALCULATED RESULTS

Several divalent cation saturation/elution experiments were performed with test cores. The brine compositions used were selected to simulate the current waterflooding and proposed preflush brine injection sequence in the Second Wall Creek reservoir. Table 12 gives the chemical make-up of both brines and of the synthetic Second Wall Creek brine with which the Second Wall Creek cores were saturated initially. Although the actual compositions of the brines varied somewhat from one preparation to the next, all batches were analyzed chemically. Generally, the fluid pore velocity was 2 ft/day in the field cores and 1.5 to 3 ft/day in the Berea cores.

Experiments With Berea Cores

Fig. 32 illustrates two Madison brine saturation/preflush-brine elution cycles in Core MC3. More than 2 PV of Madison brine was required before the effluent divalent cation concentration reached that of the injected brine. Subsequent injection of the divalent cation-free preflush brine led to a peak of produced calcium and magnesium concentration that was about three times greater than the concentration in Madison brine. The divalent ion concentration did not decrease to the level of Madison brine until approximately 1.4 PV of preflush brine had been injected. A high degree of reproducibility in the results was evident from the close agreement between the two sets of data points.

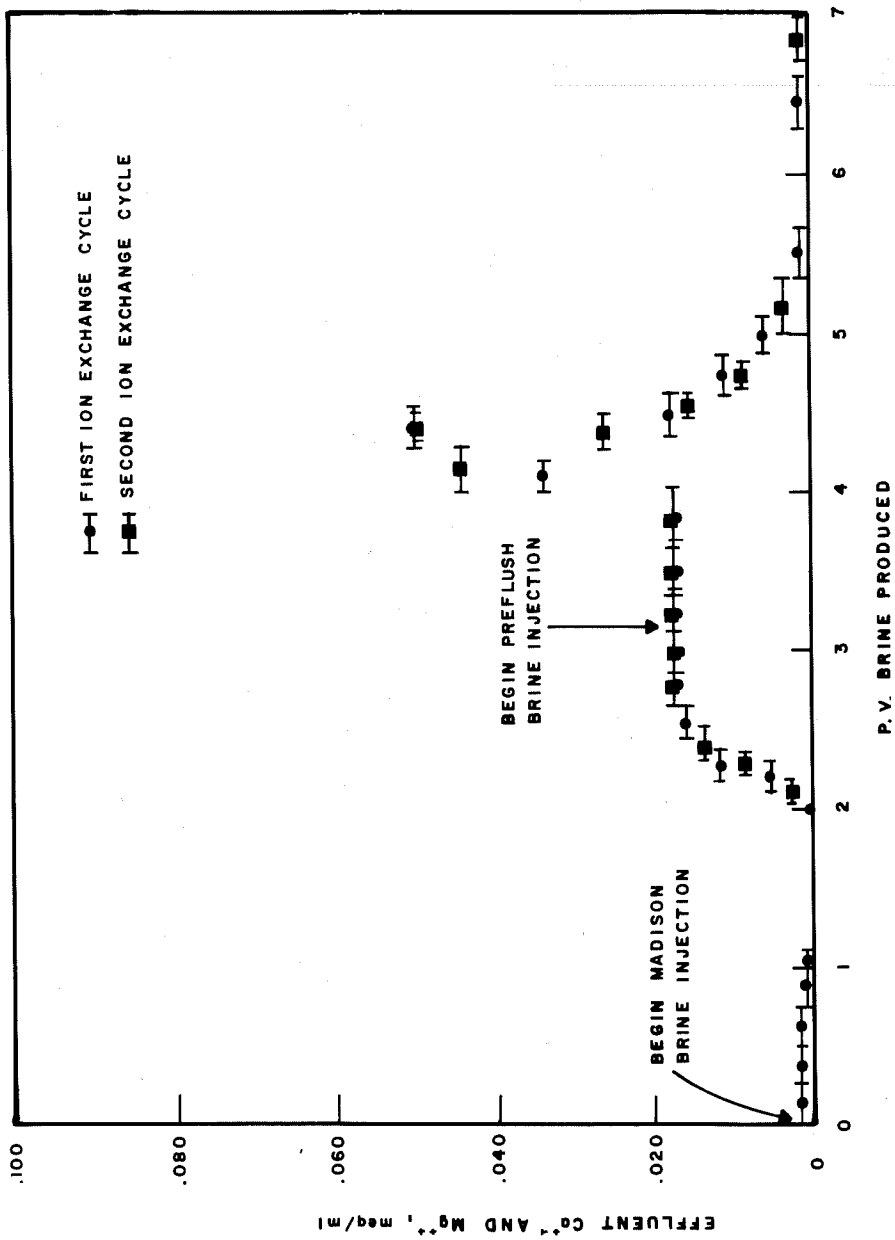


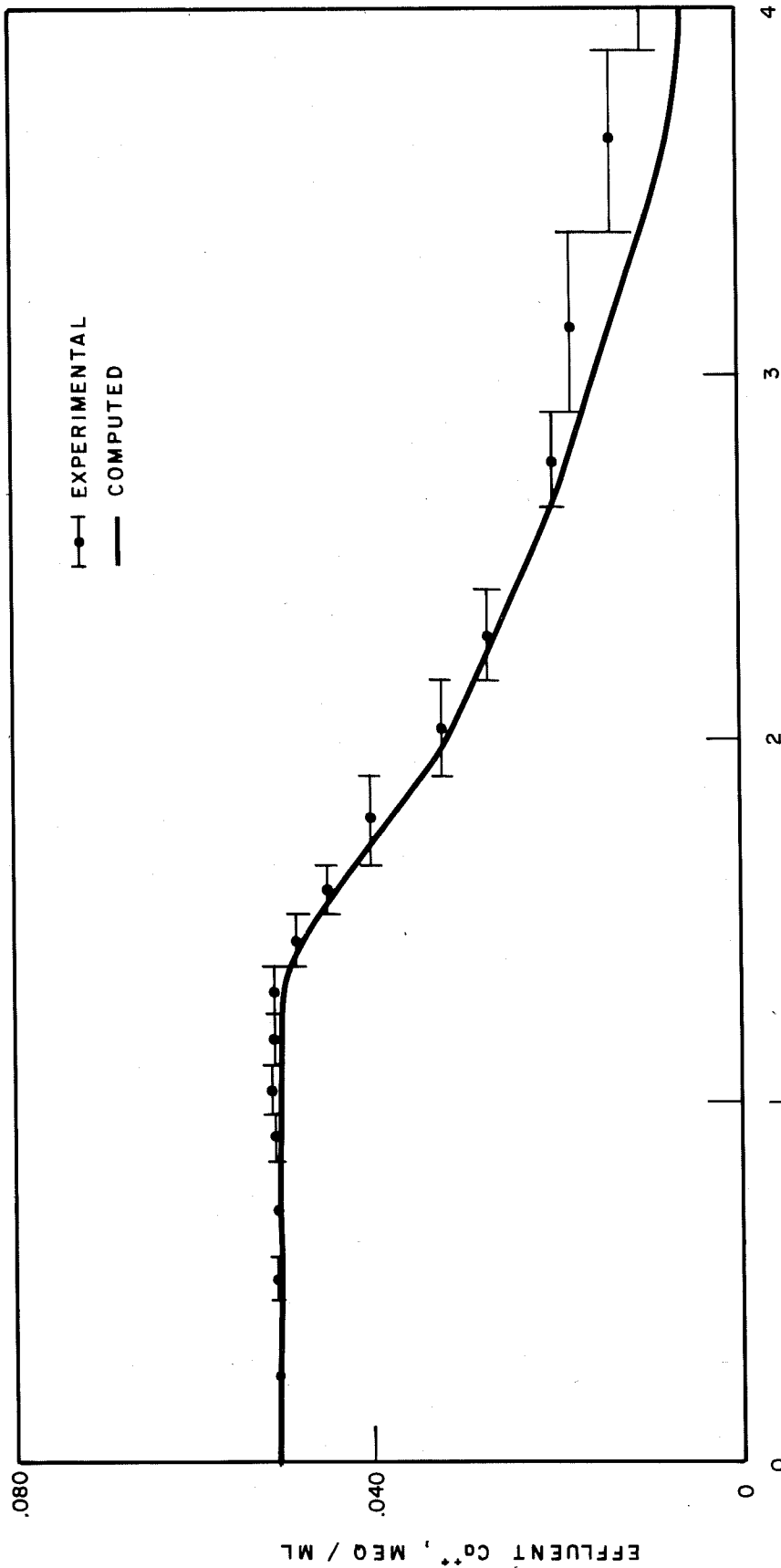
FIG. 32 — Madison brine saturation/preflush brine elution in Berea Core MS3.

A similar experiment was conducted in the companion Berea core, MS4. The saturation/elution behavior was almost identical to that shown in Fig. 32. During this experiment, however, the fluid velocity varied from 1½ to 3 ft./day before and after the eluted divalent-ion peak was produced. Results indicated the absence of flow-rate dependence, i.e., local ion exchange equilibrium existed in the core. Other results from this run were as follows:

1. Hydrogen ion exchange was negligible. After beginning preflush brine injection, the effluent pH increased from 8.0 to 9.1 at the divalent ion peak, then soon decreased to the pH value of preflush brine, 8.4. Thus, the maximum hydrogen ion concentration change amounted to less than 10^{-8} meq/ml.
2. No evidence was found for anion exchange. Produced samples near the divalent cation peak were examined for sulfate content. In spite of the large change in chloride concentration caused by the arrival of preflush brine, no significant change in sulfate concentration was observed.
3. The material balance of calcium and magnesium ions was excellent. Using a correction for presumed mineral solubility, the quantity of produced divalent cations was within 4 percent of that injected during a complete saturation/elution cycle.

Experiments with Second Wall Creek Cores

Fig. 33 describes the results of a constant salinity experiment in Core SC3. This core first was equilibrated with a solution containing 0.050 meq/ml, CaCl_2 + 0.200 meq/ml. NaCl .



P.V. BRINE PRODUCED

FIG. 33— Constant salinity elution in Second Wall Creek Core SC3: .250 meq/ml NaCl displacing .50 meq/ml CaCl₂ + .200 meq/ml NaCl.

Subsequently, several pore volumes of 0.250 meq/ml NaCl were injected to elute the absorbed calcium. Using the empirical relationship

$$y = \frac{x}{x + \left(\frac{1-x}{6}\right)} - \frac{x}{4}$$

to represent the 0.250 meq/ml exchange isotherm for the core (for $x \leq 0.2$ in Figure 30) and the approximate physical properties from Table 10, the solid curve of Fig. 33 was computed with a mathematical mode. Assuming homogeneity of the physical and chemical rock properties and using only the experimentally derived parameters of Table 10 and the preceding ion exchange expression, the simulated results agree well with experimental calcium ion effluent concentrations.

The results of a similar experiment with Core SC4 are presented in Fig. 34. The calculated curve was obtained by matching the exchange data of Fig. 31 for $x \leq 0.2$ with the equation

$$y = \frac{x}{x + \left(\frac{1-x}{15}\right)} - 0.15x$$

Again, the simulated curve agrees closely with the experimental points.

To simulate the displacement of Madison brine by preflush brine injection, one must account for the change of isotherm shape with salinity. This was done for Core SC3 by treating calcium and magnesium ions as a single specie and fitting the isotherm for each salinity level to the form of Eq. 73. By making the parameter β a linear function of salinity, C_t , an approximate description of the exchange isotherm from 0.050 to 0.250 meq/ml, was obtained as $\beta = 17.25 - 45 C_t$ where C_t is in units of milliequivalents per ml.

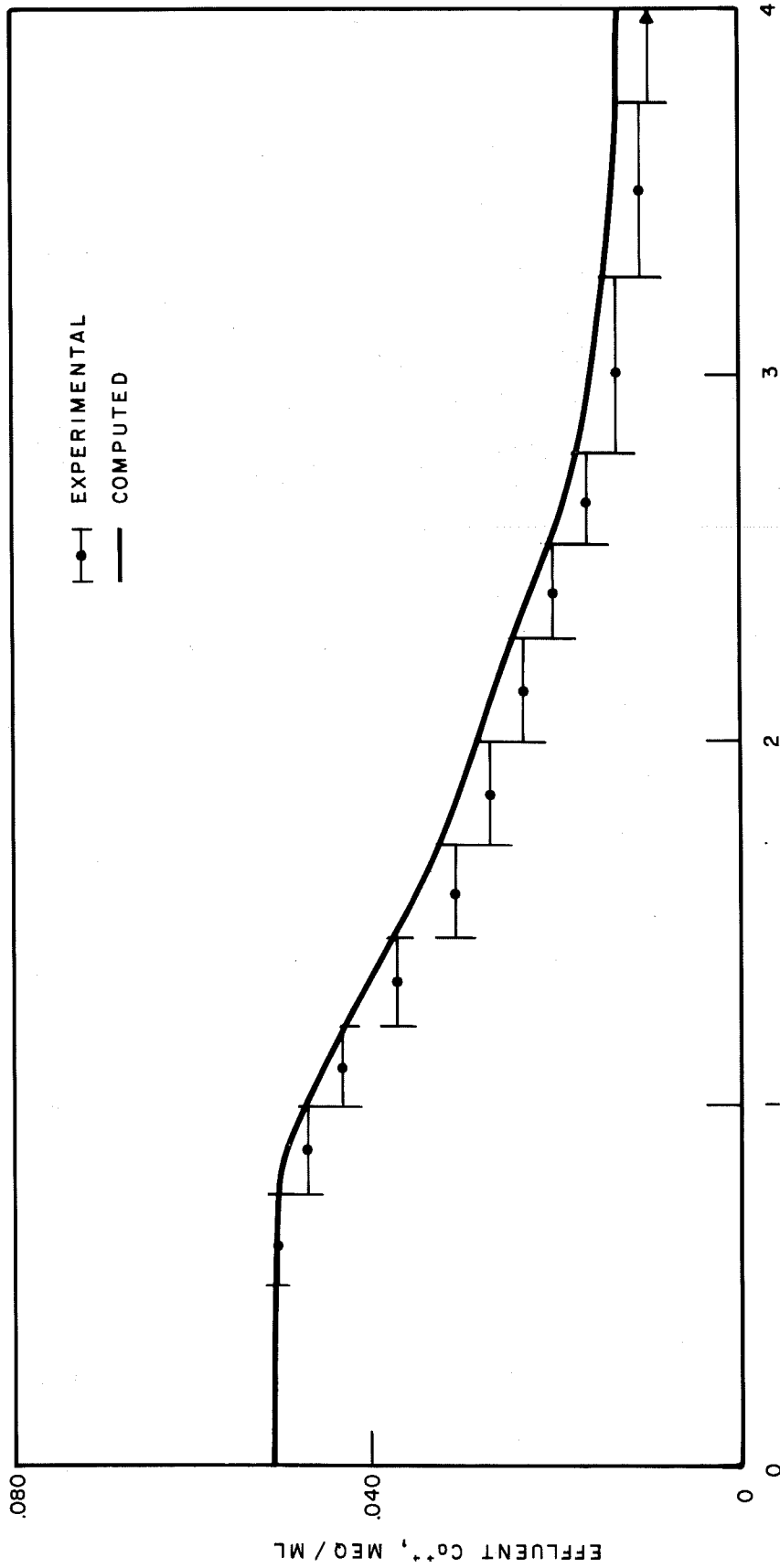


FIG. 34— Constant salinity elution in Second Wall Creek Core SC4: .250 meq/ml NaCl displacing .50 meq/ml CaCl₂ + .200 meq/ml NaCl.

Fig. 35 shows that the experimental curve closely matches the simulation. The high concentration peak in Fig. 35 occurs from two factors: (1) the absence of divalent ions and the high sodium concentration in the injected preflush brine shifts the equilibrium toward less calcium adsorption, and (2) because of the transition to higher salinity at the leading edge of the injected preflush brine, the appropriate isotherm reflects less affinity for divalent ions. An especially important feature of Fig. 35 is the slow reduction of divalent-ion concentration. After preflush brine breakthrough, another 2 PV of production is required before the divalent ion concentration decreases to the level of the Madison brine initially in place. As with Core MS4, twofold increases in flow rate had no significant effect on the effluent divalent ion concentrations.

PREDICTION OF RESERVOIR EFFICIENCY

To the degree that core samples studied in the laboratory may reflect the ion exchange properties of an entire reservoir, preflush performance in that reservoir can be estimated. Reservoir permeability variations, however, will prevent preflush efficiency from reaching levels achieved in confined, one-dimensional laboratory systems. Islands of rock, unswept by the preflush brine, may remain to contaminate the less mobile and more highly conforming chemical slug.

Froning and Trieber suggested that even after extensive preflushing, subsequently injected anionic surfactant can disrupt certain clay minerals. Consequently, divalent ions on normally inaccessible surfaces may be exposed for exchange. If this occurs, much higher divalent ion concentrations than expected could develop in the micellar slug.

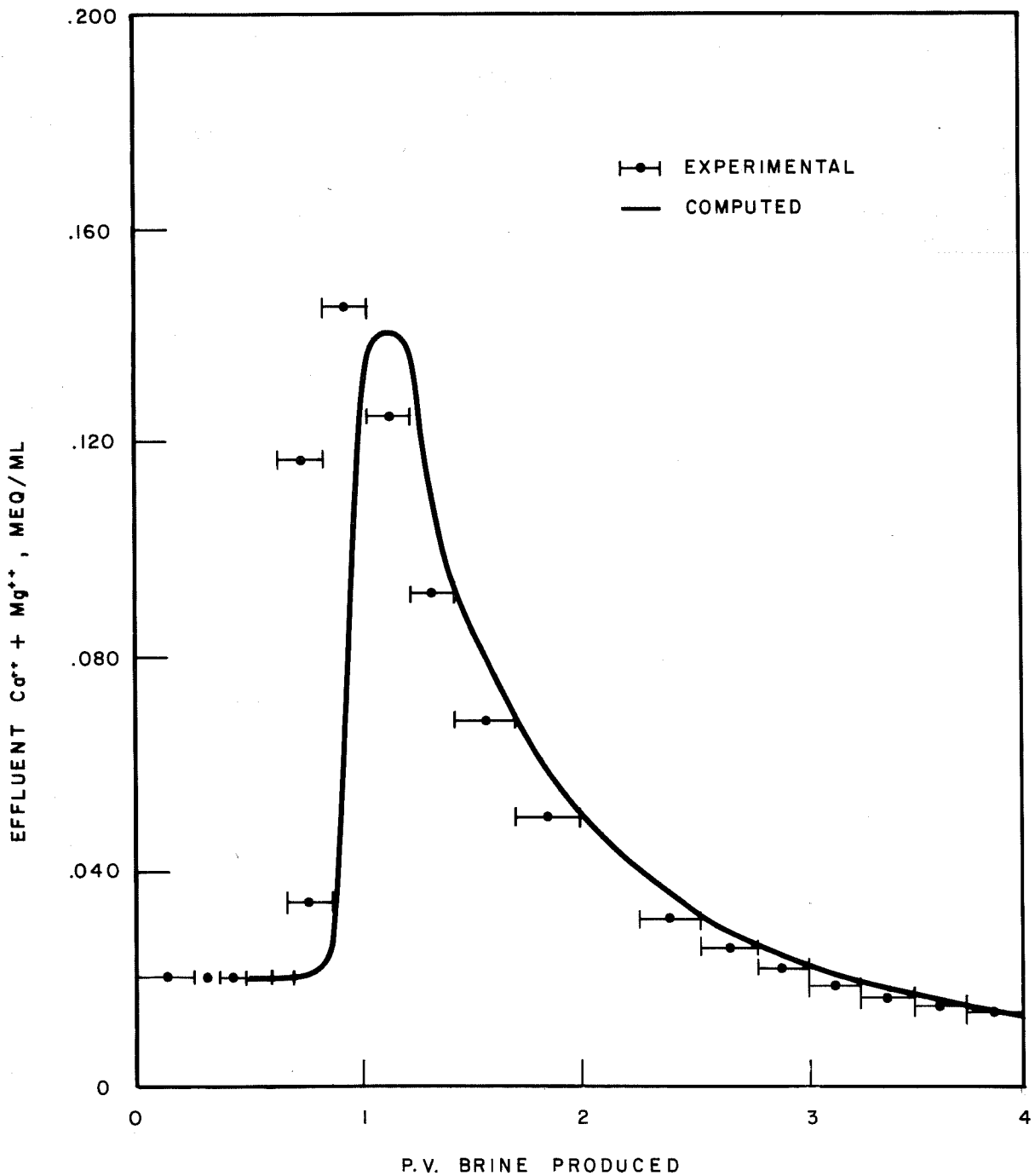


FIG. 35- Elution of Madison brine from Second Wall Creek Core SC3 by preflush brine.

Elevated temperature and resident oil saturation had no effect on preflush efficiency in one test core. Normal laboratory procedures established a waterflood residual saturation of Second Wall Creek crude in Core MS4. The connate water saturation before waterflooding was 27 percent and subsequent residual oil saturation was 43 percent. The results at 110°F for the saturation step with Madison brine and the following preflush step were practically identical to those obtained under the usual experimental conditions. Presumably, laboratory studies of preflush efficiency and ion exchange can be performed suitably in oil-free cores at ambient conditions, provided that the core is preferentially water-wet and the reservoir temperature is not extremely high.

Second Wall Creek

The effect of system length in the ion exchange calculations can be accounted for by incorporating length into a dimensionless dispersion coefficient, $K_1/(v_f L)$, where K_1/v_f is the velocity independent dispersion coefficient and L is the length. Calculations for systems having the same value of $K_1/(v_f L)$, but different lengths, give effluent divalent ion curves that are essentially superimposable. This is interpreted to mean that results of a calculation made for a short length are also valid for a large one, if dimensionless dispersion is the same. For a given value of $K_1/(v_f L)$, assuming that local equilibrium exists everywhere and other complicating factors are absent, only the shape of the ion exchange isotherm and the Q_v influence preflush efficiency. Thus, the curve presented in Fig. 35 for Core SC3, where the dimensionless dispersion coefficient was 0.0068, also would be appropriate for a heterogeneous, reservoir-like system where $K_1/v_f = 6.8$ feet and $L = 1,000$ feet. Although this scaling method is crude, it may be adequate because preflush efficiency is dominated by ion exchange equilibria, rather than by dispersion.

Not enough Madison brine has been injected into the Second Wall Creek formation to equilibrate the entire swept reservoir volume. What would be the preflush performance in a reservoir length system where a substantial gradient in divalent ion content exists? Fig. 36 illustrates the concentration profile of divalent ions resulting from preflush brine injection following 1 PV of Madison brine. The calculation assumes that no divalent ions were in the system before introducing Madison brine. In Fig. 36, $K_1/v_f = 6.8$ feet and $L = 1,000$ feet. The curves corresponding to different cumulative volumes of preflush brine injection show that the trailing edge of the divalent ion zone moves just as slowly as in a completely equilibrated system. The major difference is that because of the narrow zone width, dispersion eventually decreases the peak concentration value in the partially equilibrated system. The situation also was simulated where equilibrium with Second Wall Creek brine exists initially and absorbed divalent ions present before a Madison brine injection. Although the trailing edge of the divalent ion profile advances at the same rate as in Fig. 36, two changes are evident: (1) because of the diminished adsorption at the leading edge, the eluted divalent-ion peak travels more rapidly, and (2) a low concentration bank of divalent ions develops ahead of the peak corresponding to elution of the divalent ions initially absorbed from Second Wall Creek brine.

General Relationships

In Figs. 37 through 40, calculated results are presented showing the effects on preflush efficiency of salinity, affinity for divalent cations, and Q_v . In all cases, the injected brine has moderate salinity (0.200 meq/ml) and is free of divalent ions. In Figs. 37 and 38, the resident brine is low in total salinity, but has a relatively high concentration of divalent cations. In Figs. 39 and 40, a high salinity brine with a

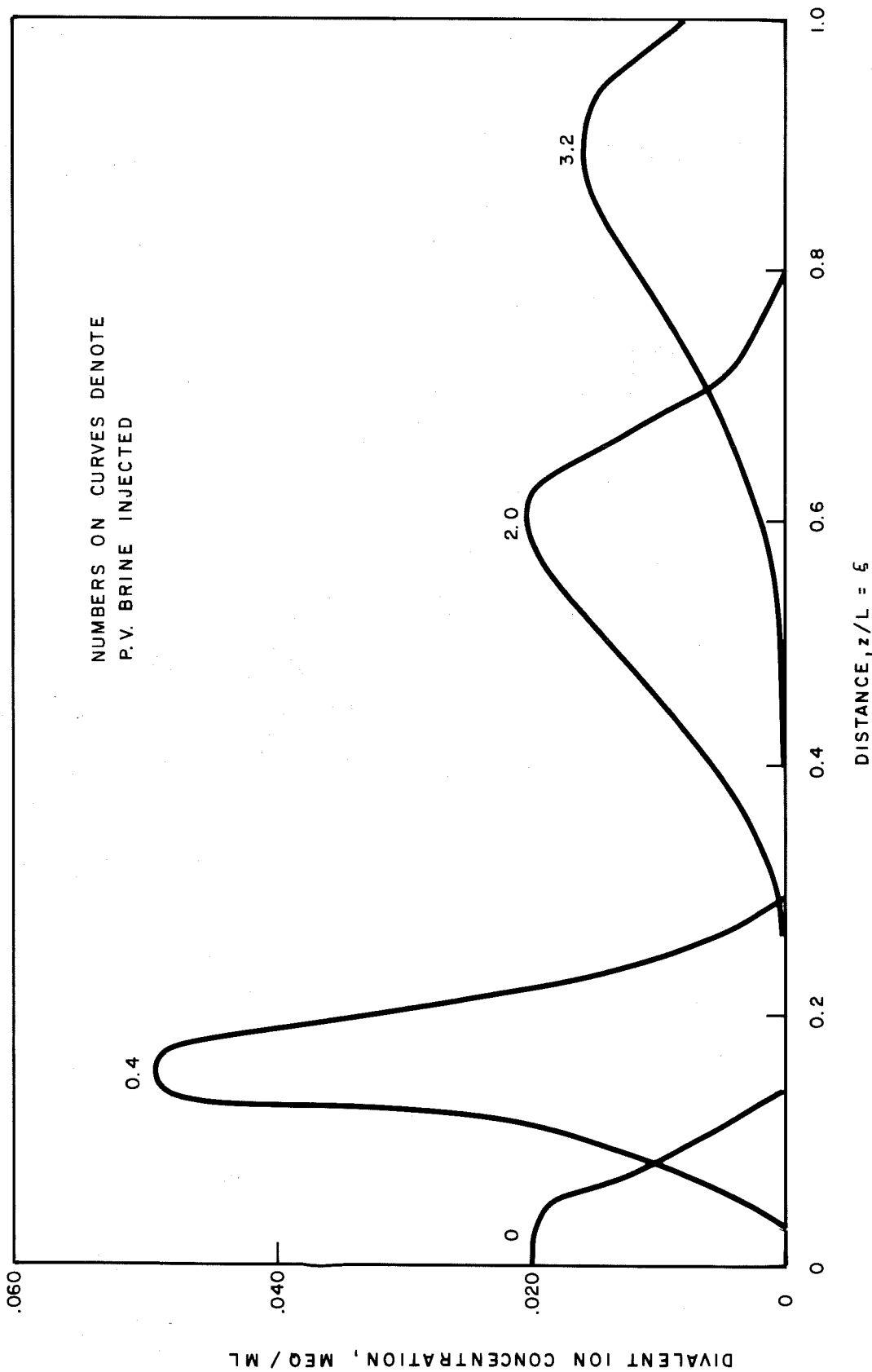


FIG. 36 - Computed displacement of divalent ions in Second Wall Creek rock following injection of 1 PV of Madison brine.

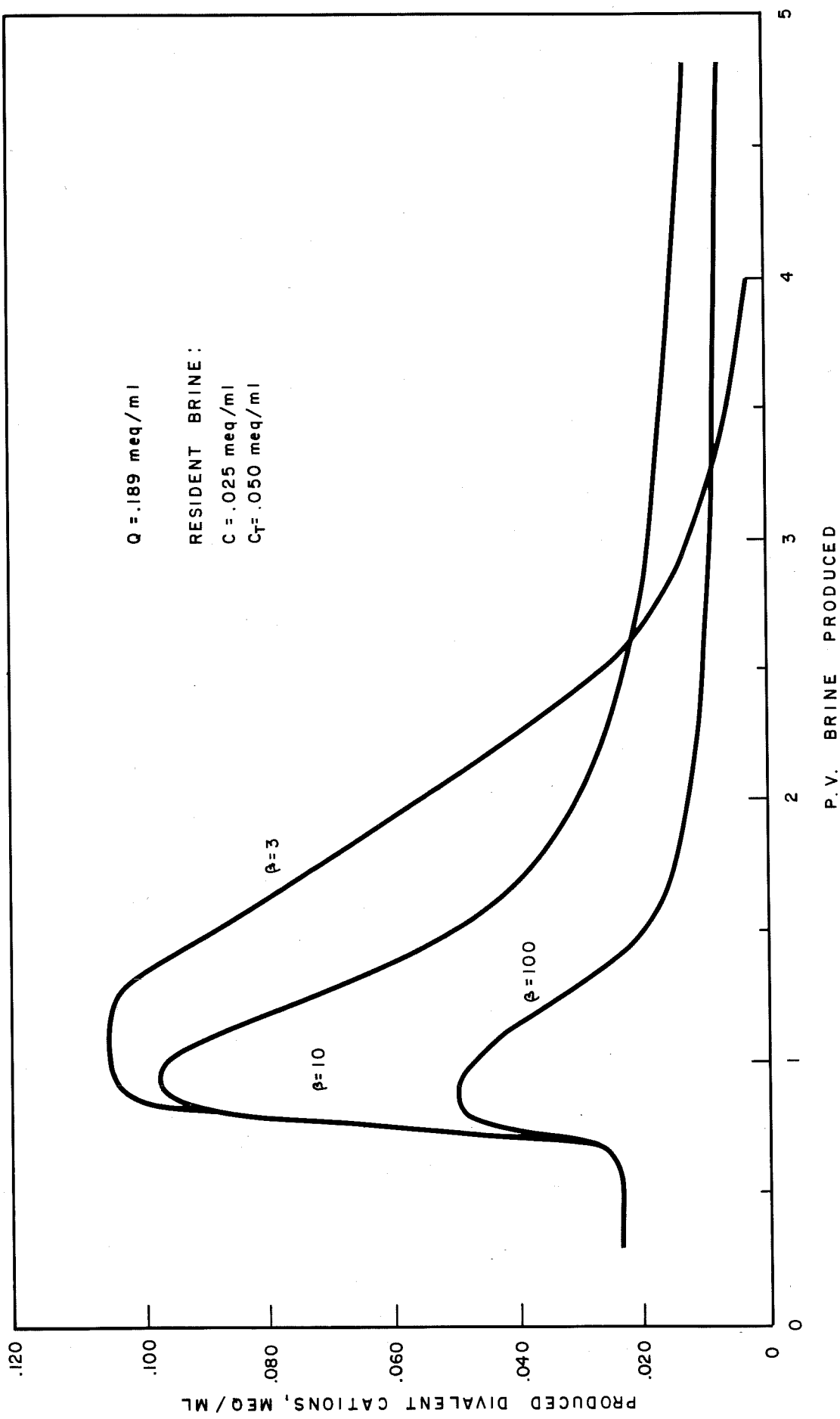


FIG. 37- Computed effect of affinity for divalent cations on preflush performance, low-salinity resident brine.

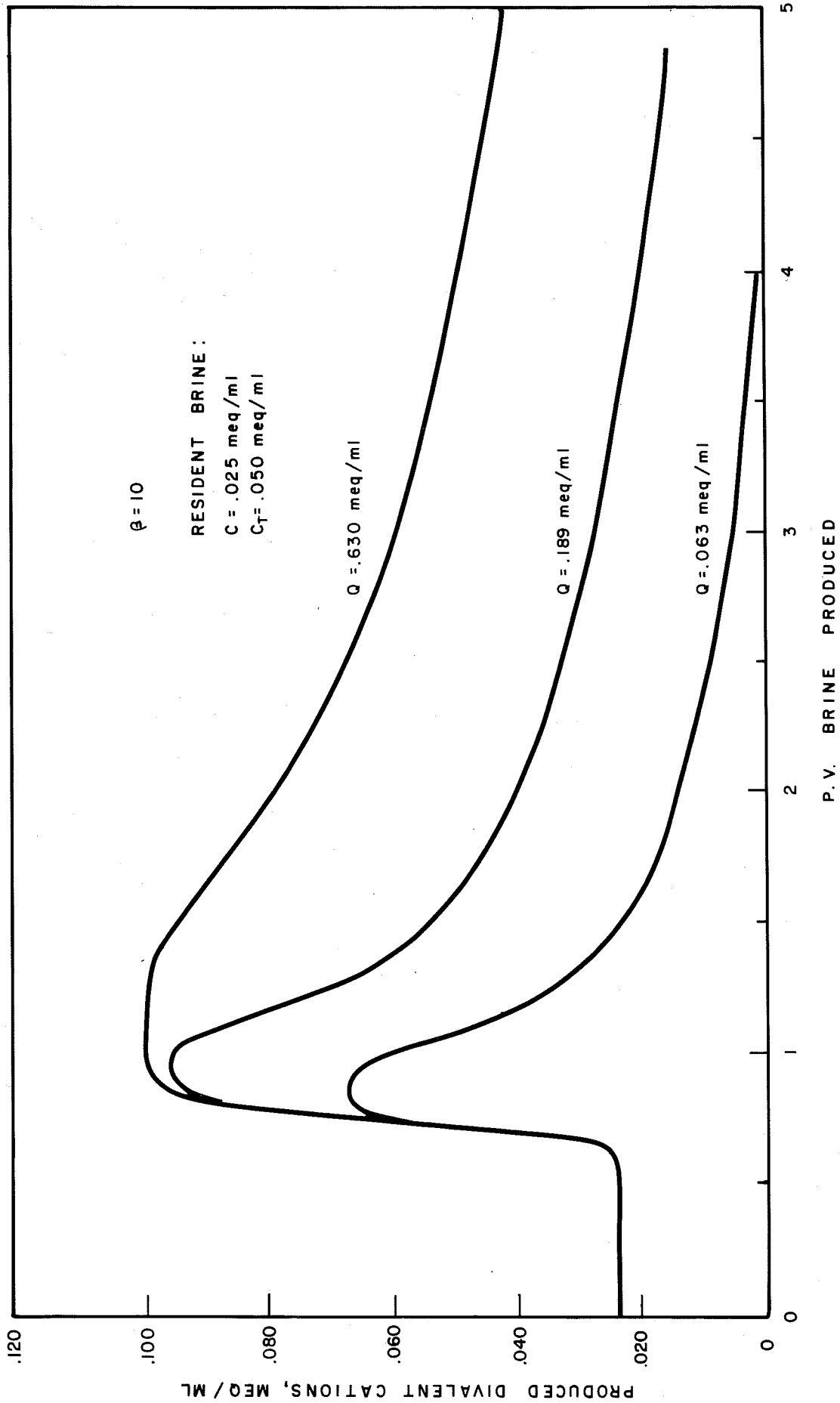


FIG. 38- Computed effect of cation-exchange capacity on preflush performance, low-salinity resident brine.

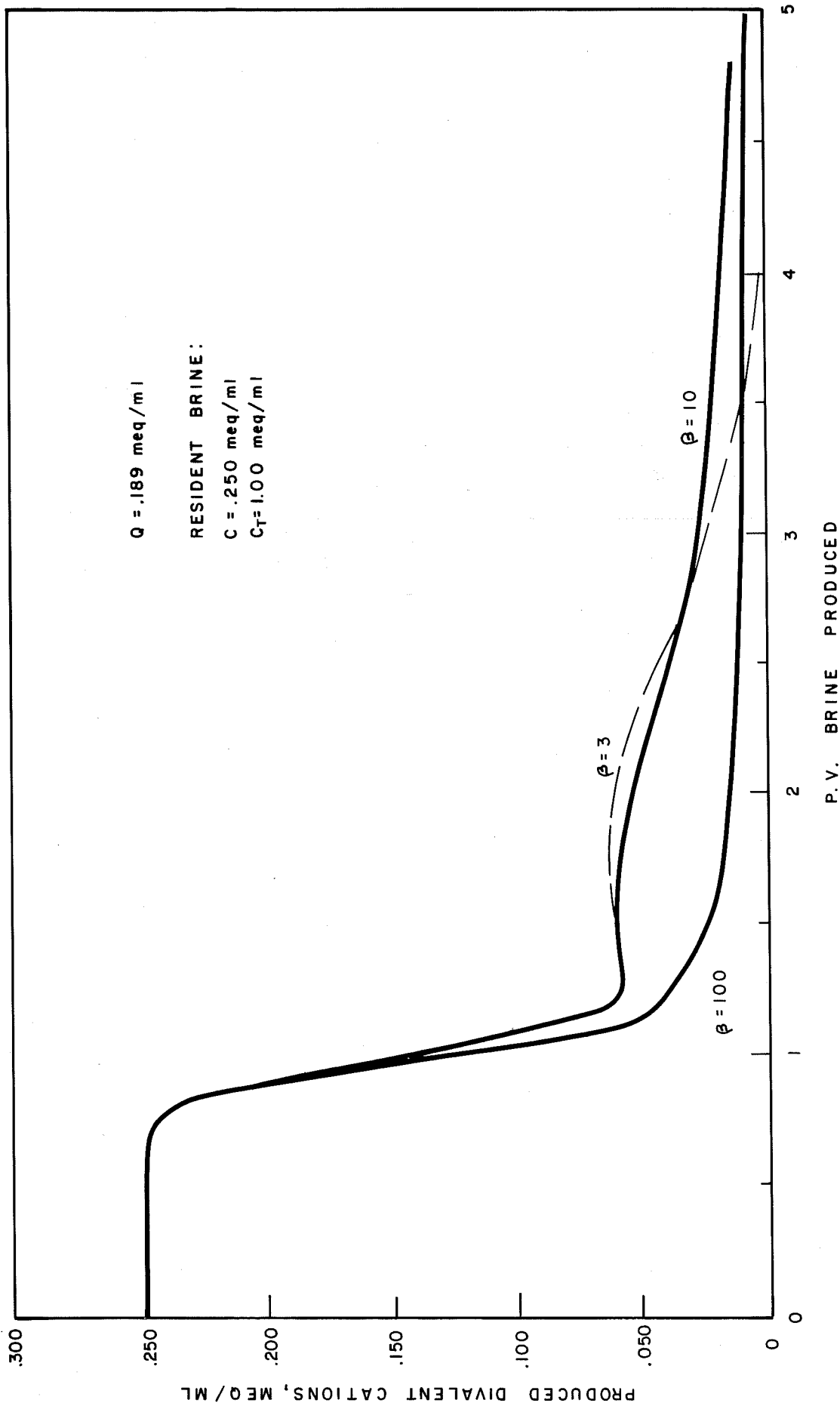


FIG. 39— Computed effect of affinity for divalent cations on preflush performance, high-salinity resident brine.

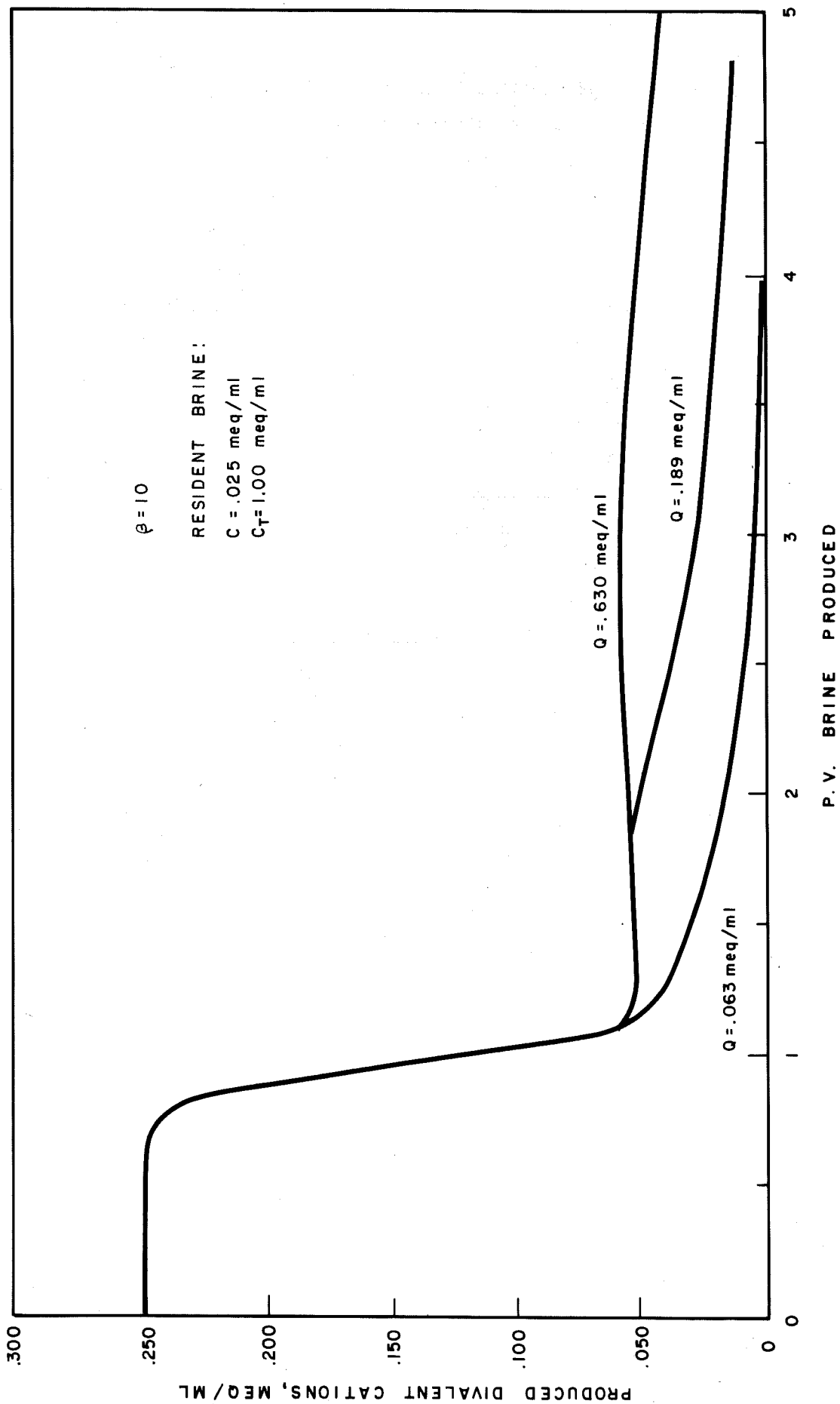


FIG. 40- Computed effect of cation-exchange capacity on preflush performance, high-salinity resident brine

moderate divalent ion content is in place. For each calculation, the shape of the exchange isotherm is independent of salinity — that is, the separation factor β is constant. The value of dimensionless dispersion, $K_T(v_f L)$, is 0.005 for all calculations.

The curves of Figs. 37 for a fixed intermediate value of exchange capacity show the effect of changes in affinity for divalent cations. As the value of β decreases, higher peak divalent ion concentrations are reached and the subsequent concentration decline is more rapid. Similar results are seen in Fig. 38 for a fixed intermediate value of β and changes in the magnitude of Q_v . In this instance the highest peak concentrations and lowest rate of decline occur with the greatest Q_v .

In Figs. 39 and 40, the results of displacing a more saline brine are shown. In spite of the differences in salinity, divalent cation concentration, and shape of the produced divalent cation curves, the effects of varying β and exchange capacity are qualitatively similar to those seen in Figs. 37 and 38. That is, following breakthrough of the injected brine, the highest effluent divalent ion concentrations correspond to the least value of β and the highest exchange capacity. Furthermore, the subsequent rate of concentration decline is greatest for lowest β and smallest capacity. Comparison of the preceding four figures shows that, regardless of the resident brine composition, the highest value of fractional divalent cation concentration displaced by the preflush brine approximates that of the resident brine. Thus, in all figures,

$$\frac{C_{\max}}{C_{t, \text{preflush}}} \sim \frac{C_{\text{resident}}}{C_{t, \text{resident}}}$$

This relationship indicates that the highest divalent ion concentrations and, subsequently, the greatest rate of elution will

be obtained with preflush brines having the highest salinity. Such behavior would be anticipated for exchange processes exhibiting a mass-action relationship.

The relative advance rate of a divalent-ion concentration level x (where $x = C/C_t$) can be defined as

$$F_i = \frac{V_x}{V_f} = \frac{1}{1 + Q/C_t \, dy/dx} \quad (75)$$

The curves of Fig. 41 were calculated by setting $Q/C_t=1$ and using Equation 73 for the exchange isotherm. Fig. 41 shows the value of F_i as a function for x for three values of β . Clearly, F_i is lowest for the lowest values of x ; that is, the lower the desired value of x , the more difficult it is to achieve. The effect of increasing β , which reflects increasing affinity for divalent ions, depends on the value of x . At high values of β , the value of F_i is very low for small x , but quite high for moderate values of x . The reason for this is that the exchange isotherm curve rises very rapidly for large β and then tends to flatten out; consequently, the value of dy/dx becomes small and F_i approaches unity.

CONCLUSIONS

Experimental and mathematical procedures were presented for studying ion exchange processes in laboratory cores. Agreement between experimentally observed and computed histories of divalent cation production indicates the adequacy of these procedures for the rock-brine systems described here. The major conclusions from studies of these particular systems are as follows.

1. The level of salinity of preflush brine is important to the efficiency of oil-exchange conditioning. Large

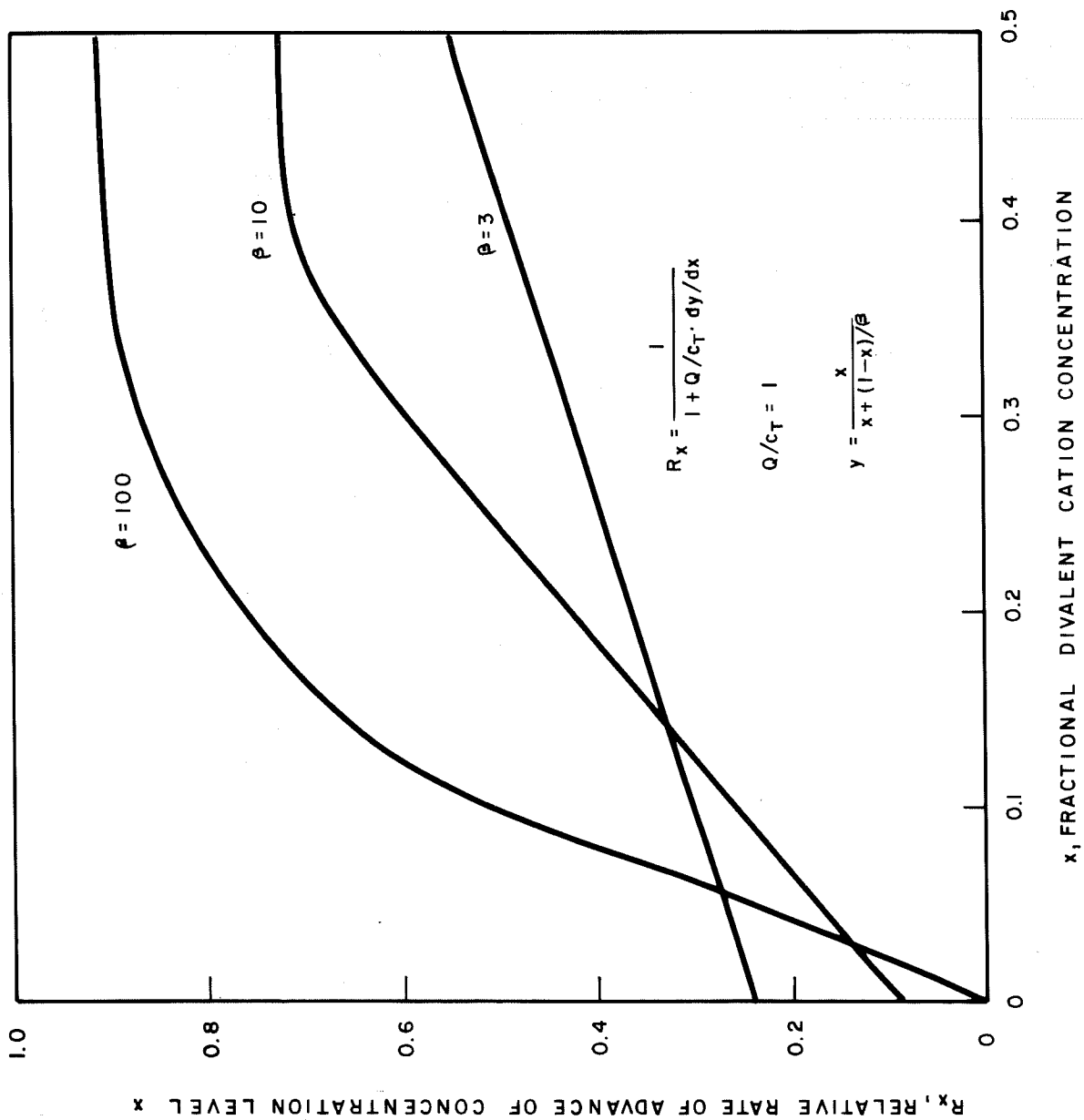


FIG. 41- Influence of divalent-ion affinity and displaced divalent-ion concentration on rate of displacement.

volumes of moderate-salinity brine may be required for elution of divalent cations, but the cation rate can be much higher with more saline brines.

2. With regard to elution of divalent cations by a preflush brine, calcium and magnesium can be treated as a single ionic species.
3. At relatively low frontal-advance, rates of 2 to 4 ft/day, the ion exchange processes are rapid enough so that local equilibrium exists throughout the system.
4. Studies of increasing and decreasing calcium concentrations in a Second Wall Creek core showed no evidence of calcium adsorption hysteresis.
5. The cation exchange capacities of the Second Wall Creek cores were considerably greater than the capacity of a Berea outcrop core.
6. The affinity of a Second Wall Creek core for calcium ions was observed to increase substantially with reduction of brine salinity.
7. Given experimental information on Q_V , shape of exchange isotherm, and compositions of resident preflush brines, idealized estimations of reservoir preflush efficiency can be made. Either the described one-dimensional model or its analytical approximation may be used.

The following excerpts were taken from a report by C.S. Chiou and H.L. Chang entitled, "Preflood Design For Chemical Flooding - A Study of Ion Exchange/Dispersion Process in Porous Media"¹².

INTRODUCTION

Most micellar slugs are intolerant of high salinity. Generally, if the salinity is higher than a few percent, the oil displacement is unsatisfactory, and further, the presence of undesirable divalent cations (calcium and magnesium) in the micellar fluid has an adverse effect upon the performance of the surface-active agents. It is the intent of the preflush to replace the formation water to reduce the salinity and divalent cation concentration in the reservoir to an acceptable level before introducing the surfactant. However, the oil recovery in field pilot tests has shown that beneficial effects are not assured by preflush because an improperly designed preflood can impair, rather than improve, the effect of a slug. It is now known that preflood type and reservoir clay play important roles in determining the ionic composition at the leading edge of the surfactant slug. It is the purpose of this work to study theoretically and experimentally the combined effects of ion exchange and dispersion on the preflood performance.

A mathematical model for a one-dimensional miscible displacement process involving ion exchange has been developed. This model is based on assumed rates of cation transfer between flooding water and reservoir solids. A numerical technique was used to solve the nonlinear partial differential equations for the three components (Na^+ , Ca^{++} , and Mg^{++}) system. The present mathematical model with the laboratory experiments would be able to give a better understanding of the kinetics aspect of ion exchange as well as to evaluate preflood performance in chemical

waterflooding process. Furthermore, it is hoped that a set of design criteria can be put forward for the pre-flood to provide optimum ionic environment for the surfactant flooding.

MODEL FORMULATION

The model considers the ion exchange/dispersion process in a three-component system consisting of sodium, calcium, and magnesium ions. The equilibrium among these ions between the flooding water and rock surfaces is assumed to follow a fairly broadly used empirical formulation, known as the "mass-action" equation,

$$\frac{\hat{C}_3}{\hat{C}_1^{1/2}} = K_{31} \frac{C_3}{C_1^{1/2}} \quad (6)$$

$$\frac{\hat{C}_1}{\hat{C}_2} = K_{12} \frac{C_1}{C_2} \quad (7)$$

where C_i is the concentration of the indicated ion in solution and \hat{C}_i is the concentration of the ion on clays in equilibrium with the solution, and K_{31} and K_{12} are the experimentally determined equilibrium constants. Here, K_{31} and K_{12} are dimensionless and determined to be 0.15 and 2.0, respectively. We recognize that these K values are functions of the type of clay, the ionic composition of the flooding water, and temperature. In practical field application, variation of rock samples complicates the determination of representative K values.

Inspection of Equation 6 shows that if the sodium ion is increased, some of the excess sodium ion will be adsorbed while some of the calcium ion will be desorbed in order to maintain the equilibrium value constant. The converse is also true. Furthermore, Equation 7 shows that if K_{12} approaches unity, there will be no selectivity between calcium and magnesium ions, or in other words, calcium and magnesium can be treated as a single divalent ion.

Under nonequilibrium conditions, the instantaneous cation concentration \hat{C}_i , on the rock surface deviates from \hat{C}_i, eq , which is the cation concentration on rocks in equilibrium with the

interstitial solution of concentration C_i . The extent of this deviation depends on the ion exchange rate.

The "linear-driving-force" relationship implies that at any time, the ion exchange rate is proportional to the concentration change between the instantaneous and the equilibrium states.

NUMERICAL SOLUTION

Implicit finite difference with Gauss' elimination method was used to solve the set of equations. The implicit finite difference form was used for each of the terms in the one-dimensional transport equation.

PARAMTERS USED IN COMPUTER SIMULATION

Some important parameters associated with the characteristics of the ion exchange/dispersion process are as follows:

1. Cation Exchange Capacity, Q_v

The cation exchange capacity was estimated to be 0.05 meq/ml of pore space for the laboratory core. This is approximately the median value for Berea and other sands of mid-continent and Gulf Coast areas. The cation exchange capacity, which is associated with the type of clay on the rock surface, is assumed to be constant throughout flooding process.

2. Ion Exchange Equilibrium Constants, K_{ij}

As mentioned earlier, the equilibrium constants between Na/Ca and Ca/Mg are assumed to be 0.15 and 2.0, respectively. These values will in general depend on the type of formation and ionic composition of flooding water.

3. Ion Exchange Rate Constant

The proportional constant for the rate law of ion exchange determines the rate at which cations are transported from the rock surface to the solid-liquid interface. Zero implies that no ion exchange occurs between the flooding water and rocks while infinity implies instantaneous equilibrium for ion exchange reactions. In this work, the constant was assumed to be 50 sec^{-1} for the comparison between simulated and experimental results. This term would not affect the calculated ionic compositions significantly from those assuming instantaneous equilibrium.

4. Dispersion Coefficient, K_1

Several types of dispersion have been given in the literature. In this work, the dispersion coefficient is assumed to be linearly dependent on the linear velocity, that is,

$$K_1 = 1 + v \quad (76)$$

The proportional constant " λ " is the characteristic dispersion length. This " λ " may be determined by matching the calculated elution curves with those of laboratory core tests. Chloride ion, which is believed to follow the fluid front closely without adsorption, was used as a reference tracer. For the Berea cores used in this work, the dispersion length was estimated to be one centimeter.

EXAMPLE CALCULATIONS AND DISCUSSIONS

Example calculations were made by using the input data listed in Table 13. Some of the calculated results were com-

TABLE 13

INPUT DATA FOR COMPUTATION

Cation Exchange Capacity (Q_v) = 0.01, 0.05, 0.10, 0.20 meq/ml of pore space

Porosity of Core (\emptyset) = 0.1789

Core Radius = 2.54 cm

Core Length (L) = 25.24 cm

Dispersion Length (l) = 1.0 cm

Injection Rate (q) = 40 ml/hr

Ion Exchange Rate Constant = 0.0, 0.5, 5.0, ∞ sec⁻¹

Preflood Slug Size = 260 ml

Equilibrium Constant K_{31} for Na/Ca = 0.15

Equilibrium Constant K_{12} for Ca/Mg = 2.0

TABLE 14

IONIC COMPOSITION IN INJECTED SOLUTION

<u>Descriptions of Fluids</u>	<u>Na⁺ meq/ml</u>	<u>Ca⁺⁺ meq/ml</u>	<u>Mg⁺⁺ meq/ml</u>
Formation water	0.8985	0.1392	0.0606
Preflood Type 1	0.1348	0.0209	0.0091
Preflood Type 2	0.3480	0.0209	0.0051
Preflood Type 3	0.2606	0.00	0.00
Simulated Chemical Slug Followed Preflood Type 1 or Type 2	0.2470	0.0035	0.0001
Simulated Chemical Slug Followed Preflood Type 3	0.1262	0.0074	0.0031

pared with experimental data. In this study, tests were conducted in 2" x 10" Berea cores which were mounted in a Hassler cell. Fluids were injected through a Ruska constant volumetric pump. A Sargent automatic fraction collector was used to collect the effluent solution for analysis. Calcium and total hardness (combination of calcium and magnesium) were readily determined by standard chemical titration. Sodium ion concentration was then calculated as the difference of chloride ion concentration (determined by automatic chloride titrator) and the total hardness.

For the experiment, we saturated the core with synthetic Madison water and flowed with this water until effluent composition was equal to the injection composition. We then displaced the formation water with a preflood solution. After injecting 260 cc of preflood (2.84 pore volume), a quasi-steady state composition was achieved. About 3 pore volumes of simulated chemical slug (without adding any sulfonate or polymer) was then injected. The flow rate was set at 40 cc/hr. Ionic compositions of all the injected solutions are listed in Table 14. Three types of preflood were tested in this study to investigate the effect of preflood design on ionic composition in the front of the chemical slug. Type 1 preflood contains 15% of formation water mixed with deionized water. In Type 2, some NaCl was added to the 15% dilution of formation water to maintain Na/Ca/Mg equilibria with the formation rock. Type 3 is a plain brine containing 1.5% sodium chloride.

Comparison of Experimental and Theoretical Results in the Case of Using Preflood Type 1 - 15% Formation Water

As will be seen later in this section, the divalent ions have a greater percent of change than monovalent ions due to ion

exchange. It was also found that calcium and magnesium ions behaved similarly. Therefore, only calcium ion concentration in effluent is presented here to compare with experimental data. Both calculated and experimentally determined calcium ions in the effluent were normalized by calcium ions in formation water and plotted against pore volume of effluent produced. Agreement between experimental and theoretical results is only fair for the preflood/formation water displacement (Fig. 42). This is due to the end effect of the short laboratory cores. The predicted "hump" of calcium ion in the front of the chemical slug is confirmed by experiment. With this type of preflood, the slug would pick up divalent ions by exchange to a concentration several times greater than the injected concentration. This preflood is not desirable.

Comparison of Experimental and Theoretical Results in the
Case of Using Preflood Type 2 - Adjusted* 15% Formation Water

As listed in Table 14, the concentration ratio of sodium and calcium in the formation water is

$$\frac{C_3}{(C_1)^{\frac{1}{2}}} = \frac{0.8985}{(0.1392)^{\frac{1}{2}}}$$

The additional Na^+ required to obtain the properly adjusted preflood with 15% formation water may be calculated as

$$\frac{(0.15 \times 0.8985) + \text{Na}^+}{(0.15 \times 0.1392)^{\frac{1}{2}}} = \frac{0.8985}{(0.1392)^{\frac{1}{2}}}$$

or $\text{Na}^+ = 0.2132$ meq/ml. By the addition of 0.2132 meq/ml of Na^+ into preflood 1, the ratios of Na^+ to Ca^{++} in preflood and formation water are balanced. In this case, there is no ion

$$* \left(\frac{\text{Na}^+}{\text{Ca}^{++}} \right)_{\text{preflood}} = \left(\frac{\text{Na}^+}{\text{Ca}^{++}} \right)_{\text{formation water}}$$

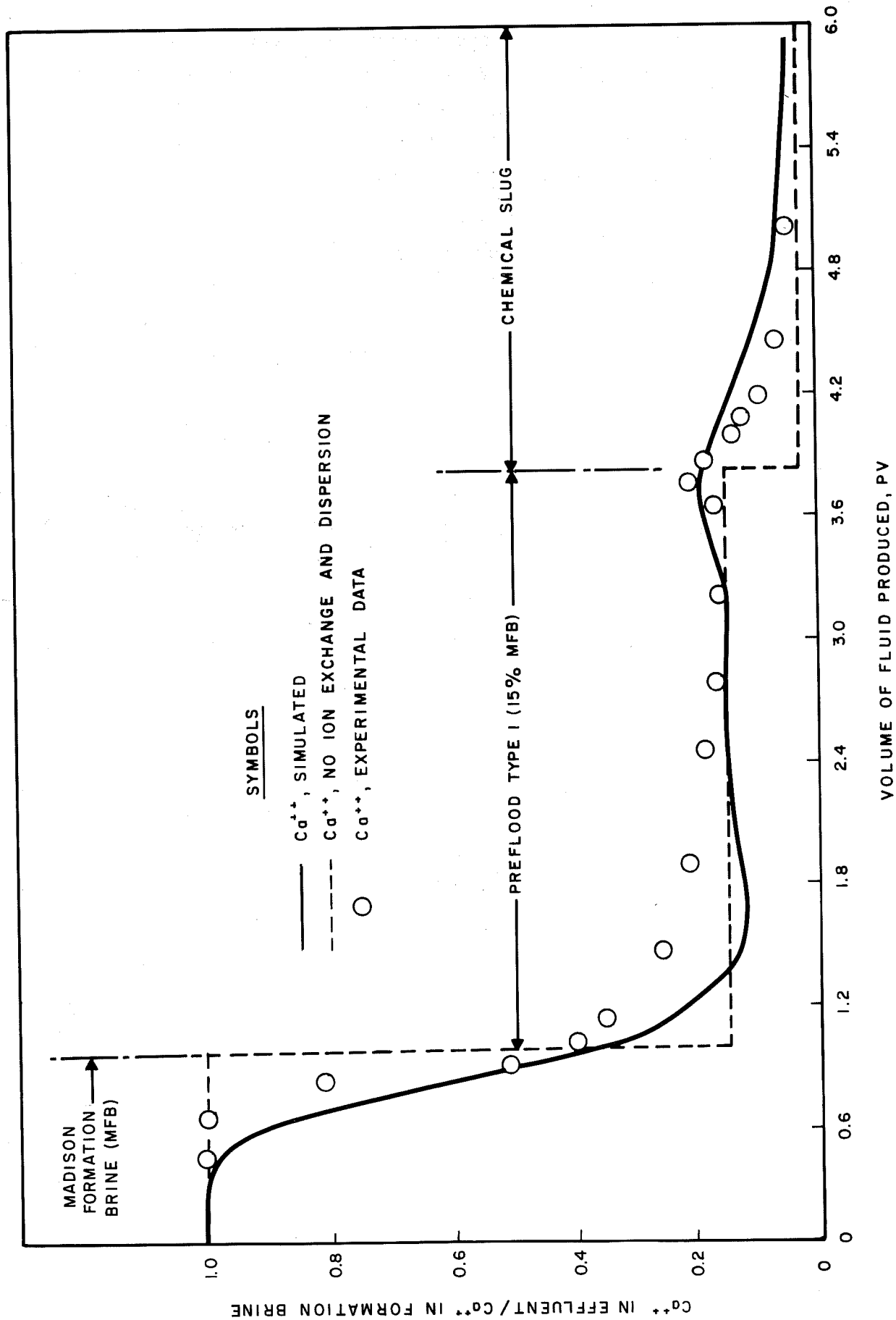


FIG. 42— Comparison of experimental and predicted calcium ion concentration in effluent preflood Type 1.

exchange between the flood water and the formation rock. Simulated and experimentally determined calcium in effluent were compared in Fig. 43. As expected, the calcium ion concentration did not increase in the chemical slug/preflood displacement. Agreement between experimental and calculated composition is good. Such a preflood would not change the reservoir rock property, and no ion exchange would occur during the preflush. This design is recommended because of its simplicity in predicting the preflood performance without knowing the ion exchange characteristics of the rocks.

Comparison of Experimental and Theoretical Results in the Case of Using Preflood Type 3 - 1.5% NaCl

In this test, plain brine containing 1.5% NaCl was used as the preflood. Fig. 44 shows that good agreement between experimental and simulated results is again achieved for the chemical slug/preflood displacement. Equation 6 indicated that if the Na/Ca ratio in flooding water is increased, the Na/Ca ratio on clays will also be increased in order to maintain equilibrium. The chemical slug following the preflood will then equilibrate with preconditioned clays by losing its calcium ion to the rock surface. If the chemical slug is designed to have optimum recovery efficiency without the presence of divalent ions, this preflood is recommended.

Effect of Cation Exchange Capacity on Preflood Performance

The cation exchange capacity is defined as the total exchangeable cation concentration on the rock surface. The higher the value of cation exchange capacity, the more the unbalanced preflood will affect the ionic composition in the front of the chemical slug due to ion exchange. The effect of cation exchange capacity on the performance of preflood Type 1 was given

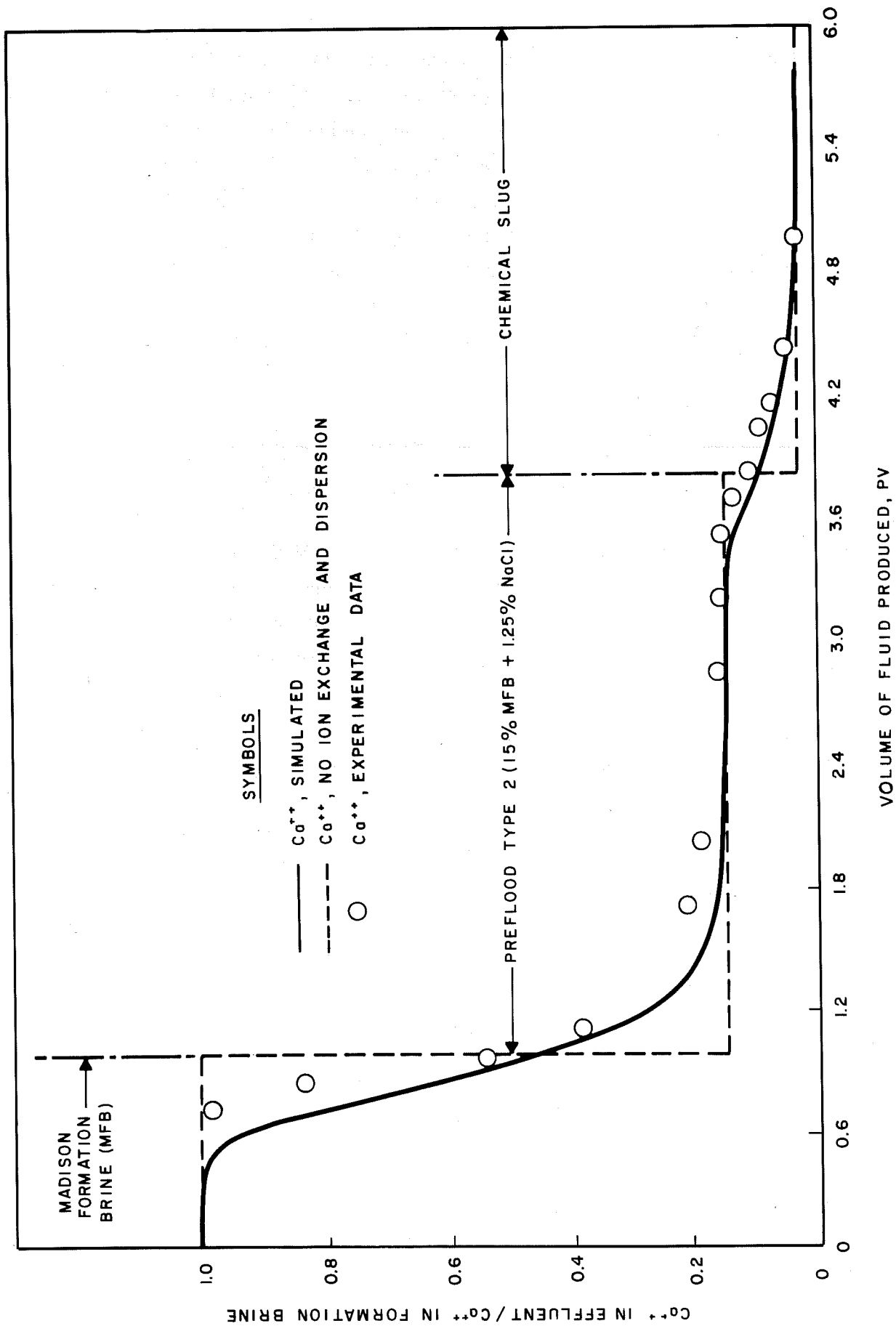


FIG. 43 - Comparison of experimental and predicted calcium concentration in effluent preflood Type 2.

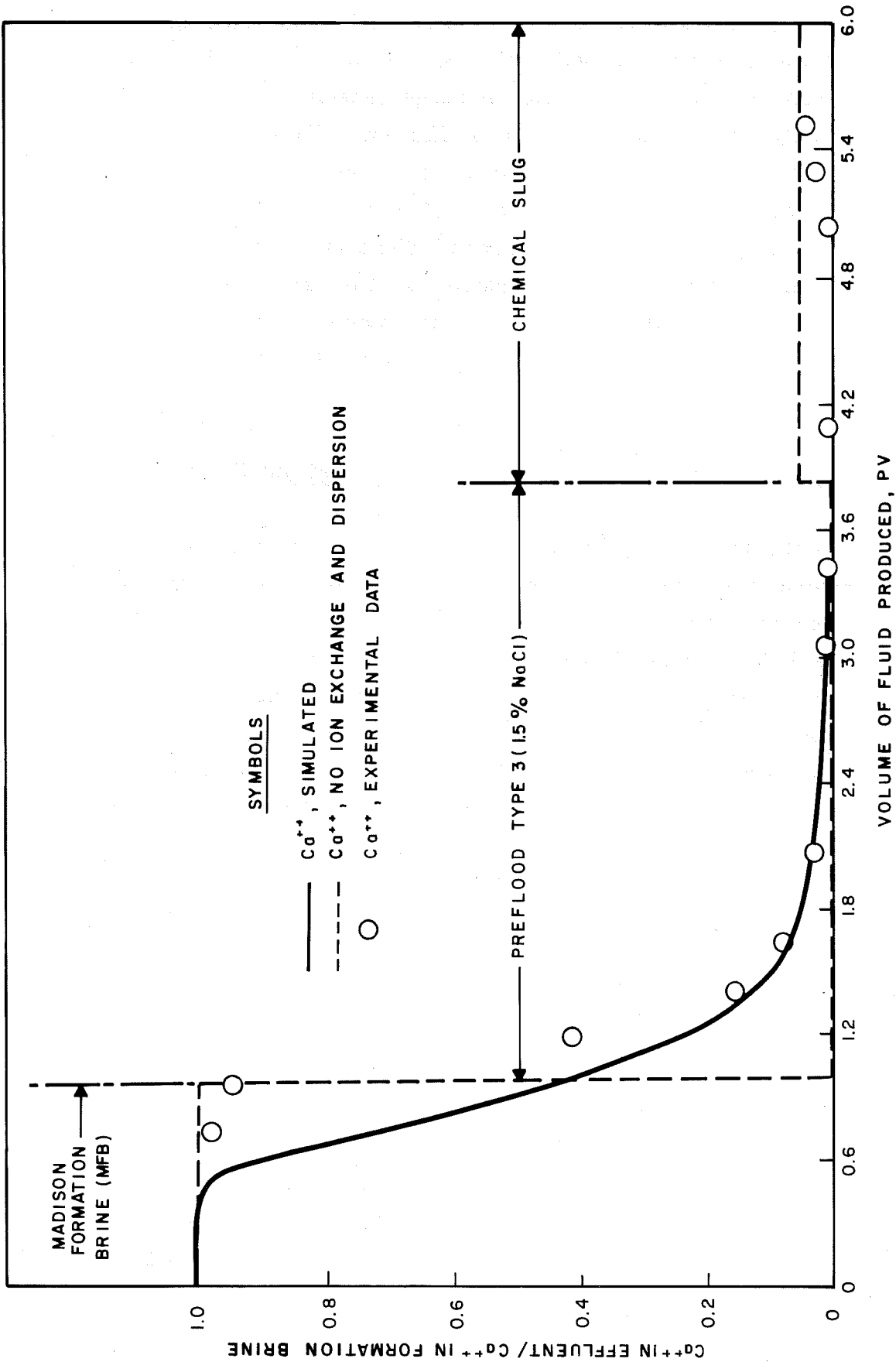


FIG. 44 - Comparison of experimental and predicted calcium ion concentration in effluent preflood Type 3.

as a typical example. Figure 45 through 47 represent the concentration of Ca^{++} , Mg^{++} , and Na^+ in the produced effluent, assuming four different cation exchange capacities with fixed ion exchange rates and dispersion coefficient. These figures indicate that the divalent ions have a greater percent change due to ion exchange than monovalent ions. The "hump" in both Ca^{++} and Mg^{++} in the chemical slug/preflood displacement increases with increasing cation exchange capacity of the clay. This implies the significance of the effect of the types of clay in determining the ionic composition of the chemical slug under operative condition.

Effect of Ion Exchange Rate Constant on Preflood Performance

The ion exchange rate is assumed to be proportional to the concentration change between the instantaneous state and the equilibrium state. Calculations were carried out for preflood Type 1 for a rate changing from zero to infinity, with constant cation exchange capacity and dispersion coefficient. Figures 48 through 50 indicate that the variation of monovalent ions due to ion exchange are much less significant compared with divalent ions even under instantaneous equilibrium condition. The divalent ion concentration in the front of the chemical slug is found to increase with increasing exchange rate, indicating quicker ion exchange reactions.

CONCLUSIONS

As indicated in the above example calculations and discussions, the following conclusions are made.

1. The present mathematical model may be used to interpret the ionic composition in preflood/formation water and chemical slug/preflood displacement in both the laboratory experiments and field pilot tests.

SODIUM

ION EXCHANGE RATE = 50.0 sec⁻¹
CATION EXCHANGE CAPACITY (Q_v) = 0.01 meq/ml —
= 0.05 meq/ml - - -
= 0.10 meq/ml - - -
= 0.20 meq/ml - - -

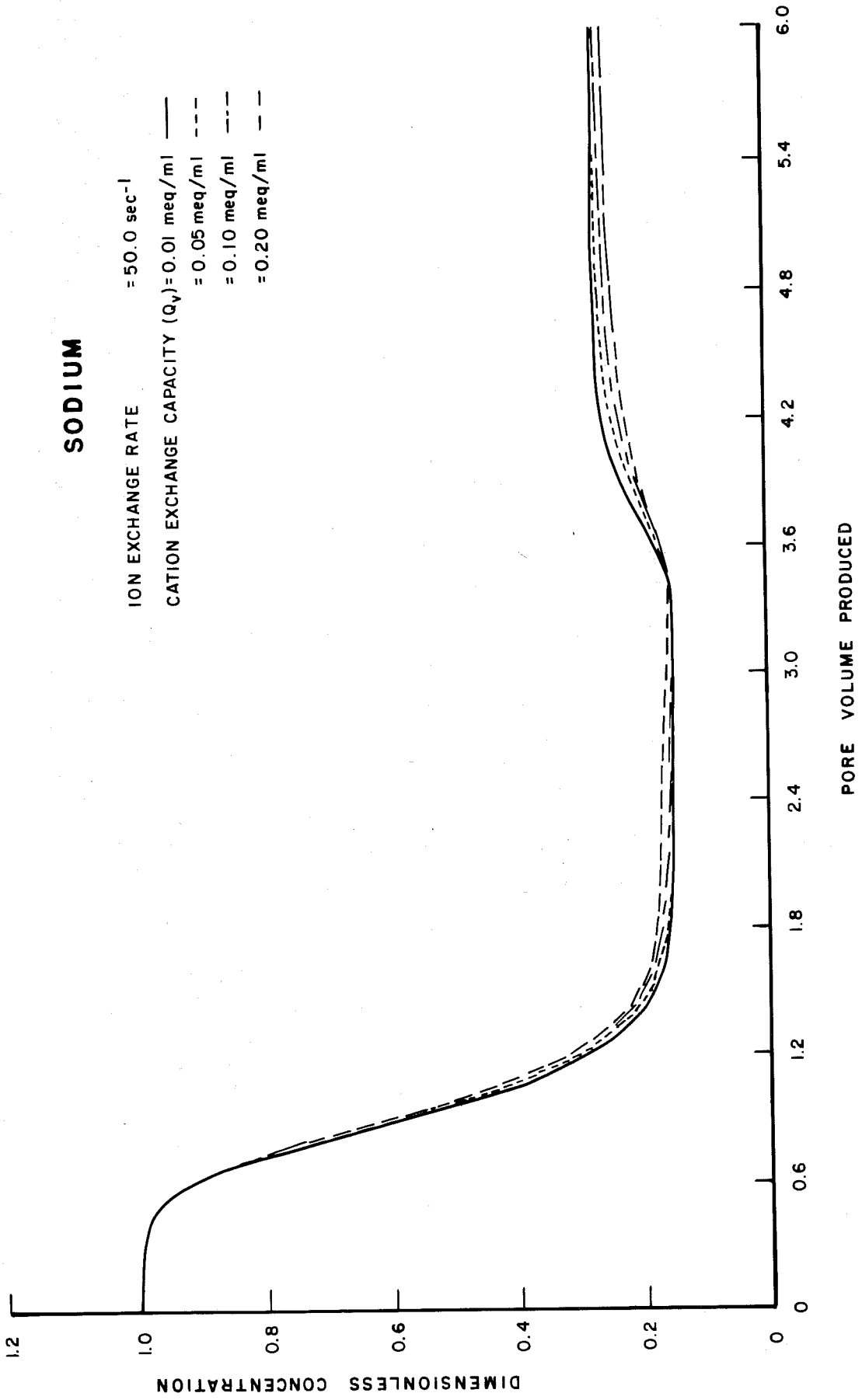


FIG. 45- Effect of cation exchange capacity on sodium ion concentration in effluent.

SODIUM

CATION EXCHANGE CAPACITY (Q_v) = 0.05 meq/ml

ION EXCHANGE RATE

- 0.0 sec⁻¹
- - - 0.5 sec⁻¹
- · - · 5.0 sec⁻¹
- · · · ∞ sec⁻¹

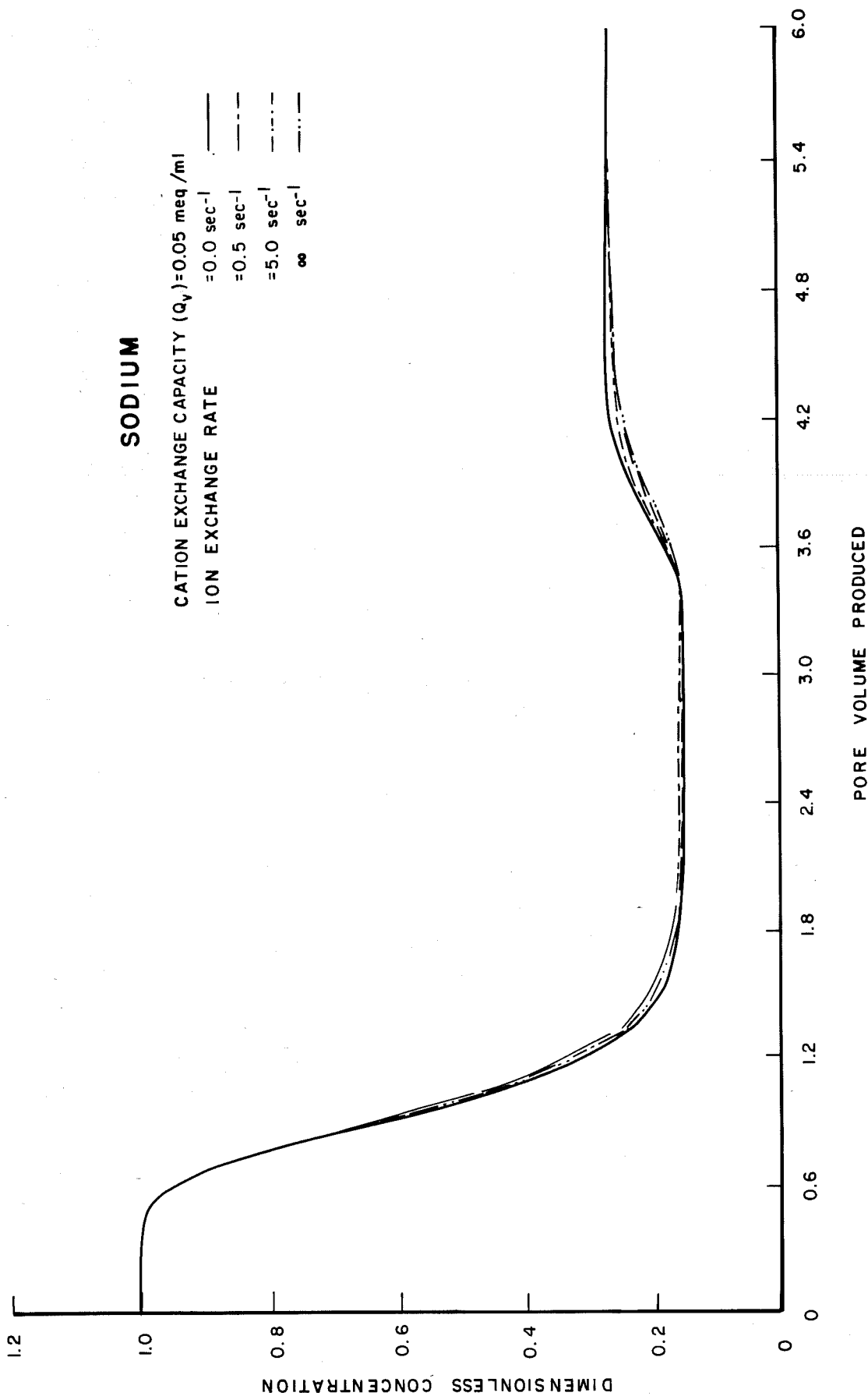


FIG. 48 - Effect of ion-exchange rate on sodium ion concentration in effluent.

CALCIUM

CATION EXCHANGE CAPACITY (Q_r) = 0.05 meq/ml

ION EXCHANGE RATE

- 0.0 sec⁻¹
- - - 0.5 sec⁻¹
- · - · 5.0 sec⁻¹
- · · ∞ sec⁻¹

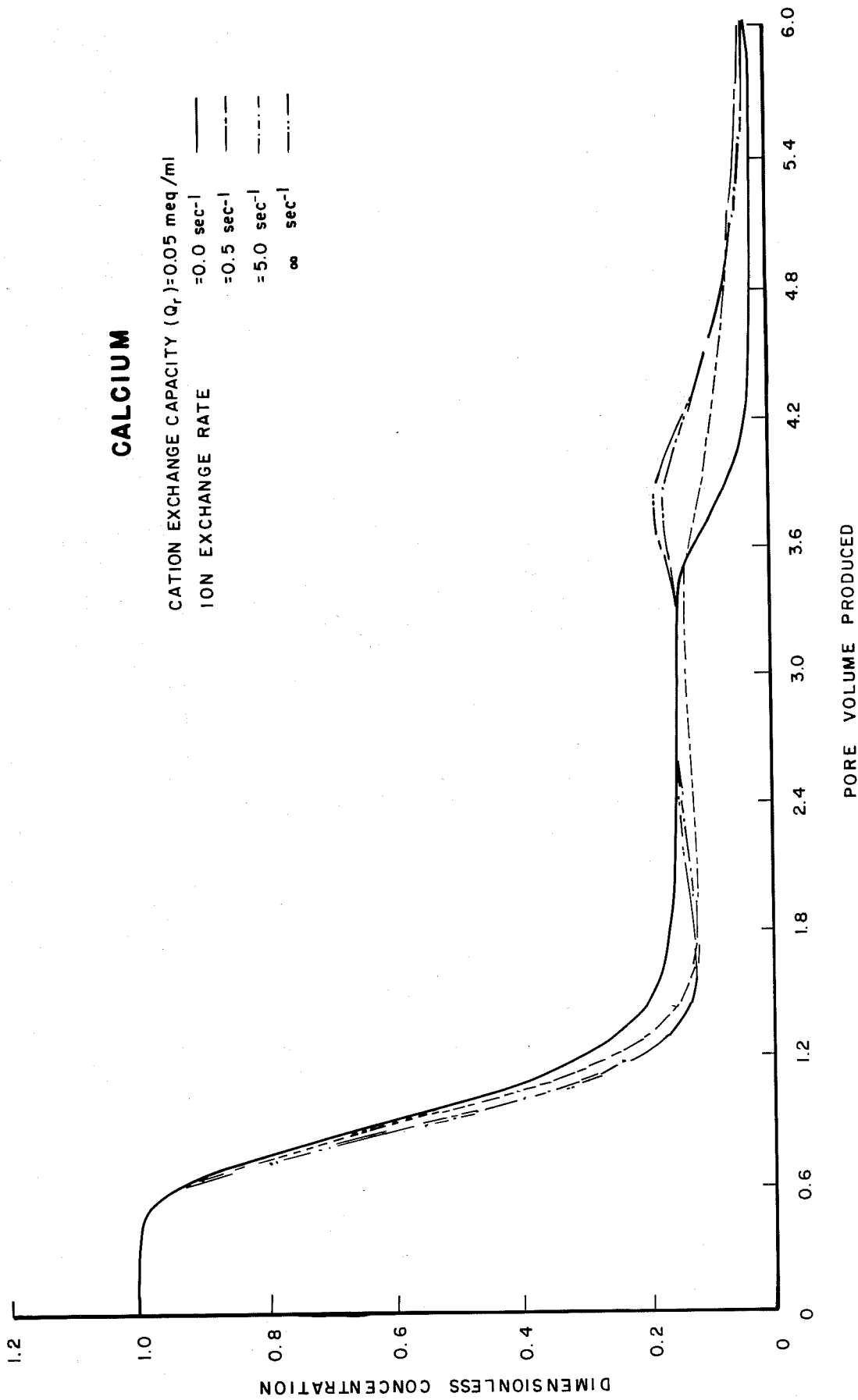


FIG. 49 - Effect of ion-exchange rate on calcium ion concentration effluent.

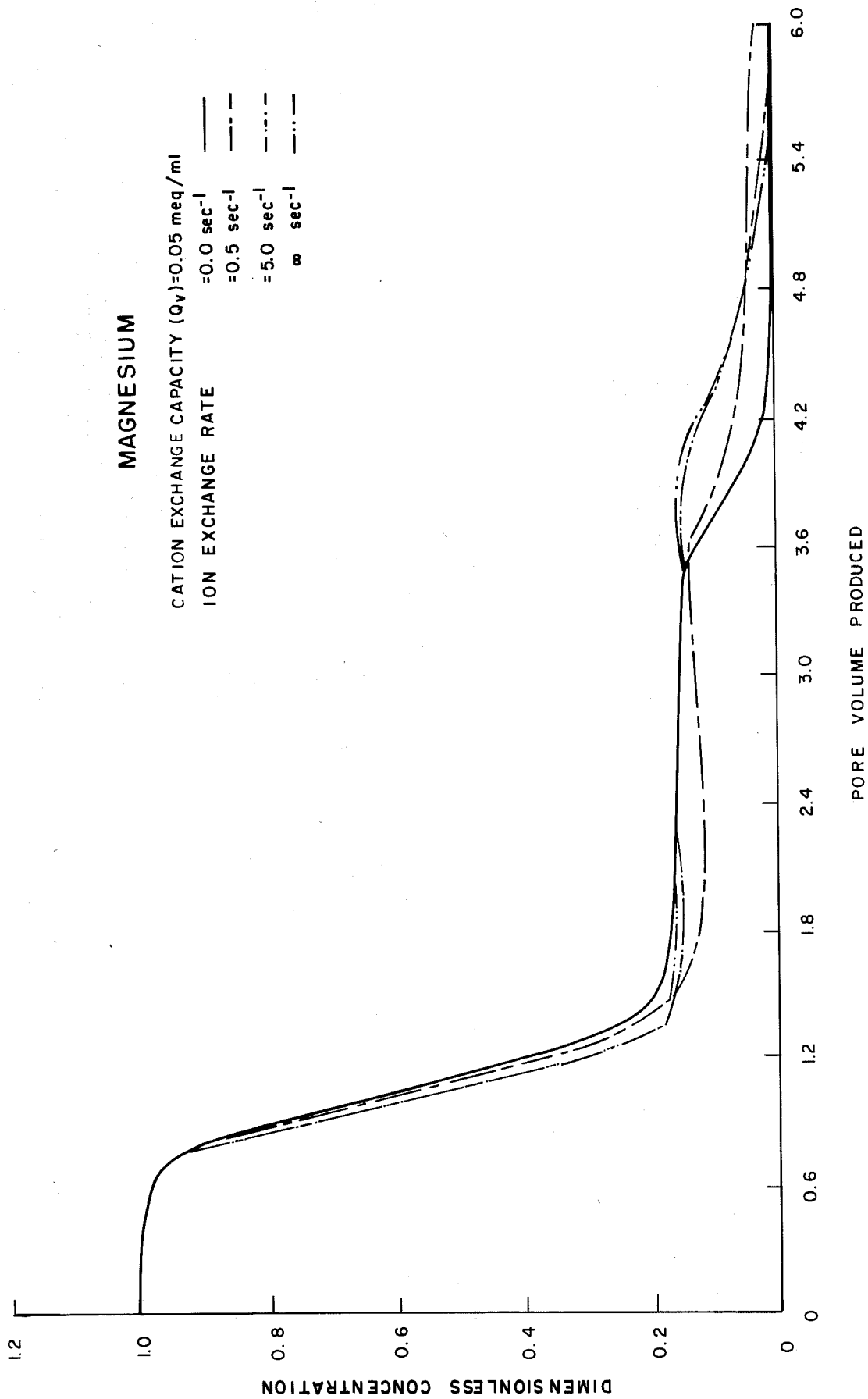


FIG. 50—Effect of ion-exchange rate on magnesium ion concentration in effluent.

2. Based on the assumed cation exchange capacity, ion exchange rate law and dispersion characteristics of the flooding system, the ionic composition in the effluent can be simulated for three different types of preflow. Preflood Type 1 is a diluted formation water, Type 2 is a balanced diluted formation water, and Type 3 is a brine without divalent ions.
3. Of all three types of preflow cited here, only Type 1 will result in an increase in divalent ion concentration in the front of the chemical slug. This design may impair the effectiveness of a chemical slug.
4. As far as the ion exchange reaction between the flooding water and rock clay is concerned, the divalent ion variation is emphasized in the flooding process. The divalent ions have a greater percent change due to ion exchange than monovalent ions.
5. The preflow performance in a chemical waterflooding process should be determined by the following factors:
 - a. Types of prefloods design
 - b. Slug size of preflow
 - d. Dispersion characteristics of porous media
 - e. Ionic composition in the chemical slug

The following account is taken from the report of Thomas Campbell of P.Q. Corporation entitled, "Chemical Flooding: A Comparison Between Alkaline and Soft Saline Preflush Systems For Removal of Hardness Ions From Reservoir Brines"¹⁰.

INTRODUCTION

In chemical flooding systems for recovery of residual crude oil, the reservoir rocks and aqueous fluids usually have to be conditioned so that an optimum environment can be provided for a surfactant-based system to mobilize the unrecovered oil. Excessive salinity and undesirable divalent cations in the reservoir brine and in the clays normally present in the reservoir rocks are some of the factors which can be significantly changes by the injection of appropriate fluids as a preflush. Several approaches have been taken to this problem, which can be generally classified as follows:

1. Design of the preflush and surfactant systems with balanced concentrations of monovalent cations and divalent cations which could minimize the ion exchange from the clays in the reservoir.
2. Preflush the reservoir with slugs of high monovalent cation salinity so that the divalent cations are exchanged from the reservoir clays and eluted through the reservoir ahead of the surfactant slug.
3. Inject alkaline chemicals which can disrupt or minimize the ion-exchange process by various mechanisms, such as adsorption, precipitations, or ionic effects.

A number of workers have published and patented work which showed that ion exchange from reservoir clays could be prevented

or controlled by using ratios of monovalent cations to divalent cations in the surfactant slug which will not disturb the ion exchange equilibrium between the fluids and the clays.

Other papers show that mass-action equilibria, dispersion, and surfactant-divalent ion interactions should be considered in modeling chemical floods. The studies described in these papers report on experimental efforts to understand and predict cation exchange and other interrelated equilibria, to apply chromatographic principles to the problems and to develop a simulator model which can predict ionic environments when the correct equilibria descriptions are provided.

Another approach to reservoir conditioning is described by experiments on reservoir cores with high ion exchange capacity from a reservoir which has been partially hardened by injection of fresh water containing relatively high levels of divalent cations. Laboratory studies showed that preflushing with low or moderate salinity soft brine would require large volumes of fluids to remove the divalent ions from the reservoir. However, injection of considerably smaller volumes of high salinity soft brines produced a sharp ion exchange peak within reasonable elution volumes. Some of the major conclusions reached from these studies, based on experimental data and modeling, were that ion exchange capacity was the most important factor in sizing high salinity preflushes, that equilibria expressions with single, non-varying constants can correlate the ion exchange data over wide ranges of salinity, and that dispersion effects can be a major factor in high salinity preflush processes.

A different system for preflushing reservoirs prior to injection of surfactant slugs has been described in which small slugs of highly alkaline sodium silicate solution ($\text{pH} > 11$) are injected to reduce or eliminate the divalent cations in the

reservoir fluids. This process also gives improved oil recovery efficiency compared to soft saline preflushes, presumably due to reduction in surfactant and polymer adsorption on the reservoir rocks. Several aspects of the use of highly alkaline fluids as a preflush were investigated. Among these were comparisons of highly alkaline sodium silicate to sodium hydroxide and highly saline soft brines, studies on the adsorption of surfactants and polymers, and studies on rock reactivity and permeability changes. Some of the conclusions reached from these studies were as follows:

1. Highly alkaline sodium silicate solution ($\text{pH} > 11$) are more effective than sodium hydroxide or highly saline soft water solutions as preflush solution, based on recovery efficiency.
2. The permeability to highly alkaline sodium silicate solutions was to the order of 75% to 85% of brine permeability in the porous media used for the studies.
3. The highly alkaline sodium silicate solutions react with hardness ions in reservoir brines and clays, with the clays themselves, and with calcium carbonate and calcium sulfate minerals.
4. The adsorption of surfactant and solvent by the reservoir rocks was significantly reduced by a preflush of highly alkaline sodium silicate.

In order to compare some of the various preflush approaches on an equivalent basis, a systematic study was undertaken on a fixed system using a standard brine solution and Berea sandstone cores. Presented here are some of the preliminary results obtained from laboratory studies on elution of calcium and magne-

sium ions from Berea cores by various types of preflush solutions. The alkaline systems studied were sodium silicate, sodium hydroxide, and sodium carbonate. The soft saline systems contained various concentrations of sodium chloride. In some of the tests, dilute petroleum sulfonate solutions were injected after the preflush to measure surfactant effects on ion exchange.

EXPERIMENTAL PROCEDURE

The brine displacement studies were performed on epoxy-coated Berea sandstone cores. The cores were evacuated and saturated with standard brine. The cores were equilibrated with several pore volumes of the standard brine at a rapid flow rate until the hardness ion concentration of the effluent was equal to that of the standard brine. The hardness ion levels were measured by a standard EDTA titration procedure and are reported in ppm of CaCO_3 for convenience. No differentiation between calcium and magnesium ions was attempted, since several workers have shown that calcium and magnesium behave essentially the same in systems similar to ours at slow flow rates. Permeability measurements were not made for the experiments performed in this study. The pH values of the effluent fractions were monitored when the alkaline solutions were injected. The effluent was collected by an automatic fraction collector in 0.05 PV fractions.

The solutions used in the study and the general experimental conditions are given in Table 15. The solution and volumes used for the individual brine displacement studies are given in Table 16.

TABLE 15

SOLUTIONS AND EXPERIMENTAL CONDITIONS

Solutions

ALKALINE

0.5% Na ₄ SiO ₄ in 3% NaCl	(pH = 12.6)
0.5% NaOH in 3% NaCl	(pH = 12.8)
0.5% Na ₂ CO ₃ in 3% NaCl	(pH = 11.0)
1.14% liquid Sodium Silicate (44% solids, SiO ₂ /Na ₂ O) ratio of 2:1 in 1% NaCl	(pH = 11.2)

SALINE

3% NaCl, 10% NaCl in deionized water

SURFACTANT

0.25% WITCO TRS 10-80 in 3% NaCl

BRINE

28,400 ppm NaCl
1,110 ppm CaCl₂
490 ppm MgCl₂

EXPERIMENTAL CONDITIONS

Berea Cores - 2" x 2" x 24"
Average Porosity - 22%
Permeability - Approximately 200 md
Flow Rate - 2 ft/day
Temperature - 22°C
Hardness Analysis - Standard EDTA Titration
(expressed as ppm CaCO₃)

TABLE 16

SOLUTIONS AND VOLUMES INJECTED FOR INDIVIDUAL
BRINE DISPLACEMENT EXPERIMENTS

<u>Core</u>	<u>Brine</u>	<u>Treatment</u>
27	Standard	3% NaCl to 3 PV
38	Standard	1) 0.25 PV of 0.5% NaOH in 3% NaCl 2) 3% NaCl to 3 PV
39	Standard	1) 0.25 PV of 0.5% Na ₄ SiO ₄ in 3% NaCl 2) 3% NaCl to 3 PV
45	Standard	1) 0.1 PV of 0.5% NaOH in 3% NaCl 2) 3% NaCl to 3 PV
46	Standard	1) 0.1 PV of 0.5% Na ₄ SiO ₄ in 3% NaCl 2) 3% NaCl to 3 PV
47	Standard	1) 0.1 PV of 0.5% Na ₂ CO ₃ in 3% NaCl 2) 3% NaCl to 3 PV
48	Standard	1) 0.5 PV of 0.5% Na ₂ CO ₃ in 3% NaCl 2) 3% NaCl to 3 PV
49	Standard	1) 0.5 PV of 1.14% "D" sodium silicate in 1% NaCl 2) 1% NaCl to 3 PV
50	Standard	1) 0.1 PV of 1.14% "D" sodium silicate in 1% NaCl 2) 1% NaCl to 3 PV
51	Standard	1) 0.25 PV of 1.14% "D" sodium silicate in 1% NaCl 2) 1% NaCl to 3 PV
57	Standard	1) 0.1 PV of 0.5% Na ₄ SiO ₄ in 3% NaCl 2) 0.25% Witco TRS 10-80 in 3% NaCl to 3 PV
58	Standard	1) 0.25 PV of 3% NaCl 2) 0.25% Witco TRS 10-80 in 3% NaCl to 3 PV
61	Standard	1) 0.1 PV of 0.5% Na ₄ SiO ₄ in 3% NaCl 2) 0.5 PV of 0.25% Witco TRS 10-80 in 3% NaCl 3) 3% NaCl to 3 PV
62	Standard	1) 0.25% PV of 3% NaCl 2) 0.5 PV of 0.25% Witco TRS 10-80 in 3% NaCl 3) 3% NaCl to 3 PV
67	Standard	1) 0.25% PV of 10% NaCl 2) 3% NaCl to 3 PV
68	Standard	1) 0.1 PV of 10% NaCl 2) 3% NaCl to 3 PV

RESULTS

High Salinity Preflush

The injection of soft saline solution (3% NaCl) of essentially the same ionic strength as the brine which was used to condition the Berea core produced a gradual decrease in the hardness ion concentration in the effluent. This behavior is shown by the curve designated Core 27 in Fig. 51. The ion exchange elution of hardness ions from the clays followed a typical pattern, decreasing rapidly to a minimum value after 2.0 pore volumes of injection.

The injection of higher salinity solutions (10% NaCl) as a preflush at 0.1 or 0.25 pore volumes, followed by 3% NaCl to a total of 3.0 pore volumes, developed significant increases in the levels of hardness ions in the effluent obtained prior to 1.0 pore volume of injected fluid. These data are shown in Fig. 51 as the curves for Cores 67 and 68. The curve for 0.1 PV of 10% NaCl (Core 68) showed a sharp ion exchange peak between 0.8 and 1.0 pore volumes with a rapid drop-off in concentration between 0.95 and 1.3 pore volumes. After 1.3 pore volumes, the curve was essentially the same as the curve for 3% NaCl. A broader ion exchange peak was observed for the injection of 0.25 pore volume of 10% NaCl (Core 67) and the hardness ion minimum level was not attained until nearly 3 pore volumes of fluid had been injected.

High Alkalinity Preflush

The results from the use of highly alkaline chemicals as preflush agents are shown in Figs. 52 and 53. A comparison between the injection of 0.1 pore volume of 0.5% sodium orthosilicate (Core 46) or 0.5% sodium hydroxide (Core 45) followed by 3%

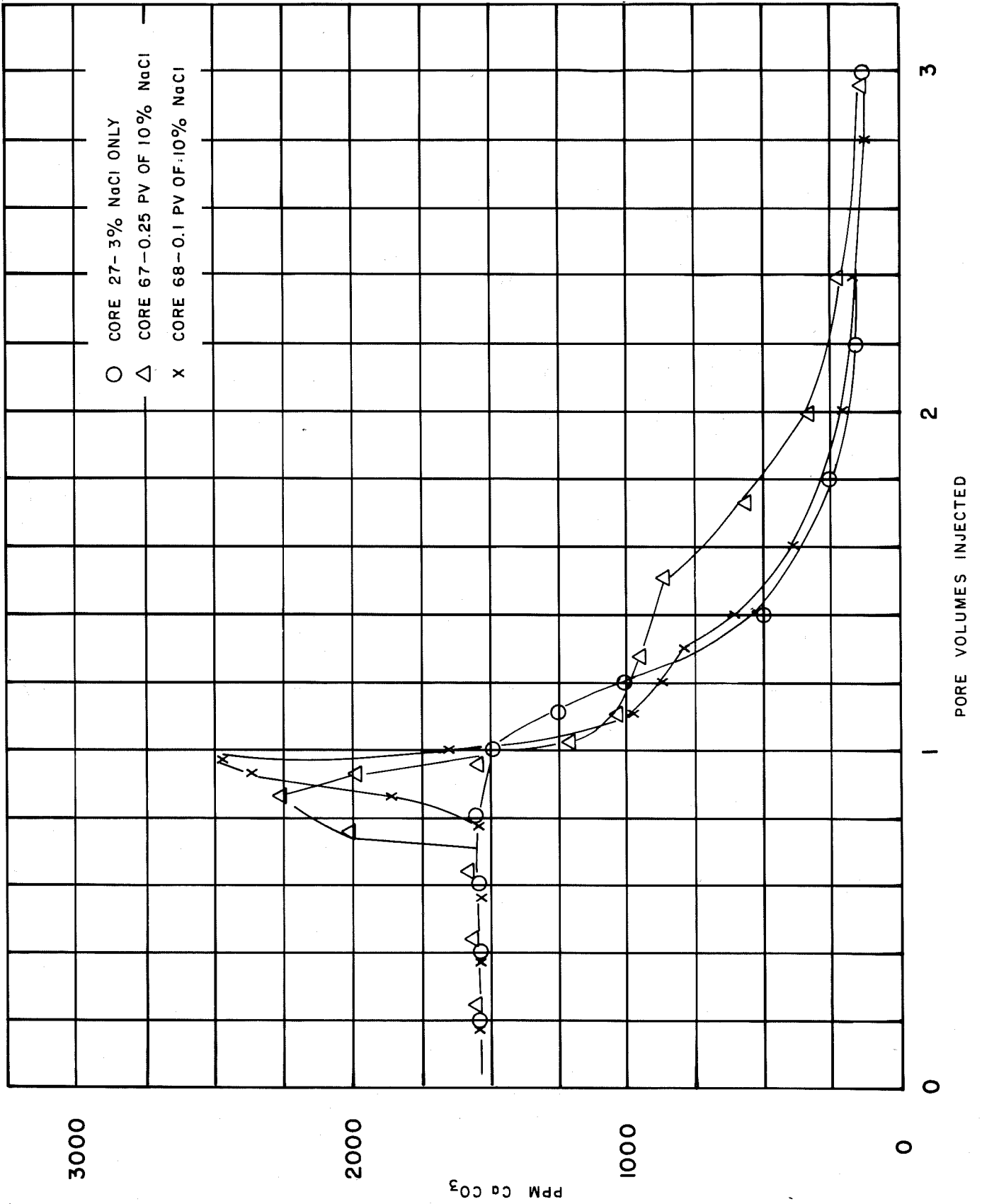


FIG. 51- High salinity preflush.

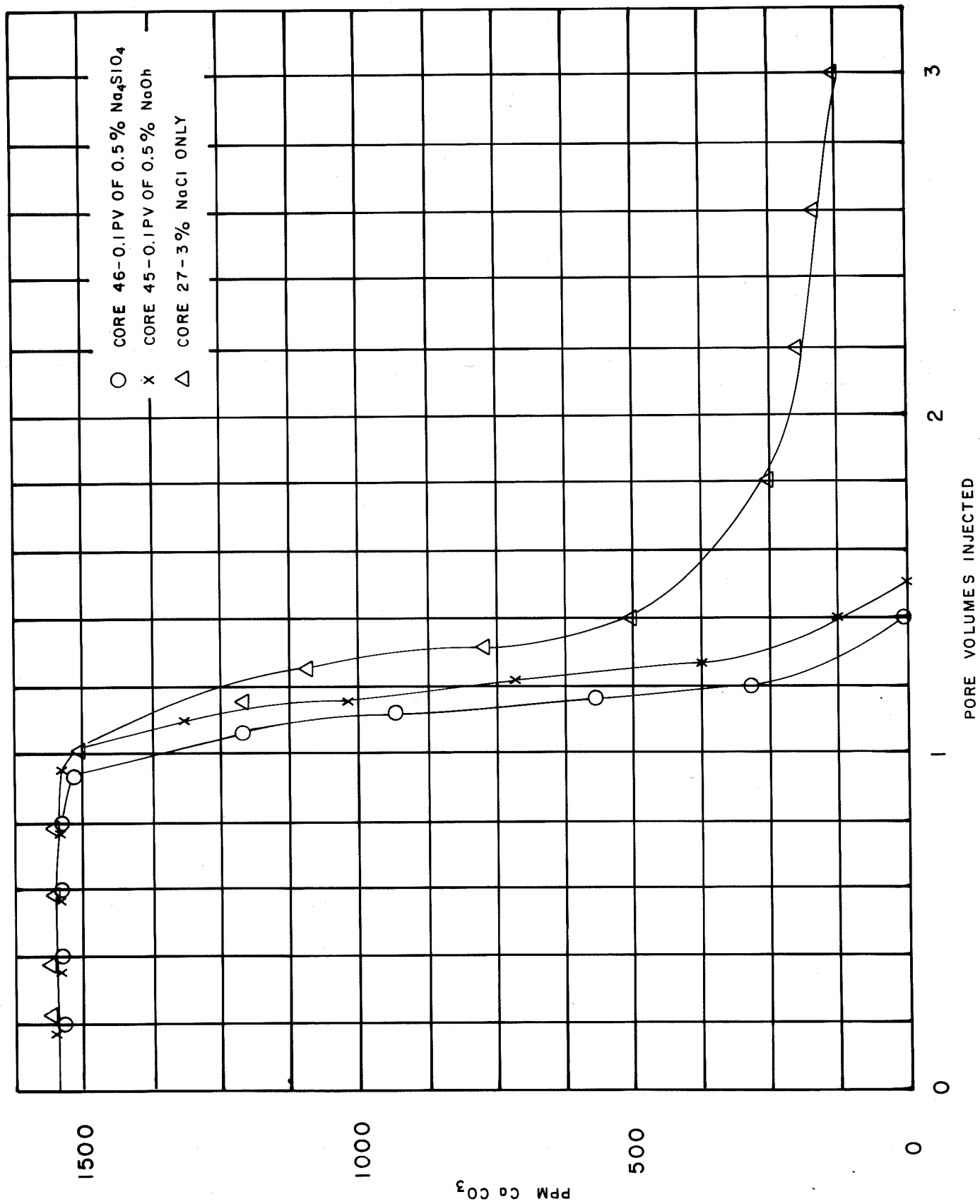


FIG. 52- Highly alkaline preflush - 0.1 PV.

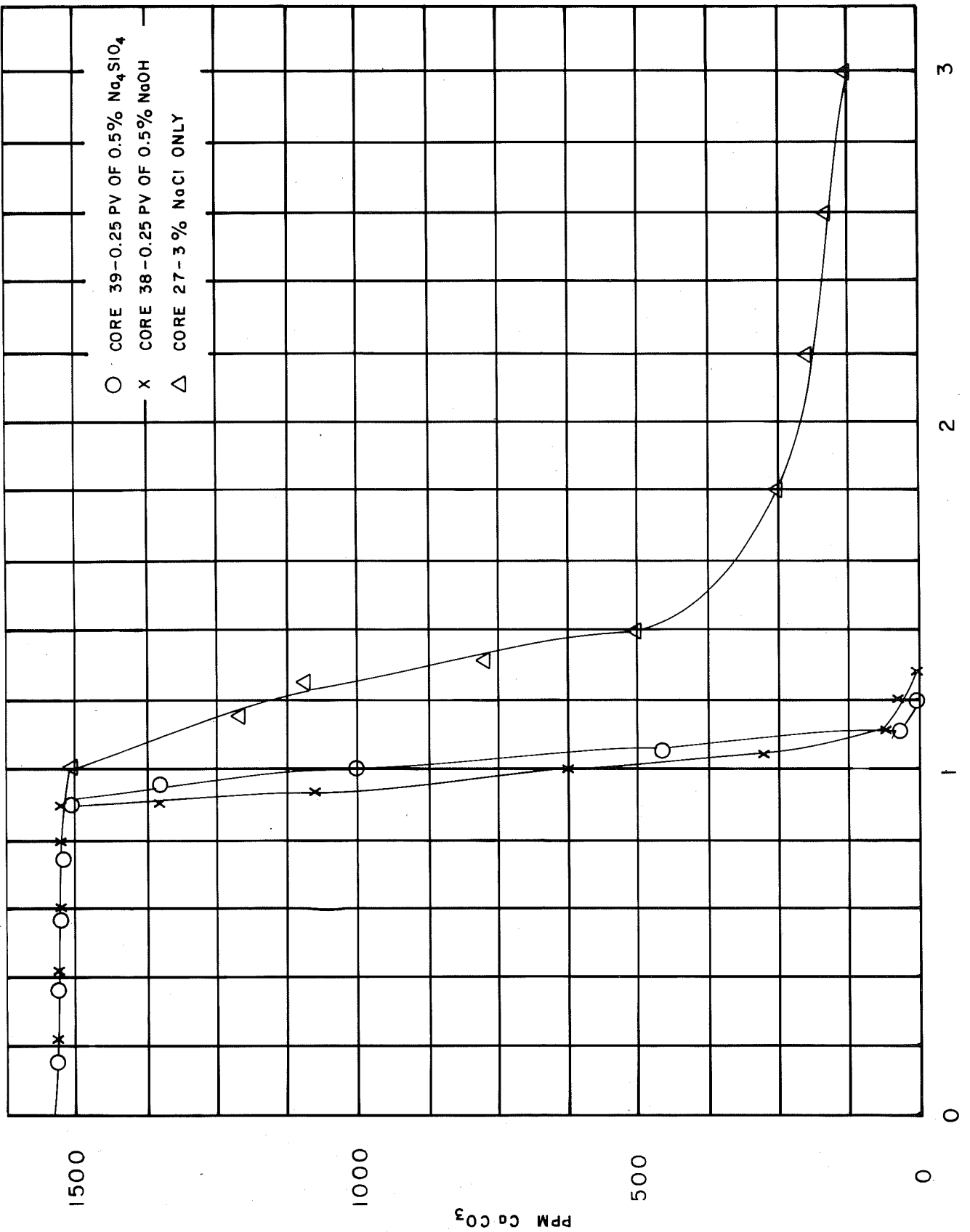


FIG. 53- Highly alkaline preflush - 0.25 PV.

NaCl to 3.0 pore volumes and the injection of 3% NaCl alone (Core 27) is shown in Fig. 52. Both alkaline solutions produced a rapid decrease in hardness ion levels between 0.95 and 1.5 pore volumes, with no further elution of hardness ions beyond this point.

The injection of 0.25 pore volume of the alkaline solution, followed by 3% NaCl to 3.0 pore volumes gave a sharper decrease in hardness ion levels, with no further elution of hardness ions beyond 1.25 pore volumes. These data are presented in Fig. 53. The curve for 3% NaCl (Core 27) is shown for comparison. The results for 0.5% sodium orthosilicate (Core 39) and 0.5% sodium hydroxide (Core 38) were essentially the same within experimental error and natural variations in the Berea cores.

Sodium Silicate Preflush

Fig. 54 presents the results obtained when increasing volumes of a less alkaline sodium silicate were injected as a preflush agent. For these tests, a 1.14% solution of liquid sodium silicate (2:1 ratio $\text{SiO}_2/\text{Na}_2\text{O}$, 44% solids) in 1% NaCl was used. The pH of the injection solution was 11.2. The results show that the less alkaline sodium silicate solutions were not as effective as the sodium orthosilicate or sodium hydroxide solutions in reducing the hardness ion level to zero.

Sodium Carbonate Preflush

The use of sodium carbonate as an alkaline preflush agent gave significantly different results compared to the highly alkaline systems. The data are plotted in Fig. 55 with the plot for 3% NaCl (Core 27) included for comparison. When 0.1 pore volume of 0.5% Na_2CO_3 in 3% NaCl solution was injected (Core 47), a response similar to the high salinity preflush was observed. An

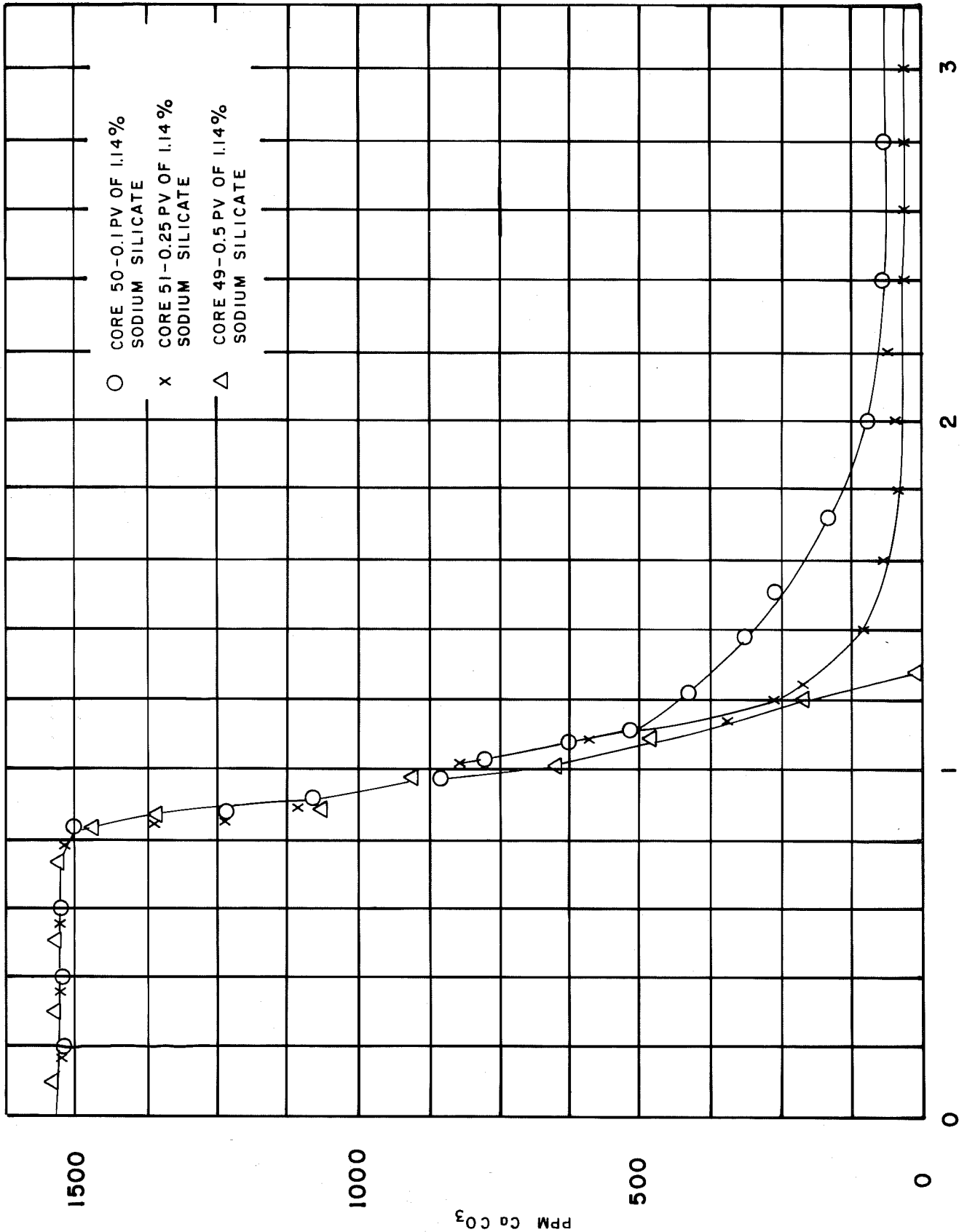


FIG. 54- Sodium silicate preflush (2.0 ratio, S_{iO_2}/Na_2O).

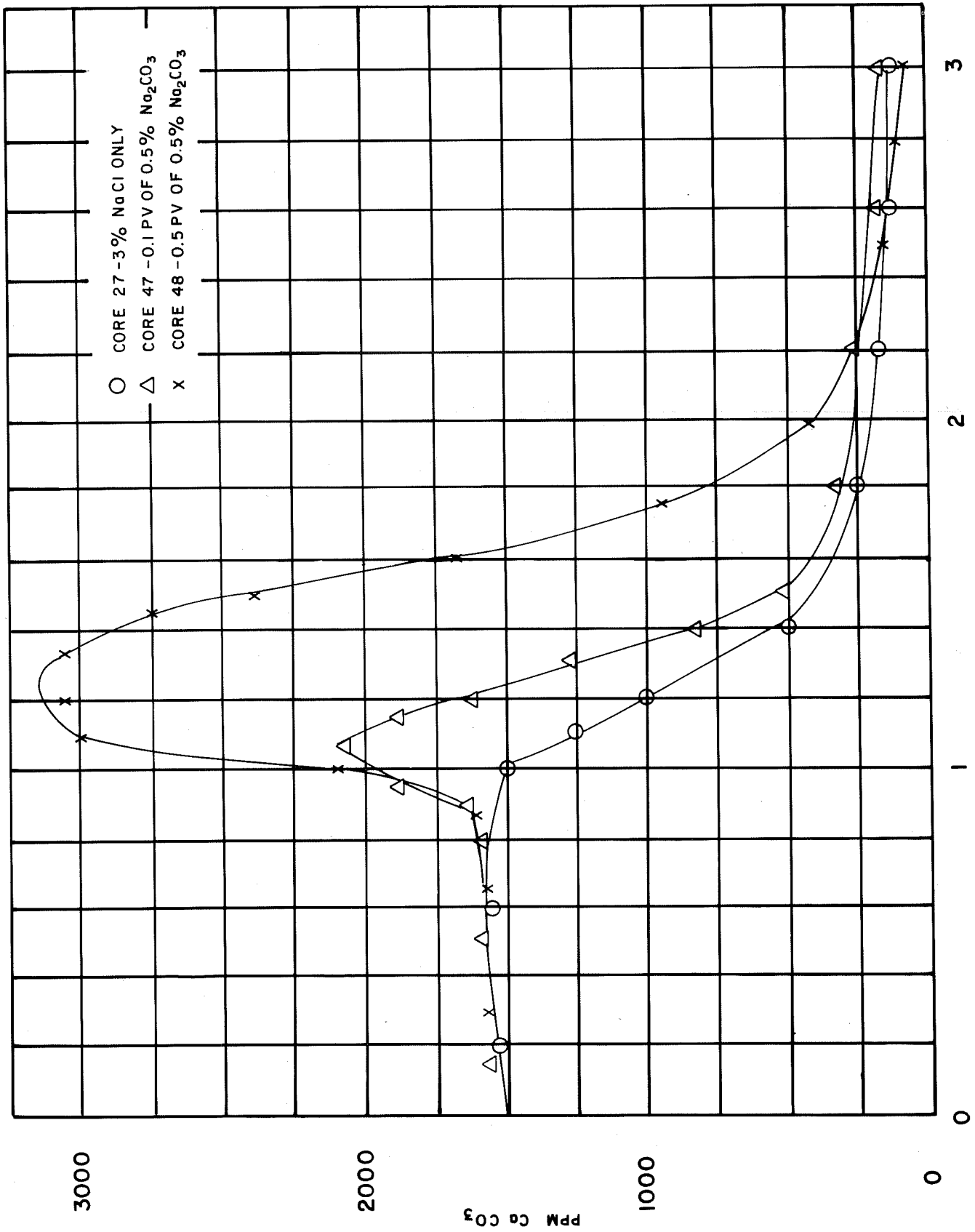


FIG. 55 - Sodium carbonate preflush.

ion exchange peak of higher hardness ion concentration occurred starting at 0.9 pore volume which peaked at 1.05 pore volumes. The curve lay above the 3% NaCl curve until 2.5 pore volumes had been injected.

The injection of 0.5 pore volume of 0.5% Na₂CO₃ in 3% NaCl (Core 48) as a preflush gave an extreme ion exchange response which started at 0.9 pore volumes, peaked at 1.25 pore volumes with a hardness ion concentration of more than twice the equilibration concentration and fell off to a minimum at 2.5 pore volumes.

Surfactant-Induced Ion Exchange

Fig. 56 shows the hardness ion elution curves for 3% NaCl alone (Core 27), for a 0.25 pore volume injection of 3% NaCl followed by 0.5 pore volume of 0.25% Witco TRS 10-80 surfactant in 3% NaCl (Core 62) and for a 0.25 pore volume injection of 3% NaCl followed by injection of 0.25% Witco TRS 10-80 in 3% NaCl to 3.0 pore volumes (Core 58). The curves for Core 27 and Core 58 were virtually superimposable, which indicated that no additional ion exchange was induced by the surfactant at an injection volume of 0.5 pore volume. The continuous injection of surfactant produced an elution curve of somewhat higher concentration of hardness ions between 1.2 and 3.0 pore volumes injected. There was no ion exchange peak observed of the type seen with sodium carbonate, but the higher level of hardness ions may have been due to an increase in ion exchange induced by the surfactant in the system.

The effect of an alkaline preflush prior to injection of a surfactant solution is depicted in Fig. 57. The elution curves for 3% NaCl alone (Curve 27) and for 0.1 pore volume of 0.5%

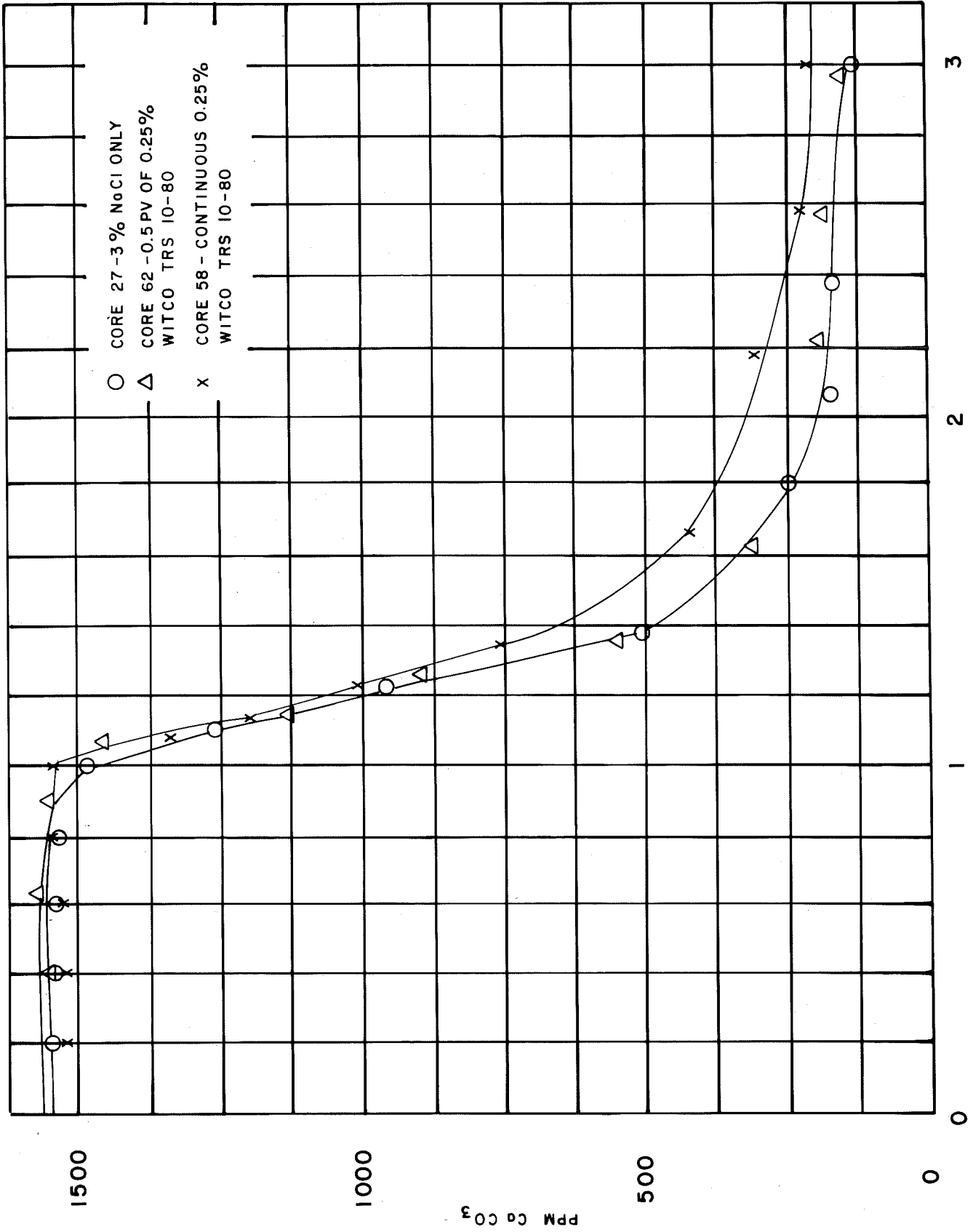


FIG. 56 - Surfactant effect on hardness ion elution.

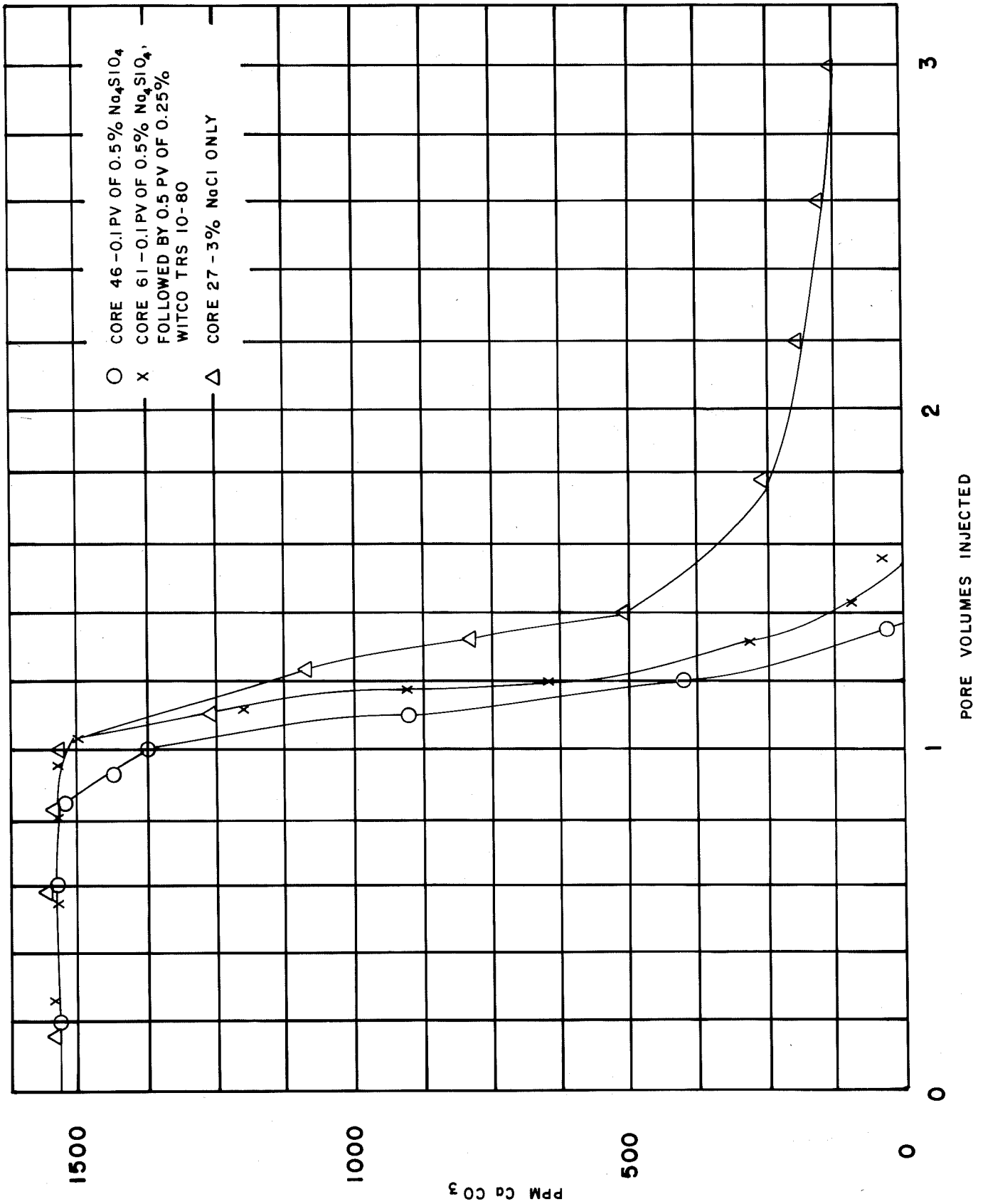


FIG. 57 - Effect of alkaline preflush and surfactant on hardness ion elution.

sodium orthosilicate in 3% NaCl, followed by 3% NaCl (Core 46) are given for comparison. The injection of 0.1 pore volume of 0.5% sodium orthosilicate in 3% NaCl, followed by 0.5 pore volume of 0.25% Witco TRS 10-80 and 3% NaCl to 3.0 pore volumes (Core 61) showed an elution curve which was similar in response to the curve for the sodium orthosilicate alone. The difference in elution volume may have been due to natural core differences or to an increase in ion exchange caused by the presence of surfactant in the solution.

DISCUSSION

The results from the above experiments showed that highly alkaline brine solutions were very effective for rapidly reducing the hardness ions in the effluent to very low levels. The alkalinity of these solutions causes precipitation of the hardness ions eluted from the clays as highly soluble hydroxides and silicates. Further elution of hardness ions from the core was not observed with the injection of additional brine. Although elution with a soft brine of essentially the same ionic strength as the standard brine gave a fairly rapid drop-off in the hardness ion level, there was still a significant level of hardness ions in the effluent after 2 pore volumes of 3% NaCl had been injected. With the highly alkaline brine solutions, the hardness ion level dropped to zero after 1.2 pore volumes when 0.25 PV of 0.5% sodium orthosilicate or sodium hydroxide in 3% NaCl was injected prior to the injection of the 3% NaCl alone, as shown in Fig. 53. The injection of 0.1 PV of the alkaline brine prior to the injection of 3% NaCl showed similar results (Fig. 52), except that 1.4 to 1.5 pore volumes of fluid were injected before the hardness ion level dropped to zero.

The injection of 0.1 PV or 0.25 PV of 10% NaCl prior to the injection of 3% NaCl gave ion exchange peaks, followed by a rapid

drop-off in hardness ion levels. However, the hardness ion levels were not reduced below that of the curve for elution with 3% NaCl alone, except between 1.0 PV and 1.2 PV of injection. The hardness ion level did not reach zero with the high salinity preflush solutions. The elution curves attained a steady-state level of about 60 ppm (as CaCO₃) at 3.0 PV of injection. Apparently, the volumes of 10% NaCl injected were not sufficient to exchange all the hardness ions in the clays, so the hardness ion level in the effluent was not reduced to zero.

The behavior of the less alkaline chemicals, sodium carbonate and sodium silicate, was quite different. The 1.14% sodium silicate solution (2.0 ratio of SiO₂/Na₂O, 44% solids) in 1% NaCl gave similar elution curves (Fig. 54) to those obtained with sodium orthosilicate and sodium hydroxide when 0.5 PV was injected prior to the injection of 3% NaCl alone. Injection of 0.1 PV of the sodium silicate solution gave an elution curve similar to the curve for 3% NaCl alone. The hardness ion level did not reach zero. Injection of 0.25 PV of sodium silicate produced a sharper drop-off in hardness ion level, but did not reduce the effluent to zero hardness.

In contrast, the injection of 0.1 PV of 0.5% sodium carbonate followed by 3% NaCl (Fig. 55) produced significant ion exchange peaks, especially when 0.5 PV of the chemical was injected. The sodium carbonate should have removed part of the calcium present in the brine by precipitation, although magnesium ions would not be affected. In this case, however, the injection of sodium carbonate gave the same type of behavior as injection of 10% NaCl, except that the hardness ion drop-off was less rapid following the ion exchange peak. These results suggest that sodium carbonate would be an uneconomical choice as a preflush agent.

In the brine displacement experiments where dilute surfactant was injected (Figs. 56 and 57), there was some evidence of additional ion exchange induced by the surfactant when the surfactant solution was injected continuously. This phenomena was shown by the curve for Core 58 in Fig. 56. However, the curve for injection of 0.5 PV of the surfactant solution, Core 62 in Fig. 56, was essentially superimposable on the curve for elution with 3% NaCl alone. The curve obtained for injection of 0.5 PV of surfactant solution following a 0.1 PV preflush with sodium orthosilicate (Core 61, Fig. 57) showed a shift to higher elution volumes compared to the curve obtained for 0.1 PV of sodium orthosilicate without surfactant (Core 46, Fig. 57). This shift may have resulted from additional ion exchange induced by the surfactant, from diffusion effects between the surfactant solution and the silicate solution or from innate differences between the Berea cores. We do not have much experimental evidence yet to determine which type of mechanism is operating in this system.

CONCLUSIONS

1. Highly alkaline preflushes are very effective in reducing hardness ions to very low levels in reservoir brine prior to injection of surfactant solutions.
2. High salinity preflush solutions are less effective in reducing hardness ions to low levels due to continued ion exchange from the clays in Berea cores.
3. The less alkaline sodium silicates, such as 2.0 ratio sodium silicate, are not as effective as sodium orthosilicate, mainly due to the lower alkalinity of the solution.

4. The use of sodium carbonate as a preflush chemical is very inefficient due to the high ion exchange peak induced by some action of the carbonate anion.

5. Dilute surfactant solution had minimal effects on the elution of hardness ions from Berea cores.

